**NTNU – Trondheim**
Norwegian University of
Science and Technology

# Integrity Evaluation of Duplex Stainless Steel Flanges

Henrik Sture

Subsea Technology
Submission date: June 2012
Supervisor: Roy Johnsen, IPM
Co-supervisor: Ragnar Gjengedal, Bergen University College (HiB)
Ørjan Fyllingen, Bergen University College (HiB)

Norwegian University of Science and Technology
Department of Engineering Design and Materials

## Preface

This thesis is the product of approximately twenty weeks of work in the period between 15th of January and 24th of June 2012. The project has been challenging, and very educational. Working with finite element modeling has been particularly interesting, as I had very limited prior experience with this kind of software. The fact that this line of research is quite new at Bergen University College (HiB), presented me with a multitude of potential areas of study. Having the freedom and responsibility to determine the project direction has been a great experience.

I would like to thank my supervisors PhD Ragnar Gjengedal and PhD Ørjan Fyllingen for their support, enthusiasm, and guidance. Without them, this thesis would not be what it is today. I would also like to thank Kjetil Gravelsæter and Nafez Mohammadi Ardestani whom aided me with preparing the test specimens and with help in regards to the testing equipment. Additionally, I would like to thank Svein Johnsen from Norske Ventiler that acquired the forged bars for material testing, and that gave advice readily when asked. Lastly, I would like to thank the unknown HiB employee that spent an hour of his Thursday evening helping me get back into my office when the school's computer system locked all the doors for the night.

Henrik Sture Bergen, 24th of June 2012

## Abstract

Duplex stainless steel flanges are normally forged to form, as required by the ASTM A182/A182M standard, but may also potentially be machined directly from forged stainless steel bar. In order to evaluate the integrity of such flanges, axisymmetric elastic-plastic finite element models have been developed, considering static effects such as bolt load and internal pressure. Additionally, tensile testing of a sample forged bar (UNS S31803) has been conducted.

The stress distribution in a flange during gasket seating and operating conditions has been determined, as well as the degree of plastic strain caused by the bolt loads. The maximum stresses have been found to be around the same values as the minimum yield strength requirement of the studied material (UNS S31803), and the location of the maximum stress concentrations have been identified as the gasket groove.

The tensile tests of the forged bar (UNS S31803) have shown that the yield and tensile strength properties are considerably higher than the standardized minimum requirements. The elastic modulus of the forged bar has also been determined, and was found to be lower than anticipated in the axisymmetric models. Some specimens have also been found to exhibit highly non-linear elastic properties.

## Sammendrag

Flenser laget av dupleks rustfritt stål er normalt smidd til form, som krevd av ASTM A182/A182M standarden, men kan potensielt bli maskinert direkte fra smidd rustfritt stål i bar form. For å kunne evaluere integriteten til slike flenser, har elementmetoden blitt brukt til å utvikle aksialsymmetriske elastisk-plastiske modeller, som vurderer statiske effekter slik som bolt laster og interne trykk. I tillegg har strekktester av smidd bar (UNS S31803) blitt gjennomført.

Spenningsfordelingen i en flens under installasjon av pakningen og driftsforhold har blitt kartlagt, i tillegg til graden av plastisk tøyning forårsaket av bolt lastene. De maksimale spenningene har blitt funnet å ligge i samme området som den minimale flytegrensen til det studerte materialet (UNS S31803), og posisjonen til de maksimale spenningskonsentrasjonene er blitt avdekket å ligge i pakningssporet.

Strekktestene av de smidde barene (UNS S31803) har vist at flytegrensen og bruddgrensen er betydelig høyere enn de standardiserte minimale kravene. Elastisitetsmodulen til smidd bar (UNS S31803) har også blitt bestemt, og funnet å være lavere enn forutsett i de aksialsymmetriske modellene. Noen av prøvene har også blitt funnet å utvise en høy grad av ikke-lineære elastiske egenskaper.

## Table of Contents

# 1 INTRODUCTION

## 1.1 Background

Duplex stainless steel flanges may potentially be manufactured by forging the source material as close to form as possible, or alternatively by machining the entire geometry from a forged bar source. The forging procedure requires available production time on highly specialized equipment, which may potentially increase the lead time of a flange product forged to form. Manufacturing the flange from bar stock, on the other hand, only requires conventional machining equipment, and available bar stock. Potential benefits from using the latter manufacturing method may be a reduction in the lead time, as well as the cost of the finished flange product.

The widely used ASTM (American Society for Testing and Materials) A182/A182M standard specifies that "Flanges of any type, elbows, return bends, tees, and header tees shall not be machined directly from bar stock", and "The material shall be forged as close as practicable to the specified shape and size". This thesis aims to independently evaluate the integrity of duplex stainless steel flanges manufactured from bar stock.

## 1.2 Objective

There are two main objectives for this thesis: The first is to develop a finite element model for a flange in both gasket seating and operating conditions. The model is to consider the static strength of a flanged joint, and simplifications in regards to transient effects may be done. The second objective is to test the bar stock material (UNS S31803) in order to determine the strength properties and elastic characteristics. A third sub-objective is to compare the axisymmetric results to existing design rules for flanged joints, defined by ASME (American Society of Mechanical Engineers).

## 1.3 Nomenclature

**Table 1: Nonmenclature**

| Acronym | Full Meaning |
|---|---|
| ASME | American Society of Mechanical Engineers |
| ASTM | American Society for Testing and Materials |
| BaPVC | Boiler and Pressure Vessel Code |
| BaPVC | Boiler and Pressure Vessel |
| CNC | Computer Numerical Control |
| DSS | Duplex Stainless Steel |
| NORSOK | Norsk Sokkels Konkurranseposisjon |
| NPS | Nominal Pipe Size |
| NS | Norwegian Standard |

# 2 PREVIOUS WORK

## 2.1 Fabrication of Duplex Stainless Steel Flanges

Duplex stainless steel (DSS) products may be fabricated through several different techniques, which includes, but is not limited to: Forging, rolling, casting, extrusion, and powder metallurgy. This chapter contains a brief introduction to forging and rolling of DSS, as well as descriptions of the micro structural similarities and differences. The main references for this chapter is the ASM International Handbook Committee. (1990), ASM International Handbook Committee. (1998), and Mateo et al. (2003).

### 2.1.1 Introduction to forging

Forging is the act of mechanically deforming a piece of metal into a desired form. Depending on the material, desired properties, and process, forging may be performed at either cold, warm, or hot temperatures.

One of the major advantages to forged products is that the "...impurities are redistributed in a more or less fibrous form." (Rollason, 1973). This is often particularly beneficial in DSS as the ferrite and austenite metallic phases are more evenly distributed throughout the product body. The microstructure of forged DSS products will be further discussed in 2.1.3 The duplex stainless steel microstructure.

While there are a multitude of different forging techniques available, many of them fall under one of the following categories: Open-die forging, closed-die forging, hot heading, cold forging or forge rolling (ASM International Handbook Committee., 1998). Forge rolling, also known as hot rolling, will be further discussed in section 2.1.2 Introduction to rolling. Cold forging will not be discussed further in this thesis.

Open-die forging utilizes generic dies, often flat-faced or v-faced, which are attached to hammers and presses in order to deform the source material into the desired shape. This form of forging is most common for products that are either too large to be produced in a closed-die process, or where the product line is too small to justify the development of a dedicated closed-die. Note however, that this form of forging is expensive and time consuming, and are used only in unusual circumstances (ASM International Handbook Committee., 1998).

Closed-die forging, or impression-die forging as it also is called, is a technique where a set of two or more matching dies are used to guide the source material to a specific form. In a two die setup, one die would be attached to a hammer or press actuator, while the other would

remain stationary with the source material inside. The actuator would then hit or press the source material, thereby forcing it to flow into the die, and eventually achieve the desired product form. For larger products, it is normal to heat both the die and the source material to high temperatures prior to starting the process. Smaller products may be produced through a cold process often referred to as coining (ASM International Handbook Committee., 1998). The coining process will not be discussed further in this thesis.

Hot heading consists of forcing a source material partly or fully into a die, or pair of matching dies. It is a process commonly used for production of bolts, wrench sockets, and flanged shafts, but also more complex shapes may be produced. Such complex products are often produced in several steps, referred to as passes, where each pass add contributions towards the final product form (ASM International Handbook Committee., 1998).

### 2.1.2 Introduction to rolling

Rolling is mainly used for reducing the thickness of a source material into bars and plates of uniform thickness. However, some mechanical parts such as axles and shafts are well suited for this kind of production method. By passing the source material, often in the form of a metal billet or slab, between two or more rotating rolls with limited clearance, it undergoes mechanical deformation. By repeating this process, it is possible to form bars, plates, or other products of reduced, uniform thickness, which in turn may be used as source material for other forming processes. Some rolling techniques also allow for forming of bars with tapered ends.

There are two main categories of rolling, cold rolling and hot rolling. As previously mentioned, the hot rolling process has much in common with forging, and is by some literature sources referred to as roll forging. Both temperatures and heating times are in many cases the same for hot rolling as for forging a specific alloy (ASM International Handbook Committee., 1998).

### 2.1.3 The duplex stainless steel microstructure

The DSS microstructure consists of ferrite and austenite phases in a duplex matrix, as implied by the name. While the fractions of said phases may vary from alloy to alloy, it is common to aim for about half of each. That said, forged and hot rolled DSS products of the same grade can be expected to have roughly the same fractions, although a significant difference in distribution may occur.

### *2.1.3.1 Intermetallic phases*

During the forming and manufacturing of DSS products it is important to carefully consider the temperature profile versus time, as precipitation of intermetallic phases may cause embrittlement and loss of toughness (Beddoes and Parr, 1999, ASM International Handbook Committee., 1998). The most important of these phases are sigma, carbides, and the so called 475˚C embrittlement, as illustrated in the precipitation diagram below (Figure 1).

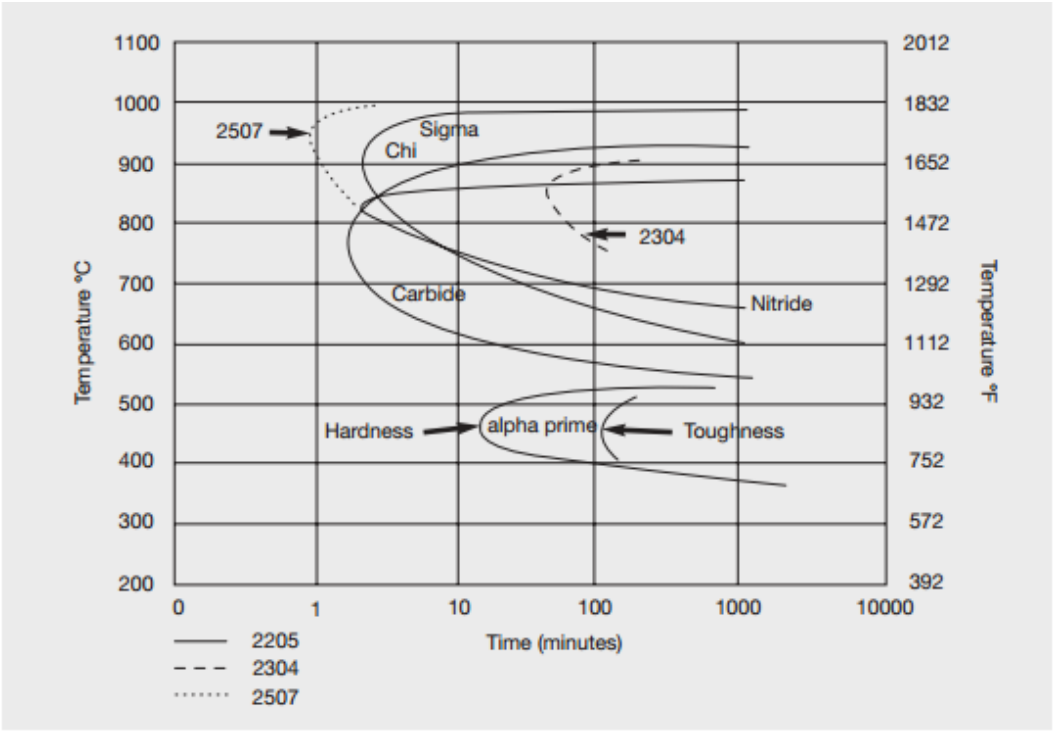


**Figure 1: Isothermal precipitation diagram for 2205 duplex stainless steel, annealed at 1050 C (TMR Stainless, 2009).**

The sigma phase is an iron-chromium compound with a hardness of approximately 68 HRC, which causes embrittlement in DSS alloys. The embrittlement effect is at its greatest once the alloy has cooled below approximately 260˚C. While the sigma phase also may affect the corrosion resistance of the DSS, it is normally not a cause for concern as the effect is small compared to the change mechanical properties (Beddoes and Parr, 1999, ASM International Handbook Committee., 1998).

The precipitation of chromium carbides, known as sensitization, occurs on the grain boundaries, and is simply put the redistribution of chromium in the matrix. Due to the ferrite phase (BCC) being a more open structure than the austenite phase (FCC), the chromium tend to diffuse much more rapidly in ferrite. This causes much of the ferrite grains around chromium carbides to be deficit of chromium, while only a narrow band in the austenite grains loses chromium. Chromium carbides can cause both a decrease in local corrosion

resistance and a loss of toughness. While it is a common problem in heat affected zones (HAZ) from welding, the problem is much lower in DSS than other stainless steels. This is both due to the duplex phase matrix and the low carbon content (Beddoes and Parr, 1999).

The 475˚C embrittlement occurs when a DSS alloy is cooled slowly through or heated to temperatures within the 400 to 550˚C range. This phenomenon causes an increase in tensile strength and hardness, while corrosion resistance, tensile ductility, and impact strength is reduced. The mechanism, in which the embrittlement occurs, is essentially a redistribution of the chromium content within the ferrite phase, where the result is one chromium rich and one chromium deficit ferrite phase (ASM International Handbook Committee., 1998).

Due to the fact that the abovementioned intermetallic phases require temperature and time to form, the simplest solution is to rapidly cool the DSS product fully below the critical temperature range. This process is called quenching, and is essentially the act of submerging the heated product in a cooling medium, such as water or oil. However, in objects of higher thickness, the centre may have substantially higher temperature profiles that what is found at the surface. The dissipation rate of thermal energy then has to be modelled to ensure that also the material in the centre has the right composition and properties.

It should be noted that the precipitation diagrams, such as Figure 1, are severely affected by any changes in the composition of the alloy. This is something metallurgists use actively to optimize the allowable cooling time of alloys.

#### *2.1.3.2 Grain Flow*

The nature of the deformations involved during the forming process induces a phenomenon known as grain flow (ASM International Handbook Committee., 1998). This phenomenon causes the ferrite and austenite phases, as well as any impurities, to be distributed as fibres of a specific alignment. In forged flanges, the dies are often designed in such a way that the fibres align parallel to the flange surface. Similarly, in hot rolling, the fibres are often aligned parallel to the rolling direction, as shown in Figure 2.

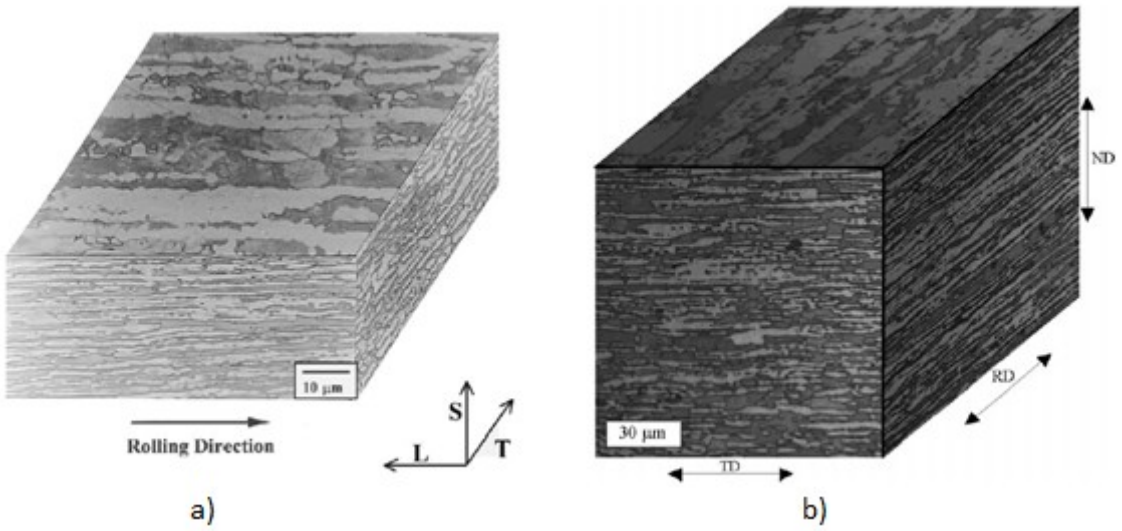


**Figure 2: a) duplex stainless steel plate, bright colour is austenite phase (Mateo et al., 2003), b) duplex stainless steel plate, bright colour is austenite phase (Moverare and Odén, 2002).**

Due to this type of alignment, forged and hot rolled products can exhibit significant anisotropic behaviour, where both the strength and ductility is greater along the direction of working (Mateo et al., 2003, Moverare and Odén, 2002). In cases where a forged or hot rolled product is machined in such a way that the fibre ends are exposed, it is called end-grain exposure. This has been known to lower the resistance towards stress corrosion cracking (SCC) in the transverse directions (ASM International Handbook Committee., 1990).

## 2.2 Materials

The objective of this chapter is to introduce the material data that will act as a basis for the finite element analyses conducted in the thesis. The chapter has been split into three sections, based on components; Flange material, gasket material, and bolt material. The most important references for this chapter are the ASME (2010) Section II Part D, and the ASTM (2011a) A182 and ASTM (2011b) A479 standards.

### 2.2.1 Flange material

The flange material chosen for the analyses conducted in the thesis is the UNS S31803 alloy, also known as AISI 2205. The composition of relevant product forms may be found in Table 2 below. The specification number refers to the ASTM standard that is valid for that product form.

**Table 2: Material data for UNS 31803**
**(based on ASME (2010), section II, part D)**

| Product Form | UNS No. | Composition | Spec No. |
|---|---|---|---|
| Bar | S31803 | 22Cr-5Ni-3Mo-N | SA-479 |
| Forgings | S31803 | 22Cr-5Ni-3Mo-N | SA-182 |

#### *2.2.1.1 Ultimate tensile and yield strength*

The minimum ultimate tensile and yield strength of the UNS S31803 alloy is listed for room temperatures in Table 3. As this is a minimum, the measured values may be substantially higher.

**Table 3: ultimate tensile and yield strength for UNS S31803**
**(based on ASME (2010), section II, part D, ASTM (2011b) A479, ASTM (2011a) A182).**

| - | Min. Value at Room Temperature | | - |
|---|---|---|---|
| Product Form | Yield Strength | Tensile Strength | Unit |
| Bar | 450 | 620 | MPa |
| Forgings | 450 | 620 | MPa |

The ASME (2010) standard, Section II, Part D, provides extensive material data for most of the alloys common in pressure vessels. This includes temperature dependent ultimate tensile and yield strengths, as shown in Table 4 and Table 5 respectively. However, it is noted in the standard that the strength values presented are to be used cautiously outside their intended application of ASME (2010) pressure vessel design. The explanation for this is that the values are selected by the ASME (2010) boiler and pressure vessel (BaPV) committee based on what they believe are suitable for use in design calculations, and the values are stated to be neither

a minimum nor an average in the traditional sense. While this limits the usefulness of the data for the purpose of finite element analysis, it should be noted that the two product forms are presented with equal values both for yield and tensile strength at all temperatures. This may indicate that the data which the ASME (2010) BaPV committee based their decisions are relative similar for both product forms.

**Table 4: Ultimate tensile Strength for UNS S31803, for temperatures (based on ASME (2010), section II, part D).**

| Product Form | Tensile Strength, for Temperatures | | | | | | | | | Unit |
|---|---|---|---|---|---|---|---|---|---|---|
| - | -30 to 40 | 65 | 100 | 125 | 150 | 200 | 250 | 300 | 325 | C |
| Bar | 621 | - | 619 | - | 598 | 577 | 564 | 558 | - | MPa |
| Forgings | 621 | - | 619 | - | 598 | 577 | 564 | 558 | - | MPa |

**Table 5: Yield strength for UNS S31803, for temperatures (based on ASME (2010), section II, part D).**

| Product Form | Yield Strength, for Temperatures | | | | | | | | | Unit |
|---|---|---|---|---|---|---|---|---|---|---|
| - | -30 to 40 | 65 | 100 | 125 | 150 | 200 | 250 | 300 | 325 | C |
| Bar | 448 | 418 | 395 | 381 | 370 | 354 | 344 | 334 | 328 | MPa |
| Forgings | 448 | 418 | 395 | 381 | 370 | 354 | 344 | 334 | 328 | MPa |

Temperature dependent ultimate tensile and yield strength data for the UNS S31803 alloy has also been obtained from producer data sheets, which may be found in Table 6 and Table 7. Note that there is a significant gap between the values obtained from the ASME (2010) Boiler and Pressure Vessel Code (BaPVC) and from the producer data sheets, where the BaPVC values are consistently higher by roughly 5 to 10 percent.

**Table 6: Ultimate tensile strength for UNS S31803, for temperatures, based on producer data sheets (Rolled Alloys, 2012, Outokumpu, 2012)**

| Producer | Tensile Strength, for Temperatures | | | | | | | | | Unit |
|---|---|---|---|---|---|---|---|---|---|---|
| - | -30 to 40 | 65 | 100 | 125 | 150 | 200 | 250 | 300 | 325 | C |
| Rolled Alloys | - | - | 589,5 | - | 569,5 | 549,5 | 539,9 | - | - | MPa |
| Outokumpu | - | - | 590 | - | 570 | 550 | 540 | - | - | MPa |

**Table 7: Yield strength for UNS S31803, for temperatures, based on producer data sheets (Rolled Alloys, 2012, Outokumpu, 2012, Sandvik Materials Technology, 2012)**

| Producer | Yield Strength, for Temperatures | | | | | | | | | Unit |
|---|---|---|---|---|---|---|---|---|---|---|
| - | -30 to 40 | 65 | 100 | 125 | 150 | 200 | 250 | 300 | 325 | C |
| Rolled Alloys | - | - | 359 | - | 338 | 317 | 303 | - | - | MPa |
| Sandvik | - | - | 360 | - | 335 | 315 | 300 | - | - | MPa |
| Outokumpu | - | - | 360 | - | 335 | 315 | 300 | - | - | MPa |

### *2.2.1.2 Young's modulus and Poisson's ratio*

Temperature dependent moduli of elasticity values obtained from the ASME (2010) BaPVC are presented in Table 8. In this case, there are no stated adaptations to or limitations to the use of the values obtained from the BaPVC. The moduli of elasticity obtained from producer data sheets are presented in Table 9.

**Table 8: Moduli of elasticity for UNS S31803, for temperatures (based on ASME (2010), section II, part D).**

| Material Grp. | Moduli of Elasticity, for Temperatures | | | | | | | | | Unit |
|---|---|---|---|---|---|---|---|---|---|---|
| - | 25 | 65 | 100 | 125 | 150 | 200 | 250 | 300 | 325 | C |
| Grp. H | 200 | - | 194 | - | 190 | 186 | 183 | 180 | - | GPa |

Both the Sandvik and Outokumpu data sheets present identical values to the BaPVC, while the values from the Rolled Alloys data sheet are consistently lower than all other sources. This gap may be due to fact that the Rolled Alloys data sheet is valid for a broad range of product forms, and the value thereby represent the lower end of said range.

**Table 9: Moduli of elasticity for UNS S31803, for temperatures, based on producer data sheets (Outokumpu, 2012, Rolled Alloys, 2012, Sandvik Materials Technology, 2012)**

| Producer | Moduli of Elasticity, for Temperatures | | | | | | | | | Unit |
|---|---|---|---|---|---|---|---|---|---|---|
| - | 20 to 25 | 65 | 100 | 125 | 150 | 200 | 250 | 300 | 325 | C |
| Rolled Alloys | 193 | - | 179 | - | - | 172 | - | 165 | - | GPa |
| Sandvik | 200 | | 194 | | | 186 | | 180 | - | GPa |
| Outokumpu | 200 | - | 194 | - | - | 186 | - | 180 | - | GPa |

The Poisson's ratio is necessary for the finite element material models, and is assumed to be constant at 0.30 in accordance with the ASME (2010), Section II, Part D.

### *2.2.1.3 Maximum allowable stress*

The maximum allowable stress values are used for pressure vessel design in the ASME (2010) BaPVC. It is important to note that these values are neither intended as limits on the actual stresses present during operation, nor on the stresses found during finite element analysis. The maximum allowable stresses for relevant product forms of the alloy UNS S31803 is presented in Table 10.

**Table 10: Maximum allowable stress, for UNS S31803, for temperatures (based on the ASME (2010), Section II, Part D)**

| Section | Division | Product Form | Maximum Allowable Stress, for Temperatures | | | | | | | | | Unit |
|---|---|---|---|---|---|---|---|---|---|---|---|---|
| - | | | -30 to 40 | 65 | 100 | 125 | 150 | 200 | 250 | 300 | 325 | C |
| VIII | Div. 1 | Bar | 177 | 177 | 177 | 174 | 171 | 165 | 161 | 160 | 159 | MPa |
| VIII | Div. 1 | Forgings | 177 | 177 | 177 | 174 | 171 | 165 | 161 | 160 | 159 | MPa |
| VIII | Div. 2 | Bar | N/A | | | | | | | | | MPa |
| VIII | Div. 2 | Forgings | 259 | 259 | 259 | 254 | 247 | 236 | - | - | - | MPa |

The three divisions of the ASME (2010) BaPVC Section VIII have different requirements, among others the level of verification and material testing. Applications that are to be used at pressures below 20.69 MPa are normally designed according to division 1, while applications that are intended for pressures between 20.69 MPa and 68.95 MPa are normally designed according to division 2. Division 3 is for applications where the pressures are exceeding 68.95 MPa. Based on this, it should be noted that the bar product form is not listed as a possible alternative in the table containing maximum allowable stresses for division 2. This will be discussed further in 2.4 Design Rules for Flanged Joints.

#### *2.2.1.4 Stress-strain curves*

As material stress-strain data for UNS S31803 has proven difficult to obtain from previous research, a simplified curve based upon the minimum yield and ultimate strength values has been approximated for use in the finite element analyses. The tensile tests performed on UNS S31803 forged bar will either validate or falsify this assumption. The ultimate strain has been assumed to be 80 percent of the minimum total elongation, which is specified by the ASTM (2011b) A479 as 25 percent for UNS S31803. Yield strain is calculated by dividing yield strength on the assumed elastic modulus. Table 11 contains the engineering stress-strain data.

**Table 11: Assumed engineering stress-strain data for room temperature ASTM (2011b) A479.**

| Temp. | Ultimate Strength | Ultimate Strain | Yield Strength | Total Strain | Young's Modulus | Yield Strain |
|---|---|---|---|---|---|---|
| ˚C | MPa | mm/mm | MPa | mm/mm | GPa | mm/mm |
| 20,0 | 620,0 | 0,200 | 450,0 | 0,250 | 200 | 0,00225 |

As the Abaqus software requires the stress-strain data to be input as true stress and true plastic strain, the values in Table 11 will have to be converted. This may be done using the following well known equations:

$$\sigma_{true} = \sigma_{nominal}(1 + \epsilon_{nominal}),$$

$$\epsilon_{true} = \ln(1 + \epsilon_{nominal}),$$

and

$$\epsilon_{true-plastic} = \epsilon_{true} - \frac{\sigma_{true}}{E}.$$

Here, the engineering stress and strain values are denoted with a nominal suffix, and the true stress and strain values are denoted with a true suffix. The true-plastic suffix is used for calculating the amount of true plastic strain at a given point along the true stress-strain curve.

**Table 12: Assumed true stress-strain data for room temperature, for UNS S31803, based on Table 11.**

| Temp. | Ultimate Strength | Ultimate Strain | U. Plastic Strain | Yield Strength | Yield Strain |
|---|---|---|---|---|---|
| ˚C | MPa | mm/mm | mm/mm | MPa | mm/mm |
| 20,0 | 744,0 | 0,182 | 0,179 | 451,0 | 0,00225 |

Figure 3 describes the assumed simplified stress-strain curve for the UNS S31803 alloy, which will be used for the finite element models described in later chapters.

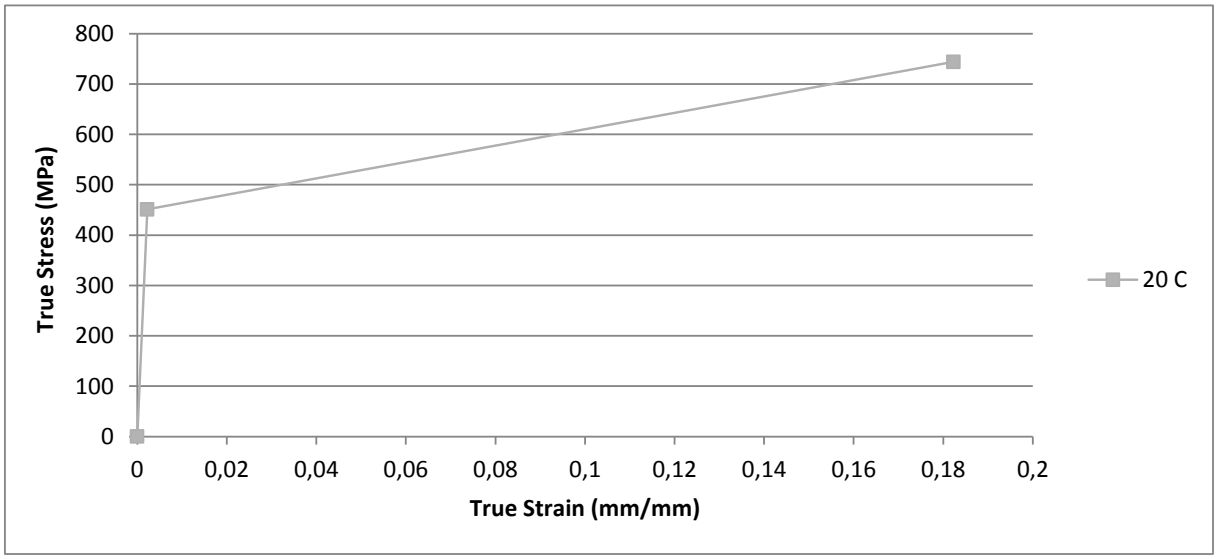


**Figure 3: Assumed simplified true stress-strain curves, for UNS S31803, for room temperature, based on Table 12.**

### 2.2.2 Bolt material

The bolt material was selected based on the requirements found in the NORSOK (2004) M-001 standard. The five bolt grades that are allowed are presented in Table 13.

**Table 13: Material data for NORSOK M-001 bolt grades (based on NORSOK (2004) M-001 and ASME (2010), section II, part D)**

| Product Form | UNS No. | Composition | Spec No. | Grade | Temperature Range |
|---|---|---|---|---|---|
| Bolting | G41400 | 1Cr-$^{1}/_{5}$Mo | SA-320 | L7 | -100 to +400 ˚C |
| Bolting | G43400 | 1$^{3}/_{4}$Ni-$^{3}/_{4}$Cr-$^{1}/_{4}$Mo | SA-320 | L43 | -100 to +400 ˚C |
| Bolting | G41400 | 1Cr-$^{1}/_{5}$Mo | SA-193 | B7 | -46 to +400 ˚C |
| Bolting | K14072 | 1Cr-$^{1}/_{5}$Mo-V | SA-193 | B16 | -29 to +540 ˚C |
| Bolting | S31600 | 16Cr-12Ni-2Mo | SA-193 | B8M | -196 to +540 ˚C |

It should be noted that both the B16 and the B8M grades are subjected to environmental limitations, and may not be suitable for all applications (NORSOK, 2004). However, the thesis does not specifically address the external environment outside the flanges, and the bolt grades will continue to be included for the purpose of comparison. For the finite element modelling that is described in following chapters, the properties of the L7 grade will be used a basis for the bolt material model.

#### *2.2.2.1 Ultimate tensile and yield strength*

The minimum ultimate tensile and yield strength for the previously introduced bolt grades may be found in Table 14.

**Table 14: Ultimate tensile and yield strength for bolt grades (based on ASME (2010), section II, part D)**

| - | Min. Value at Room Temperature | | |
|---|---|---|---|
| Grade | Yield Strength | Tensile Strength | Unit |
| L7 | 725 | 860 | MPa |
| L43 | 725 | 860 | MPa |
| B7 | 725 | 860 | MPa |
| B16 | 725 | 860 | MPa |
| B8M | 550 | 690 | MPa |

Temperature dependent values for ultimate tensile and yield strength are presented in Table 15 and Table 16 respectively. However, as these values also are obtained from the same table in the ASME (2010) BaPVC as the flange material, it is believed that the values may be equally inaccurate. Even so, the values seem to indicate the ultimate tensile strength of the four top bolt grades remain more or less constant even at high temperatures. The different bolt

grades also retain most of their yield strength, even at higher temperatures, which is important in order to stay within the range of pure elastic strain.

**Table 15: Ultimate tensile strength for bolt grades, for temperatures (based on ASME (2010), section II, part D)**

| Grade | Tensile Strength, for Temperatures | | | | | | | | | Unit |
|---|---|---|---|---|---|---|---|---|---|---|
| - | -30 to 40 | 65 | 100 | 125 | 150 | 200 | 250 | 300 | 325 | C |
| L7 | 862 | - | 862 | - | 862 | 862 | 862 | 862 | 862 | MPa |
| L43 | - | - | - | - | - | - | - | - | - | MPa |
| B7 | 862 | - | 862 | - | 862 | 862 | 862 | 862 | 862 | MPa |
| B16 | 862 | - | 862 | - | 862 | 862 | 862 | 862 | 862 | MPa |
| B8M | 689 | - | 689 | - | 680 | 665 | 660 | 660 | 660 | MPa |

**Table 16: Yield strength for bolt grades, for temperatures (based on ASME (2010), section II, part D)**

| Grade | Yield Strength, for Temperatures | | | | | | | | | Unit |
|---|---|---|---|---|---|---|---|---|---|---|
| - | -30 to 40 | 65 | 100 | 125 | 150 | 200 | 250 | 300 | 325 | C |
| L7 | 724 | 698 | 671 | 658 | 648 | 632 | 614 | 595 | 583 | MPa |
| L43 | 724 | 702 | 679 | 669 | 659 | 635 | 615 | 590 | 576 | MPa |
| B7 | 724 | 698 | 671 | 658 | 648 | 632 | 614 | 595 | 583 | MPa |
| B16 | 724 | 711 | 696 | 688 | 680 | 664 | 648 | 631 | 623 | MPa |
| B8M | 552 | 509 | 472 | 460 | 451 | 414 | 383 | 364 | 350 | MPa |

#### *2.2.2.2 Young's modulus and Poisson's ratio*

The temperature dependent moduli of elasticity are presented in Table 17, obtained from the ASME (2010) standard, section II, part D.

**Table 17: Moduli of elasticity for bolt grades, for temperatures (based on ASME (2010), section II, part D).**

| Grade | Moduli of Elasticity, for Temperatures | | | | | | | | | Unit | Material Grp. |
|---|---|---|---|---|---|---|---|---|---|---|---|
| - | 25 | 65 | 100 | 125 | 150 | 200 | 250 | 300 | 325 | C | - |
| L7 | 204 | - | 200 | - | 197 | 193 | 190 | 186 | - | GPa | Grp. C |
| L43 | 191 | - | 187 | - | 184 | 181 | 178 | 174 | - | GPa | Grp. B |
| B7 | 204 | - | 200 | - | 197 | 193 | 190 | 186 | - | GPa | Grp. C |
| B16 | 204 | - | 200 | - | 197 | 193 | 190 | 186 | - | GPa | Grp. C |
| B8M | 195 | - | 189 | - | 186 | 183 | 179 | 176 | | GPa | Grp. G |

Poisson's ratio is assumed to be 0.30 for all the bolt grades listed above.

### *2.2.2.3 Maximum allowable stress*

The maximum allowable stress for the different bolt grades are listed in Table 18. While the values remain constant across the entire listed temperature range, the magnitude of the values will become lower as the temperature is increased outside the range of the table.

**Table 18: Maximum allowable stress for bolt grades, for temperatures (based on the ASME (2010), section II, part D)**

| Grade | Maximum Allowable Stress, for Temperatures | | | | | | | | | Unit |
|---|---|---|---|---|---|---|---|---|---|---|
| - | -30 to 40 | 65 | 100 | 125 | 150 | 200 | 250 | 300 | 325 | C |
| L7 | 172 | 172 | 172 | 172 | 172 | 172 | 172 | 172 | 172 | MPa |
| L43 | 172 | 172 | 172 | 172 | 172 | 172 | 172 | 172 | 172 | MPa |
| B7 | 172 | 172 | 172 | 172 | 172 | 172 | 172 | 172 | 172 | MPa |
| B16 | 172 | 172 | 172 | 172 | 172 | 172 | 172 | 172 | 172 | MPa |
| B8M | 138 | 138 | 138 | 138 | 138 | 138 | 138 | 138 | 138 | MPa |

For detailed information of how the maximum allowable stress values are calculated, please refer to the ASME (2010) Section II Mandatory Appendix 10. Note that the maximum allowable stress values remain the same for all three divisions of the ASME (2010) Section VIII.

## 2.2.3 Gasket material

The alloy UNS S31603, also commonly known as 316L, has been chosen as the ring joint gasket material. Some material data for the alloy may be found in Table 19.

**Table 19: Material data for UNS S31603 (based on (ASME, 2010), section II, part D)**

| Grade | UNS No. | Composition | Spec No. |
|---|---|---|---|
| 316L | S31603 | 16Cr-12Ni-2Mo | SA-240 |

### *2.2.3.1 Ultimate tensile and yield strength*

The minimum ultimate tensile and yield strength for the UNS S31603 alloy may be found in Table 20. It is considered likely that in a real application a 316L gasket ring would be fully annealed to obtain as soft a material as possible within given limits, resulting in strength values close to the minimum values presented in Table 20.

**Table 20: Ultimate tensile and yield strength for UNS S31603 (based on ASME (2010), section II, part D, and ASTM (2011b) A479)**

| - | Min. Value at Room Temperature | | |
|---|---|---|---|
| Grade | Yield Strength | Tensile Strength | Unit |
| 316L | 170 | 485 | MPa |

Temperature dependent ultimate tensile and yield strength for the UNS S31603 may be found in Table 21 and Table 22. However, as the data is obtained from the ASME (2010) BaPVC, the same limitations as discussed in 2.2.1.1 Ultimate tensile and yield strength apply.

**Table 21: Ultimate tensile strength for UNS S31603, for temperatures (based on ASME (2010), section II, part D)**

| Grade | Tensile Strength, for Temperatures | | | | | | | | | Unit |
|---|---|---|---|---|---|---|---|---|---|---|
| - | -30 to 40 | 65 | 100 | 125 | 150 | 200 | 250 | 300 | 325 | C |
| 316L | 483 | - | 467 | - | 441 | 429 | 426 | 426 | 425 | MPa |

**Table 22: Yield strength for UNS S31603, for temperatures (based on ASME (2010), section II, part D)**

| Grade | Yield Strength, for Temperatures | | | | | | | | | Unit |
|---|---|---|---|---|---|---|---|---|---|---|
| - | -30 to 40 | 65 | 100 | 125 | 150 | 200 | 250 | 300 | 325 | C |
| 316L | 172 | - | 145 | 137 | 131 | 121 | 114 | 109 | 107 | MPa |

### *2.2.3.2 Young's modulus and Poisson's ratio*

Temperature dependent moduli of elasticity for UNS S31603 were obtained from the ASME (2010) Section II Part D, and may be found in Table 23.

**Table 23: Moduli of elasticity for UNS S31603, for temperatures (based on ASME (2010), section II, part D)**

| Grade | Moduli of Elasticity, for Temperatures | | | | | | | | | Unit | Material Grp. |
|---|---|---|---|---|---|---|---|---|---|---|---|
| - | 25 | 65 | 100 | 125 | 150 | 200 | 250 | 300 | 325 | C | - |
| 316L | 195 | - | 189 | - | 186 | 183 | 179 | 176 | | GPa | Grp. G |

Poisson's ratio is assumed to be equal to 0.3 for the UNS S31603 alloy.

### *2.2.3.3 Stress-strain curves*

Engineering stress-strain data was obtained for the UNS S31603 alloy (Blandford et al., 2007), and the average values are presented in Table 24. The original stress-strain data may be found in Appendix A: Original Stress Strain Data for 316L. The Young's moduli presented in Table 24 were obtained from the ASME (2010) Section II Part D. Table 25 contains the true stress-strain data converted from Table 24 using the equations presented in 2.2.1.4 Stress-strain curves.

As shown, the stress-strain data presented in Table 24 and Table 25 is significantly higher than the minimum values listed by ASTM A479. The source materials for the test data provided by Blandford et al. (2007) were hot rolled and annealed plates, which may have resulted in significantly higher strength than that which is found in ring gaskets. However,

this argument is highly dependent on the ring gasket manufacturing method and source material. As it was found difficult to obtain material data specifically for metallic ring gaskets, the provided data will have to serve as an approximation.

**Table 24: Engineering stress-strain data for UNS S31603, for temperatures (average based on Blandford et al. (2007)).**

| Temp. | Ultimate Strength | Ultimate Strain | Yield Strength | Total Strain | Young's Modulus | Yield Strain |
|---|---|---|---|---|---|---|
| ˚C | MPa | mm/mm | MPa | mm/mm | GPa | mm/mm |
| -28,9 | 782,4 | 0,588 | 332,2 | 0,747 | 198 | 0,00168 |
| 21,1 | 617,1 | 0,557 | 258,2 | 0,723 | 195 | 0,00132 |
| 148,9 | 497,5 | 0,338 | 206,0 | 0,463 | 186 | 0,00111 |
| 315,6 | 470,2 | 0,308 | 168,2 | 0,402 | 175 | 0,00096 |

**Table 25: Calculated true stress-strain data for UNS S31603, for temperatures (based on data in Table 24)**

| Temp. | Ultimate Strength | Ultimate Strain | U. Plastic Strain | Yield Strength | Yield Strain |
|---|---|---|---|---|---|
| ˚C | MPa | mm/mm | mm/mm | MPa | mm/mm |
| -28,9 | 1242,6 | 0,463 | 0,456 | 332,7 | 0,00168 |
| 21,1 | 961,0 | 0,443 | 0,438 | 258,6 | 0,00132 |
| 148,9 | 665,6 | 0,291 | 0,288 | 206,2 | 0,00111 |
| 315,6 | 615,1 | 0,268 | 0,265 | 168,4 | 0,00096 |

Figure 4 illustrates the true stress-strain curves for different temperatures up until the point of ultimate strength.

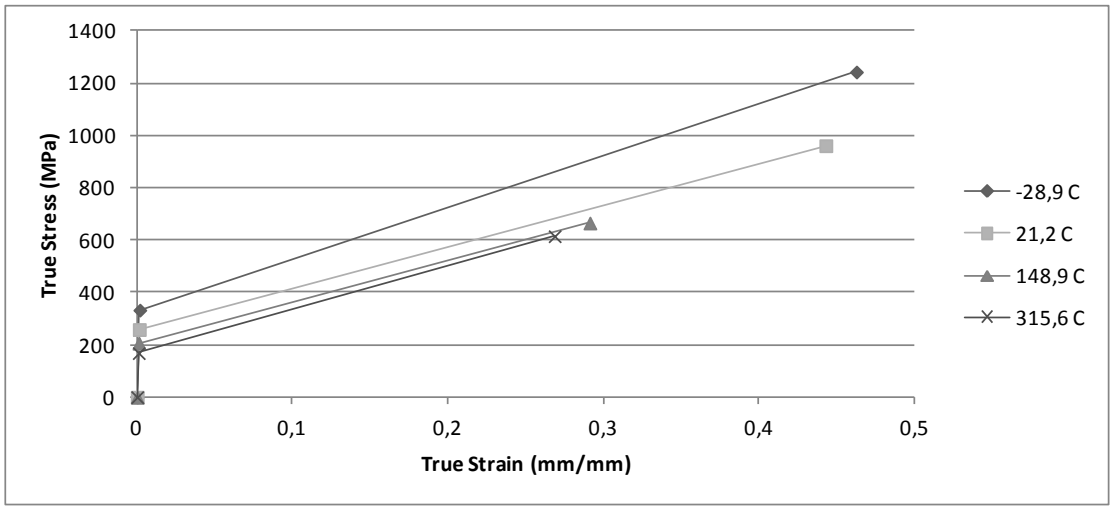


**Figure 4 Simplified true stress-strain curves, for UNS S31603, for temperatures (based on Table 25 and Blandford et al. (2007))**

## 2.3 Dimensions

The dimensions that are presented in this chapter are the basis for both the design rules for flanged joints and the finite element models. The flange dimensions were obtained from the ASME (2009) B16.5 standard, and the ring gasket dimensions from the ASME (2007) B16.20 standard. The bolt dimensions were obtained partly from the ASME B16.5 and partly from the NS (1973) 963 standard.

### 2.3.1 Flanges

The flange dimensions presented in this chapter are valid for a 1500 pressure class, weld neck flange, with a ring joint face, and a nominal pipe size of two inches. Figure 5 provides the legend for the face dimensions provided in Table 26.

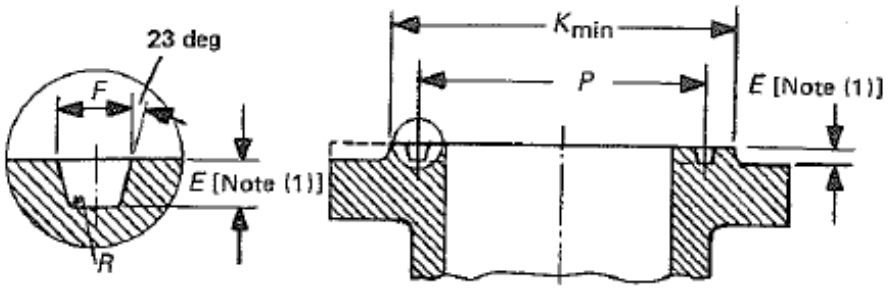


**Figure 5: Legend, ring joint face dimensions (ASME, 2009).**

Figure 6 illustrates where the approximate distance between flanges is measured. However, the distance is highly dependent on the ring gasket material, and a higher strength material will not yield sufficiently to reach the approximate distance listed in ASME (2009) B16.5.

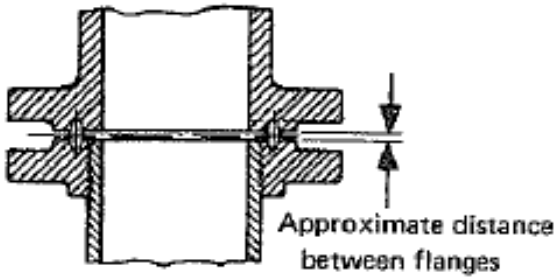


**Figure 6: Legend, ring joint face dimensions (ASME, 2009).**

**Table 26: Ring joint face dimensions (ASME, 2009).**

| Name | Symbol | Value | Unit |
|---|---|---|---|
| Nominal Pipe Size | NPS | 2 | in. |
| Nominal Pipe Size | - | 50,8 | mm |
| Pressure Class | - | 1500 | psi |
| Groove Number | - | R24 | - |
| Pitch Diameter | P | 95,25 | mm |
| Depth | E | 7,92 | mm |
| Width | F | 11,91 | mm |
| Radius at Bottom | R | 0,8 | mm |
| Diameter of Raised Portion | K | 124 | mm |
| Approximate Distance Between Flanges | - | 3 | mm |

Note that the bore dimension is not specified in the ASME (2009) B16.5 standard, and is assumed to be equal to the nominal pipe size (NPS) of two inches (50.8 mm). Figure 7 describes the legend for the bolt hole dimensions listed in Table 27. Note that the bolt holes should be evenly distributed around the bolt circle.

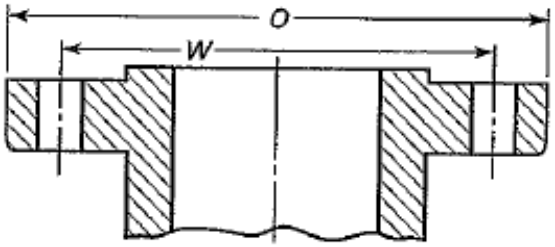


**Figure 7: Legend, bolt hole dimensions (ASME, 2009).**

A conversion factor of 25.4 millimetres per inch is used for the conversion of the bolt diameter.

**Table 27: Bolt hole dimensions (ASME, 2009)**

| Name | Symbol | Value | Unit |
|---|---|---|---|
| Outside Diameter of Flange | O | 215 | mm |
| Diameter of Bolt Circle | W | 165.1 | mm |
| Diameter of Bolt Holes | - | 1 | in. |
| Diameter of Bolt Holes | - | 25,4 | mm |
| Number of Bolts | - | 8 | - |
| Diameter of Bolts | - | 7/8 | in. |
| Diameter of Bolts | - | 22,225 | mm |

Figure 8 illustrates the legend for the flange body dimensions, which are presented in Table 28.

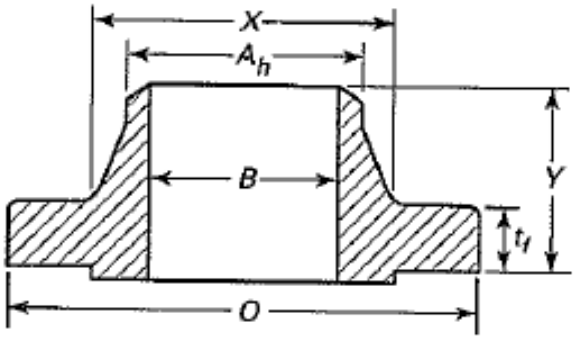


**Figure 8: Legend, flange body dimensions (ASME, 2009).**

The minimum thickness of the flange is assumed to disregard the additional thickness due to the gasket ring groove, and is roughly equal to the length of the bolt hole perforations.

**Table 28: Flange body dimensions (ASME, 2009).**

| Name | Symbol | Value | Unit |
|---|---|---|---|
| Minimum Thickness of Flange | $t_f$ | 38,1 | mm |
| Diameter of Hub | X | 105 | mm |
| Hub Diameter Beginning of Chamfer | $A_h$ | 60,3 | mm |
| Length Through Hub | Y | 102 | mm |
| Bore Diameter | B | 50,8 | mm |
| Wall Thickness | t | 4,75 | mm |

As illustrated by Figure 9, the maximum slope of the flange hub is 45 degrees. This is the hub slope that will be used for the finite element models described in later chapters.

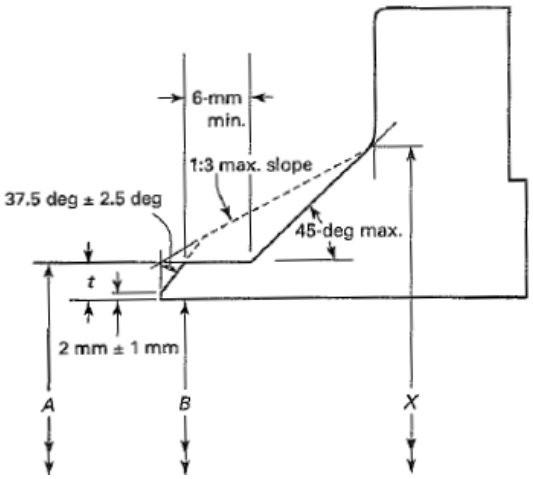


**Figure 9: Legend, flange hub dimensions (ASME, 2009).**

### 2.3.2 Gasket ring

The gasket ring dimensions were obtained from the ASME (2007) B16.20 standard, and are valid for a groove number of R24. Figure 10 illustrates the legend for the dimensions found in Table 29.

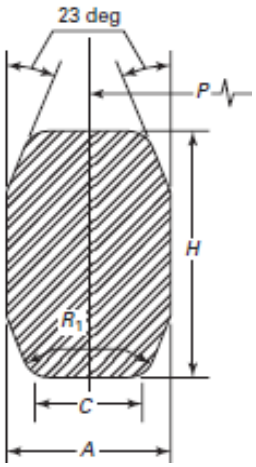


**Figure 10: Legend, type R octagonal ring gasket dimensions (ASME, 2007).**

**Table 29: Type R octagonal ring gasket dimensions (ASME, 2007).**

| Name | Symbol | Value | Unit |
|---|---|---|---|
| Groove Number | - | R24 | - |
| Average Pitch Diameter of Ring | P | 95,25 | mm |
| Width of Ring | A | 11,13 | mm |
| Height of Ring | H | 16 | mm |
| Width of Flat | C | 7,75 | mm |
| Radius | $R_1$ | 1,5 | mm |

### 2.3.3 Bolts

Based on the nominal bolt diameter specified in the ASME (2009) B16.5 standard, the remaining bolt dimensions were obtained from the NS (1973) 963 standard.

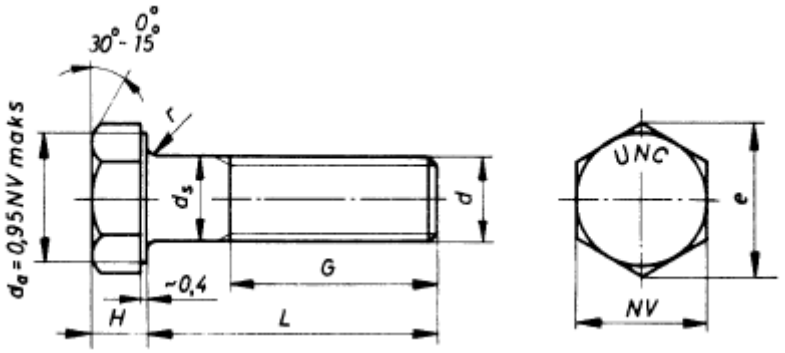


**Figure 11: Legend, bolt dimensions (NS, 1973).**

The average head diameter is used for the finite element modelling of the bolt part, and this will be further discussed in 3.1 Finite element modelling of flanged joint.

**Table 30: Bolt dimensions (NS, 1973).**

| Name | Symbol | Value | Unit |
|---|---|---|---|
| Nominal Diameter | d | 7/8 | in. |
| Max Head Diameter | e | 38,5 | mm |
| Min Head Diameter | NV | 33,3 | mm |
| Average Head Diameter | - | 35,9 | mm |
| Head Thickness | H | 13,9 | mm |

## 2.4 Design Rules for Flanged Joints

This chapter covers the design rules of flanges as set forth by the ASME (2010), Section VIII. The design rules utilizes established formulas, both theoretical and empirical, in order to determine parameters such as stresses, bending moments, and minimum bolt loads. They are intended as a way of checking the validity of your flange design, and might be considered as an alternative to using finite element analysis (FEA). This chapter will be an introduction to the design rules, and for the original design rules one may look to Appendix L: ASME Design Rules for Flanged Joints.

### 2.4.1 Design considerations

As defined in the ASME (2010), Section VIII, a flanged joint has to be able to withstand two different sets of conditions; Gasket seating condition and operating conditions. The gasket seating condition is, as the name implies, the conditions in effect when the gasket is initially seated between a flange pair. Likewise, the operating conditions are the worst pressurized conditions that the flange should be exposed to during its lifetime. It should be noted that it is common practice to consider atmospheric pressure and temperature at the time of gasket seating.

For the purpose of computation, the ASME (2010) also defines two major categories of flanges: Loose type and integral type. Flanges that have weak structural connections to the vessel or pipe wall, are considered to be the loose type, while flanges that are more rigidly connected, are considered to be the integral type. The weld neck flange design is defined as an integral flange with a hub. Due to this, the design rules presented below will be limited to those of relevance to said type with ring joint flange face.

It should also be noted that the following is specified in the design rules: "Flanges with hubs may be machined from a hot rolled or forged billet or forged bar. The axis of the finished flange shall be parallel to the long axis of the original billet or bar, but these axis need not be concentric." (ASME (2010), Section VIII, Division 2, Paragraph 4.16.4.3).

### 2.4.2 Bolt loads

For ring joint flange faces, the basic gasket seating width may be found using the expression

$$b_o = \frac{w}{8},$$

where w is the width of the gasket ring, which is defined in 2.3.2 Gasket ring as width of ring, A. For cases where

$$b_o \leq 6\,mm,$$

the effective gasket seating width is defined as

$$b = b_o,$$

while for the remaining cases

$$b = 0.5\sqrt{C_{ul} b_o},$$

where $C_{ul}$ is a length conversion factor, and may be set equal to 25.4 for metric units.

The operating design load may be found using the expression

$$W_o = 0.785G^2P + 2b\pi GmP.$$

Here, G is the diameter of the gasket load reaction, P is the pressure, and m is a gasket factor. For ring joint gaskets, the diameter of the gasket load reaction may be set equal to the average pitch diameter of the gasket ring, and the gasket factor is tabulated in the design rules as 6.50 for stainless steel ring joint gaskets. The first part of the equation estimates the total force exerted by a pressure P on the area inside the gasket ring, which is the force that would act towards separating the flange pair. As shown below

$$Effective\ gasket\ seating\ area = \pi\left(\frac{G+2b}{2}\right)^2 - \pi\left(\frac{G-2b}{2}\right)^2 = 2b\pi G,$$

the second part of the equation may also be considered the product of the effective gasket seating area, the pressure, and the gasket factor, resulting in the approximate force required for maintaining the desired gasket compression.

The gasket seating design load is expressed as

$$W_{gs} = \pi bGy,$$

where y is the minimum design seating stress, tabulated as 180 MPa for stainless steel ring joint gaskets. Here, the effective gasket seating area is calculated based on one effective gasket seating width, unlike in the operating design load. Wright (2005) offers some indications of the use of $b$ in stead of $2b$ to calculate the effective gasket seating area, may be

due to flange rotation. However, this is only speculations, and the ASME (2010) does not provide any references or explanation to why this particular method is defined.

The total minimum required cross-sectional area of the bolts is expressed as

$$A_m = \max\left[\left(\frac{W_o + F_A + \frac{4M_E}{G}}{S_{bo}}\right), \left(\frac{W_{gs}}{S_{bg}}\right)\right],$$

where $F_A$ is the external tensile net-section axial force, $M_E$ is the absolute value of the external net-section bending moment, $S_{bo}$ is the maximum allowed bolt stress at operating conditions, and $S_{bg}$ is the maximum allowed bolt stress at gasket seating conditions. Note that the gasket seating portion of the expression does not take the axial force or bending moment into account, as it is assumed that no such forces are present during installation.

The design bolt load for the gasket seating condition is defined as

$$W_g = \left(\frac{A_m + A_b}{2}\right) S_{bg},$$

where the $A_b$ is the total cross-sectional area of the selected bolt diameter. Note that the following expression has to be true

$$A_m \leq A_b.$$

It is assumed that the average between $A_m$ and $A_b$ is used in order to establish a conservative bolting stress, and in that way prevent potential overstressing the bolt material. That said, the ASME (2010) also allows for calculating the design bolt load for the gasket seating condition by an alternative method, using

$$W_g = A_b S_{bg},$$

which results in a greater buffer between the pressure forces and the bolt forces.

The ASME (2010), section VII, division 1, appendix S, also defines an expression that may be used to estimate the achievable bolt stress with normal hand held wrenches, defined as

$$S = \frac{45000}{\sqrt{d}},$$

where S is the average bolt stress in pounds per square inch (psi), and d is the nominal diameter of the bolt in inches (in.). The stress may then be converted to megapascals (MPa) by dividing the stress in psi with a conversion factor of 145.0377.

### 2.4.3 Flange bending moments

According to the ASME (2010), there are three main components of the flange design bending moment; $M_D$, $M_T$, and $M_G$, expressed as

$$M_D = H_D h_D,$$

$$M_T = H_T h_T,$$

and

$$M_G = H_G h_G.$$

Here, the capital $H$ is the respective force component, and the lower case $h$ is the moment arm. There is also an additional bending moment component originating from the external tensile net-section axial force, $F_A$, and the external net-section bending moment, $M_E$. This component is expressed as

$$M_{oe} = 4M_E \left[\frac{I}{0.3846 I_p + I}\right]\left[\frac{h_D}{(C - 2h_D)}\right] + F_A h_D,$$

where $I$ is the bending moment of inertia of the flange cross-section, $I_p$ is the polar moment of inertia of the flange cross-section, and $C$ is the bolt circle diameter. Figure 12 illustrates the locations where the force components act, as well as the moment arms.

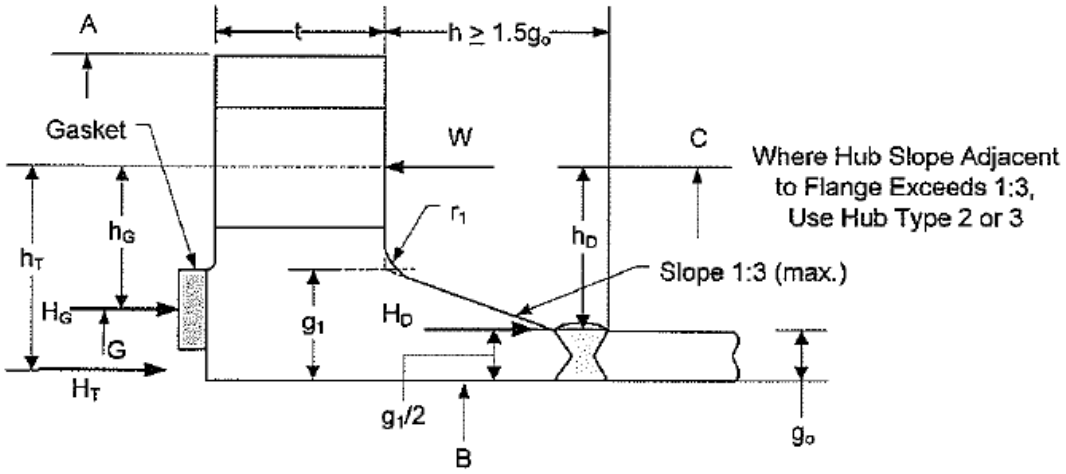


**Figure 12: Legend for design rules (ASME (2010), section VIII, division 2)**

The hydrostatic end force inside the flange bore is expressed as

$$H_D = \frac{\pi B^2 P}{4},$$

where $B$ is the bore diameter. The equation is the product of the bore area and the internal pressure. The moment arm for this pressure force is

$$h_D = \frac{C - B - g_1}{2},$$

where $g_1$ is the hub thickness at the large end. The difference between the total hydrostatic end force and the hydrostatic end force inside the flange bore is defined as

$$H_T = H - H_D,$$

where

$$H = \frac{\pi G^2 P}{4}.$$

The radial distance from the bolt circle to where the force $H_T$ acts, which is midways between point of gasket load reaction and the bore, is expressed as

$$h_T = \frac{1}{2}\left[\frac{C - B}{2} + h_G\right].$$

The difference between flange design load and the total hydrostatic end force is defined as

$$H_G = W_o - H$$

and the radial distance between the bolt circle and the gasket load reaction is

$$h_G = \frac{C - G}{2}.$$

The flange design bending moment for the operating condition is then defined as

$$M_o = abs\left[\left((H_D h_D + H_T h_T + H_G h_G)B_{sc} + M_{oe}\right)\right],$$

Here, $B_{sc}$ is a bolt spacing correction factor, which may be calculated using

$$B_{sc} = \sqrt{\frac{B_s}{2a+t}} = \sqrt{\frac{\pi C}{n(2a+t)}},$$

where $B_s$ is the bolt spacing, which may be expressed as bolt circle circumference divided by the $n$ number of bolts, $a$ is the nominal bolt diameter, and $t$ is the flange thickness. The flange design moment for the gasket seating condition is defined as

$$M_g = \frac{W_g(C-G)B_{sc}}{2}.$$

### 2.4.4 Flange stresses

The design rules define a set of equations that may be used to estimate the design stresses that can be expected in a flange pair. Three forms of stress equations are defined; Flange hub stress, flange radial stress, and flange tangential stress. All three equation forms are calculated both for operating and gasket seating conditions. The stress factors that are used in the equations may be calculated using tabulated formulas found in the original design rules. These stress factors will not be discussed in further detail here, and for the original design rules, please look to Appendix L: ASME Design Rules for Flanged Joints.

The flange hub stress is defined as

$$S_{Ho} = \frac{fM_o}{Lg_1^2B}$$

for operating conditions, and as

$$S_{Hg} = \frac{fM_g}{Lg_1^2B}$$

for gasket seating conditions. Here, $f$ is a hub stress correction factor for integral flanges, and $L$ is a stress factor. The flange radial stress is expressed as

$$S_{Ro} = \frac{(1.33te+1)M_o}{Lt^2B}$$

for operating conditions, and as

$$S_{Rg} = \frac{(1.33te+1)M_g}{Lt^2B}$$

for the gasket seating conditions, where $e$ is a stress factor. The flange tangential stress is defined as

$$S_{To} = \frac{YM_o}{t^2 B} - ZS_{Ro}$$

for operating conditions, and as

$$S_{Tg} = \frac{YM_g}{t^2 B} - ZS_{Rg}$$

for gasket seating conditions. Here, both $Y$ and $Z$ are stress factors. As a final note, Nagata and Sawa (2007) presented results indicating that there is a substantial gap between stresses calculated according to the design rules and finite element analysis. The results presented show that the gap is particularly big for flanges with a nominal size of two inches, where the flange radial stress estimated by the design rules were shown to be greater by a factor of approximately 7.7 to the stress observed in the finite element analysis. The flange hub stress and flange tangential stress found through the design rules were also larger by a factor of approximately 3.25 and 2 respectively. This indicates that the stresses calculated with the design rules in some cases are conservative, and should be used with caution.

### 2.4.5 Acceptance criteria

The design rules provide two sets of acceptance criteria that may be used to evaluate the results from the equations discussed in the previous sections. The first set of criteria involves the maximum allowable stress values, which were presented in 2.2.1 Flange material. The following five equations describe the maximum limits for the three different forms of stress found through the design rules, and all of them have to be satisfied in order to verify the design. The $S_{fo}$ is the maximum allowable stress for the flange material at operating conditions, and the $S_{no}$ is the maximum allowable stress for the pipe material at operating conditions.

$$S_{Ho} \leq \min\left[1.5S_{fo}, 2.5S_{no}\right]$$

$$S_{Ro} \leq S_{fo}$$

$$S_{To} \leq S_{fo}$$

$$\frac{S_{Ho} + S_{Ro}}{2} \leq S_{fo}$$

$$\frac{S_{Ho} + S_{To}}{2} \leq S_{fo}$$

As in the previous portions of the design rules, the criteria also have to be checked both for the operating and the gasket seating conditions. However, they are more or less identical to the previous presented equations, only with different maximum allowable stress values.

$$S_{Hg} \leq \min\left[1.5S_{fg}, 2.5S_{ng}\right]$$

$$S_{Rg} \leq S_{fg}$$

$$S_{Tg} \leq S_{fg}$$

$$\frac{S_{Hg} + S_{Rg}}{2} \leq S_{fg}$$

$$\frac{S_{Hg} + S_{Tg}}{2} \leq S_{fg}$$

The second set of acceptance criteria is the flange rigidity criterion, which is intended as a way of checking the flange flexibility. The goal is to verify that the flange is sufficiently rigid to ensure that leakage are below established limits, and that the flange thereby is likely to perform sufficiently when put into operation. The two following equations are the rigidity criteria for operating and gasket seating conditions respectively.

$$J_o = \frac{52.14VM_o}{LE_{yo}g_0^2K_Rh_o} \leq 1.0$$

$$J_g = \frac{52.14VM_o}{LE_{yg}g_0^2K_Rh_o} \leq 1.0$$

Here, $V$ is a flange stress factor, $h_o$ is a hub length parameter, $E_{yo}$ is the modulus of elasticity at the operating conditions, and $E_{yg}$ is the modulus of elasticity at gasket seating conditions. For the flanges of the integral type, $K_R$ may be set equal to 0.3 in most cases.

## 2.6 Static Stress Analysis with ABAQUS Standard

This chapter will introduce the static stress analysis method, and describe some of the contact models available in Abaqus Standard. It is intended as a basis for the choice of methodology described in 3.1 Finite element modelling of flanged joint. The main references for this chapter are the Abaqus/CAE User's Manual, Abaqus Analysis User's Manual, and the Abaqus Theory Manual (Dassault Systèmes, 2010c, Dassault Systèmes, 2010a, Dassault Systèmes, 2010b).

### 2.6.1 Static stress analysis

A static stress analysis is essentially an analysis where time dependent effects such as material creep and swelling is ignored, and where inertia may be neglected. Abaqus offers two finite element analysers capable of handling static problems; Abaqus Standard is a general purpose analyser that utilizes the traditional implicit approach. Abaqus Explicit is a more special purpose analyser that applies the explicit scheme, which is intended for dynamic problems. While Abaqus Explicit is capable of handling static problems, it requires approximations in order to get a time-independent solution. Such approximations may cause loss of accuracy, and the rest of this chapter will thereby focus on the implicit approach provided by Abaqus Standard.

### 2.6.2 Contact behaviour

#### *2.6.2.1 Nonlinearity*

Linear behaviour may be mathematically defined as the scaling of an input parameter resulting in the same scaling of the output parameter. That said, there are three sources of nonlinearity in Abaqus stress analyses; Geometric nonlinearity, material nonlinearity, and boundary nonlinearity.

Abaqus Standard provides two ways of handling the geometric nonlinearity. The first is to define the analysis as a small displacement analysis, where all geometric nonlinearities are ignored during element calculations (Dassault Systèmes, 2010c). When using this approach, the elements are formulated based on the initial nodal coordinates. As this is an approximation, some error is to be expected when enabling small displacement. The second method involves defining the analysis as a large displacement analysis. The element calculations are then based upon the most recent nodal coordinates throughout the analysis. This will in turn causes the elements to distort as the deformation increases, and may in some cases cause the element to become unsuitable for use (Dassault Systèmes, 2010c). One may

switch from small to large displacement analysis in Abaqus Standard by turning on the NLGEOM option. However, once the NLGEOM option is turned on, it cannot be turned off for the subsequent steps.

Material nonlinearity is often due to the material models which are inherently nonlinear, such as plasticity and creep models. By comparison, a linear material model could involve a perfect elastic material. However, all analyses involving plastic strain should be considered to yield a nonlinear response. Boundary nonlinearity is commonly found in contact problems, where it is due to the nonlinear behaviour of the contact interactions.

Two of the types of steps that are available in Abaqus Standard are the general analysis step and the linear perturbation analysis step. The general analysis step allows for both linear and nonlinear response, while the linear perturbation analysis step allows only linear behaviour. A single nonlinear contribution is enough to cause an entire step to yield a nonlinear response, and all possible sources of nonlinearity needs to be considered prior to using the linear perturbation analysis step.

#### *2.6.2.2 Contact discretization method*

There are two discretization methods available in Abaqus Standard; Node-to-surface and surface-to-surface. While both may be used to define how contact surfaces interact during a simulation, there are significant differences between the two.

The node-to-surface discretization method utilizes what is considered a traditional approach, where master surface is defined as an interpolated surface, and the slave surface is defined as a set of nodes. As a node-to-surface surface pair initiates contact, the nodes on the slave surface will interact with the points on the master surface that are the closest, as illustrated in Figure 13. Thus, the slave nodes may essentially interact with any point along the master surface, but no interaction will occur if the master surface penetrates the slave surface where no slave nodes are located.

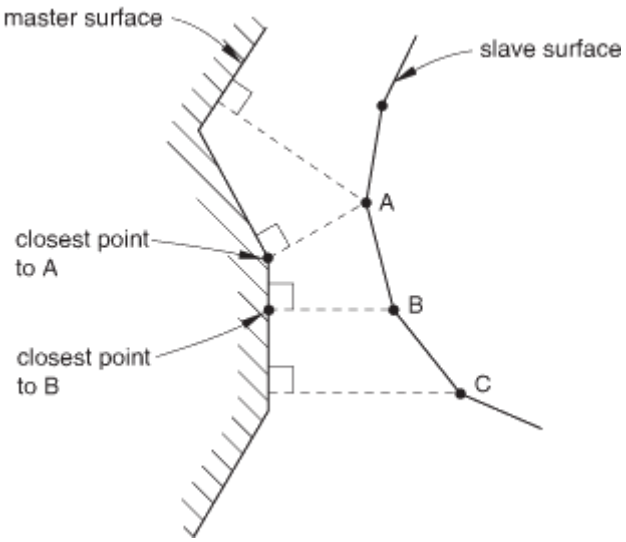


**Figure 13: Node-to-surface discretization method (Dassault Systèmes, 2010a).**

There are several limitations to using this method in analyses. First, the method potentially allows for the master surface to penetrate into the slave surface in-between the slave nodes, which may cause quite large and hidden overclosures. This in turn may cause phenomena such as snagging, where a sliding master surface hooks a slave node, as opposed to sliding across it. Secondly, as described in the Abaqus Analysis User Manual 6.10 (Dassault Systèmes, 2010c), there may be significant differences in contact pressures as a result of the forces being concentrated at the location where the slave nodes interact with the master surface. Thirdly, the method may be highly dependent on the slave and master assignment.

The surface-to-surface discretization method, on the other hand, will not only consider the slave surface nodes, but also nearby surface regions. The technique thereby avoids the large penetrations that may occur when using the node-to-surface discretization method. This method will in the case of most well defined geometries yield more accurate stresses and contact pressures (Dassault Systèmes, 2010a). However, it should be noted that the surface-to-surface method may result in increased computational cost due to the complexity of the contact behaviour. For most contact problems, the increase in computational cost is low enough not to be of concern. However, it should be specifically considered when analyzing problems where the contact surfaces cover a large portion of the model, or where the master surface is more refined than the slave surface. The increase in computational cost may prove to be very high in such cases.

### *2.6.2.3 Contact tracking*

Contact tracking is the approach used for determining the relative motion of two interacting surfaces, and there are essentially two models available in Abaqus Standard; Finite sliding and small sliding. The main differences between the two forms of contact tracking is that finite sliding allows for the sliding, rotation, and separation of the interacting surfaces, while small sliding assumes that only small relative sliding will occur between the two surfaces. The finite sliding method is thereby considered the more robust of the two, while the small sliding method is considered to have considerably lower computational cost.

When applying the finite sliding method to a contact problem, the software tracks the positions of the slave nodes relative to the master surface. This allows for a slave node to contact anywhere along the master surface, and slide along the surface regardless of the orientation or deformation of the master surface. An example presented in the Abaqus Analysis User Manual 6.10 (Dassault Systèmes, 2010a) is shown in Figure 14 and Figure 15, where node 101 is put into contact with the master surface, followed by sliding contact, then separation, and finally sliding contact again. When node 101 is in contact with the master surface in-between two master nodes, the contact force is split between the two master nodes.

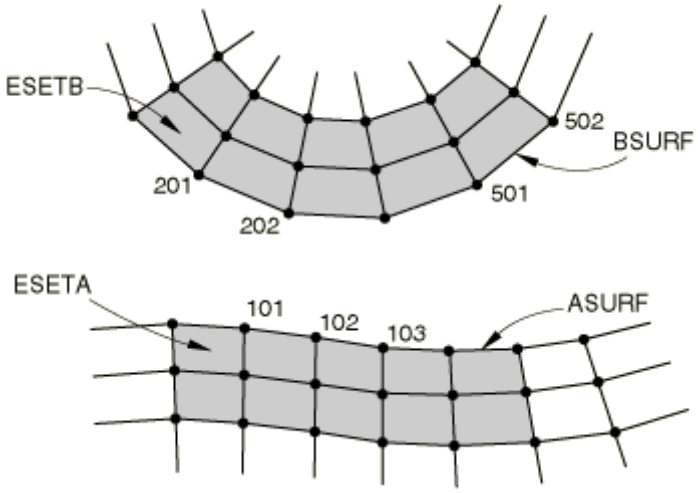


**Figure 14: Contact tracking example (Dassault Systèmes, 2010c).**

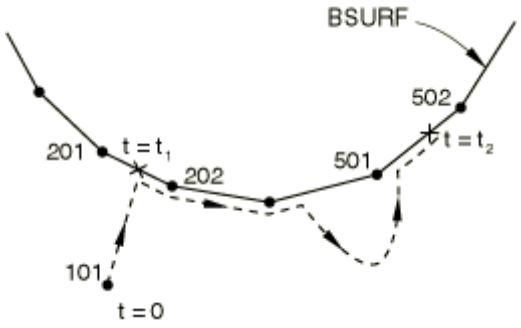


**Figure 15: Contact tracking example (Dassault Systèmes, 2010a).**

The small sliding utilizes tangent planes in order to guide the sliding motion. Slave node penetration of the tangent plane is commonly not allowed. The tangent plane is defined through anchor points and anchor normals, shown as $X_0$ and $N(X_0)$ respectively in Figure 16. Abaqus Standard uses smoothly varying master surface normal in order to determine the point along the master surface that has an equivalent normal that aligns with the position of the matching slave node, which in the case of Figure 16 would be node 103. The tangent plane would then be perpendicular to the anchor normal. It should be noted that both the anchor points and normals are based on the models initial geometry, and are chosen before the analysis starts.

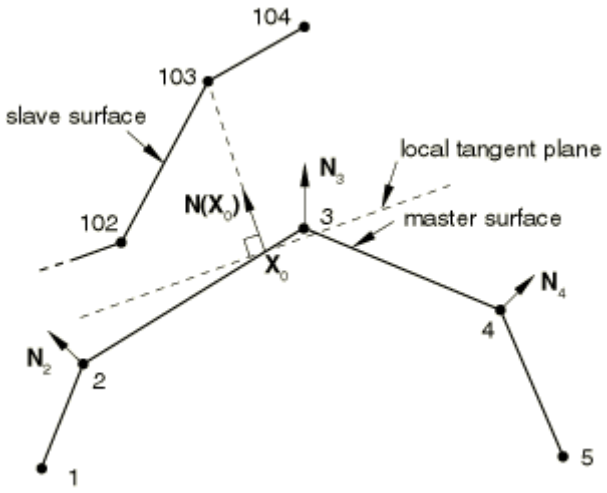


**Figure 16: Small sliding example (Dassault Systèmes, 2010a)**

The Abaqus Analysis User Manual 6.10 (Dassault Systèmes, 2010a) has provided a set of specific requirements for models that intend to use the small sliding contact tracking. The essence of the requirements is that the slave nodes should not slide more than an element length from their corresponding anchor point, and should not experience any separation from

their tangent plane. For highly curved surfaces, the allowable sliding distance is further reduced to a fraction of an element length.

#### *2.6.2.4 Contact pressure-overclosure relationship*

The pressure-overclosure relationship describes how the contact pressure relates to the clearance between two surfaces. There are several relationship models available in Abaqus, some of them being hard contact, soft tabulated contact, soft exponential contact, and soft contact without separation. All of the aforementioned models will be briefly described below.

The conventional hard contact, illustrated in Figure 17, is the most common pressure-overclosure relationship, and is selected by default for most surface-based contacts. As illustrated, the contact pressure remain at zero as long there is clearance between the two surfaces, but once the clearance reaches zero or less, the model allows for any positive value of contact pressure. Note that the conventional hard contact does not allow for tensile stress to be transferred between contact surfaces, and is also considered to minimize the penetration of the master surface by the slave surface. A modified version of the hard contact is also available in Abaqus, providing additional functionality such as allowing limited penetration and tensile stress transfer.

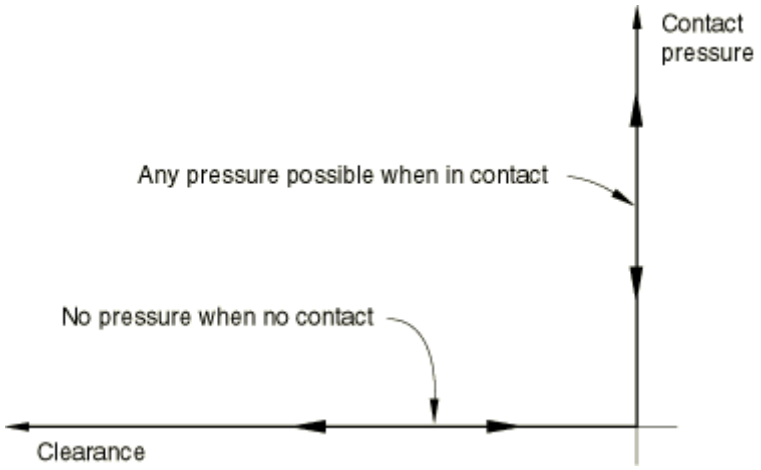


**Figure 17: Hard contact pressure-overclosure relationship (Dassault Systèmes, 2010a).**

Common for all soft contact models in Abaqus is that they allow for custom contact pressures at specified clearance values. It is thereby possible to for example model contacts that behave the same way as a hard material coated with a soft material, and may also be used for damping in contacts that are found difficult to converge. The soft tabulated relationship, illustrated in Figure 18, is defined through a set of contact pressure (p) values versus

clearances (h) values. Once the overclosure is greater than the largest defined value $h_n$, the curve will be extrapolated indefinitely based on the previous slope.

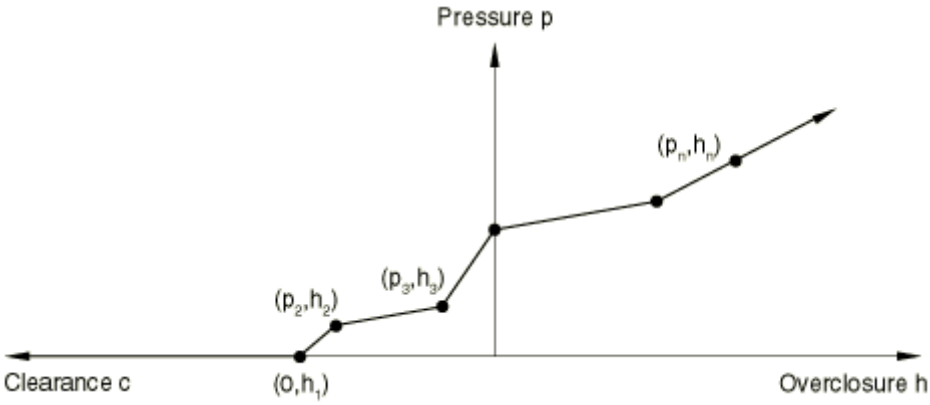


**Figure 18: Soft pressure-overclosure relationship (Dassault Systèmes, 2010a).**

The soft exponential contact, shown in Figure 19, is defined by two values; the lowest clearance at which the contact pressure is zero $C_0$ and the contact pressure at zero clearance $P_0$. The value $K_{max}$ shown in Figure 19 is only available in Abaqus Explicit, and in Abaqus Standard the contact pressure will follow the exponential curve with no maximum slope.

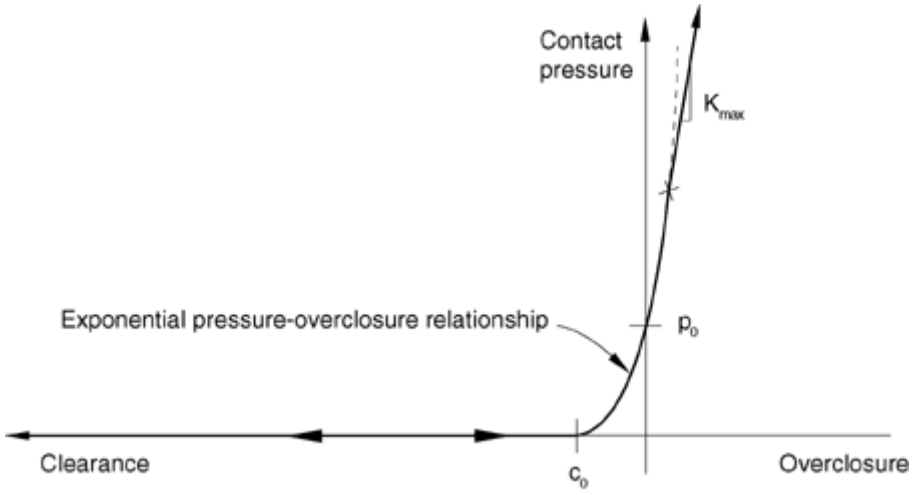


**Figure 19: Exponential pressure-overclosure relationship (Dassault Systèmes, 2010a).**

The soft contact without separation, shown in Figure 20, will as the name implies not allow separation of the two contact surfaces. A positive clearance will be counteracted by a tensile contact stress, and overclosure will likewise be counteracted by contact pressure. The curve is specified in the same manner as the soft tabulated contact, where sets of pressures and clearances / overclosures define the slopes. The slope at the extremes will be equal to those defined by the first and last set of values.

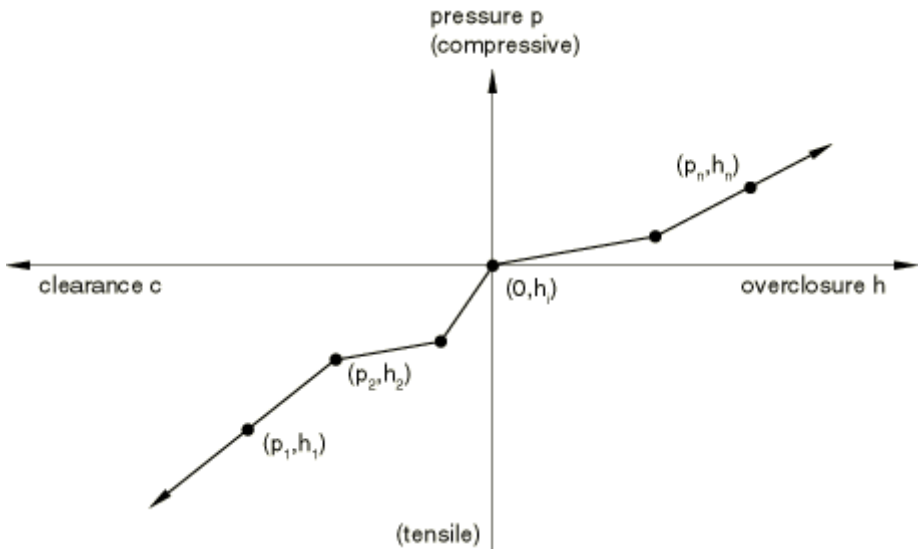


**Figure 20: Soft contact without separation pressure-overclosure relationship (Dassault Systèmes, 2010a).**

### *2.6.2.5 Contact constraint enforcement method*

The contact constraint enforcement method determines how the constraints imposed by the pressure-overclosure relationship are solved numerically. The actual contact pressure can either be a strict enforcement of the defined pressure-overclosure relationship, or an approximation, and can be modified in order to obtain convergence in difficult analyses. There are three available contact constraint enforcement methods in Abaqus Standard; The penalty method, the augmented Lagrange method, and the direct method.

The penalty method approximates the hard pressure-overclosure behaviour. The contact force is proportional to the degree of penetration, which may cause a small degree of overclosure in the results. An advantage to the penalty method is that it may require a lower number of iterations, and may thereby prove to be more efficient than the direct method. The downside to this is that there is a small loss of accuracy. The penalty method is used by default for finite sliding with surface-to-surface contact formulation.

The augmented Lagrange method is only applicable to hard pressure-overclosure relationships. Initially the enforcement will follow the penalty method, but as the overclosure passes a specified tolerance, the method will attempt to reduce the overclosure through augmenting the contact pressures. Similar to the penalty method, the augmented Lagrange method may prove cheaper than the direct method in regards to computational cost. The augmented Lagrange method is default for three dimensional self-contact with node-to-surface contact formulation and hard pressure-overclosure relationship.

The direct method strictly enforces the defined pressure-overclosure relationship, and is required for soft contact formulations. Note that overlapping contact definitions may cause convergence issues in directly enforced hard contacts, and should be avoided. The direct method is default for all cases except those that were defined for the penalty and the augmented Lagrange method.

#### *3.6.2.6 Tangential contact behaviour*

When two surfaces are in contact, tangential behaviour determines the amount of frictional shear forces that are transferred between surfaces. There are several models available in Abaqus Standard, but the models that will be discussed in this thesis are penalty, frictionless, and rough.

The penalty model utilizes the Coulomb friction model by default, where the critical frictional stress $\tau_{crit}$ relates to the contact pressure $p$ through the following equation:

$$\tau_{crit} = \mu p,$$

where $\mu$ is the friction constant. The friction constant may be defined as a function of parameters such as contact pressure, slip rate, or surface temperature. When the critical frictional stress is larger than the equivalent frictional stress $\tau_{eq}$, it is assumed that no relative motion can occur, which is often referred to as sticking. The equivalent frictional stress is defined as

$$\tau_{eq} = \sqrt{\tau_1^2 + \tau_2^2}.$$

If, on the other hand, the critical frictional stress is lower than the equivalent frictional stress, then relative motion, also known as slipping, may occur. A third possible state that a contact may be in is open, which implies that there is no contact between the two surfaces. This may both be due to the surfaces not having made contact yet, or that the surfaces have separated, if the contact model allows it.

The frictionless model assumes that there is no transfer of frictional stresses between the two surfaces. In practice this translates into no friction induced shear stresses, and motion can occur as long as there is a net force driving it.

The rough friction model does not allow for any slipping of the surfaces. This is done by specifying the friction constant as infinite, making the critical frictional stress infinite as well.

However, the model should only be used with surfaces that are intended to stay closed once contact is initiated. Opening a closed surface with the rough friction model may cause severe convergence issues, especially if large shear stresses have been established.

# 3 RESEARCH METHODOLOGY

This chapter is split into three sections; the first describing the axisymmetric finite element models, the second describing the ASME design rules for flanged joints, and the third describing the tensile testing of UNS S31803 forged bar.

## 3.1 Finite element modelling of flanged joint

This chapter describes the methodology applied when analysing a two inch flanged joint using Abaqus Standard.

### 3.1.1 Axisymmetric model

The concept of modelling a flanged joint as an axisymmetric structure has been well established within the pressure vessel community, among others by Nagata and Sawa (2007), Sato and Kado (2005), and Hwang and Stallings (1992). However, most of the published papers that look at flanged joints have been limited to flanged joints with flat gaskets. As a step towards determining the viability of ring joint weld neck flanges machined from forged bar, an attempt has been made to model such a flange assembly in Abaqus. For this purpose, the static analysis technique is selected, where all time dependent phenomena, such as creep, is considered to be negligible.

Both the gasket seating and operating temperatures is assumed to be atmospheric, which impose restrictions on the temperature of the medium traveling within the flanged joint. The low temperatures will also cause any creep to develop at slower rates, enforcing the assumption about it not being included in the model.

#### *3.1.1.1 Parts*

The axisymmetric model assembly is based upon three parts; the flange, the gasket ring, and the bolt. The parts are all modelled after the dimensions presented in 2.3 Dimensions, and have individually been split into smaller sections in order to facilitate better mesh generation and enable application of necessary loads. The individual sectioning of the parts is illustrated in Figure 21 through Figure 24.

The flange part was split into three different kinds of sections. The section denoted A in Figure 21 represents the cross sectional area of the bolt hole ring, which will be further discussed in 3.1.1.6 Materials.

Section B was added in order to allow for consistent element alignment and mesh refinement around the contact surfaces located in the gasket ring groove. As illustrated in Figure 22, the

sections follow the contour of the contact surfaces at a constant distance, which is set equal to the length of two elements. The square section surrounding the contact section was added as a transition area from refined element size to the larger overall element size. The series of sections denoted C was added to force the Abaqus meshing algorithm to distribute the elements in an orderly fashion, and thereby avoid some observed problems with distorted elements. The final mesh of all the parts will be described in 3.1.1.2 Element mesh.

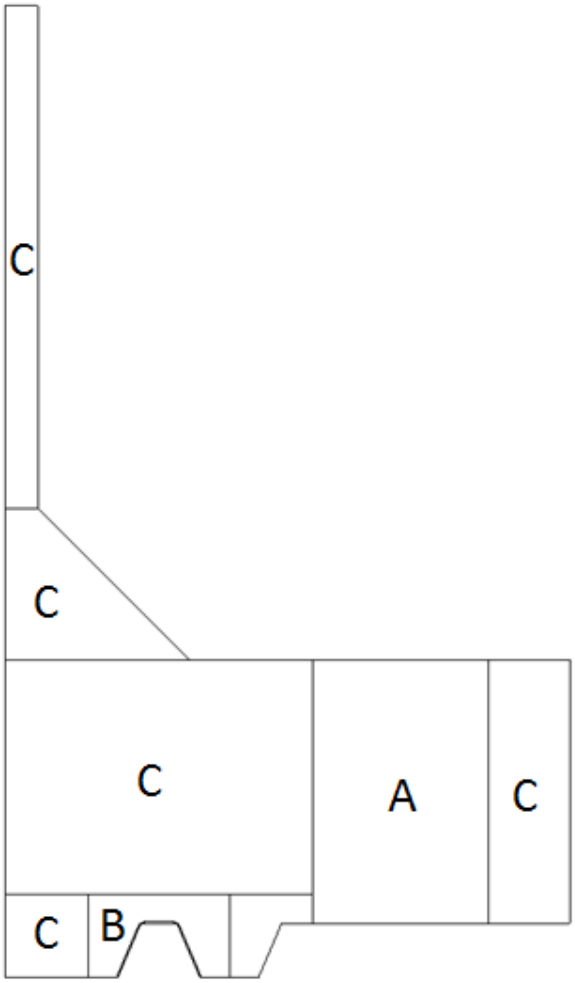


**Figure 21: Flange sections as modelled in Abaqus Standard.**

**Figure 22: Enlarged sections of flange contact area, shown as B in Figure 21, as modelled in Abaqus Standard.**

The ring gasket part was split into sections like those found in the gasket ring groove, again to ensure element alignment and mesh refinement. The width of these sections is also two times the element length.

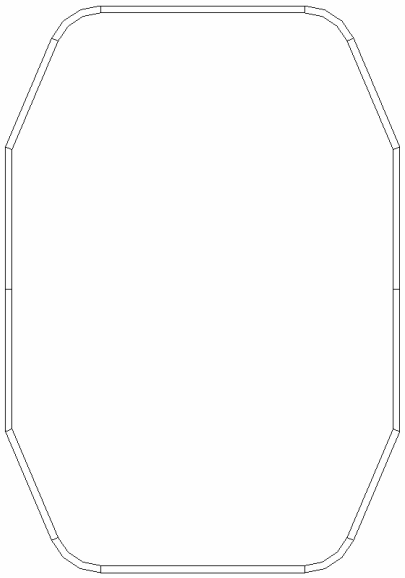

**Figure 23: Ring sections as modelled in Abaqus Standard.**

The bolt part is sectioned in order to force a structured mesh, and to allow for the application of the bolt load at the vertical centre. Bolt loads will be described further in 3.1.1.3 Loads. Note that the bolt width is consistent with the bolt diameter found in ASME (2009) B16.5, and is slightly smaller than the bolt hole ring section found on the flange part.

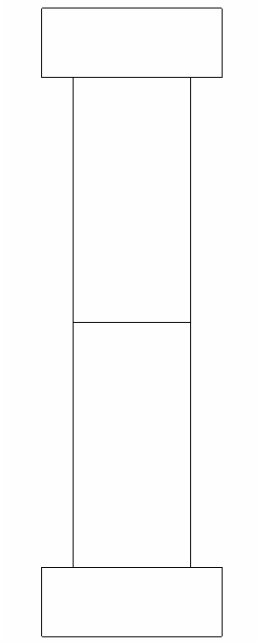

**Figure 24: Bolt sections as modelled in Abaqus Standard.**

The final assembly consisted of two instances of the flange part, one ring gasket instance, and one bolt instance, which is illustrated in Figure 25. Note that even if the bolt and the flange parts overlap, no interaction occurs between them outside the defined contact surfaces. This will be further described in 3.1.1.5 Contacts.

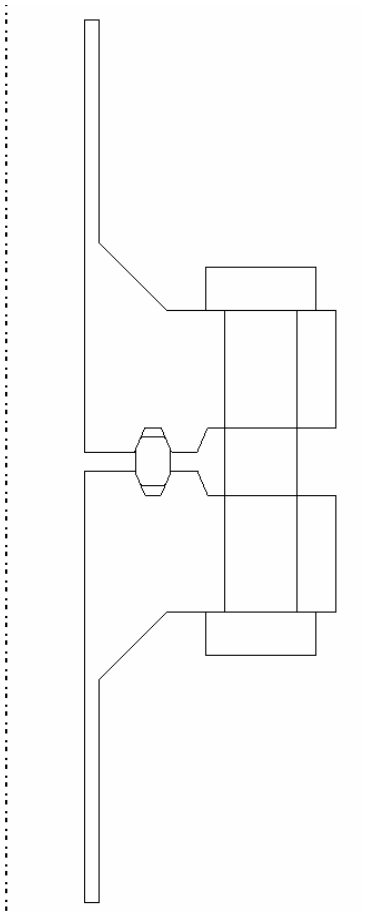

**Figure 25: Flanged joint assembly as modelled in Abaqus Standard.**

### *3.1.1.2 Element mesh*

Based on the information available in Dassault Systèmes (2010a), the Abaqus element CAX4R was chosen for all the axisymmetric analyses. The CAX4R element is a 4-node linear quadrilateral with reduced integration. In addition, the CAX4R elements used in these analyses also have the enhanced hourglass control option enabled, which reduces the distortion that can occur when using first order elements. Table 31 contains information regarding the element size and bolt load used in each of the analysis cases. The contact element size applies to the ring gasket groove of the flanges and the entire ring gasket part. The general element size applies to the remaining portion of the flange part, as well as the bolt part. The bolt stress aim will be described in 3.1.1.3 Loads, while the friction coefficient will be described in 3.1.1.5 Contacts.

.

**Table 31: List of axisymmetric analyses conducted in this thesis.**

| Analysis Name | Analysis Number | Contact Element Size | General Element Size | Analysis Type | Element Type | Bolt Stress Aim | Friction Coeff. |
|---|---|---|---|---|---|---|---|
| - | # | mm | mm | - | - | MPa | - |
| Quad-138-F-0-E-0_1 | 1 | 0,1 | 1 | 2D | CAX4R | 138 | 0 |
| Quad-172-F-0-E-0_1 | 2 | 0,1 | 1 | 2D | CAX4R | 172 | 0 |
| Quad-331-F-0-E-0_1 | 3 | 0,1 | 1 | 2D | CAX4R | 331 | 0 |
| Quad-172-F-0_05-E-0_1 | 4 | 0,1 | 1 | 2D | CAX4R | 172 | 0,05 |
| Quad-172-F-0_10-E-0_1 | 5 | 0,1 | 1 | 2D | CAX4R | 172 | 0,1 |
| Quad-138-F-0_15-E-0_1 | 6 | 0,1 | 1 | 2D | CAX4R | 138 | 0,15 |
| Quad-172-F-0_15-E-0_1 | 7 | 0,1 | 1 | 2D | CAX4R | 172 | 0,15 |
| Quad-331-F-0_15-E-0_1 | 8 | 0,1 | 1 | 2D | CAX4R | 331 | 0,15 |
| | | | | | | | |
| Quad-172-F-0-E-0_05 | 9 | 0,05 | 0,5 | 2D | CAX4R | 172 | 0 |
| Quad-172-F-0-E-0_01 | 10 | 0,01 | 0,1 | 2D | CAX4R | 172 | 0 |
| Quad-172-F-0_15-E-0_05 | 11 | 0,05 | 0,5 | 2D | CAX4R | 172 | 0,15 |
| Quad-172-F-0_15-E-0_01 | 12 | 0,01 | 0,1 | 2D | CAX4R | 172 | 0,15 |

The flange part mesh, as it is modelled in Abaqus Standard, is shown in Figure 26 and Figure 27. The mesh of the flange part was checked with the "Verify Mesh" tool available in Abaqus CAE, and the results are presented in Table 32.

**Table 32: Mesh verification results for the flange part.**

| Parameter | Value | Unit |
|---|---|---|
| Max Face Corner | 138,93 | Degrees |
| Average Max Face Corner | 96,03 | Degrees |
| Min Face Corner | 41,67 | Degrees |
| Average Min Face Corner | 84,38 | Degrees |
| Errors | 0 | % |
| Warnings | 0 | % |

The ring gasket part mesh is shown in Figure 29, and Table 33 contains the results from the mesh verification tool.

**Table 33: Mesh verification results for the ring gasket part.**

| Parameter | Value | Unit |
|---|---|---|
| Max Face Corner | 138,93 | Degrees |
| Average Max Face Corner | 96,03 | Degrees |
| Min Face Corner | 41,67 | Degrees |
| Average Min Face Corner | 84,38 | Degrees |
| Errors | 0 | % |
| Warnings | 0 | % |

The bolt part mesh is likewise shown in Figure 28, and the mesh verification results are described in Table 34.

**Table 34: Mesh verification results for the bolt part.**

| Parameter | Value | Unit |
|---|---|---|
| Max Face Corner | 90,87 | Degrees |
| Average Max Face Corner | 90,15 | Degrees |
| Min Face Corner | 89,13 | Degrees |
| Average Min Face Corner | 89,85 | Degrees |
| Errors | 0 | % |
| Warnings | 0 | % |

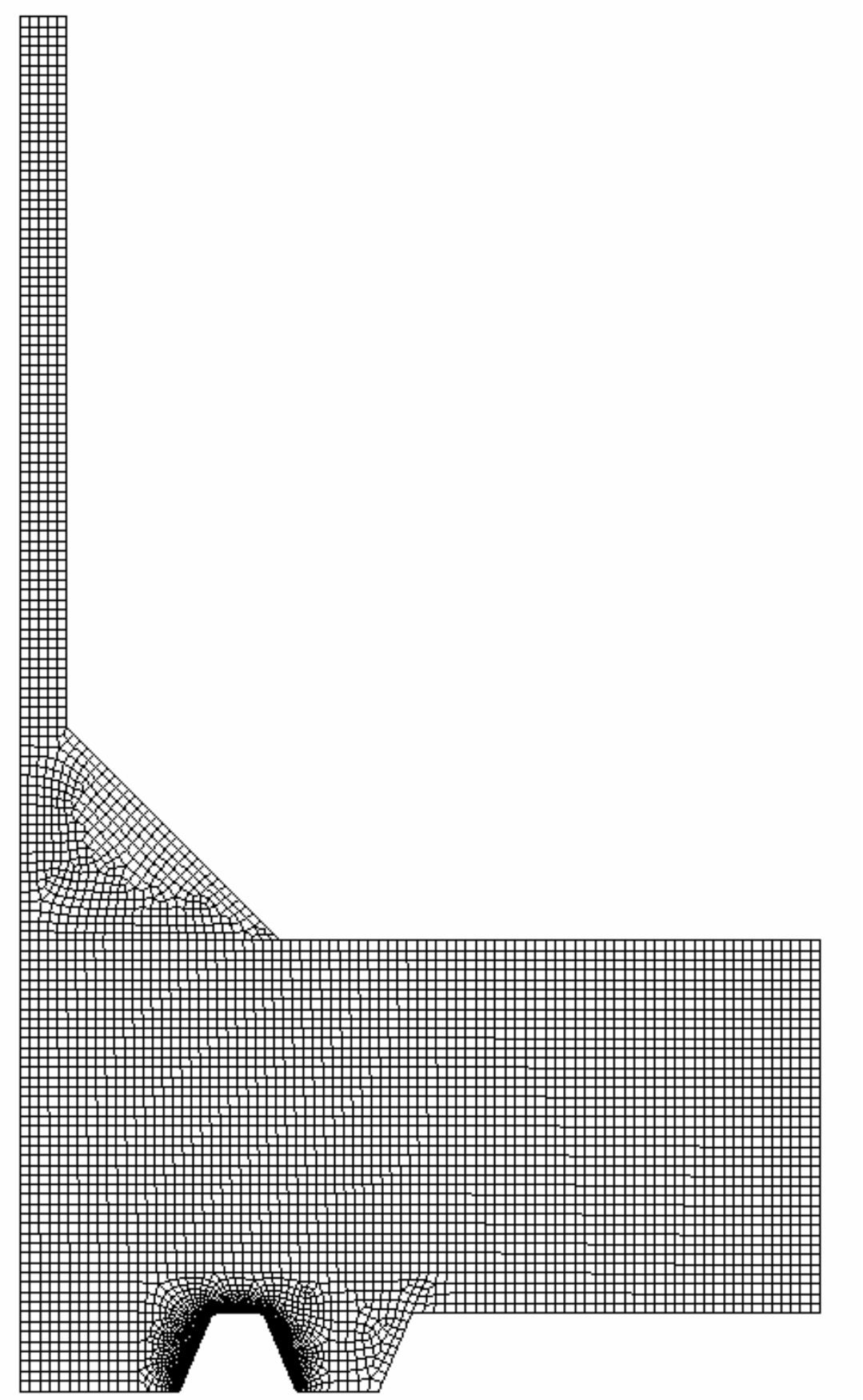

**Figure 26: Flange part mesh.**

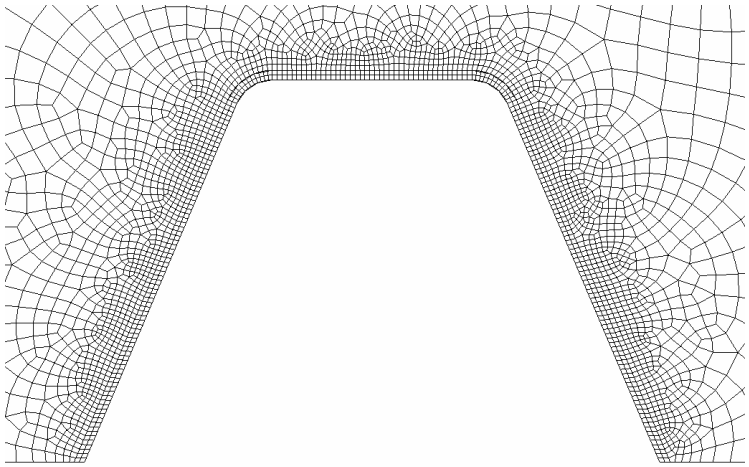

**Figure 27: Enlarged mesh of ring gasket groove on the flange part.**

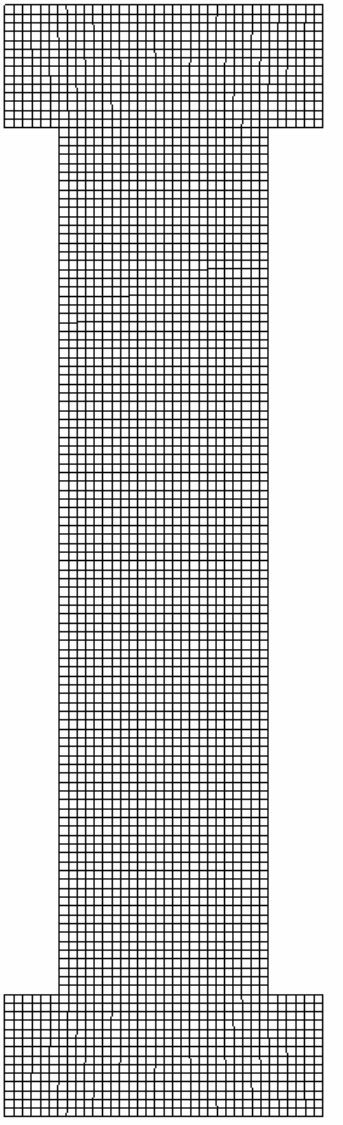

**Figure 28: Bolt part mesh.**

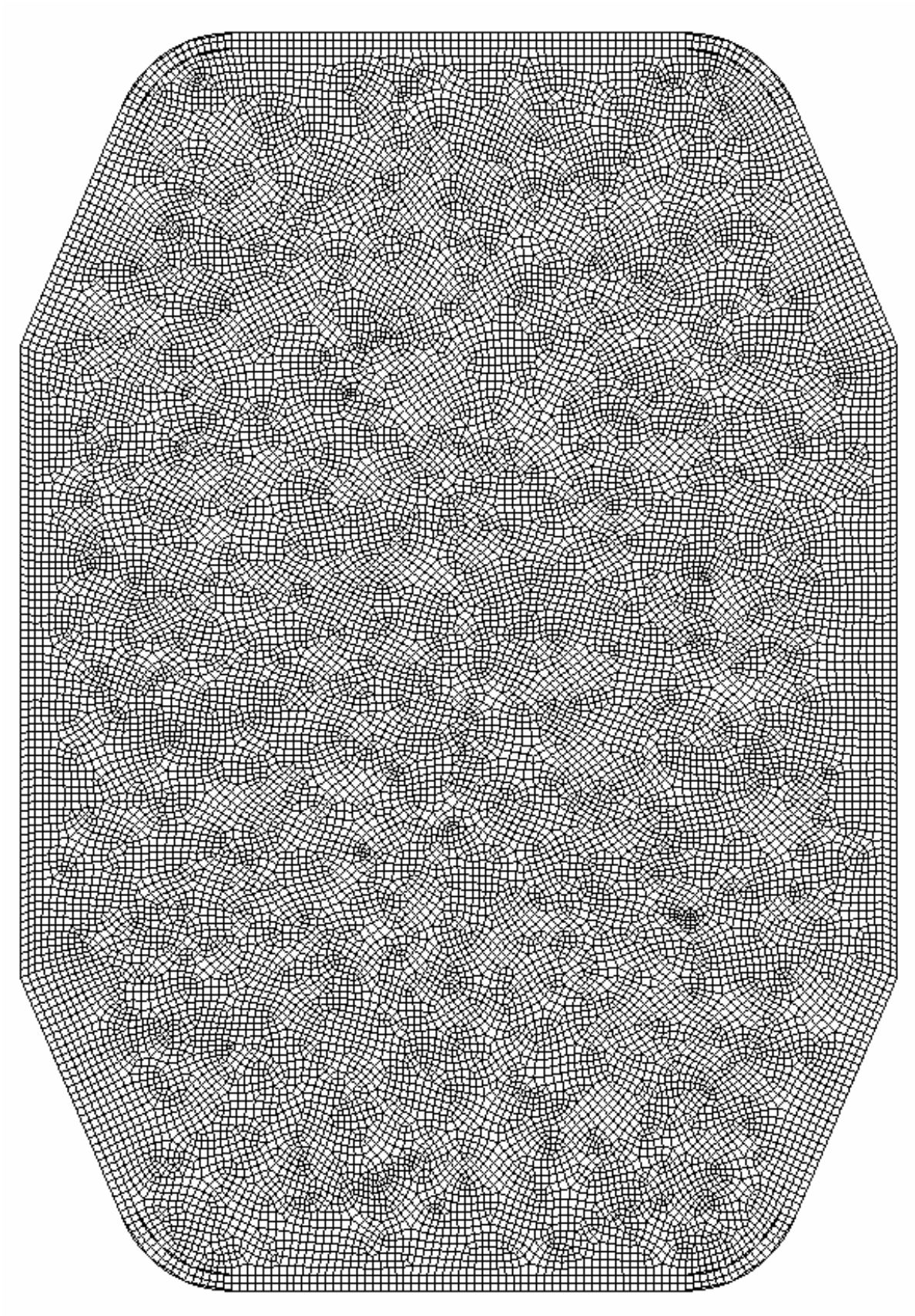

**Figure 29: Ring gasket part mesh.**

### *3.1.1.3 Loads*

There are three loads used in the axisymmetric model; bolt load, internal pressure, and pressure end force. The steps are described in Table 35, where the percentage value is the percentage of the load values presented in Table 36. As shown, the bolt load is applied in the first step, and then held for the remainder of the analysis. Note that it is the length of the bolt that is held, and higher bolt stress will be present as the internal pressure increases and causes further elastic strain in the bolt part.

**Table 35: Loads versus steps for axisymmetric analyses.**

| Step Name | Bolt Load | Internal Pressure | Pressure End Force |
|---|---|---|---|
| Bolt Load | 100 % | | |
| Pressure 1 | HOLD | 100 % | 100 % |
| Pressure 2 | HOLD | 150 % | 150 % |
| Pressure 3 | HOLD | 200 % | 200 % |
| Pressure 4 | HOLD | 300 % | 300 % |

The bolt loads presented in Table 36 is calculated using the ASME (2010) Design Rules for Flanged Joints, as described in 2.4.2 Bolt loads. The internal pressure value is based upon the ASME B16.5 pressure rating, and is described in 3.2 Basis for Flange Design Rules. The pressure end force is calculated using the equation

$$p_{end} = \frac{p_{internal} * A_{internal}}{A_{end}},$$

where $A_{end}$ is the area of the pipe wall, $p_{internal}$ is the internal pressure, and $A_{internal}$ is the bore area of the pipe.

The bolt load is generated by using the Abaqus load function “Bolt Load”, where the length of the elements next to the line of application are reduced without causing local strain. However, the overall strain of the bolt will increase due to the net reduction of bolt length. Figure 30 illustrates where the bolt load is applied. Note that throughout the thesis, the bolt load is uniformly distributed. The external net axial forces and bending moments is assumed to be zero.

**Table 36: List of loads for axisymmetric analyses conducted in this thesis.**

| Analysis Name | Bolt Stress Aim | Internal Pressure | Pressure End Force |
|---|---|---|---|
| - | MPa | MPa | MPa |
| Quad-138-F-0-E-0_1 | 138 | 25,86 | -78,2 |
| Quad-172-F-0-E-0_1 | 172 | 25,86 | -78,2 |
| Quad-331-F-0-E-0_1 | 331 | 25,86 | -78,2 |
| Quad-172-F-0_05-E-0_1 | 172 | 25,86 | -78,2 |
| Quad-172-F-0_10-E-0_1 | 172 | 25,86 | -78,2 |
| Quad-138-F-0_15-E-0_1 | 138 | 25,86 | -78,2 |
| Quad-172-F-0_15-E-0_1 | 172 | 25,86 | -78,2 |
| Quad-331-F-0_15-E-0_1 | 331 | 25,86 | -78,2 |
| | | | |
| Quad-172-F-0-E-0_05 | 172 | 25,86 | 78,2 |
| Quad-172-F-0-E-0_01 | 172 | 25,86 | 78,2 |
| Quad-172-F-0_15-E-0_05 | 172 | 25,86 | 78,2 |
| Quad-172-F-0_15-E-0_01 | 172 | 25,86 | 78,2 |

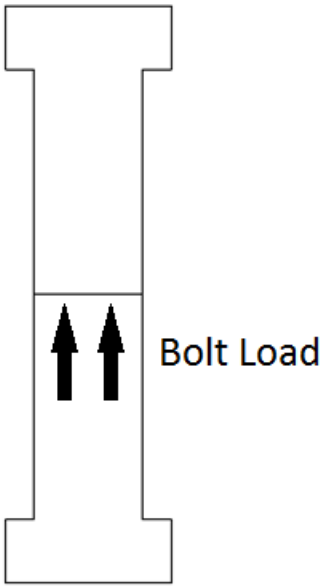


**Figure 30: The section edge where the bolt load is applied to the bolt part.**

The internal pressure is applied to both the gasket ring part and the two flange parts. As illustrated in Figure 31, the internal pressure is applied to the inwards facing side of the ring gasket part. Figure 32 show how the internal pressure is applied to the bore surface and the internal portion of the flange face. Note that the internal pressure is applied identically to the other flange part, and that no pressure loads are applied to the small portion of the ring gasket groove that is left exposed in the full assembly.

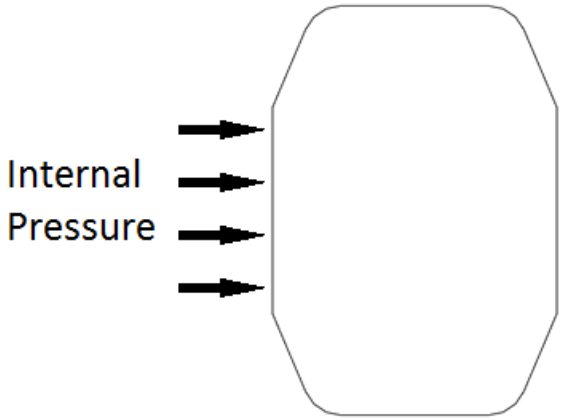


**Figure 31: The surface where the internal pressure is applied on the ring gasket part.**

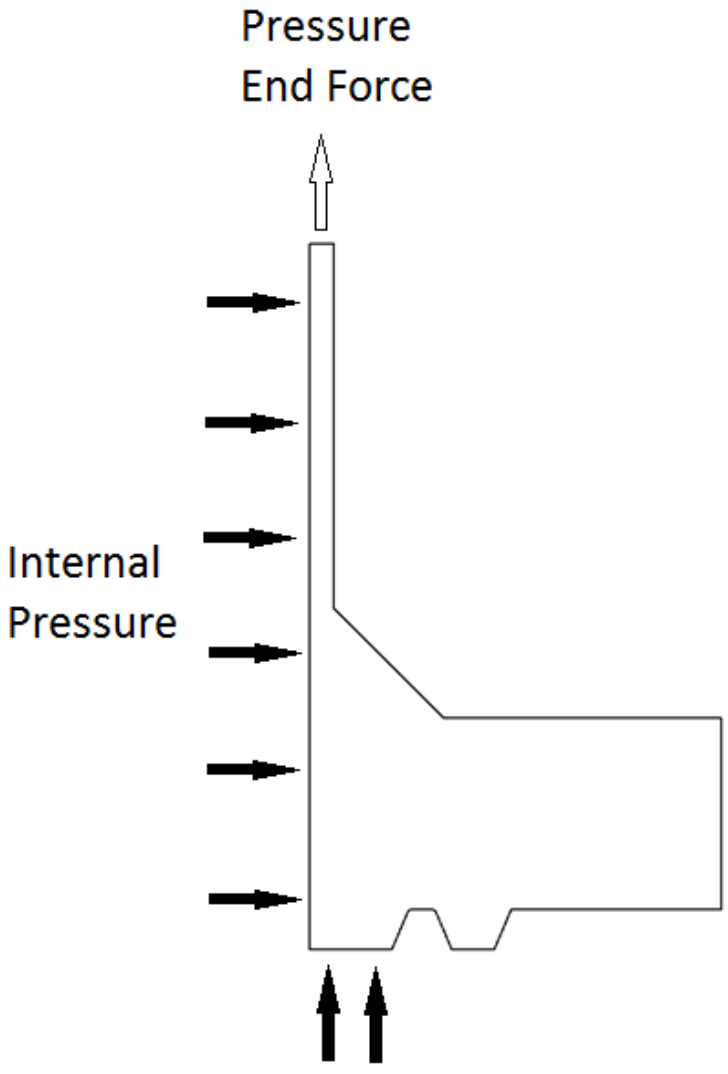


**Figure 32: The surfaces where the internal pressure is applied on the flange part.**

The pressure end force, as illustrated in Figure 32, utilizes a negative pressure load, and is applied at the pipe end of the top flange part in the assembly.

#### *3.1.1.4 Boundary conditions*

The only boundary condition defined in the axisymmetric model is defined at pipe end of the lower flange in the assembly, as illustrated by Figure 33. The boundary condition is defined as YSYMM, which implies that the part cannot move rigidly along the y-axis, nor rotate around the x- or z-axis. It does, however, allow for expansion of the pipe along the x- and z- axis, such as can be the case when the pipe / flange is internally pressurized. The main reason for including this boundary condition is to prevent the assembly from moving rigidly when pressures and loads are applied throughout the analyses.

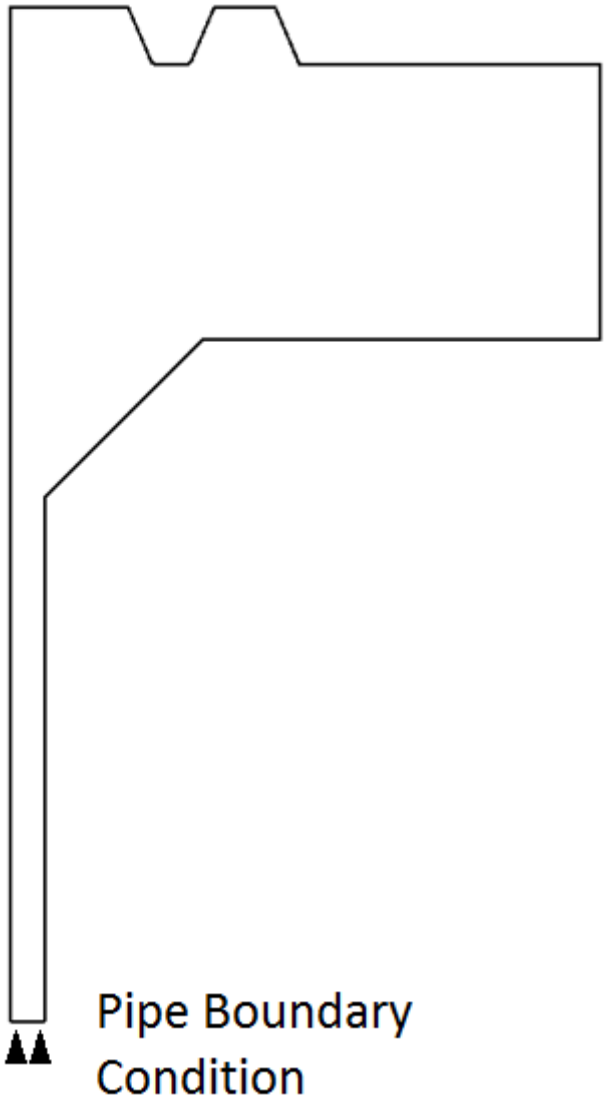


**Figure 33: Pipe boundary condition for the flange part.**

### *3.1.1.5 Contacts*

There are six contact interactions defined in the axisymmetric models; four which are located at the flange to gasket ring contact surfaces, and two which are located at the interface between bolt head and flange body.

The top left contact pair in the ring gasket groove is illustrated Figure 34 and Figure 35. As shown, the flange contact surface is applied to the respective wall of the ring gasket groove, up until the fillet at the groove bottom. The ring gasket contact surface is applied from a quarter down on the vertical side, up until the end of the fillet near the top of the ring gasket. The ring gasket contact surface is defined in this manner to allow for the expansion of the contact as the ring gasket is deformed, and to reduce the overclosure at the sharp corner of the contact.

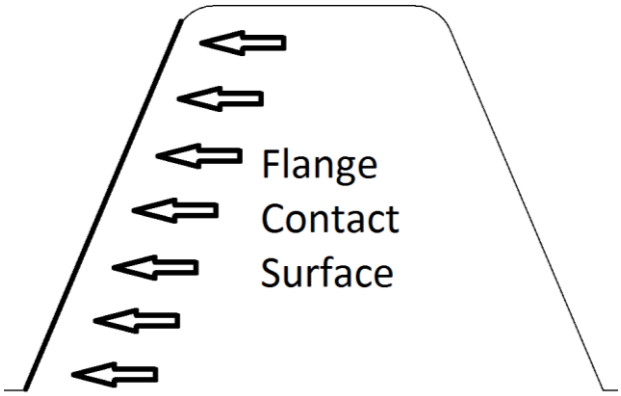


**Figure 34: Top left flange contact interaction surface.**

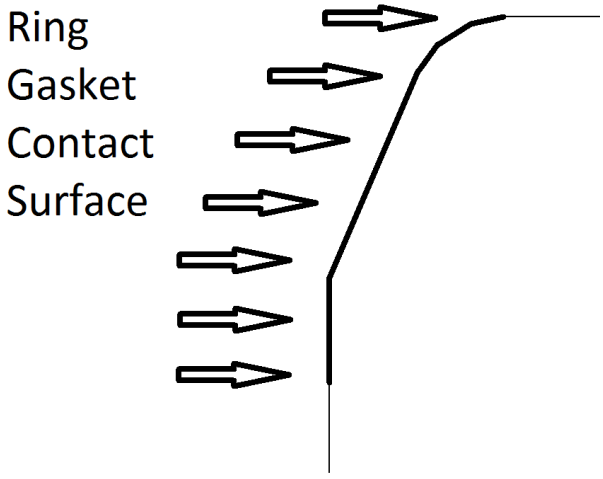


**Figure 35: Top left ring gasket contact interaction surface.**

The surfaces on which the bolt-flange contact pairs are applied are illustrated in Figure 36 and Figure 37. The top bolt contact pair is tied, meaning that there is no sliding, and that the contact transfer both tensile and pressure loads. This is done in order to reduce the number of contact calculations, and thereby simplify the model. The bottom bolt contact pair is defined as a standard surface-to-surface hard contact with a frictionless tangential behaviour.

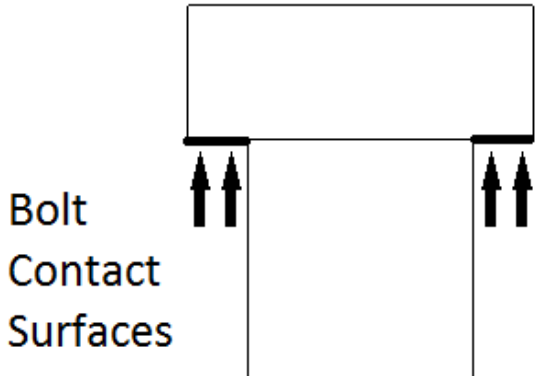


**Figure 36: Bolt contact interaction surfaces.**

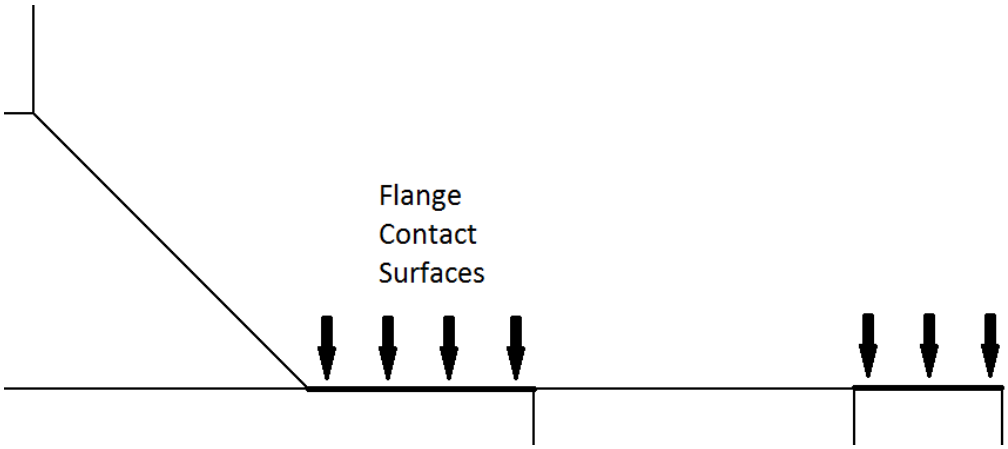


**Figure 37: Flange bolt ring contact interaction surfaces.**

The contact properties for each of the contact pairs are summarized in Table 37. The pressure-overclosure relationship and the constraint enforcement method were chosen as hard contact and penalty method respectively, as this is considered the most representative model for contact between two elastic-plastic metal bodies. The finite sliding discretization method was chosen due the sliding distance being larger than one element length. Small sliding could have been applied to the bottom bolt-flange contact pair, but as that particular contact is quite simple, and the potential reduction in computational cost were relative small, the choice was made to keep all contact pairs as finite sliding.

**Table 37: The contact properties for the axisymmetric models.**

| Master Surface | Slave Surface | Position | Discretization Method | Sliding Formulation | Pressure-Overclosure | Constraint Enforcement |
|---|---|---|---|---|---|---|
| Top Flange | Ring Gasket | Top Left | Surface-to-Surface | Finite Sliding | Hard Contact | Penalty |
| Top Flange | Ring Gasket | Top Right | Surface-to-Surface | Finite Sliding | Hard Contact | Penalty |
| Bottom Flange | Ring Gasket | Bottom Left | Surface-to-Surface | Finite Sliding | Hard Contact | Penalty |
| Bottom Flange | Ring Gasket | Bottom Right | Surface-to-Surface | Finite Sliding | Hard Contact | Penalty |
| Top Flange | Bolt | Top | Tied | N/A | N/A | N/A |
| Bottom Flange | Bolt | Bottom | Surface-to-Surface | Finite Sliding | Hard Contact | Penalty |

The coefficient of friction was chosen as 0.15 based on Johannessen (2002).

### *3.1.1.6 Materials*

As previously described, the axisymmetric model consists of three types of parts; the flange, the ring gasket, and the bolt part. The assignment of material properties is section based, where each section can be assigned individual material sets. The general material properties of the three parts are presented in Table 38. Isotropic elasticity and isotropic hardening were selected for all material property sets. Note that Abaqus requires the stress-strain data to be input as true stress and true plastic strain.

**Table 38: The general material properties of the axisymmetric parts.**

| | Bolt | Flange | Ring Gasket | Unit |
|---|---|---|---|---|
| Young's Modulus | 204 | 200 | 195 | GPa |
| Poisson's Ratio | 0,3 | 0,3 | 0,3 | - |
| True Yield Strength | - | 450 | 258,6 | MPa |
| True Plastic Strain at Yield | - | 0 | 0 | mm/mm |
| True Ultimate Strength | - | 775 | 961 | MPa |
| True Plastic Strain at Ultimate | - | 0,223 | 0,438 | mm/mm |

Due to the presence of bolt hole perforations, a bolted flange is not fully axisymmetric. However, an approximation may be made by altering the elastic modulus of the axisymmetric section spanning the bolt holes, denoted A in Figure 21. This is a technique has been applied in previous studies by Sato and Kado (2005). The bolt hole ring is illustrated in Figure 38, where the smaller circles represent the bolt hole perforations, and the two larger circles represent the inner and outer boundary of the bolt hole ring. Based on this, the fraction of surface within the bolt hole ring that is not perforated may be calculated using

$$f_{bolt\ hole\ ring} = \frac{A_{bolt\ hole\ ring} - A_{bolt\ holes}}{A_{bolt\ hole\ ring}},$$

where $A_{bolt\ hole\ ring}$ is the area of the ring spanned by the bolt holes, and $A_{bolt\ holes}$ is the total area of the bolt holes. This fraction may also be interpreted as a measure for how much material is present in the bolt hole ring section of the axisymmetric model, and may thereby be multiplied with the original elastic modulus to calculate a reduced elastic modulus. The result is that the bolt hole section will behave less rigidly when exposed to loads, which should be closer to how a three dimensional model would react to the same loads. However, the stress values presented by Abaqus for this particular section will artificially low due to the material stress still being spread over the entire bolt hole ring area, and it will be necessary to use the following equation in order to convert the stress to more realistic values:

$$\sigma = \frac{\sigma_{reduced\ section}}{f_{reduction\ factor}}.$$

The bolt material properties were calculated using the same method as the bolt hole ring section, but the ring was then spanned by the bolt diameter. The bolt circle fraction is calculated using the equation

$$f_{bolt\ ring} = \frac{A_{bolts}}{A_{bolt\ ring}},$$

where $A_{bolts}$ is the total area of the bolts, and $A_{bolt\ ring}$ is the area of the ring spanned by the bolt diameter. Note that the equation for converting the stress in the reduced section to realistic values also has to be applied to the bolt ring section. The reduced Young's Modulus for the flange bolt hole ring and the bolt ring section is presented in Table 39 and Table 40.

**Table 39: Reduced Young's Modulus for the flange bolt hole ring section.**

| | Flange | Unit |
|---|---|---|
| Total Area of Bolt Holes | 4053,7 | $mm^2$ |
| Total Area of Bolt Hole Ring | 13174,4 | $mm^2$ |
| Fraction | 0,692 | - |
| Reduced Young's Modulus | 138,5 | GPa |

**Table 40: Reduced Young's Modulus for the bolt ring section.**

| | Bolt | Unit |
|---|---|---|
| Total Area of Bolts | 3103,6 | $mm^2$ |
| Total Area of Bolt Ring | 11527,6 | $mm^2$ |
| Fraction | 0,269 | - |
| Reduced Young's Modulus | 54,9 | GPa |

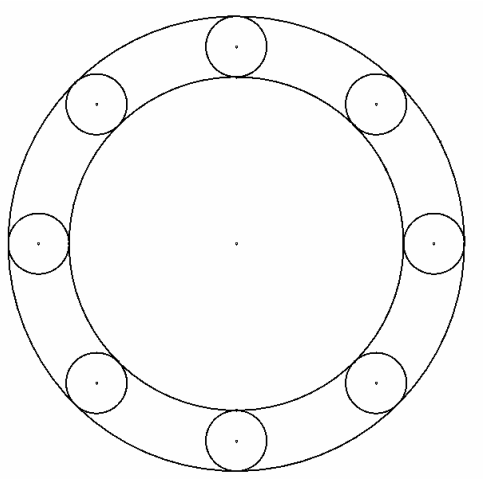

**Figure 38: Bolt hole ring of a flange with eight bolts viewed from above.**

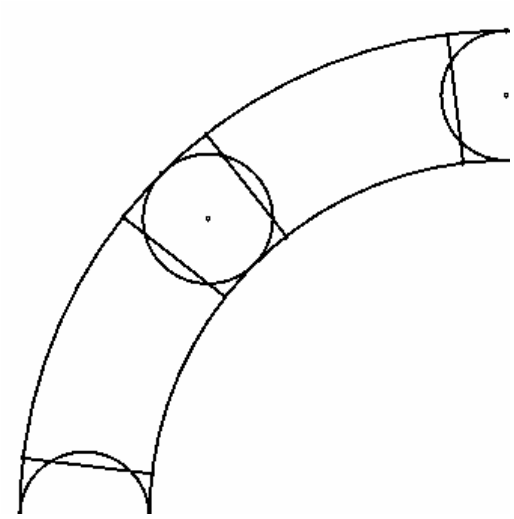

**Figure 39: Comparison of real bolt hole geometry and geometry resulting from the axisymmetric approximation.**

A source of inaccuracy when using the circle approximation in an axisymmetric model is that the bolt and bolt hole material gets distributed uniform and slightly inaccurate, as illustrated in Figure 39. There are also more material in the outer parts of the bolt ring than in the inner parts. However, it is believed that the difference is small enough to not cause any notable changes in flange stress distribution, and additional steps will not be taken to compensate for this in the model.

## 3.2 Basis for Flange Design Rules

This chapter describes the basis for the equations presented in 2.4 Design Rules for Flanged Joints, as well as any assumptions regarding the nature of the flanged connection studied. The assumed temperatures and pressures for both gasket seating and operating conditions are presented in Table 41. The operating pressures were obtained from the ASME (2009) B16.5 pressure-temperature ratings, as shown in Table 42, and is valid for multiple alloys, among them UNS S31803 (22Cr-5Ni-3Mo-N).

**Table 41: Assumed gasket seating and operating conditions (ASME, 2009).**

| Name | Symbol | Case I | Case II | Unit |
|---|---|---|---|---|
| Gasket Seating Pressure | $P_1$ | 0.1 | 0.1 | MPa |
| Gasket Seating Temperature | $T_1$ | 20 | 20 | C |
| Operating Pressure | $P_2$ | 25.86 | 38.79 | MPa |
| Operating Temperature | $T_2$ | 20 | 20 | C |

**Table 42: Pressure-temperature ratings, class 1500, for group 2.8 materials (ASME, 2009).**

| Pressure Class | Maximum Internal Pressure, for Temperatures | | | | | | | | | Unit |
|---|---|---|---|---|---|---|---|---|---|---|
| - | -29 to 38 | 50 | 100 | 150 | 200 | 250 | 300 | 325 | 350 | C |
| Class 1500 | 25,86 | 25,86 | 25,33 | 22,96 | 21,33 | 20,23 | 19,43 | 19,08 | 18,82 | MPa |

Note that the pressure and temperature conditions remain constant in set 1 through 3. However, set one will utilize the bolt load $W_g$ obtained through the averaged equation, while set two will utilize the non-averaged equation, as described in 2.4.2 Bolt loads. Set three will utilize the bolt load as estimated by the equation for the maximum obtainable manual bolt load. Set four has a higher operational pressure in order to account for a fifty percent overpressure, and will utilize the normal averaged equation.

The design rules specify that any design process should consider the flange dimensions both in the corroded and the uncorroded state. However, for the design calculations conducted in this thesis, one of the two following assumptions are made: Both the external and internal corrosion, as well as any internal erosion, is considered to be negligible. Alternatively, the dimensions presented may be considered to be the corroded state. Corrosion and/or erosion allowance has to be added to the dimensions if applied to a real application.

**Table 43: Assumed dimensions, gasket factors, and allowable bolt stresses (ASME, 2010, ASME, 2009).**

| Name | Symbol | Value | Unit |
|---|---|---|---|
| Gasket Factor | m | 6.5 | - |
| Gasket Factor | y | 180 | MPa |
| Gasket Ring Width | w | 11.13 | mm |
| External Bending Moment | $M_E$ | 0 | N mm |
| External Axial Tension Force | $F_A$ | 0 | N |
| Modulus of Elasticity at Operating Cond. | $E_{yo}$ | 200 | GPa |
| Modulus of Elasticity at Gasket Seating Cond. | $E_{yg}$ | 200 | GPa |
| Gasket Load Reaction Diameter | G | 95.25 | mm |
| Bore Diameter | B | 50.8 | mm |
| Bolt Circle Diameter | C | 165.1 | mm |
| Outside Diameter of Flange | A | 215 | mm |
| Flange Thickness | t | 38.1 | mm |
| Thickness of Hub at Large End | $g_1$ | 27.1 | mm |
| Thickness of Hub at Small End | $g_0$ | 4.75 | mm |
| Hub Length | h | 27.1 | mm |
| Allowable Bolt Stress at Design Temp. | $S_{bo}$ | 172 | MPa |
| Allowable Bolt Stress at Gasket Seating Temp. | $S_{bg}$ | 172 | MPa |
| Number of Bolts | n | 8 | - |
| Bolt Diameter | $D_b$ | 22.225 | mm |
| Bolt Root Area | $A_{br}$ | 387.95 | $mm^2$ |
| Unit Correction Factor | $C_{us}$ | 1 | - |

Most of the necessary input parameters for the design calculations are presented in Table 43. The table is based on the information provided in

2.2 Materials and 2.3 Dimensions. An exception is the gasket factors, which were presented in 2.4 Design Rules for Flanged Joints.

As previously stated, the flange type studied in this thesis is a weld neck flange with a ring joint face. This is considered an integral type by the design rules, and for the entirety of the design calculations, integral flanges are the only types considered.

In Table 44, case I and II are the cases which full design rules calculations are going to be performed. Alt. I and alt. II are only calculated in order to determine the bolt stress, as described in 2.4 Design Rules for Flanged Joints. These bolt stresses will be used in the axisymmetric models.

**Table 44: Results from bolt load calculations.**

| Name | Symbol | Case I | Case II | Alt. I | Alt. II | Unit |
|---|---|---|---|---|---|---|
| Basic Gasket Seating Width | $b_o$ | 1.391 | 1.391 | 1.391 | 1.391 | mm |
| Effective Gasket Seating Width | b | 1.391 | 1.391 | 1.391 | 1.391 | mm |
| Design Bolt Load for Operating Condition | $W_o$ | 324130 | 486195 | 324130 | 324130 | N |
| Minimum Gasket Compression Load | $W_{gs}$ | 74936 | 74936 | 74936 | 74936 | N |
| Minimum Required Total Area of Bolts | $A_m$ | 1884 | 2827 | 1884 | 1884 | $mm^2$ |
| Selected Total Area of Bolts | $A_b$ | 3104 | 3104 | 3104 | 3104 | $mm^2$ |
| Design Bolt Load for Gasket Seating Condition | $W_g$ | 428973 | 510006 | 533816 | 1027286 | N |
| Preload Stress in Bolt Material | $S_{eb}$ | 138 | 164 | 172 | 331 | MPa |

## 3.3 Tensile testing

### 3.3.1 Specimen dimensions

In order to determine both the elastic modulus and the plastic stress-strain behaviour of the UNS S31803 bar stock source material, specimens of two sizes were manufactured. The smaller sized specimens were used for developing full range stress-strain curves, while the larger specimens were used for the measurement of the elastic modulus. The dimensions of the specimens are illustrated in Figure 40.

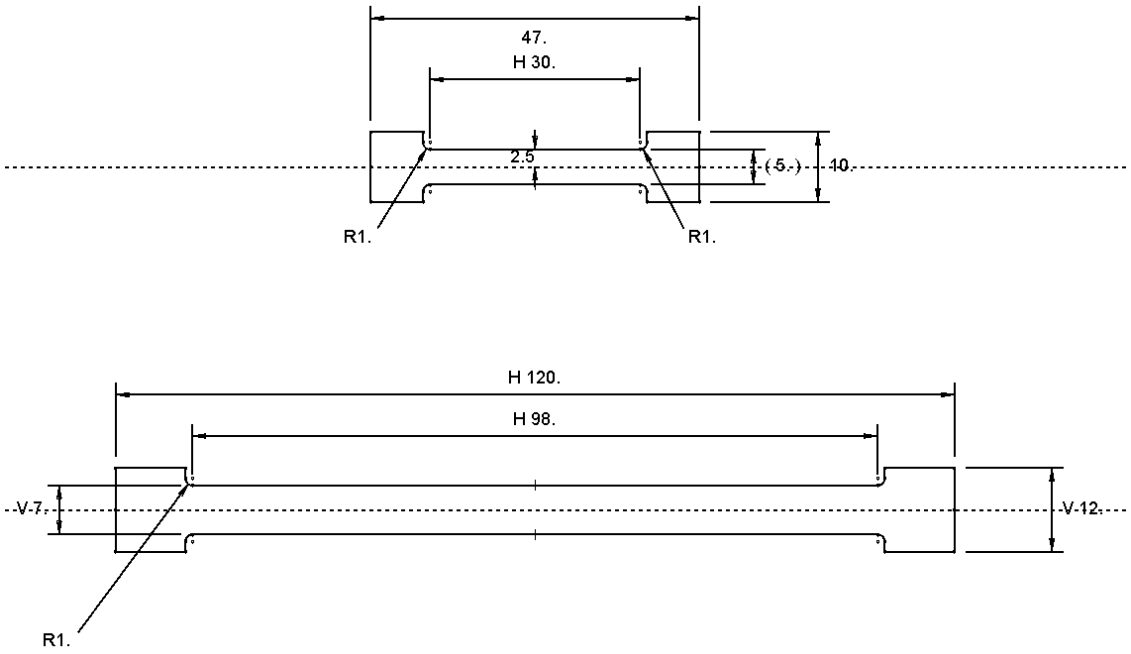


**Figure 40: Specimen dimensions.**

While specimens of even larger dimensions would be preferred, as specified by the ASTM (2011c) A370 standard for material testing, the available testing equipment at Bergen University College (HiB) is limited to a maximum 20 kN tensile load. This imposed a limit on the maximum cross-sectional area that could be tested.

### 3.3.2 Specimen orientation

The test specimens were cut from two forged, round bars with diameters of 220 and 250 millimetres, and a common length of 140 millimetres. The data sheets provided by the supplier may be found in the Appendix K: Manufacturer Data Sheets for Forged Bar. It was assumed that any flange that was potentially fabricated from a forged bar stock material, would be positioned in such a way that the bar and the flange would have a common radial centre, regardless of the bar diameter. With the centre of the bar as reference, a common layout for cutting the bars into smaller parts was made, as illustrated in Figure 41. The specific dimensions may be found in the Appendix B: Part Drawings with Dimensions.

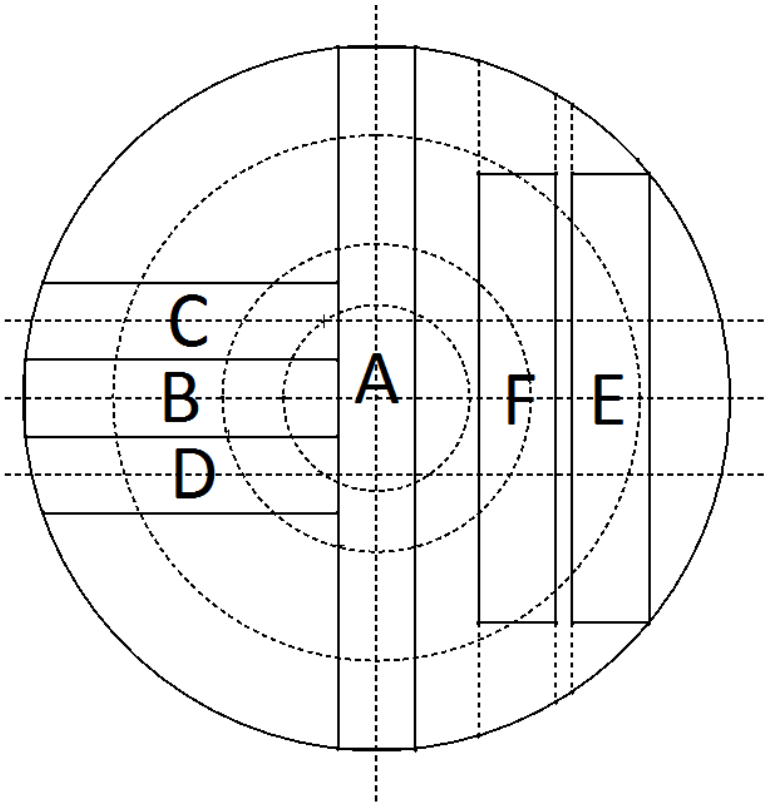


**Figure 41: Common layout for dividing the bar stock.**

While the tensile tests investigate the possibility of asymmetric plastic and elastic properties, the bar is assumed to be axisymmetric with regards to the same properties. Testing of two specimens of equal orientation and radial position should thereby in principle yield the same results. Based on this assumption, three radial positions were selected as areas of interest, illustrated by three dotted circles in Figure 41. The innermost circle is positioned 29 mm from the centre, and represents the bore wall. The middle circle has a radius of 48 mm, which roughly equals the position of the ring gasket groove. The outermost ring is located at a radius of 82 mm, which is close to the bolt circle diameter.

The parts described in Figure 41 were then split into smaller segments that were positioned roughly according to the areas of interest. However, as illustrated in Figure 42, the larger specimens cut from part A was positioned at the centre. This position was chosen based on the assumption that the material in the centre would be exposed to high temperatures for the longest time during the forging process, and the properties are most likely to deviate from the specifications there. Note that all the sections machined from part A were considered of radial orientation.

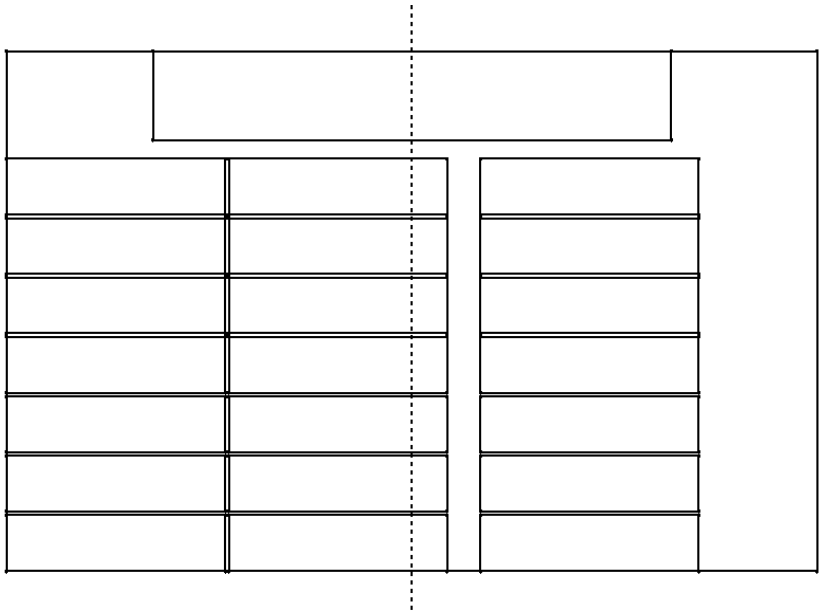

**Figure 42: Part A, viewed from the side.**

Part B were split into three large segments, as illustrated in Figure 43, which were to be machined into larger specimens of axial orientation. The vertical dotted lines represent the radial position where the circles indicating the areas of interest intersect the centre plane of the part. As shown, the middle segment is slightly offset from the intended radial position. However, considering that the ring gasket groove area of interest span roughly 5 mm in each direction, the impact on the actual results is assumed to be small.

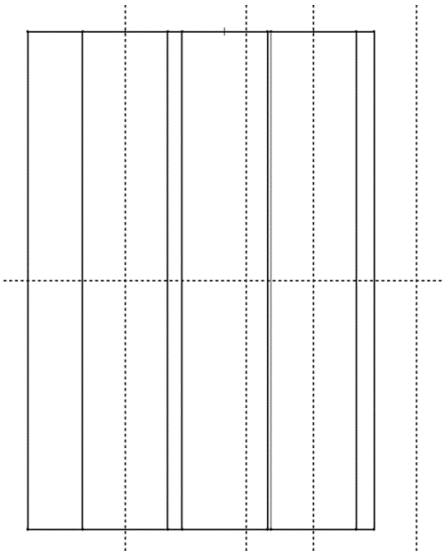

**Figure 43: Part B, viewed from the side.**

Part C and D were cut identically as they were symmetrical around the centre plane of part B. Both were split into six smaller segments, as illustrated in Figure 44. The rightmost vertical dotted line indicates the position of the centre plane of Part A. With the exception of the leftmost line indicating curvature, the remaining dotted vertical lines indicate the intersection between the dotted circles shown in Figure 41, and the centre plane of Part C and D.

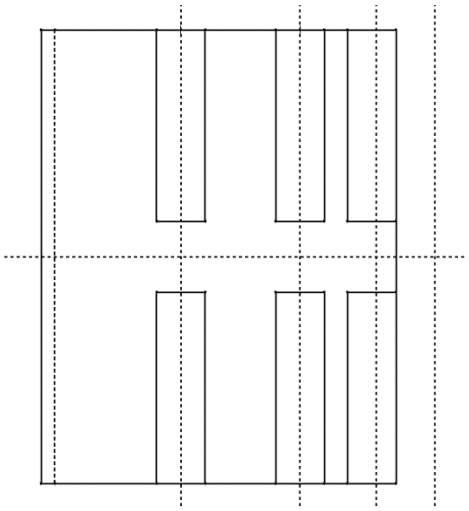

**Figure 44: Part C and D, viewed from the side.**

Part E and F, as illustrated in Figure 45, were also cut in an identical manner. One large and six small sections were cut from each of the two parts. They were all positioned at the horizontal centre of the figure, as indicated by the vertical dotted lines, and were considered of tangential orientation. As shown in Figure 41, the positions of the parts do not align perfectly with the dotted circles. However, due to the small magnitude of the offsets, the sections are considered of equal radial position as the respective sections from other parts.

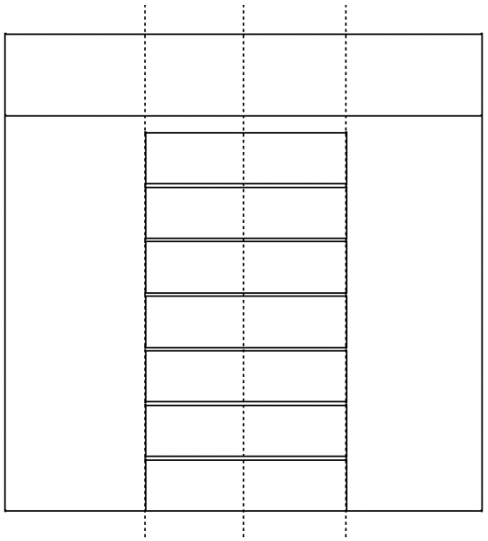

**Figure 45: Part E and F, viewed from the side.**

### 3.3.3 Specimen preparation

The initial cutting of the parts was done using a band saw with bi-metal saw blades. After the bar stock was split into smaller sections, each section was rounded at one end using a milling machine. The round section then provided a grip that could be fastened in the turning machine for processing to the final shape of the test specimens. Figure 46 shows the CNC assisted turning machine that was used for the final shaping of the test specimens.


**Figure 46: The CNC assisted turning machine.**

For a full list of specimens, please look to Table 54 and Table 55 in Appendix C: Lists of Manufactured Specimens. However, note that some of the specimens are listed as broken, poor finish, or N/A. The specimens that are listed as N/A were according to the laboratory technician unable to be completed due to turning machine limitations when working in very hard materials.

### 3.3.4 Test equipment

The tests were all conducted using the Hounsfield H20K-W machine for material testing, as shown in Figure 47. The small specimens were tested using the basic setup, where both force measurement and displacement is measured by the machine's internal sensors. However, when determining the elastic modulus, the Hounsfield PS50C external extensometer was attached to the specimens in order to obtain better strain measurement resolution.


**Figure 47: The Hounsfield H20K-W material testing machine.**

Figure 48 shows the attachments used for mounting the small specimens in the H20K-W. The large specimens were mounted in a set of similar attachments, only with larger holes. Figure 49 shows how the extensometer was attached to the large test specimens using metal clips.

**Figure 48: The attachments used for mounting the small specimens.**

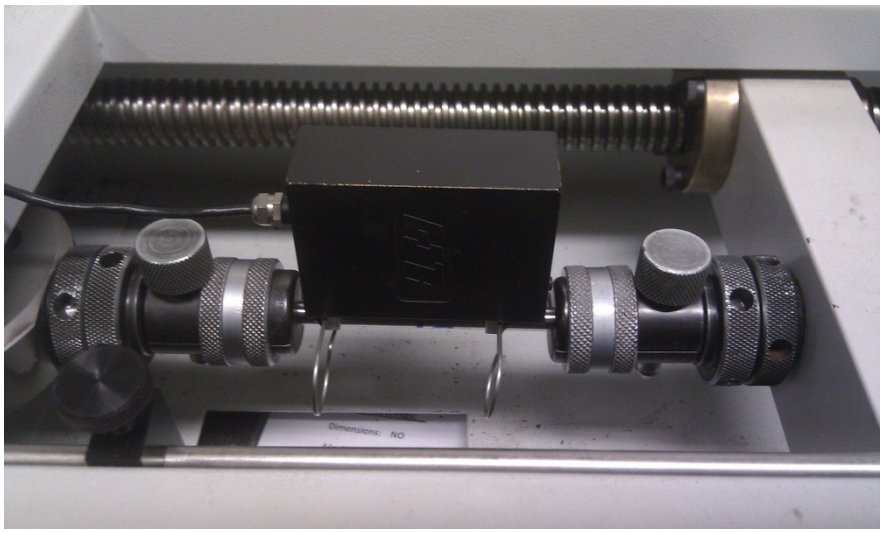

**Figure 49: The extensometer mounted to a large test specimen.**

As previously mentioned, the H20K-W has a limitation of 20 kN on the maximum tensile load, which limits the cross-sectional area of the specimens to be tested. The specimen dimensions thereby had to be selected with this in mind. Note that the length of the extensometer at zero elongation is 50 millimetre.

### *3.3.4.1 Testing procedures*

Two testing procedures were used during the testing of the UNS S31803 alloy. The first procedure was used for the development of full range stress-strain curves from the smaller specimens described in section 3.3.2 Specimen orientation. The second procedure was used for measuring the elastic elongation of the larger specimens, which was the basis for calculating the elastic modulus.

Both of the testing procedures described above were conducted according to the parameters presented in Table 45. The strain rate was defined as 1.54 millimetres per minute and remained constant throughout the tests, and according to the manufacturer data sheet, should not deviate by more than one percent. The temperature was measured at the start of each test, and verified not to deviate from the prescribed range by more than 0.5˚C. A simple electronic thermometer with 0.1˚C resolution was used for measuring the temperature. Prior to the tensile testing of a specimen, the diameter at both ends of the reduced section was measured, and used as a basis for calculating the cross-sectional area.

**Table 45: Test Parameters Used for Tensile Testing.**

| Legend | Value | Unit |
|---|---|---|
| Strain Rate | 1.54 | mm/min |
| Temperature | 22-24 | ˚C |

During the testing of the small specimens, the force and elongation values were measured using the internal sensors in the testing equipment. The values were then temporarily stored in the memory, and finally transferred to a work station through a RS232 connection. The sampling rate of the force measurements are listed as 60 times per second.

As previously mentioned, an external extensometer was used when testing the larger specimens. The specimens were loaded in intervals, and the elongation and force values were manually logged at start and end of each interval. The preload and the magnitude of the force intervals are listed in Table 46. Each set was tested in total seven times, where the first two measurements were disregarded, resulting in a total of five measurements for each set. The whole testing procedure was repeated for all large specimens.

**Table 46: Target Force Intervals for Large Specimens.**

| Set # | Preload | ax Fororce Interv | | Unit |
|---|---|---|---|---|
| Set 1 | 2000 | 8000 | 6000 | N |
| Set 2 | 4000 | 10000 | 6000 | N |
| Set 3 | 6000 | 12000 | 6000 | N |
| Set 4 | 2000 | 4000 | 2000 | N |
| Set 5 | 4000 | 6000 | 2000 | N |
| Set 6 | 6000 | 8000 | 2000 | N |
| Set 7 | 8000 | 10000 | 2000 | N |
| Set 8 | 10000 | 12000 | 2000 | N |

### *3.3.4.2 Measurement accuracy*

The manufacturer data sheets contain values for elongation, force, and speed accuracy, as presented in Table 47. The force accuracy is stated as valid only for total tensile loads between 1 kN and 20 kN.

**Table 47: Equipment data for the W20K-W and PS50C, obtained from manufacturer data sheets.**

| W20K-W | | |
|---|---|---|
| Elongation Accuracy | 1 | % |
| Force Accuracy | 1 | % |
| Speed Accuracy | 1 | % |
| Elongation Resolution | 0.01 | mm |
| Force Resolution | 0.625 | N |
| PS50C | | |
| Elongation Accuracy | 1 | % |
| Elongation Resolution | 0.1 | µm |

In order to verify that the testing equipment perform as prescribed by the data sheets, a set of tests were initially conducted using two generic materials; an aluminium alloy and a fully annealed steel that both have been tested previously on multiple occasions. However, data

sheets for the materials were not available, and the verification is thereby only valid in regards to repeatability and stability of the measurements. Systemic error may still affect the test equipment and the results.

When measuring the elastic modulus, an initial preload of approximately 1000 N was applied to the aluminium and steel specimens. Once the preload was applied, the extensometer was mounted on the samples and the elongation value was reset.. Table 48 and Table 49 contain both the intervals and the results from the initial verification tests.

Based on the tensile force and elongation values, the elastic modulus was calculated for each test using the following form of Hooke's Law:

$$E = \frac{\Delta\sigma}{\Delta\varepsilon} = \frac{\frac{\Delta F}{A_0}}{\frac{\Delta l}{l_0}},$$

where $\sigma$ is the stress, $\varepsilon$ is the strain, $\Delta F$ is the differential force within an interval, $A_0$ is the cross-sectional area of the specimen, $\Delta l$ is the measured elongation within one interval, and $l_0$ is the length of the extensometer at zero elongation. The accuracy of the measurements were then approximated using standard deviation.

**Table 48: Elastic Modulus Results for Aluminum Alloy.**

| Legend | Set 1 | Set 2 | Set 3 | Unit |
|---|---|---|---|---|
| Number of Force Intervals | 3 | 7 | 1 | - |
| Magnitude of Force Interval(s) | 2000 | 1000 | 7000 | N |
| Total Minimum Force | 1000 | 1000 | 1000 | N |
| Total Maximum Force | 7000 | 8000 | 8000 | N |
| | | | | |
| Test 1 Elastic Modulus | 69354 | 69001 | 69919 | MPa |
| Test 2 Elastic Modulus | 69607 | 69173 | 70119 | MPa |
| Test 3 Elastic Modulus | 68544 | 69907 | 68782 | MPa |
| Test 4 Elastic Modulus | 69842 | 68924 | 69763 | MPa |
| Test 5 Elastic Modulus | 69719 | 69064 | 69513 | MPa |
| | | | | |
| Average Elastic Modulus | 69413 | 69214 | 69619 | MPa |
| Calculated Accuracy | 518 | 398 | 518 | MPa |

**Table 49: Elastic Modulus Results for Steel Alloy.**

| Legend | Set 1 | Set 2 | Unit |
|---|---|---|---|
| Number of Force Intervals | 4 | 4 | - |
| Magnitude of Force Intervals | 2000 | 2000 | N |
| Total Minimum Force | 9000 | 1000 | N |
| Total Maximum Force | 17000 | 9000 | N |
| | | | |
| Test 1 Elastic Modulus | 201164 | 207431 | MPa |
| Test 2 Elastic Modulus | 201046 | 204826 | MPa |
| Test 3 Elastic Modulus | 200227 | 204086 | MPa |
| Test 4 Elastic Modulus | 204706 | 206988 | MPa |
| Test 5 Elastic Modulus | 200453 | 207403 | MPa |
| Test 6 Elastic Modulus | 201053 | 208002 | MPa |
| | | | |
| Average Elastic Modulus | 201441 | 206456 | MPa |
| Calculated Accuracy | 1643 | 1600 | MPa |

The elastic modulus for the aluminium alloy has previously been measured to approximately 69-70 GPa, while the elastic modulus of the steel alloy has been measured to approximately 195-205 GPa. As shown, both the values for the aluminium and steel alloy were mostly within the expected ranges.

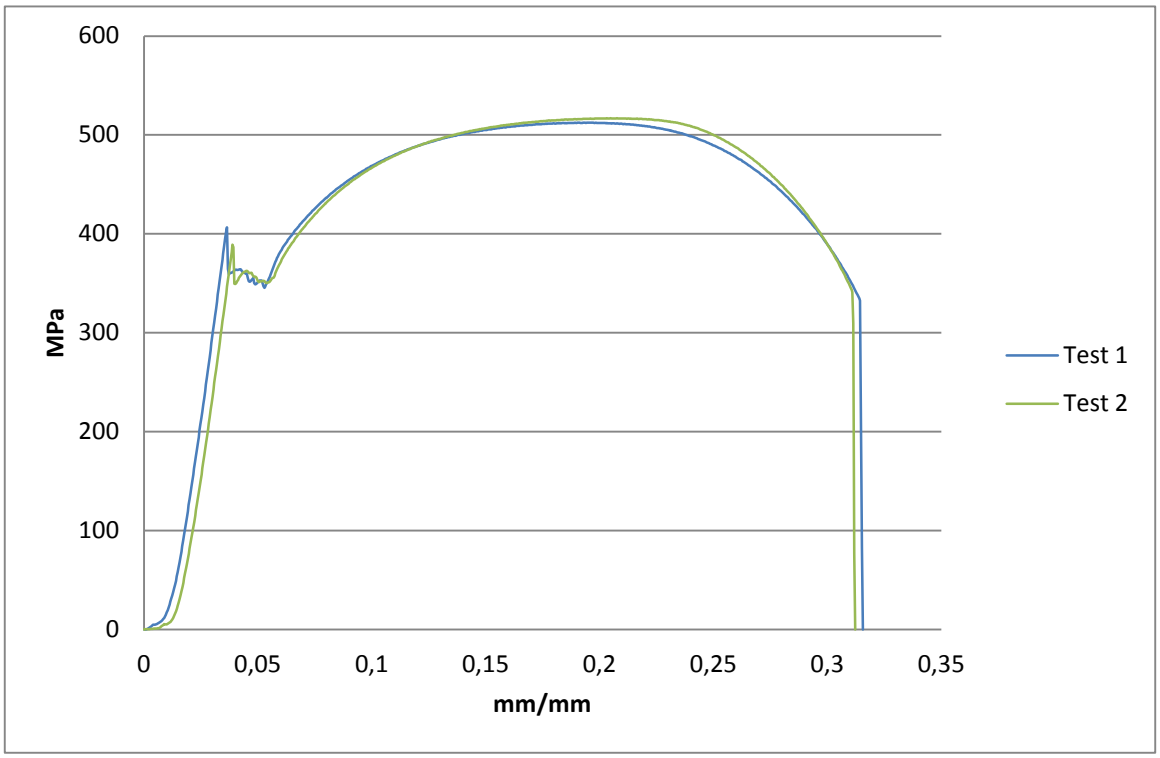


**Figure 50: Stress-Strain Curves for Generic Steel Alloy.**

The stress-strain curves obtained by testing the generic steel alloy until fracture are presented in Figure 50. As shown by the graph, no preload is applied at the start of the test, resulting in a

slight displacement of the two graphs in regards to strain. The difference in ultimate tensile strength between the two test specimens was found to be 4.3 MPa, which translates into approximately 0.85 percent of the average total value. Note that the low number of samples may cause the calculated accuracy to be inaccurate.

# 4 RESULTS

This chapter is split into five sections, where the three first are describing the results from the axisymmetric finite element model, the fourth section contains the stresses calculated according to the ASME Design Rules for Flanged Joints, and the within the fifth section one may find the results from the tensile testing of the UNS S31803 alloy. The results presented in each section will only be briefly introduced, and then discussed in 5 DISCUSSION.

## 4.1 Effect of Bolt Loads

The stress distributions for the axisymmetric flange model under varying bolt loads are presented in Figure 51. As shown, the stress concentrations are centred around the gasket groove, which is presented in greater detail in Figure 52. Note that the bolt hole ring sections are not presented with the correct stress levels, as described in 3.1.1.6 Materials.

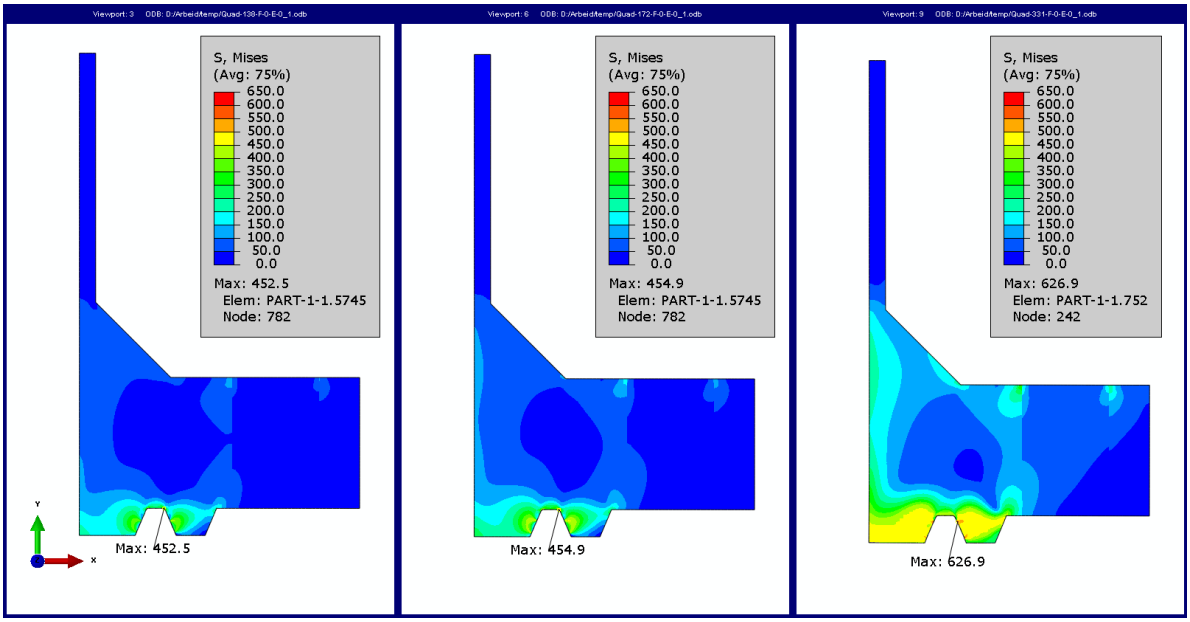


**Figure 51: Stress distribution of the flange at varying bolt stresses, no internal pressure, (left = 138 MPa bolt stress, middle = 172 MPa bolt stress, right = 331 MPa bolt stress).**

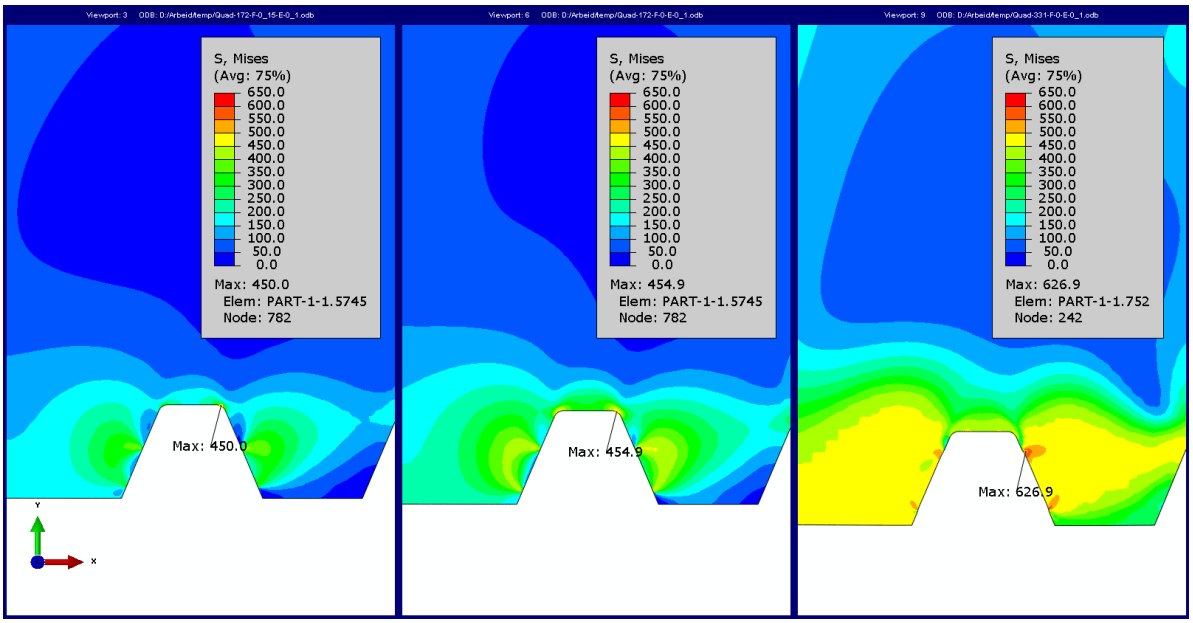


**Figure 52: Gasket groove stress distribution of the flange at varying bolt stresses, no internal pressure, (left = 138 MPa bolt stress, middle = 172 MPa bolt stress, right = 331 MPa bolt stress).**

The equivalent plastic strain of the axisymmetric flange model during bolt up with varying bolt loads are presented in Figure 53. An equivalent plastic strain of less than 0.5 percent will be displayed as grey.

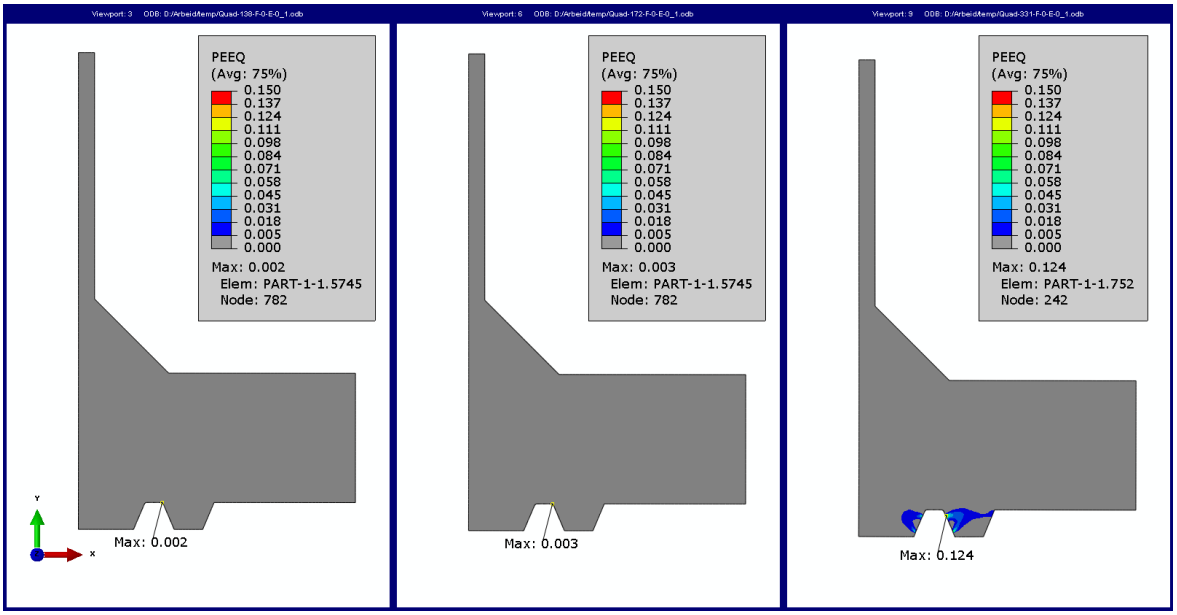


**Figure 53: Equivalent plastic strain of the flange at varying bolt stresses, no internal pressure, (left = 138 MPa bolt stress, middle = 172 MPa bolt stress, right = 331 MPa bolt stress).**

As the axisymmetric flange model only resulted in significant equivalent plastic strain when subjected to the load from 331 MPa bolt stress, that instance is presented in greater detail in Figure 54.

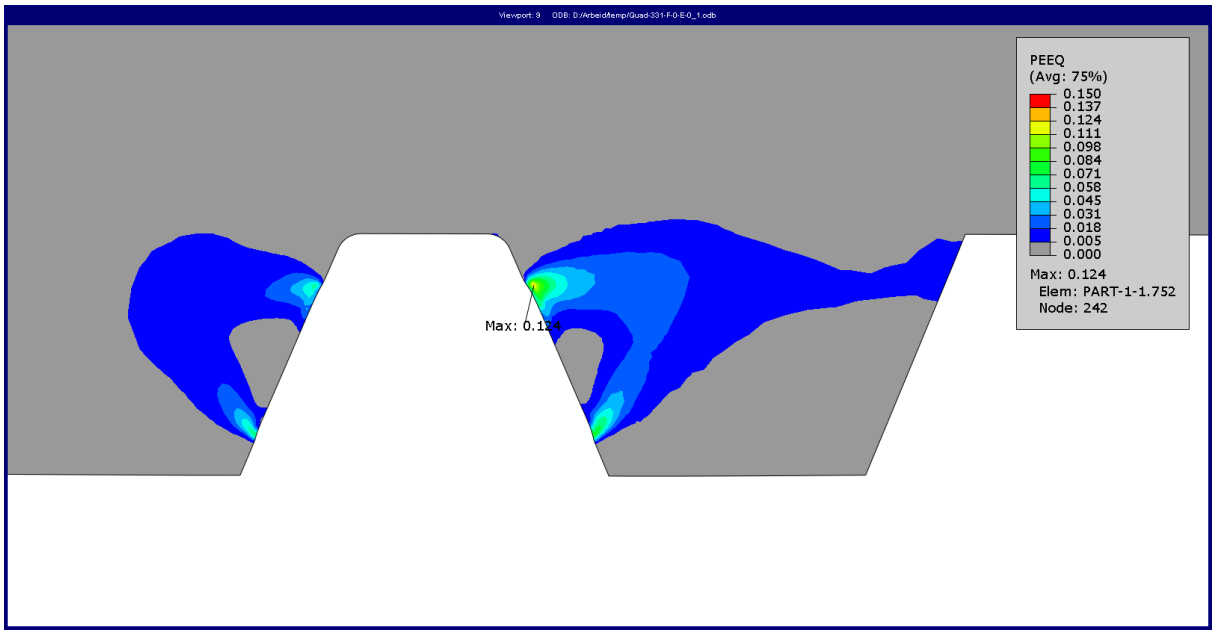


**Figure 54: Gasket groove equivalent plastic strain at 331 MPa bolt stress, no internal pressure.**

The equivalent plastic strains of the gasket ring for varying bolt loads are presented in Figure 55. Note that the contour plots are more or less symmetric due to the absence of internal pressure.

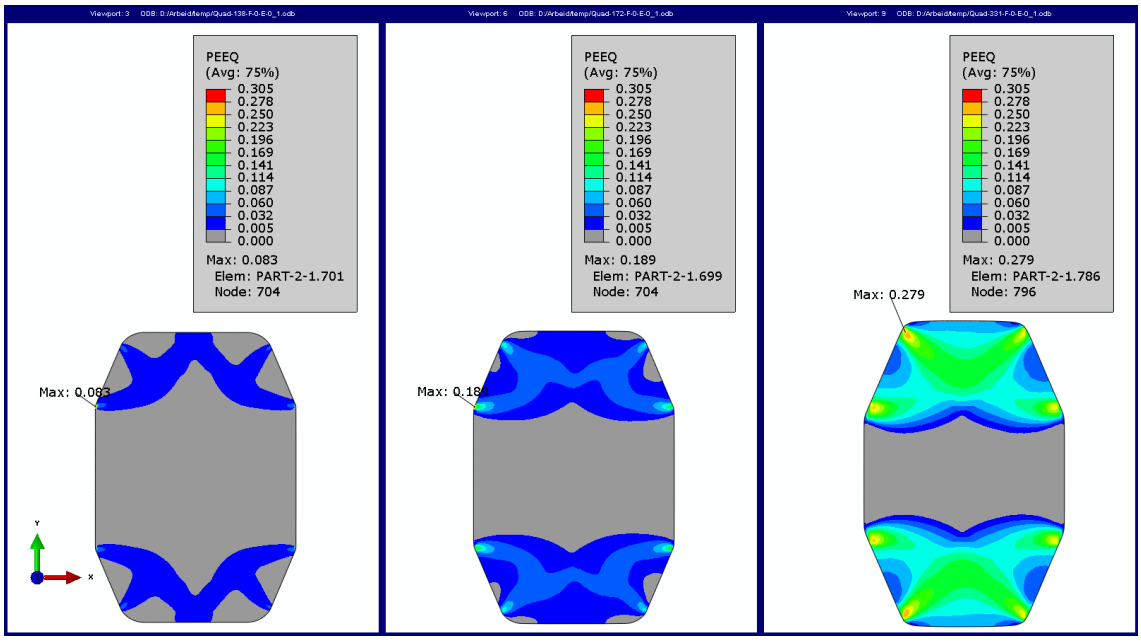


**Figure 55: Equivalent plastic strain of the gasket ring at varying bolt stresses, no internal pressure, (left = 138 MPa bolt stress, middle = 172 MPa bolt stress, right = 331 MPa bolt stress).**

The contact pressures at the top left and top right gasket groove contact surfaces are presented for varying bolt loads in Figure 56. The node number is zero at the face of the flange, and then increases node by node until the start of the fillet at the bottom of the gasket groove.

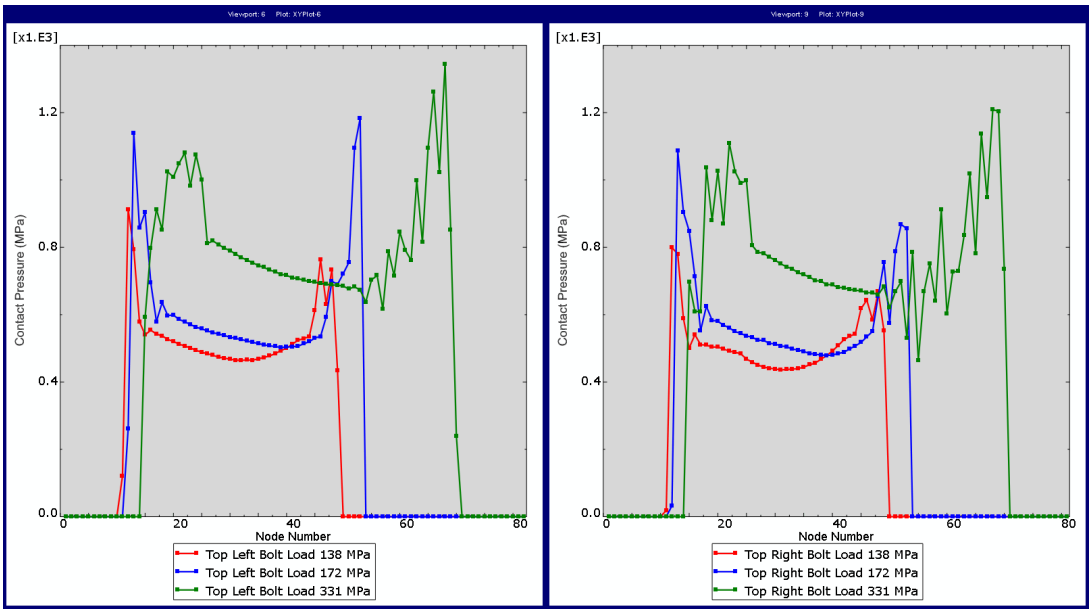


**Figure 56: Contact pressure for the top left and top right gasket groove at varying bolt stresses, no internal pressure, (left = 138 MPa bolt stress, middle = 172 MPa bolt stress, right = 331 MPa bolt stress).**

## 4.2 Effect of Internal Pressure

The maximum Von Mises flange stresses versus the different pressurized steps are presented in Figure 57 for the defined bolt stresses. Note that the location of maximum Von Mises stress changes to the pipe section in step four and five for 138 MPa bolt stress. The same occurs in step five for 172 MPa bolt stress.

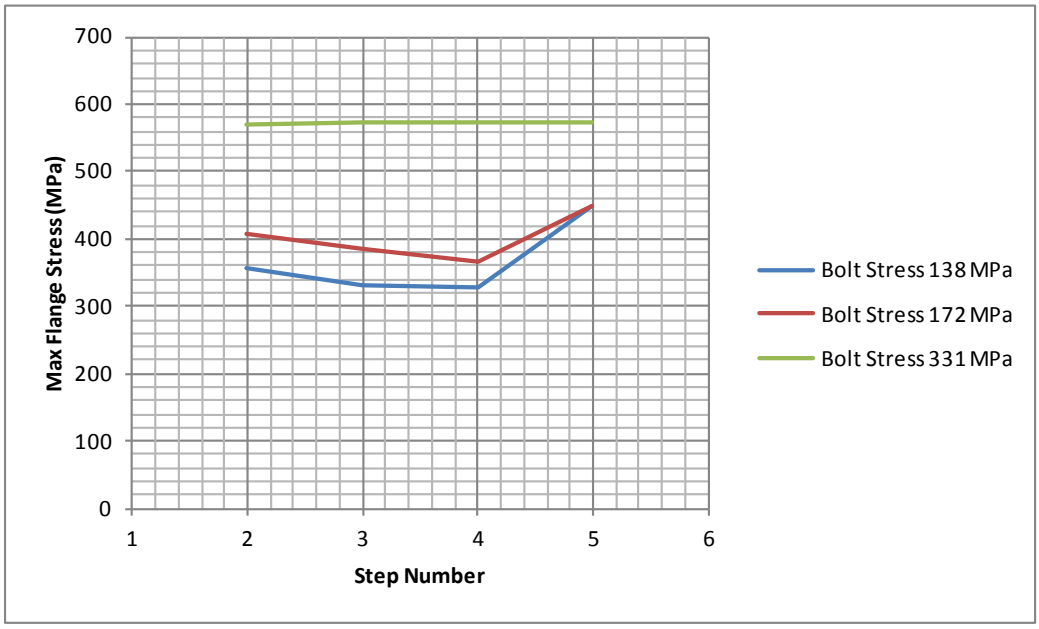


**Figure 57: Maximum Von Mises flange stress versus step number, for varying bolt stresses.**

The contact pressures for the defined bolt loads and pressure steps are presented in Figure 58 through Figure 60. The node numbers are defined the same way as for Figure 56. Note the asymmetric distribution of contact pressure that occurs, especially on the right (outer) gasket groove contact surface. The exception is the contact pressures for the 331 MPa bolt stress, presented in Figure 60.

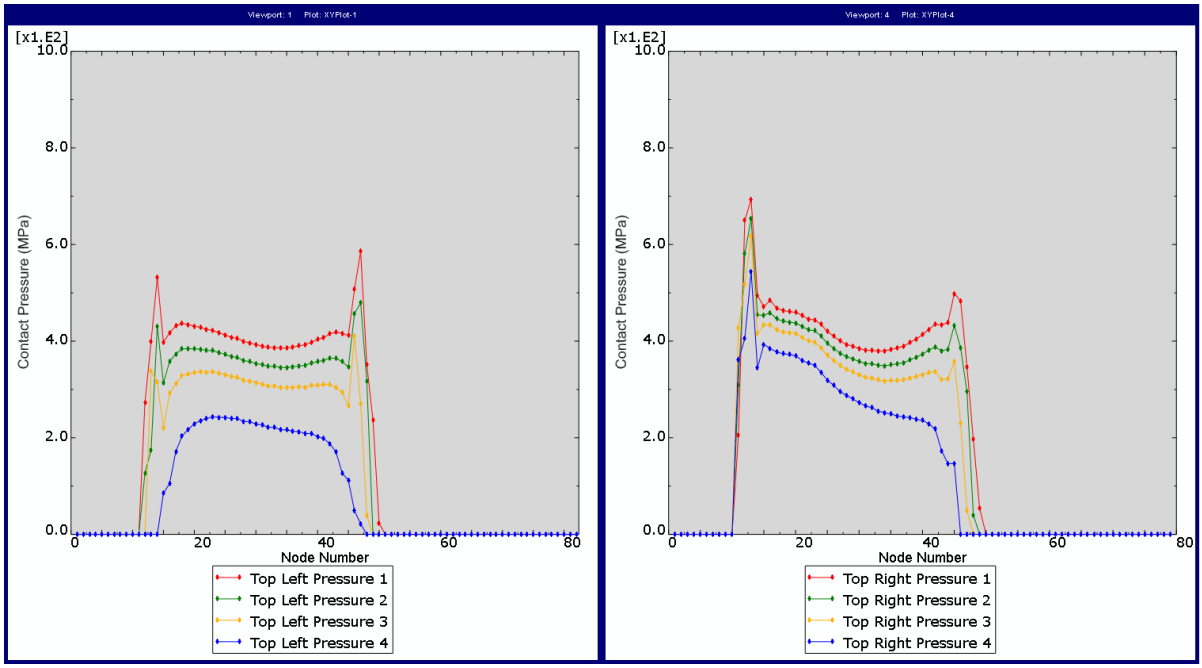


**Figure 58: Contact pressures for top left and top right gasket groove of assembly, for 138 MPa bolt stress.**

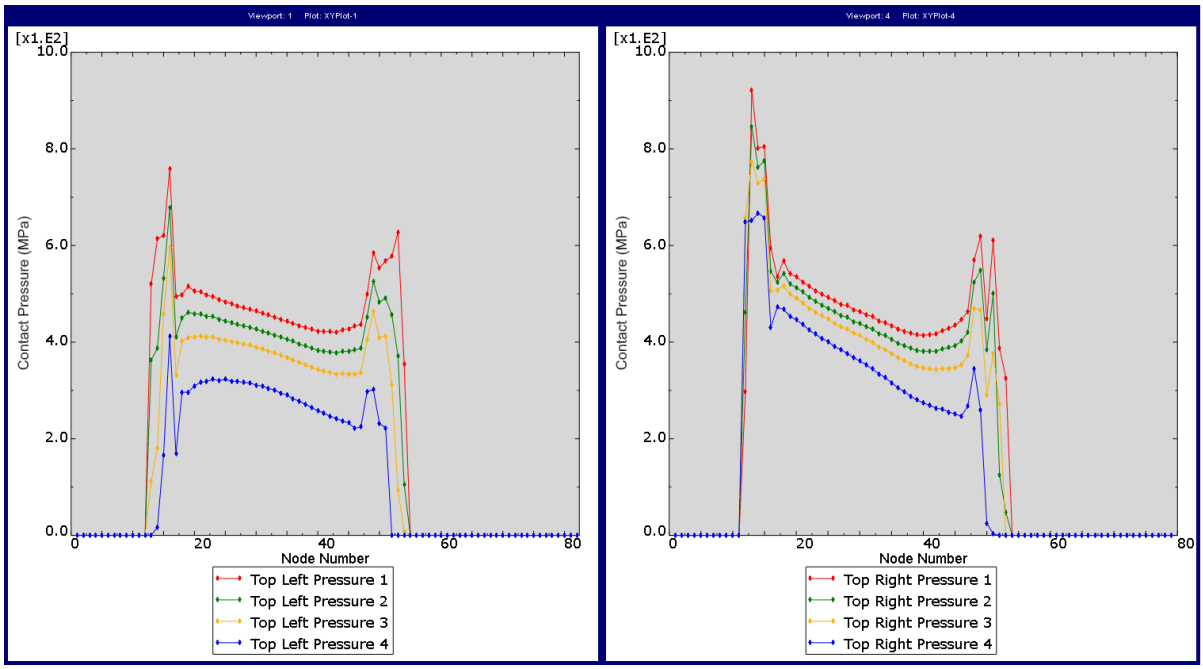


**Figure 59: Contact pressures for top left and top right gasket groove of assembly, for 172 MPa bolt stress.**

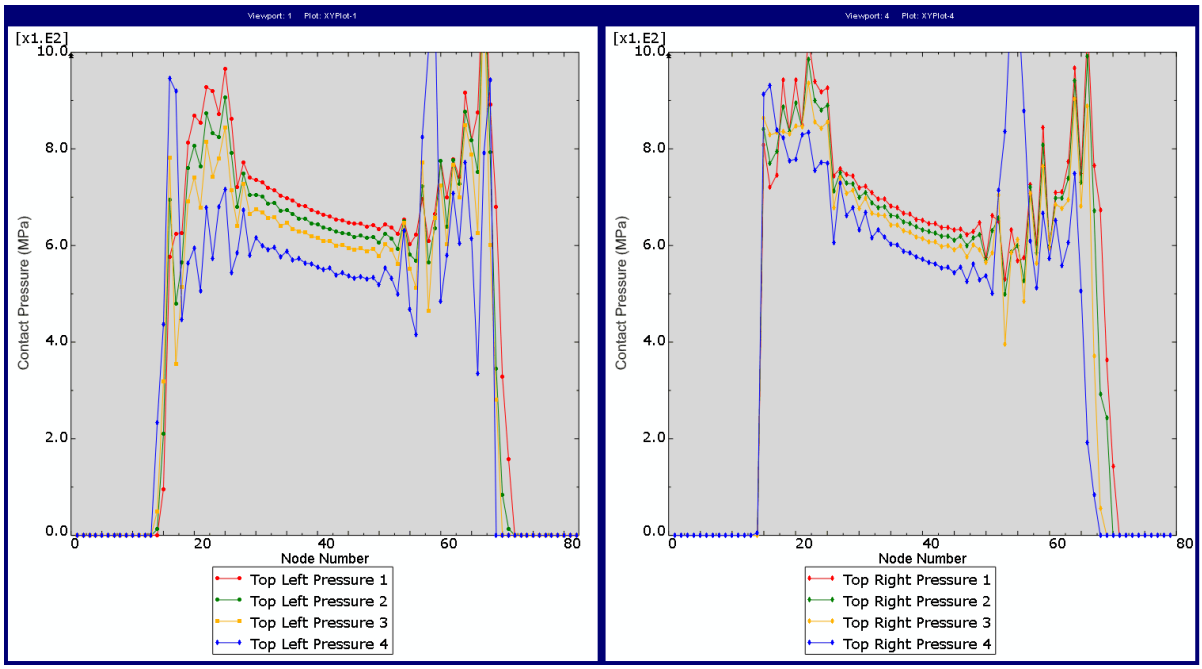


**Figure 60: Contact pressures for top left and top right gasket groove of assembly, for 331 MPa bolt stress.**

## 4.3 Effect of Friction

The effect of friction on the integrity of flanged joints has been investigated in this thesis, and is split into split into two section; the first section describes the influence of bolt loads with friction, and the second section describes internal pressures with friction present.

### 4.3.1 Bolt loads with friction

The Von Mises stress distribution of flanges with varying degree of friction is presented in Figure 61. Note that while the maximum stress level only decreases slightly, there is a significant reduction in the overall stress distribution surrounding the gasket groove.

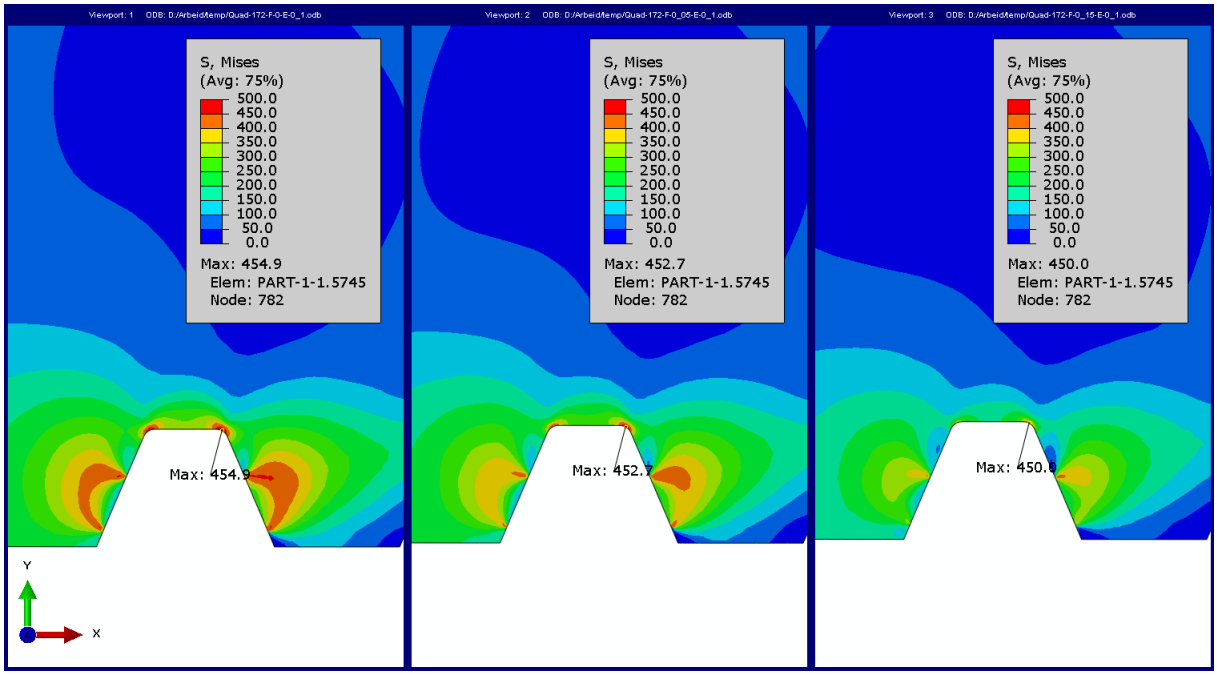


**Figure 61: Stress distribution for 172 MPa bolt stress with varying coefficient of friction, no internal pressure, (left: μ = 0, middle: μ = 0.05, right: μ = 0.15).**

Figure 62 illustrates the maximum Von Mises stress in the flange for varying coefficients of friction and bolt stresses. While the maximum stress remains more or less constant for 172 MPa bolt stress, there is a noticeable decrease in stress for the other two bolt stress values as the coefficient of friction increases. The Von Mises contour plots for the 138 MPa and 331 MPa bolt stress may be found in Appendix F: Additional Abaqus Results for Varying Friction, listed as Figure 86 and Figure 87.

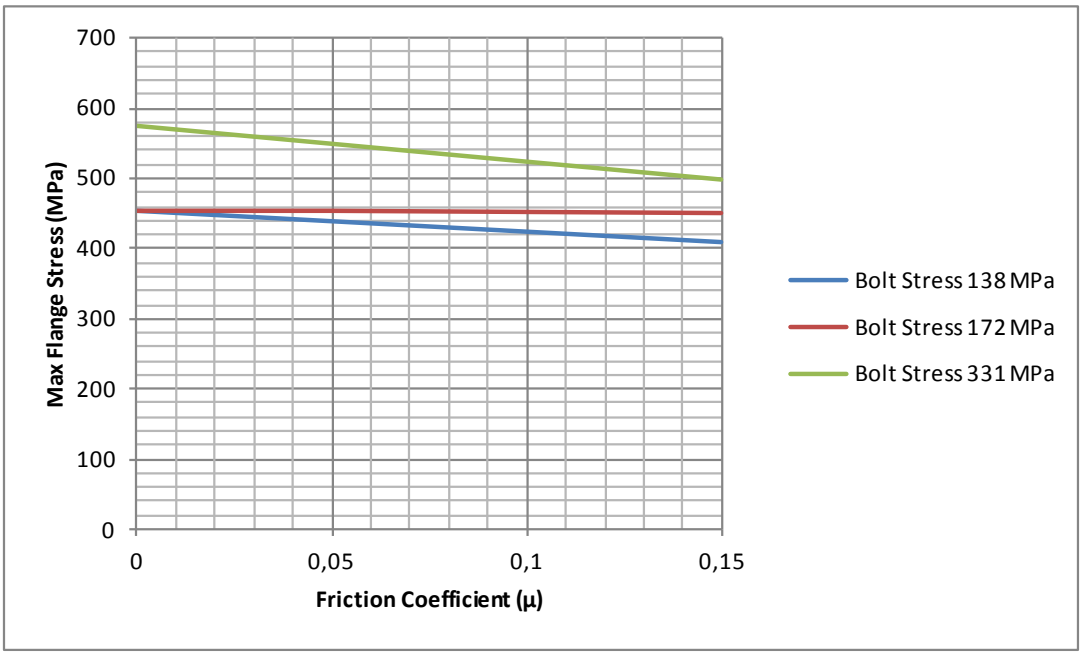


**Figure 62: Maximum flange stress versus friction coefficient, for varying bolt stresses, no internal pressure.**

As described above, the presence of friction has been observed to reduce the stress levels surrounding the gasket groove, and as a result, the equivalent plastic strain is also reduced. The equivalent plastic strain for 331 MPa bolt stress and a friction coefficient of 0.15 is presented in Figure 63. Note that the equivalent plastic strain observed in Figure 54 is significantly reduced in the presence of friction. As before, any equivalent plastic strain below 0.5 percent is shown as grey.

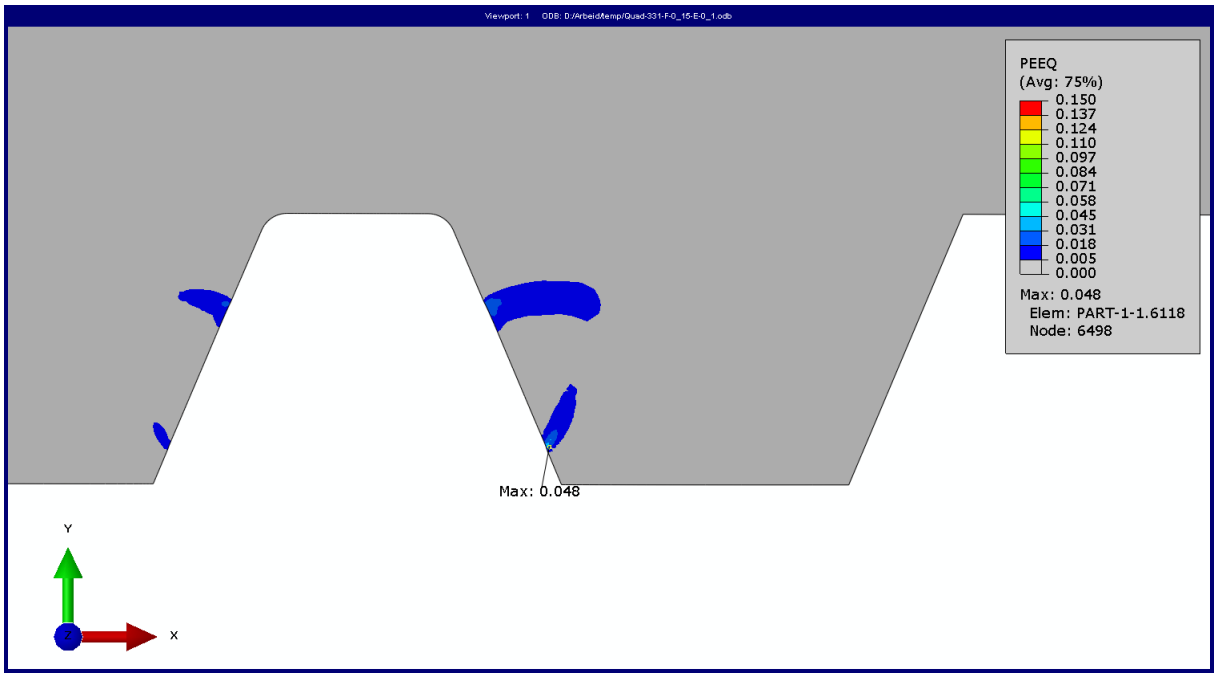


**Figure 63: Equivalent plastic strain for 331 MPa bolt stress with μ = 0.15, no internal pressure.**

### 4.3.2 Internal pressure with friction

The maximum Von Mises stress versus step number is presented for varying coefficient of frictions in Figure 64. The full contour plots may be found in Appendix F: Additional Abaqus Results for Varying Friction, listed as Figure 88, Figure 89, and Figure 90. Note that the degree of relaxation found in the gasket ring to flange contact seems to decrease with increasing coefficient of friction. At a coefficient of friction equal to 0.15, the maximum Von Mises changes little in spite of increasing pressures counteracting the bolt load.

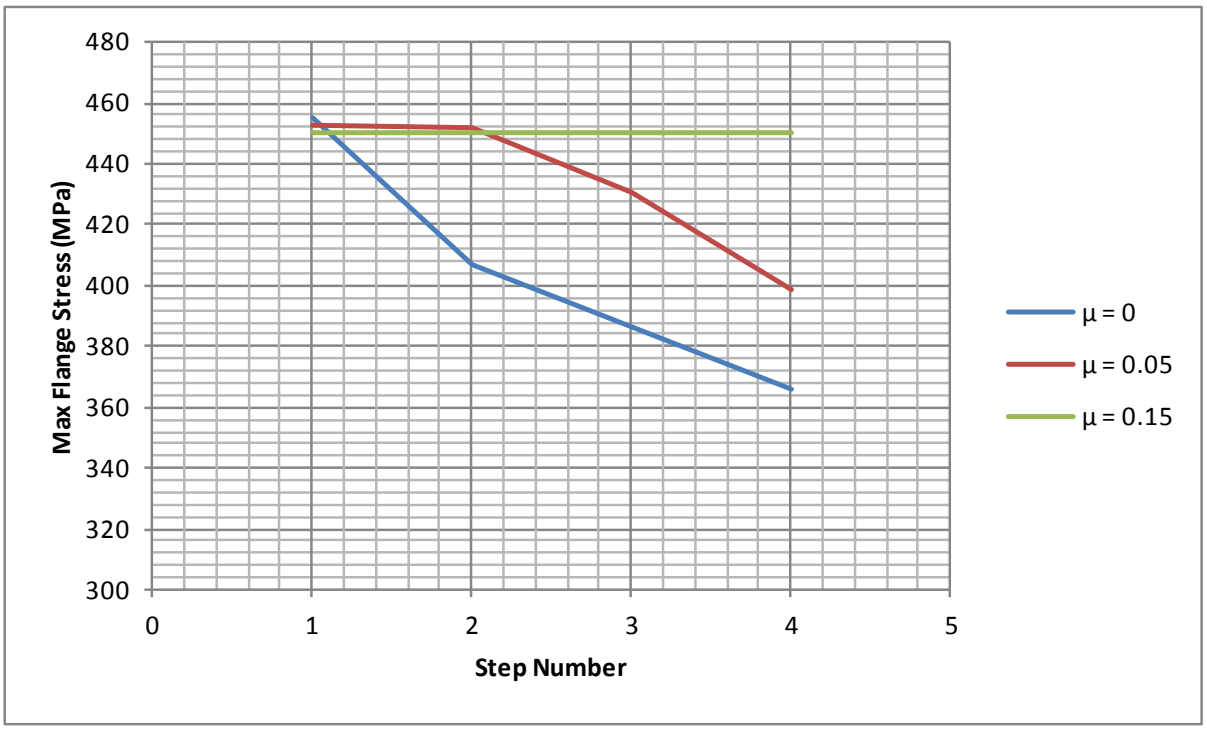


**Figure 64: Max flange stress versus steps for varying coefficient of friction, for 172 MPa bolt stress.**

The contact pressures of contact with and without friction are compared in Figure 65 and Figure 66, where the friction coefficient is set to 0.15 for the frictional case. The node numbers are distributed in the same manner as previously described for other contact pressure graphs.

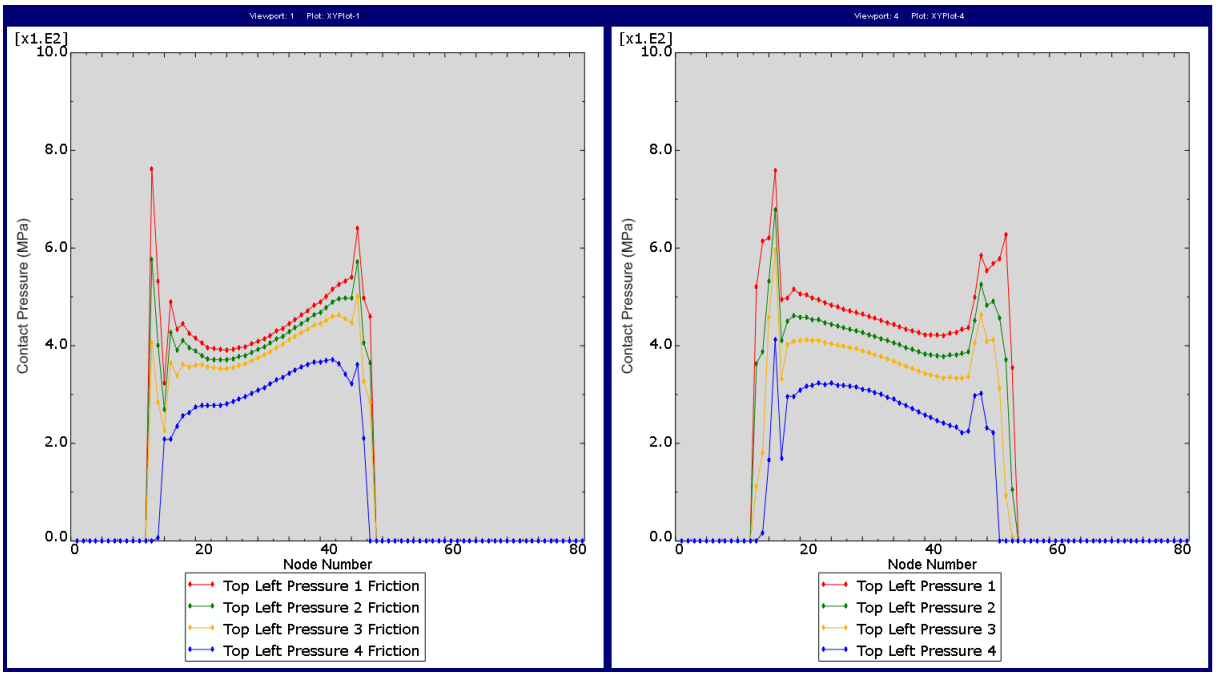


**Figure 65: Contact pressures of top left gasket groove surface for varying internal pressures, for 172 MPa bolt stress, (left: μ = 0.15, right: μ = 0)**

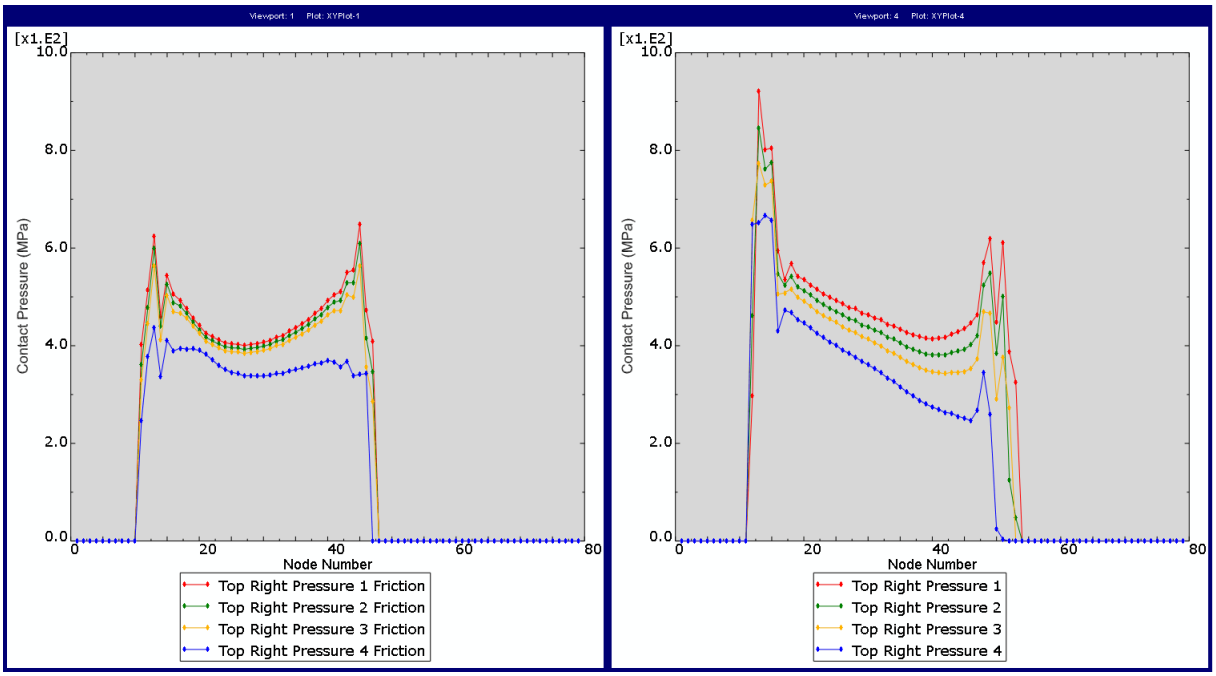


**Figure 66: Contact pressures of top right gasket groove surface for varying internal pressures, for 172 MPa bolt stress, (left: μ = 0.15, right: μ = 0).**

## 4.4 ASME Design Rules for Flanged Joints

As described in 2.4 Design Rules for Flanged Joints, the ASME design rules provide formulas for calculating the stresses in flanged joints. The flange axial hub stresses, radial stresses, and tangential stresses are presented in Table 50. As defined previously, case 1 uses the maximum allowable pressure defined by the ASME B16.5 standard, while case 2 uses 1.5 times the same pressure.

**Table 50: Calculated stresses from ASME design rules.**

| Name | Symbol | Case I | Case II | Unit |
|---|---|---|---|---|
| Hub Stress for Operating Conditions | $S_{Ho}$ | 77.06 | 115.60 | MPa |
| Radial Stress for Operating Conditions | $S_{Ro}$ | 104.56 | 156.85 | MPa |
| Tangential Stress for Operating Conditions | $S_{To}$ | 102.73 | 154.09 | MPa |
| Hub Stress for Gasket Seating Conditions | $S_{Hg}$ | 87.21 | 103.68 | MPa |
| Radial Stress for Gasket Seating Conditions | $S_{Rg}$ | 118.33 | 140.68 | MPa |
| Tangential Stress for Gasket Seating Conditions | $S_{Tg}$ | 131.64 | 120.13 | MPa |

The principle stresses found through the axisymmetric finite element model for the same case, are presented in Figure 67. Note that lower and upper limits equal to the respective calculated stresses are imposed on the contour plot. Stress values below the minimum are thereby shown as black, while stress values above the maximum are shown as grey. As shown, most of the stress concentrations surpassing the design rules' calculations are located around the gasket groove.

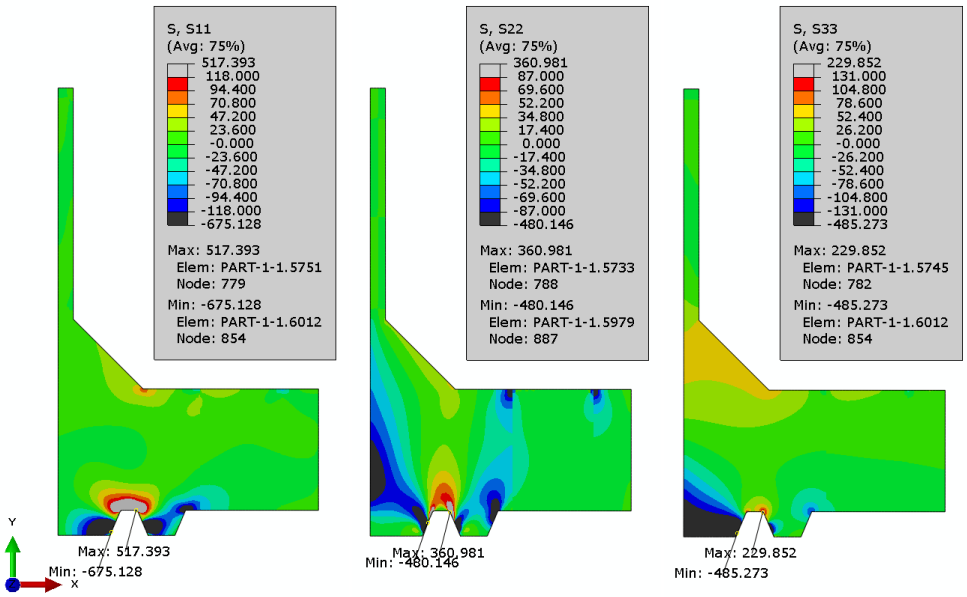


**Figure 67: Principle stresses for gasket seating with 138 MPa bolt stress, no internal pressure, (left: radial stresses, middle: axial stresses, right: tangential stresses).**

## 4.5 Tensile Testing of UNS S31803

The results from the tensile testing of the UNS S31803 alloy in forged bar product form are presented in two sections; the first section describes the results from the elastic tensile tests, and the second section describes the elastic-plastic stress-strain results.

### 4.5.1 Elastic modulus

The averaged elastic moduli for forged bar (UNS S31803) are presented in Table 51, and illustrated as a bar graph in Figure 68.

**Table 51: Averaged elastic moduli for forged bar (UNS S31803).**

| - | A | B1 | B2 | B3 | E | F | Unit |
|---|---|---|---|---|---|---|---|
| Average E (Set 1-3) | 192249 | 194939 | 189838 | 195983 | 198991 | 188123 | MPa |
| St. Dev. (Set 1-3) | 8433 | 401 | 2248 | 2820 | 1696 | 898 | MPa |
| Average E (Set 4-8) | 194763 | 191972 | 187873 | 194475 | 200045 | 184721 | MPa |
| St. Dev. (Set 4-8) | 16933 | 1513 | 2489 | 3411 | 1472 | 3021 | MPa |

It should be noted that the source data set for the specimen originating in part A have significant variations to it, causing a higher standard deviation. Also, the elastic moduli of specimen B2 and F, which both originate approximately the same radial distance from centre, are notable lower than the rest of the data set. This will be discussed further in 5 DISCUSSION.

.

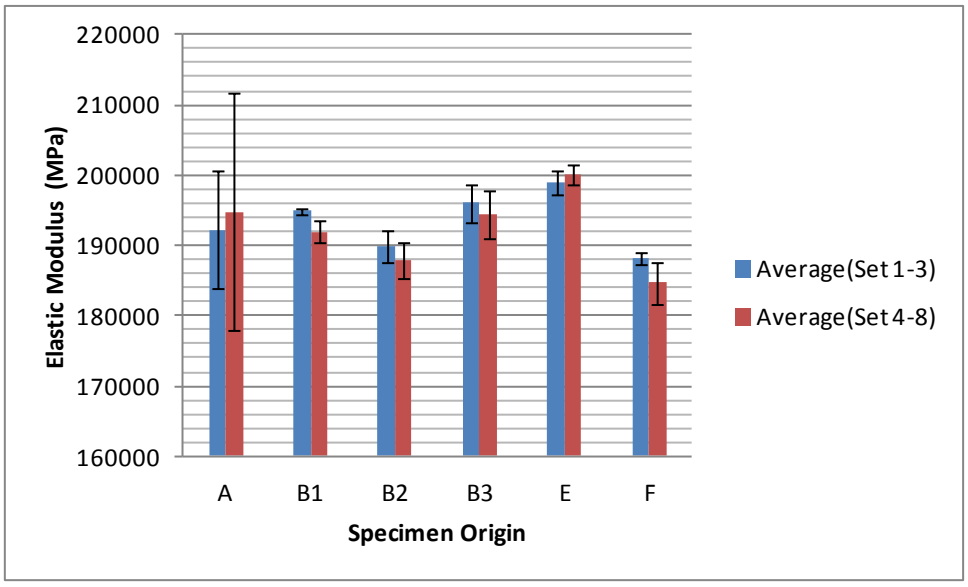


**Figure 68: Averaged elastic moduli with bars to indicate the standard deviation in the source data set.**

Figure 69 contains the elastic modulus test results for specimen A, obtained from the 250 mm diameter forged bar.

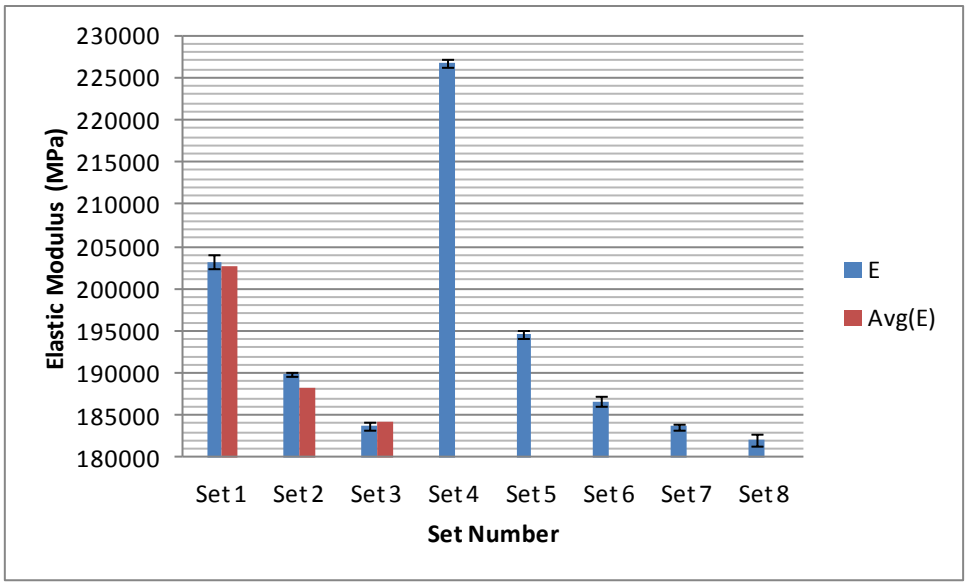


**Figure 69: Elastic modulus test results for specimen A from 250 mm diameter forged bar.**

The source data set may be found in Appendix G: Elastic Modulus Data for UNS S31803, and more detailed graphs may be found in Appendix H: Elastic Modulus Graphs for UNS S31803.

### 4.5.2 Stress-strain behaviour

The elastic-plastic stress-strain behaviour found through the tensile tests are presented in condensed form as averaged yield strength and ultimate tensile strength values, split into sub-sections based on specimen orientation. For the full range stress-strain graphs, please look to Appendix J: Stress-Strain Curves for UNS S31803, and for the data basis for the figures presented within this chapter, please see Appendix I: Stress-Strain Data for UNS S31803.

#### *4.5.2.1 Axial*

The yield strength and ultimate tensile strength values for the specimens of axial orientation are presented in this section. Figure 70 describes the yield and ultimate tensile strength of the specimens obtained from the 220 mm forged bar, while Figure 71 describes the same properties for 250 mm forged bar.

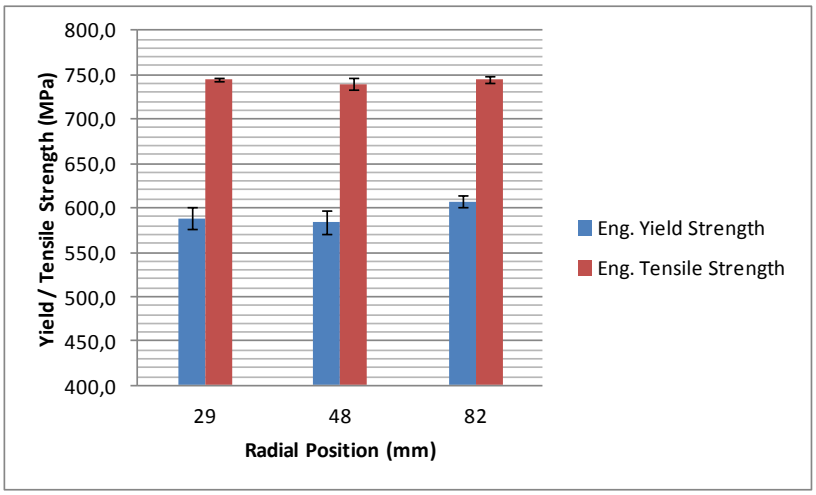


**Figure 70: Engineering yield strength and ultimate tensile strength for specimens of axial orientation, from the forged bar with diameter of 220 mm.**

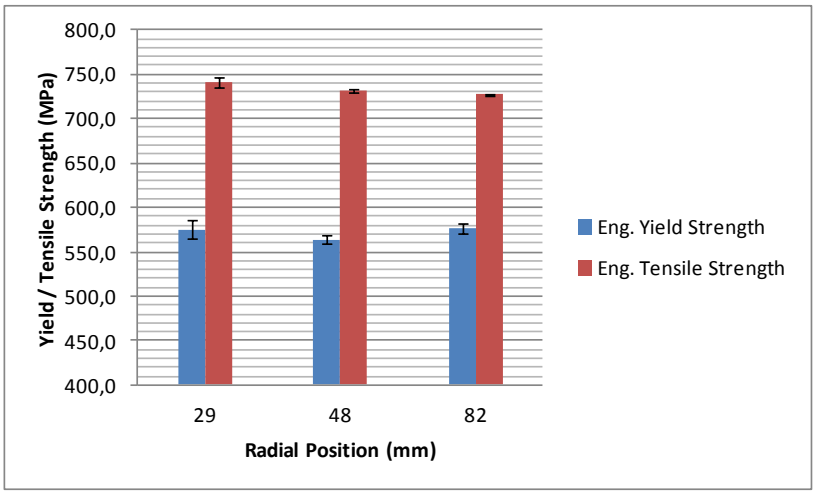


**Figure 71: Engineering yield strength and ultimate tensile strength for specimens of axial orientation, from the forged bar with diameter of 250 mm.**

### *4.5.2.2 Tangential*

The yield and ultimate tensile strength results from the specimens of tangential orientation are presented in this section. Figure 72 contains the result for the specimens obtained from the 220 mm diameter forged bar, and Figure 73 illustrates the results from the 250 mm diameter forged bar.

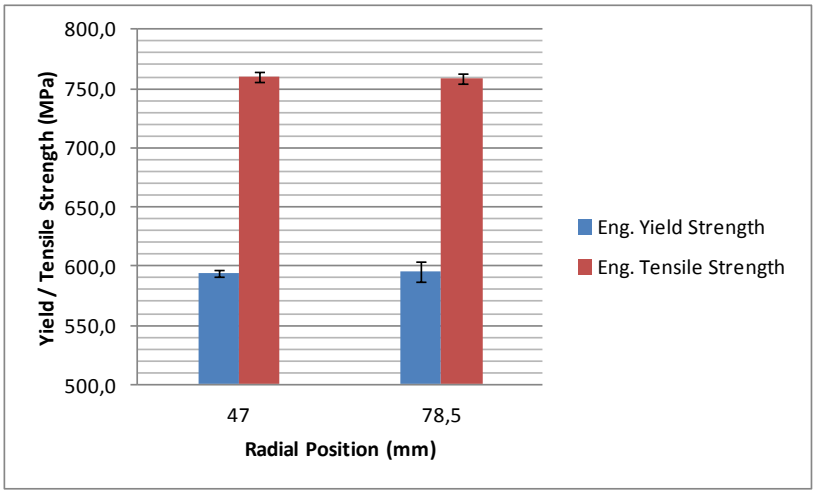


**Figure 72: Engineering yield strength and ultimate tensile strength for specimens of tangential orientation, from the forged bar with diameter of 220 mm.**

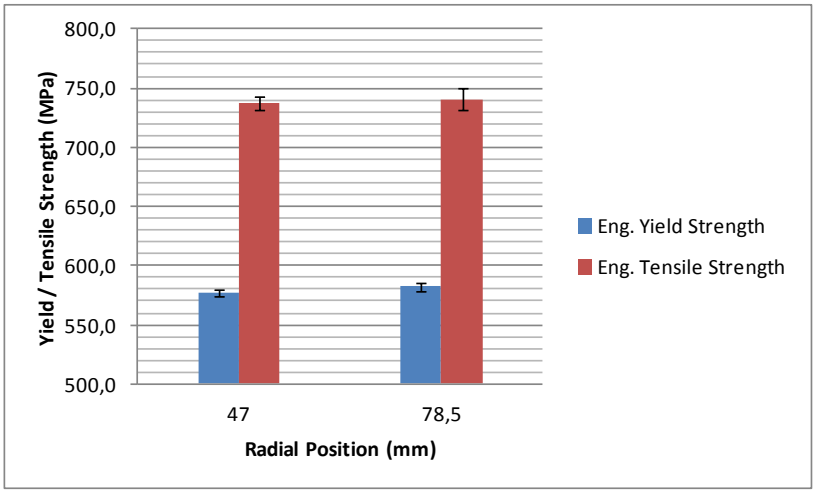


**Figure 73: Engineering yield strength and ultimate tensile strength for specimens of tangential orientation, from the forged bar with diameter of 250 mm.**

### *4.5.2.3 Radial*

This section contains the yield and ultimate tensile strength results for the specimens of radial orientation, which are presented in Figure 74 and Figure 75 for forged bar of 220 mm and 250 mm diameter respectively.

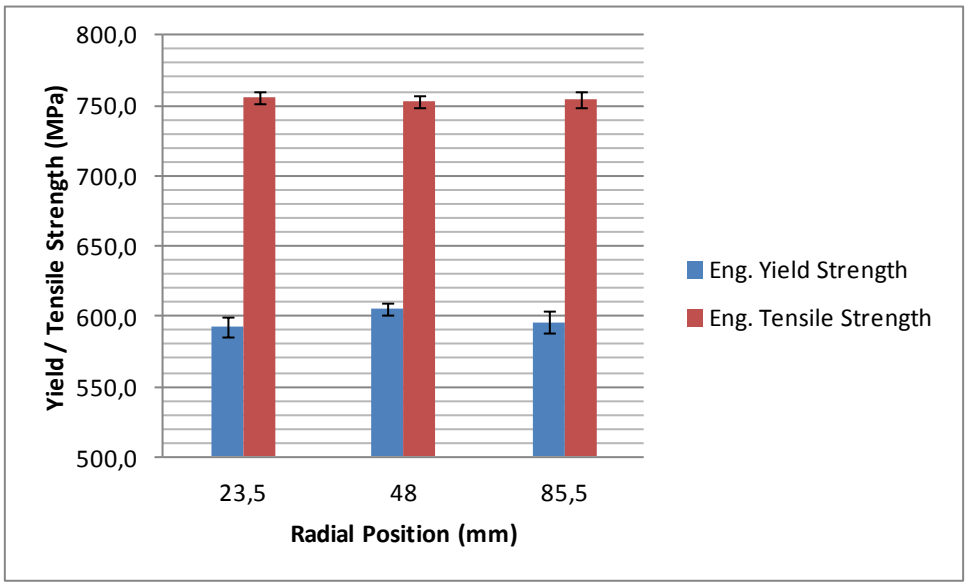


**Figure 74: Engineering yield strength and ultimate tensile strength for specimens of radial orientation, from the forged bar with diameter of 220 mm.**

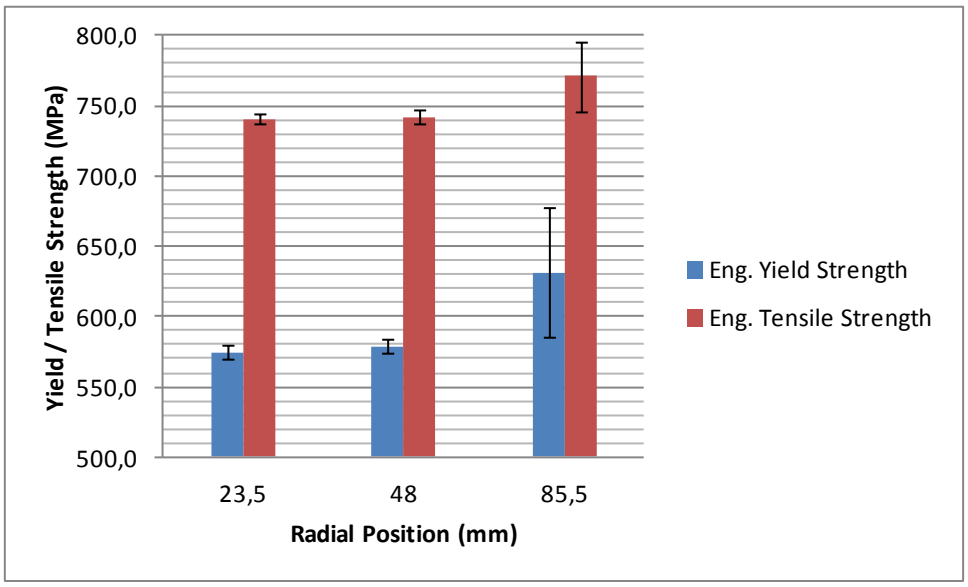


**Figure 75: Engineering yield strength and ultimate tensile strength for specimens of radial orientation, from the forged bar with diameter of 250 mm.**

Figure 76 shows the stress strain curve for the radial specimens from 85.5 mm radial position, which was obtained from the 250 mm diameter forged bar. Note the large variations in yield and ultimate tensile strength.

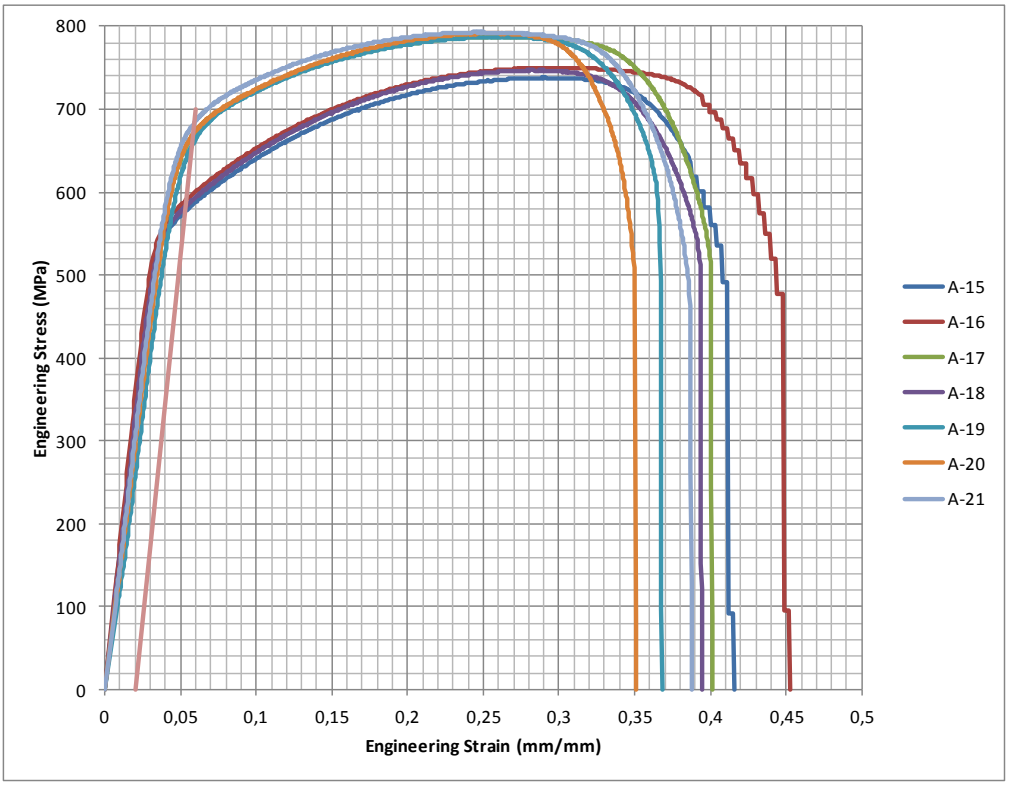


**Figure 76: Engineering stress-strain curve for radial specimens at 85.5 mm eccentricity, from 250 mm diameter forged bar.**

# 5 DISCUSSION

## 5.1 Axisymmetric Finite Element Models

The axisymmetric finite element models has shown that there is a significant potential for applying too high bolt loads to flanged joints, even with manual tools. Such high bolt loads might cause considerable plastic deformation in the flange, as shown in Figure 54. While the strain for this particular case is low compared to the fracture strain, it illustrates the need for correctly applied bolt loads at small flange dimensions. However, as shown in Figure 53, very little equivalent plastic strain occurs at the bolt loads equivalent to 138 MPa and 172 MPa bolt stress.

The simulations also indicate that the highest stress concentrations will be located at the gasket groove for both gasket seating and normal operating conditions. In the case of extraordinary operating conditions, such as overpressure tests and burst tests, the highest stress concentrations will eventually be found at the pipe section of the flange. This is due to pressure counteracting the bolt load, relieving some of the contact pressure in the gasket groove, and increasing the hoop stress in the pipe section of the flange. The pressure at which the transfer of highest stress occur, depend on the initial bolt stress, as well as the friction coefficient. However, at all studied cases, the transferred occurred at pressure levels outside the normal operating conditions.

As shown in Figure 61, an overall reduction in the stress levels was observed when friction was applied during initial bolting. However, only a slight to small reductions in maximum Von Mises stresses were observed for the same simulations. During the pressurized steps, friction has been shown to decrease the relaxation of the gasket groove material, causing the contact pressures to decrease less with increasing pressure. Still, the results indicate that this effect first comes into effect at higher than normal pressures. As the contact pressures for frictionless contacts are slightly higher than frictional contacts at normal pressures, the frictionless contact should be the preferred choice at normal operating conditions.

In the case of extreme bolt loads, the results presented in Figure 63 indicate that the presence of friction may reduce the degree of equivalent plastic strain. The friction will counteract the bolt load, and prevent the ring gasket from being forced as deep into the gasket groove. This is a beneficial side effect of friction in flanged joints, but again, it only applies to cases where there is high enough bolt loads to cause plastic deformations.

It is worth mentioning that the axisymmetric analyses are based upon assumed material models, and any property deviating from the assumed values may have a large impact on the results. Also, the models do not take into account effects such as fatigue and creep, which may have a significant impact on the integrity of a flanged joint. By nature, both the axisymmetric model and finite element modelling in general are approximations to real life systems, and there are thereby general inaccuracies attached to the method. This was studied by among others Hwang and Stallings (1992).

## 5.2 ASME Design Rules for Flanged Joints

The ASME design rules have previously been compared to axisymmetric finite element models by Nagata and Sawa (2007), and was found to be conservative in regards to calculated stress levels for most flange dimensions. However, the flanges studied were flat faced flanges, which are believed to have significantly different stress distributions than ring joint flanges. It should also be noted that Nagata and Sawa (2007) did not compare the stresses at the contact surface, only hub and flange body.

The principle stress distributions were thereby compared to the stress levels calculated according to the ASME design rules. As shown in Figure 67, there are several areas with higher absolute stress than predicted by the ASME design rules. However, most of them are located in proximity to the gasket groove. Two exceptions are found for the axial principle stress, one around the bolt to flange contact surface, and one in the bore wall inside the flange. In both these locations the principle stresses indicate that the material is being compressed, which is a natural result of bolt loads being applied and the gasket ring being forced into the gasket groove. Both of these locations were identified as areas of interest through initial simulations, and is the basis for the locations of the tensile specimens.

## 5.3 Tensile Testing of UNS S31803

The results presented in Figure 68, indicate that the elastic moduli range from 184 GPa to 200 GPa depending on specimen location and orientation. However, the results presented there are the averaged results based on several sets of tests at different load ranges, and the results are thereby only accurate if one makes the assumption that the modulus of elasticity is linear. The detailed results, shown in Figure 69, indicate a high non-linearity in that particular specimen, which is reflected by the high standard deviation shown in Figure 68. As the standard deviation of the individual sets is quite low for the detailed results, the high standard deviation of the averaged values originates from the large variations between sets.

The results also indicate that the elastic modulus is noticeable lower for specimen B2 and F, which both are located roughly the same radial distance from the centre of the forged bar. For the flange studied in this thesis, this is the same radial position as the gasket groove. These findings indicate that the elastic modulus chosen for the axisymmetric finite element model may be too high, which in turn may have reduced the accuracy of the results.

The elastic-plastic stress-strain data are presented as yield and ultimate tensile strength values in Figure 70 through Figure 75 for both the 220 mm and 250 mm diameter forged bars. The results presented indicate that especially the yield strength, but also the ultimate tensile strength, are noticeable lower for the specimens originating from the 250 mm diameter forged bar. The exception is radial specimens of 85.5 mm eccentricity. However, as shown in Figure 76, large variations were observed in the data from this particular set. The specimens seem to yield results in one of two ranges, indicating that there is common influences acting on some of the specimens. A possible source for this variation might be work hardening that occurred during machining, or potentially heating due to lack of cooling fluid. Note that no visible signs of differences were detected when the specimens were inspected prior to testing.

The yield and ultimate tensile strength were found to be considerably higher than the minimum requirements set forth by ASTM (2011b) A479/A479M, which was to be expected. However, the results also indicate that the manufacturer data sheets, found in Appendix K: Manufacturer Data Sheets for Forged Bar, are conservative compared to the actual results. This poses the question, is there a systemic error to the testing procedure, or are the manufacturers conservative in order to be sure that the product are of sufficient strength.

The minimum yield strength found throughout the tensile tests were 563.9 MPa for the 250 mm diameter forged bar, and 584 MPa for the 220 mm diameter forged bar. The maximum Von Mises stress found through the axisymmetric models, which was approximately 455 for the 172 MPa bolt stress. A safety factor of 1.28 may be calculated for the 220 mm diameter forged bar, and 1.24 for the 250 mm diameter forged bar. However, it should be noted that these maximum stresses are as previously discussed, highly localized, and the overall stress in the flange is far lower. It is believed that small local plastic deformation in the gasket groove will not pose any structural risks, but may change the sealing properties of the gasket contact. However, this does not seem to be the case in studied cases where extreme bolt load has been applied and subsequent plastic deformation has occurred.

# 6 CONCLUSION

The axisymmetric models indicate that the maximum Von Mises stress is within or slightly above the minimum material yield strength established by the ASTM (2011b) A479/A479M standard. The maximum Von Mises stresses were found to be the most severe during gasket seating conditions, and were found to be located in and around the gasket groove.

It has also been shown that the presence of friction may reduce the plastic deformation at very high bolt loads. However, friction was also shown to reduce the overall contact pressure at the sealing surfaces, which may be interpreted as a reduction in sealing ability.

Little equivalent plastic strain, less than 0.5 percent, was found in the flange when the two lower bolt loads were applied. At the highest bolt load, some equivalent plastic strain was observed. No increase in equivalent plastic strain was observed during operating conditions.

The ASME design rules were found to predict conservative results for most of the flange body, with the exception of the stresses surrounding the gasket groove. The localized stresses caused by the sealing contacts were not adequately predicted by the design rules. However, the areas which these stresses are present are small compared to the overall area of the flange cross-section.

The elastic moduli for the forged bar has been found to be ranging from 184 GPa to 200 GPa. Some of the results indicated that there are parts of the forged bar where the elastic modulus is highly non-linear, which is not considered by the axisymmetric model. Also, a lower elastic modulus was found at approximately 48 mm radial eccentricity, both for the tangential and longitudinal orientation.

The yield and ultimate tensile strengths were found to be above the values presented in the manufacturer data sheet, as well as the assumed material properties. Safety factors of 1.28 and 1.24 were calculated for yield strength of 220 mm and 250 mm diameter forged bar respectively.

As for the integrity of DSS flanges manufactured from forged bar, the tensile tests show that the static strength is more than sufficient. However, further research should be conducted into the fatigue and creep behaviour of the forged UNS S31803 forged bar product form, as well as experimental verification of the axisymmetric model. Corrosion properties should also be studied further, as inter granular corrosion may prove to affect the integrity of the flanged joint if exposed to corrosive mediums.

# REFERENCES


ASM INTERNATIONAL HANDBOOK COMMITTEE. 1990. *Volume 01 - Properties and Selection: Irons, Steels, and High-Performance Alloys*, ASM International Handbook Committee.

ASM INTERNATIONAL HANDBOOK COMMITTEE. 1998. *Metals handbook,* Materials Park, Oh., ASM International.

ASME 2007. Metallic Gaskets for Pipe Flanges. *B16.20.* The American Society of Mechanical Engineers.

ASME 2009. Pipe Flanges and Flanged Fittings. *B16.5.* The American Society of Mechanical Engineers.

ASME 2010. ASME Boiler and Pressure Vessel Code. New York, USA: ASME Boiler and Pressure Vessel Committee on Materials.

ASTM 2011a. Standard Specification for Forged or Rolled Alloy and Stainless Steel Pipe Flanges, Forged Fittings, and Valves and Parts for High Temperature Service. *A182/A182M.*

ASTM 2011b. Standard Specification for Stainless Steel Bars and Shapes for Use in Boilers and Other Pressure Vessels. *A479/A479M.*

ASTM 2011c. Standard Test Methods and Definitions for Mechanical Testing of Steel Products. *A370.*

BEDDOES, J. & PARR, J. G. 1999. *Introduction to Stainless Steels*, ASM International.

BLANDFORD, R. K., MORTON, D. K., SNOW, S. D. & RAHL, T. E. Tensile Stress-Strain Results for 304L and 316L Stainless Steel Plate at Temperature. 2007 ASME Pressure Vessels and Piping Division Conference, 2007. ASME.

DASSAULT SYSTÈMES 2010a. Abaqus Analysis User's Manual. *6.10.* Dassault Systèmes.

DASSAULT SYSTÈMES 2010b. Abaqus Theory Manual. *6.10.* Dassault Systèmes.

DASSAULT SYSTÈMES 2010c. Abaqus/CAE User's Manual. *6.10.* Dassault Systèmes.

HWANG, D. Y. & STALLINGS, J. M. 1992. Finite Element Analysis of Bolted Flange Connections. *Computers & Structures,* 51**,** 13.

JOHANNESSEN, J. 2002. *Tekniske Tabeller*, Cappelen.

MATEO, A., LLANES, L., AKDUT, N., STOLARZ, J. & ABGKADA, M. 2003. Anisotropy effects on the fatigue behaviour of rolled duplex stainless steel. *International Journal of Fatigue,* 25**,** 8.

MOVERARE, J. J. & ODÉN, M. 2002. Deformation behaviour of a prestrained duplex stainless steel. *Materials Science & Engineering,* A337**,** 14.

NAGATA, S. & SAWA, T. Comparison of Flange Stress Calculated by ASME Design Code and Finite Element Analysis. *In:* BOUZID, H. & MARTIN, J., eds. ASME Pressure Vessels and Piping Division Conference, 2007 San Antonio, Texas USA. ASME.

NORSOK 2004. Materials selection. *M-001.*

NS 1973. Hexagon bolts - Unified - Semifinished - UNC threads 1/4" to 1 1/2". *NS 963.* Standard Online Forlag.

OUTOKUMPU. 2012. *Duplex Stainless Steel* [Online]. Available: http://www.outokumpu.com/SiteCollectionDocuments/Duplex_Stainless_Grade_Data sheet.pdf [Accessed 12. May 2012].

ROLLASON, E. C. 1973. *Metallurgy for Engineers*, Edward Arnold (Publishers) Ltd.

ROLLED ALLOYS. 2012. *2205 Duplex Data Sheet* [Online]. Available: http://www.rolledalloys.com/products/duplex-stainless-steels/2205 [Accessed 12. May 2012].

SANDVIK MATERIALS TECHNOLOGY. 2012. *Sandvik SAF 2205* [Online]. Available: http://www.smt.sandvik.com/en/materials-center/material-datasheets/plate-and-sheet/sandvik-saf-2205/ [Accessed 12. May 2012].

SATO, T. & KADO, K. 2005. Inelastic Analysis of Dissimilar Material Flanges with Metal Ring Gaskets at Elevated Temperatures. *2005 ASME Pressure Vessels and Piping Division Conference.* Denver, Colorado, USA: ASME.

TMR STAINLESS 2009. Practical Guidelines for the Fabrication of Duplex Stainless Steel. London, UK: International Molybdenum Association (IMOA).

WRIGHT, D. 2005. *Fluid pressurised joints* [Online]. Department of Mechanical and Materials Engineering: The University of Western Australia. Available: http://school.mech.uwa.edu.au/~dwright/DANotes/threads/joints/joints.html [Accessed 17. May 2012].

# APPENDICES

## Appendix A: Original Stress Strain Data for 316L

**Table 52: Engineering stress-strain data (based on Blandford et al. (2007)).**

| Heat | Temp. | Ultimate Strength | Ultimate Strain | Yield Strength | Total Strain | Young's Modulus | Yield Strain |
|---|---|---|---|---|---|---|---|
| # | ˚C | MPa | mm/mm | MPa | mm/mm | GPa | mm/mm |
| 230468 | -28,9 | 790,8 | 0,498 | 267,5 | 0,652 | 198 | 0,00135 |
| | 21,1 | 568,1 | 0,591 | 199,3 | 0,751 | 195 | 0,00102 |
| | 148,9 | 473,7 | 0,356 | 175,8 | 0,470 | 186 | 0,00095 |
| | 315,6 | 443,3 | 0,316 | 149,6 | 0,413 | 175 | 0,00085 |
| | | | | | | | |
| 67K0 | -28,9 | 779,1 | 0,536 | 364,7 | 0,699 | 198 | 0,00184 |
| | 21,1 | 615,0 | 0,437 | 286,8 | 0,591 | 195 | 0,00147 |
| | 148,9 | 515,7 | 0,304 | 255,8 | 0,416 | 186 | 0,00138 |
| | 315,6 | 496,4 | 0,287 | 195,1 | 0,375 | 175 | 0,00111 |
| | | | | | | | |
| 48R8 | -28,9 | 780,5 | 0,637 | 346,8 | 0,794 | 198 | 0,00175 |
| | 21,1 | 645,4 | 0,585 | 259,9 | 0,766 | 195 | 0,00133 |
| | 148,9 | 515,0 | 0,326 | 160,6 | 0,459 | 186 | 0,00086 |
| | 315,6 | 471,6 | 0,316 | 182,0 | 0,410 | 175 | 0,00104 |
| | | | | | | | |
| 76H3 | -28,9 | 779,1 | 0,682 | 349,6 | 0,844 | 198 | 0,00177 |
| | 21,1 | 639,8 | 0,616 | 286,8 | 0,782 | 195 | 0,00147 |
| | 148,9 | 485,4 | 0,366 | 231,7 | 0,506 | 186 | 0,00125 |
| | 315,6 | 469,5 | 0,313 | 146,2 | 0,410 | 175 | 0,00084 |

**Table 53: True stress-strain data (based on Blandford et al. (2007))**

| Heat | Temp. | Ultimate Strength | Ultimate Strain | U. Plastic Strain | Yield Strength | Yield Strain |
|---|---|---|---|---|---|---|
| # | ˚C | MPa | mm/mm | mm/mm | MPa | mm/mm |
| 230468 | -28,9 | 1184,7 | 0,404 | 0,398 | 267,9 | 0,00135 |
| | 21,1 | 903,9 | 0,464 | 0,460 | 199,5 | 0,00102 |
| | 148,9 | 642,3 | 0,305 | 0,301 | 176,0 | 0,00094 |
| | 315,6 | 583,4 | 0,275 | 0,271 | 149,7 | 0,00085 |
| | | | | | | |
| 67K0 | -28,9 | 1196,7 | 0,429 | 0,423 | 365,4 | 0,00184 |
| | 21,1 | 883,8 | 0,363 | 0,358 | 287,2 | 0,00147 |
| | 148,9 | 672,5 | 0,265 | 0,262 | 256,1 | 0,00137 |
| | 315,6 | 638,9 | 0,252 | 0,249 | 195,3 | 0,00111 |
| | | | | | | |
| 48R8 | -28,9 | 1277,7 | 0,493 | 0,486 | 347,4 | 0,00175 |
| | 21,1 | 1022,9 | 0,461 | 0,455 | 260,3 | 0,00133 |
| | 148,9 | 682,9 | 0,282 | 0,278 | 160,8 | 0,00086 |
| | 315,6 | 620,6 | 0,275 | 0,271 | 182,2 | 0,00104 |
| | | | | | | |
| 76H3 | -28,9 | 1310,5 | 0,520 | 0,513 | 350,2 | 0,00176 |
| | 21,1 | 1034,0 | 0,480 | 0,475 | 287,2 | 0,00147 |
| | 148,9 | 663,0 | 0,312 | 0,308 | 232,0 | 0,00124 |
| | 315,6 | 616,5 | 0,272 | 0,269 | 146,3 | 0,00083 |

# Appendix B: Part Drawings with Dimensions

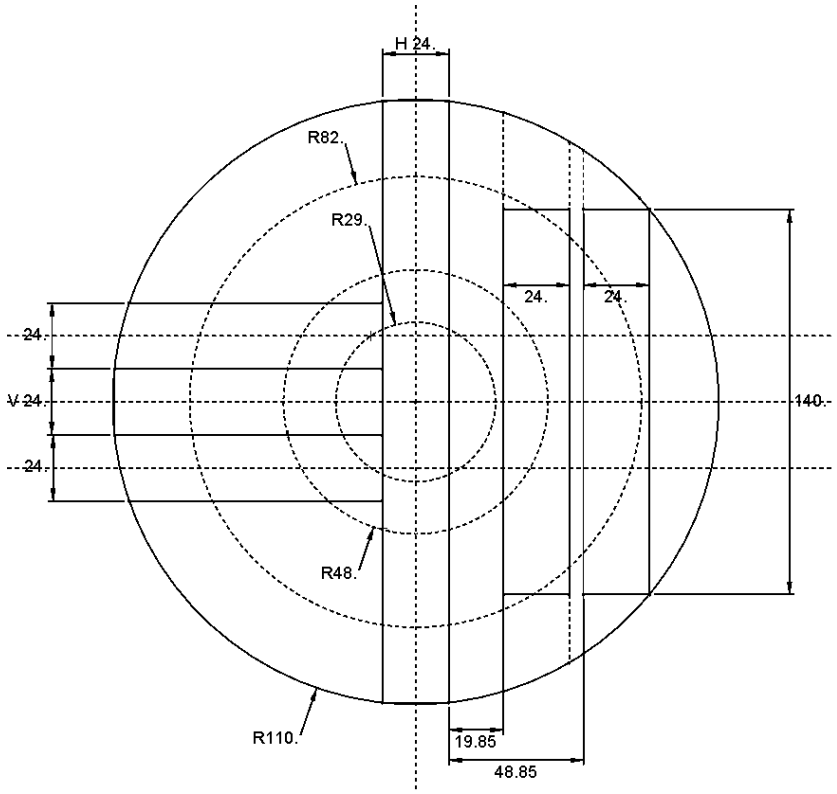


**Figure 77: Common layout for dividing the bar stock, with dimensions.**

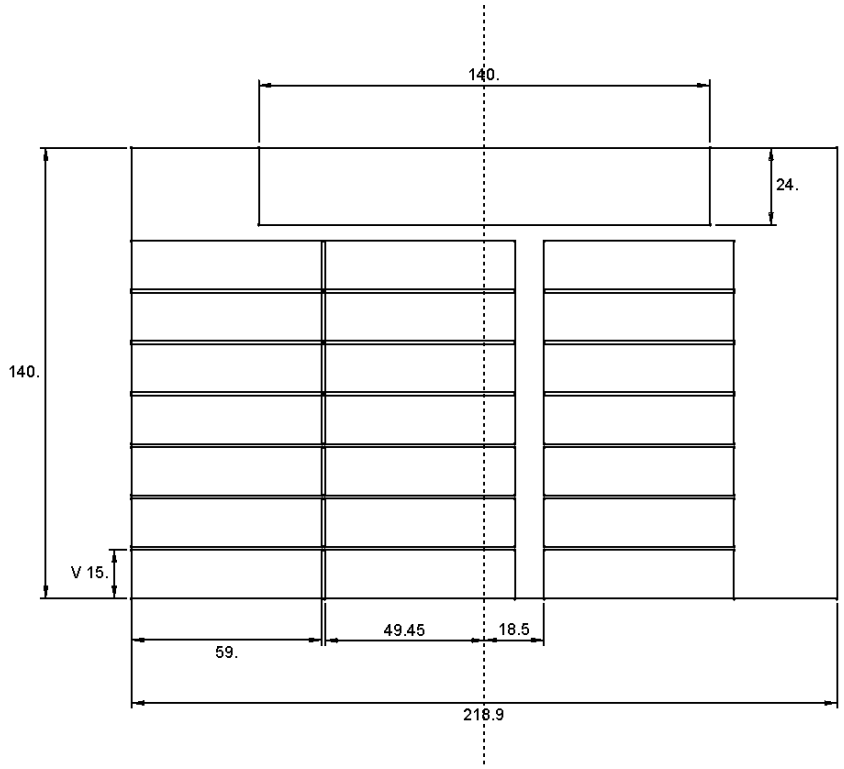


**Figure 78: Layout for part A, with dimensions.**

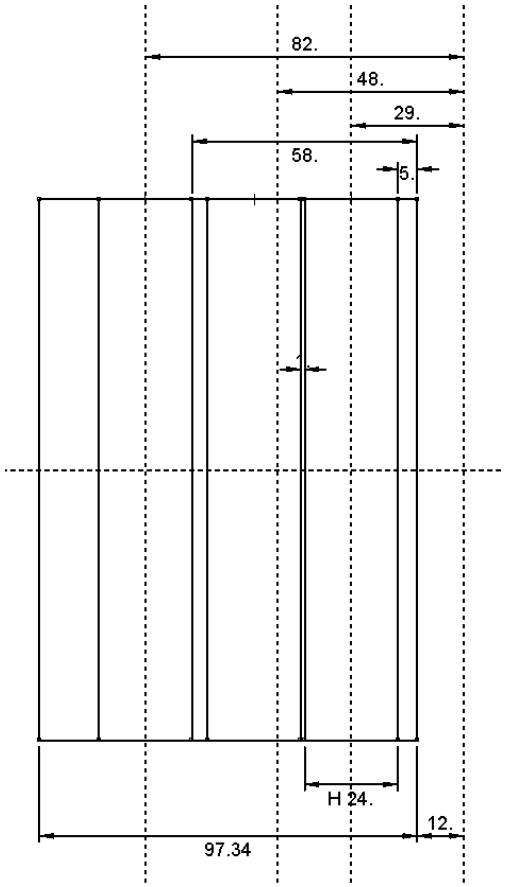


**Figure 79: Layout for part B, with dimensions.**

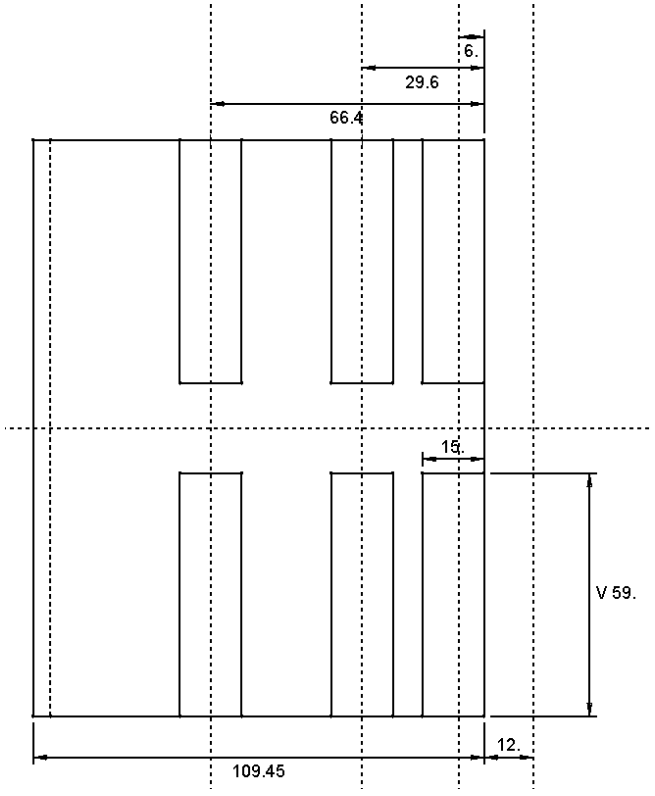


**Figure 80: Layout for part C and D, with dimensions.**

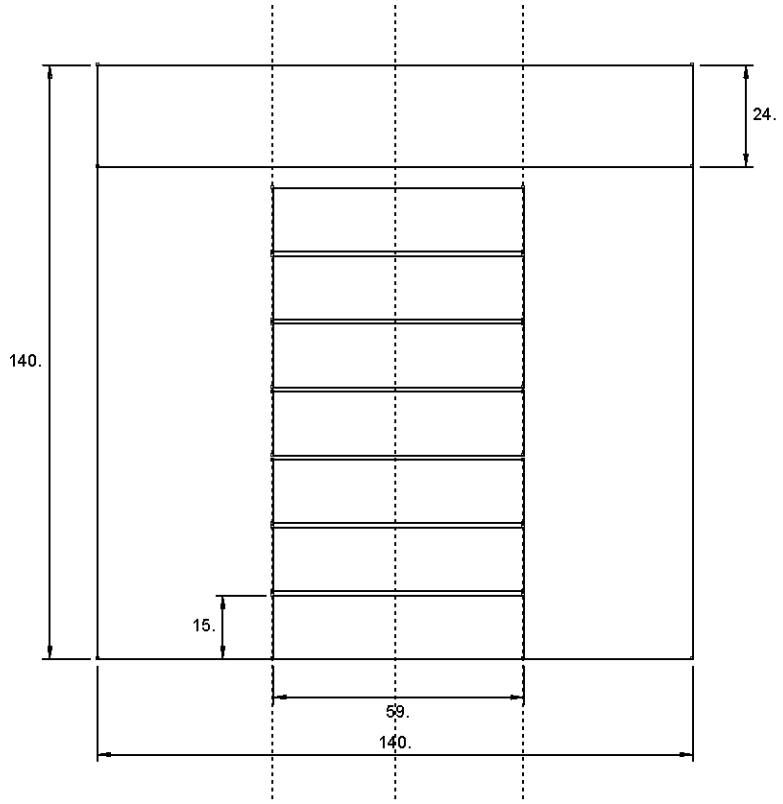


**Figure 81: Layout for part E and F, with dimensions.**

# Appendix C: Lists of Manufactured Specimens

**Table 54: List of specimens machined from 220 mm diameter bar stock.**

| Alignment | Type | Radial Pos. | Cut | ID | Status |
|---|---|---|---|---|---|
| Long | Small | 29 | C | 220-LS-C-01 | OK |
| Long | Small | 29 | C | 220-LS-C-02 | OK |
| Long | Small | 29 | D | 220-LS-D-01 | OK |
| Long | Small | 29 | D | 220-LS-D-02 | OK |
| Long | Small | 48 | C | 220-LS-C-03 | OK |
| Long | Small | 48 | C | 220-LS-C-04 | OK |
| Long | Small | 48 | D | 220-LS-D-03 | OK |
| Long | Small | 48 | D | 220-LS-D-04 | OK |
| Long | Small | 82 | C | 220-LS-C-05 | OK |
| Long | Small | 82 | C | 220-LS-C-06 | OK |
| Long | Small | 82 | D | 220-LS-D-05 | OK |
| Long | Small | 82 | D | 220-LS-D-06 | OK |
| Long | Large | 29 | B | 220-LL-B-01 | Not Tested |
| Long | Large | 48 | B | 220-LL-B-02 | Not Tested |
| Long | Large | 82 | B | 220-LL-B-03 | N/A |
| Tang | Small | 47 | F | 220-TS-F-01 | OK |
| Tang | Small | 47 | F | 220-TS-F-02 | OK |
| Tang | Small | 47 | F | 220-TS-F-03 | OK |
| Tang | Small | 47 | F | 220-TS-F-04 | OK |
| Tang | Small | 47 | F | 220-TS-F-05 | OK |
| Tang | Small | 47 | F | 220-TS-F-06 | Poor Finish |
| Tang | Small | 47 | F | 220-TS-F-07 | Broken |
| Tang | Small | 78,5 | E | 220-TS-E-01 | OK |
| Tang | Small | 78,5 | E | 220-TS-E-02 | OK |
| Tang | Small | 78,5 | E | 220-TS-E-03 | OK |
| Tang | Small | 78,5 | E | 220-TS-E-04 | OK |
| Tang | Small | 78,5 | E | 220-TS-E-05 | OK |
| Tang | Small | 78,5 | E | 220-TS-E-06 | OK |
| Tang | Small | 78,5 | E | 220-TS-E-07 | OK |
| Tang | Large | 47 | F | 220-TL-F-01 | Broken |
| Tang | Large | 78,5 | E | 220-TL-E-01 | N/A |
| Radial | Small | 23,5 | A | 220-RS-A-01 | OK |
| Radial | Small | 23,5 | A | 220-RS-A-02 | OK |
| Radial | Small | 23,5 | A | 220-RS-A-03 | OK |
| Radial | Small | 23,5 | A | 220-RS-A-04 | OK |
| Radial | Small | 23,5 | A | 220-RS-A-05 | OK |
| Radial | Small | 23,5 | A | 220-RS-A-06 | OK |
| Radial | Small | 23,5 | A | 220-RS-A-07 | OK |
| Radial | Small | 48 | A | 220-RS-A-08 | OK |
| Radial | Small | 48 | A | 220-RS-A-09 | OK |
| Radial | Small | 48 | A | 220-RS-A-10 | OK |
| Radial | Small | 48 | A | 220-RS-A-11 | OK |
| Radial | Small | 48 | A | 220-RS-A-12 | OK |
| Radial | Small | 48 | A | 220-RS-A-13 | OK |
| Radial | Small | 48 | A | 220-RS-A-14 | Broken |
| Radial | Small | 85,5 | A | 220-RS-A-15 | OK |
| Radial | Small | 85,5 | A | 220-RS-A-16 | OK |
| Radial | Small | 85,5 | A | 220-RS-A-17 | OK |
| Radial | Small | 85,5 | A | 220-RS-A-18 | OK |
| Radial | Small | 85,5 | A | 220-RS-A-19 | OK |
| Radial | Small | 85,5 | A | 220-RS-A-20 | OK |
| Radial | Small | 85,5 | A | 220-RS-A-21 | Broken |
| Radial | Large | 0 | A | 220-RL-A-01 | N/A |

**Table 55: List of specimens machined from 250 mm diameter bar stock.**

| Alignment | Type | Radial Pos. | Cut | ID | Status |
|---|---|---|---|---|---|
| Long | Small | 29 | C | 250-LS-C-01 | OK |
| Long | Small | 29 | C | 250-LS-C-02 | OK |
| Long | Small | 29 | D | 250-LS-D-01 | OK |
| Long | Small | 29 | D | 250-LS-D-02 | OK |
| Long | Small | 48 | C | 250-LS-C-03 | OK |
| Long | Small | 48 | C | 250-LS-C-04 | OK |
| Long | Small | 48 | D | 250-LS-D-03 | OK |
| Long | Small | 48 | D | 250-LS-D-04 | OK |
| Long | Small | 82 | C | 250-LS-C-05 | OK |
| Long | Small | 82 | C | 250-LS-C-06 | OK |
| Long | Small | 82 | D | 250-LS-D-05 | OK |
| Long | Small | 82 | D | 250-LS-D-06 | OK |
| Long | Large | 29 | B | 250-LL-B-01 | OK |
| Long | Large | 48 | B | 250-LL-B-02 | OK |
| Long | Large | 82 | B | 250-LL-B-03 | OK |
| Tang | Small | 47 | F | 250-TS-F-01 | OK |
| Tang | Small | 47 | F | 250-TS-F-02 | OK |
| Tang | Small | 47 | F | 250-TS-F-03 | OK |
| Tang | Small | 47 | F | 250-TS-F-04 | OK |
| Tang | Small | 47 | F | 250-TS-F-05 | OK |
| Tang | Small | 47 | F | 250-TS-F-06 | OK |
| Tang | Small | 47 | F | 250-TS-F-07 | OK |
| Tang | Small | 78,5 | E | 250-TS-E-01 | OK |
| Tang | Small | 78,5 | E | 250-TS-E-02 | OK |
| Tang | Small | 78,5 | E | 250-TS-E-03 | OK |
| Tang | Small | 78,5 | E | 250-TS-E-04 | OK |
| Tang | Small | 78,5 | E | 250-TS-E-05 | OK |
| Tang | Small | 78,5 | E | 250-TS-E-06 | OK |
| Tang | Small | 78,5 | E | 250-TS-E-07 | OK |
| Tang | Large | 47 | F | 250-TL-F-01 | OK |
| Tang | Large | 78,5 | E | 250-TL-E-01 | OK |
| Radial | Small | 23,5 | A | 250-RS-A-01 | OK |
| Radial | Small | 23,5 | A | 250-RS-A-02 | Broken |
| Radial | Small | 23,5 | A | 250-RS-A-03 | OK |
| Radial | Small | 23,5 | A | 250-RS-A-04 | OK |
| Radial | Small | 23,5 | A | 250-RS-A-05 | Miscoloring |
| Radial | Small | 23,5 | A | 250-RS-A-06 | OK |
| Radial | Small | 23,5 | A | 250-RS-A-07 | OK |
| Radial | Small | 48 | A | 250-RS-A-08 | OK |
| Radial | Small | 48 | A | 250-RS-A-09 | OK |
| Radial | Small | 48 | A | 250-RS-A-10 | OK |
| Radial | Small | 48 | A | 250-RS-A-11 | OK |
| Radial | Small | 48 | A | 250-RS-A-12 | OK |
| Radial | Small | 48 | A | 250-RS-A-13 | OK |
| Radial | Small | 48 | A | 250-RS-A-14 | OK |
| Radial | Small | 85,5 | A | 250-RS-A-15 | OK |
| Radial | Small | 85,5 | A | 250-RS-A-16 | OK |
| Radial | Small | 85,5 | A | 250-RS-A-17 | OK |
| Radial | Small | 85,5 | A | 250-RS-A-18 | OK |
| Radial | Small | 85,5 | A | 250-RS-A-19 | OK |
| Radial | Small | 85,5 | A | 250-RS-A-20 | OK |
| Radial | Small | 85,5 | A | 250-RS-A-21 | OK |
| Radial | Large | 0 | A | 250-RL-A-01 | OK |

# Appendix D: Additional Calculations and Results for the ASME Design Rules

**Table 56: Flange stress factors calculated according to the ASME (2010) Design Rules for Flanged Joints.**

| Name | Symbol | Value | Unit |
|---|---|---|---|
| Flange Diameter Ratio | K | 4,23 | - |
| Flange Stress Factor | Y | 1,38 | - |
| Flange Stress Factor | T | 0,97 | - |
| Flange Stress Factor | U | 1,52 | - |
| Flange Stress Factor | Z | 1,12 | - |
| Hub Length Parameter | $h_0$ | 15,53 | - |
| - | $X_h$ | 1,74 | - |
| - | $X_g$ | 5,71 | - |
| Flange Stress Factor | F | 0,52 | - |
| Flange Stress Factor | e | 0,0332 | - |
| Flange Stress Factor | V | 0,0169 | - |
| Flange Stress Factor | d | 31525 | - |
| Flange Stress Factor | L | 4,08 | - |
| Hub Stress Correction Factor | f | 1 | - |

**Table 57: Flange calculations conducted according to the ASME (2010) Design Rules for Flanged Joints.**

| Name | Symbol | Case I | Case II | Unit |
|---|---|---|---|---|
| Hydrostatic End Force in Flange Bore | $H_D$ | 52387 | 78581 | N |
| Total Hydrostatic End Force | H | 184174 | 276261 | N |
| Hydrostatic End Force outside Flange Bore | $H_T$ | 131787 | 197680 | N |
| Gasket Load for Operating Conditions | $H_G$ | 139956 | 209934 | N |
| Moment Arm for $H_D$ | $h_D$ | 43,60 | 43,60 | mm |
| Moment Arm for $H_T$ | $h_T$ | 46,04 | 46,04 | mm |
| Moment Arm for $H_G$ | $h_G$ | 34,93 | 34,93 | mm |
| Bolt Spacing Correction Factor | $B_{sc}$ | 0,8862 | 0,8862 | - |
| Bending Moment of Inertia | I | 376500 | 376500 | $mm^4$ |
| Average Hub Thickness | $G_{avg}$ | 15,93 | 15,93 | mm |
| Inertia Calculation Factor | $A_A$ | 82,10 | 82,10 | - |
| Inertia Calculation Factor | $B_B$ | 38,10 | 38,10 | - |
| Inertia Calculation Factor | $C_C$ | 27,10 | 27,10 | - |
| Inertia Calculation Factor | $D_{DG}$ | 15,93 | 15,93 | - |
| Inertia Calculation Factor | $K_{AB}$ | 1,07E+06 | 1,07E+06 | - |
| Inertia Calculation Factor | $K_{CD}$ | 29734 | 29734 | - |
| Polar Moment of Inertia | $I_P$ | 1,10E+06 | 1,10E+06 | $mm^4$ |
| External Component of the Design Moment | $M_{oe}$ | 0 | 0 | N mm |
| Moment Factor for Split Rings (Not Used) | $F_S$ | 1 | 1 | - |
| Design Moment for Operating Conditions | $M_o$ | 1,17E+07 | 1,76E+07 | N mm |
| Design Moment for Gasket Seating Conditions | $M_g$ | 1,33E+07 | 1,58E+07 | N mm |

**Table 58: Stress criteria, for ASME (2010), section VIII, division I and II (1 = true, 0 = false).**

| Name | Symbol | Case I | Case II | Case I | Case II | Unit |
|---|---|---|---|---|---|---|
| Max Allowable Stress for Operating Cond. | $S_{fo}$ | 177 | 177 | 259 | 259 | MPa |
| Max Allowable Stress for Gasket Seating Cond. | $S_{fg}$ | 177 | 177 | 259 | 259 | MPa |
| $S_{Ho} < 1.5 * S_{fo}$ | - | 1 | 1 | 1 | 1 | - |
| $S_{Ro} < S_{fo}$ | - | 1 | 1 | 1 | 1 | - |
| $S_{To} < S_{fo}$ | - | 1 | 1 | 1 | 1 | - |
| $(S_{Ho} + S_{Ro}) * 0.5 < S_{fo}$ | - | 1 | 1 | 1 | 1 | - |
| $(S_{Ho} + S_{To}) * 0.5 < S_{fo}$ | - | 1 | 1 | 1 | 1 | - |
| $S_{Hg} < 1.5 * S_{fg}$ | - | 1 | 1 | 1 | 1 | - |
| $S_{Rg} < S_{fg}$ | - | 1 | 1 | 1 | 1 | - |
| $S_{Tg} < S_{fg}$ | - | 1 | 1 | 1 | 1 | - |
| $(S_{Hg} + S_{Rg}) * 0.5 < S_{fg}$ | - | 1 | 1 | 1 | 1 | - |
| $(S_{Hg} + S_{Tg}) * 0.5 < S_{fg}$ | - | 1 | 1 | 1 | 1 | - |

**Table 59: Calculated rigidity criteria from ASME (2010) Design Rules for Flanged Joints.**

| Name | Symbol | Case I | Case II | Unit |
|---|---|---|---|---|
| Rigidity Index for Operating Conditions | $J_o$ | 0.1202 | 0.1804 | - |
| Rigidity Index for Gasket Seating Conditions | $J_g$ | 0.1361 | 0.1618 | - |

# Appendix E: Additional Abaqus Results for Varying Pressures

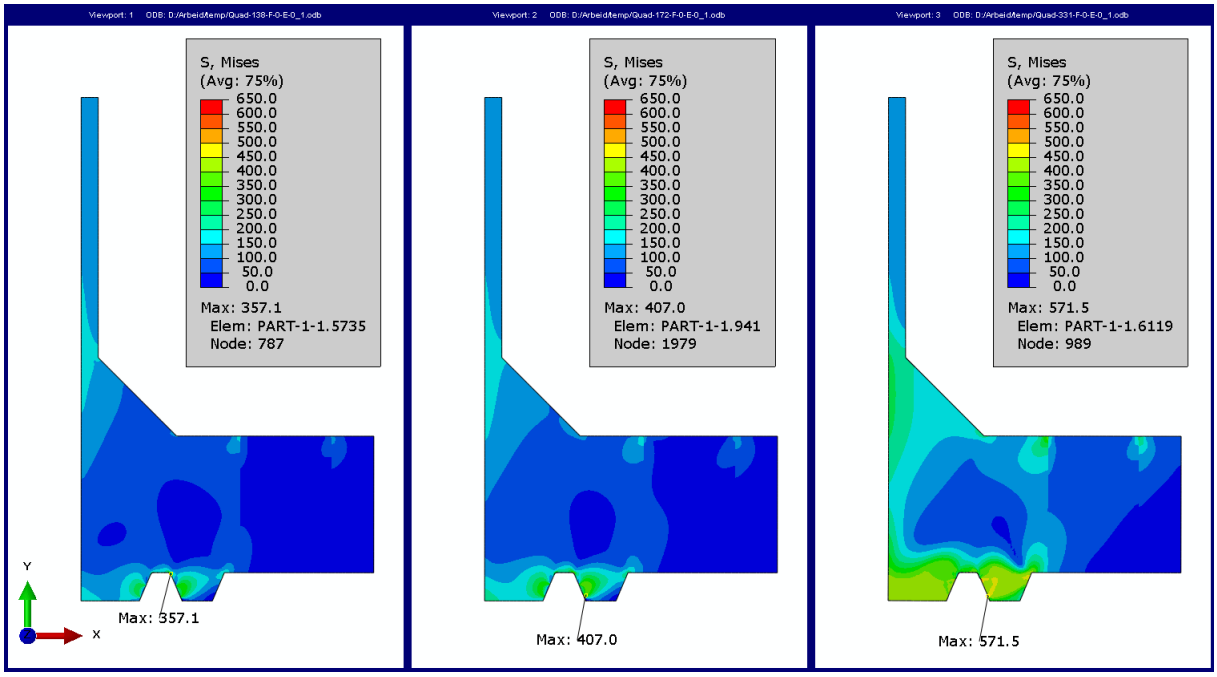


**Figure 82: Von Mises stress contour plots for varying bolt loads, for the step pressure 1, (left: 138 MPa bolt stress, middle: 172 MPa bolt stress, right: 331 MPa bolt stress).**

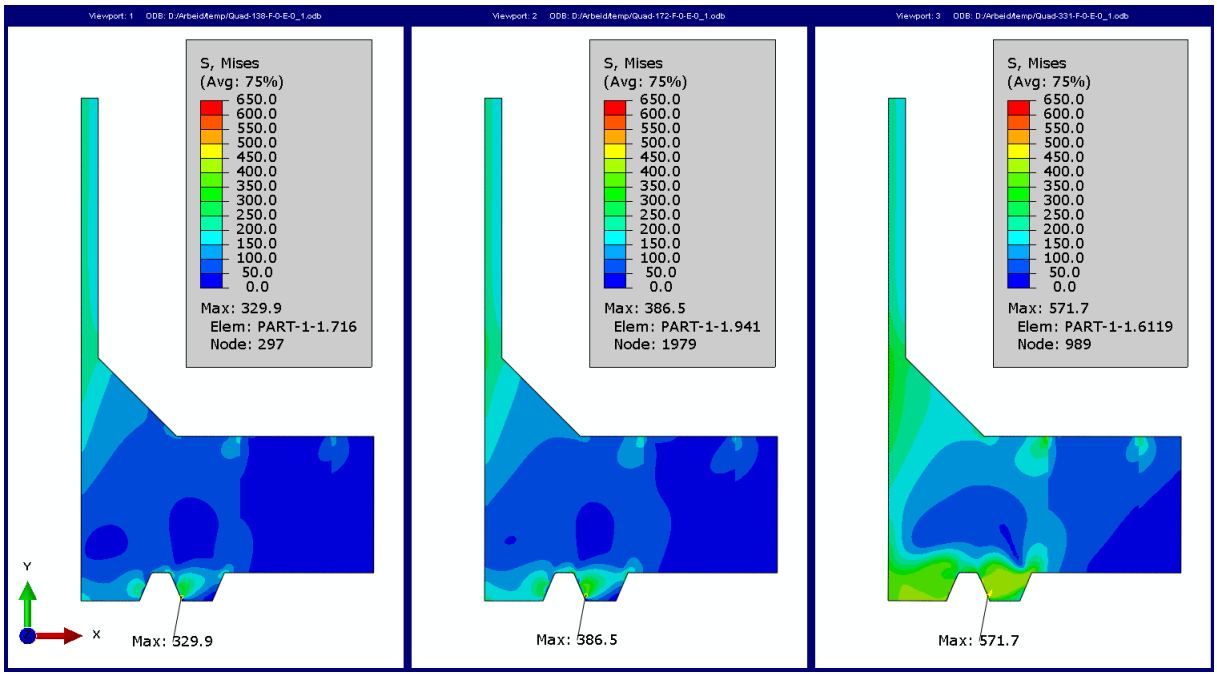


**Figure 83: Von Mises stress contour plots for varying bolt loads, for the step pressure 2, (left: 138 MPa bolt stress, middle: 172 MPa bolt stress, right: 331 MPa bolt stress).**

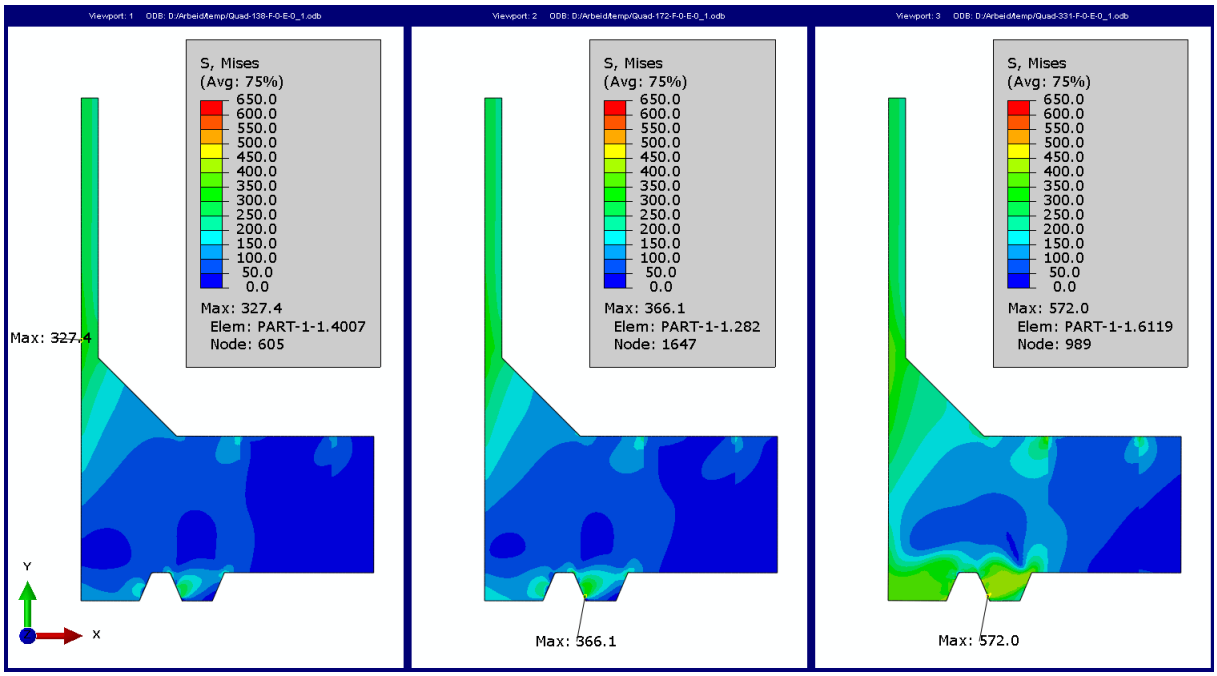


**Figure 84: Von Mises stress contour plots for varying bolt loads, for the step pressure 3, (left: 138 MPa bolt stress, middle: 172 MPa bolt stress, right: 331 MPa bolt stress).**

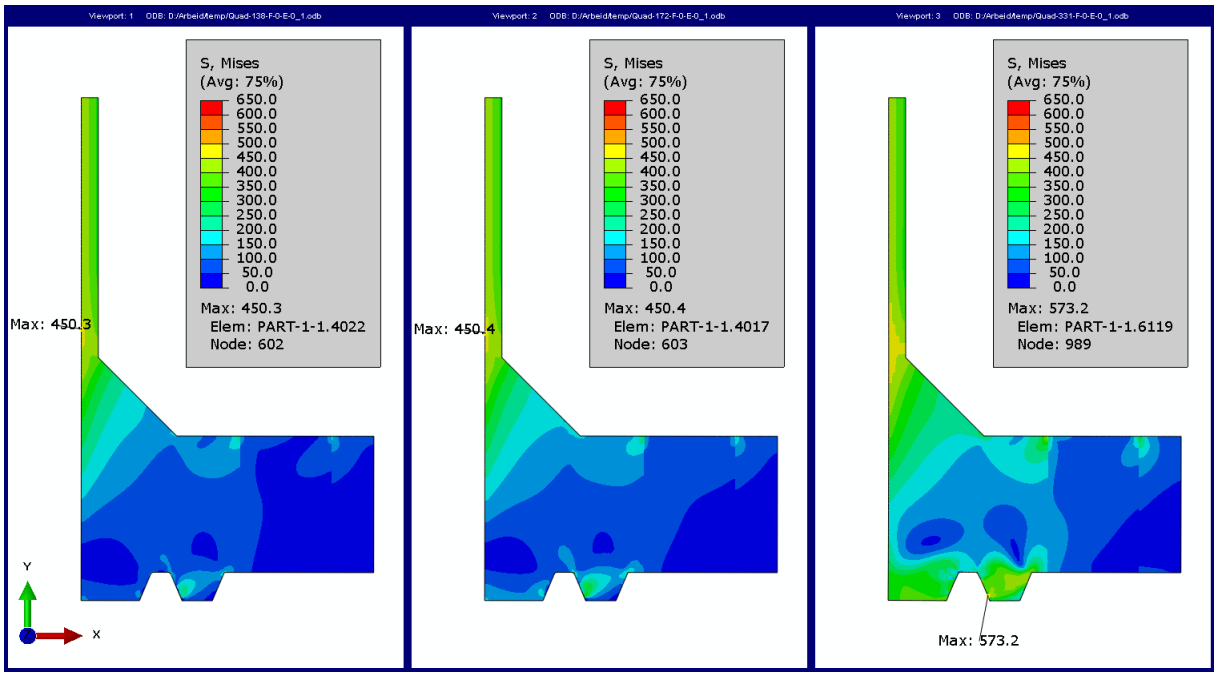


**Figure 85: Von Mises stress contour plots for varying bolt loads, for the step pressure 4, (left: 138 MPa bolt stress, middle: 172 MPa bolt stress, right: 331 MPa bolt stress).**

# Appendix F: Additional Abaqus Results for Varying Friction

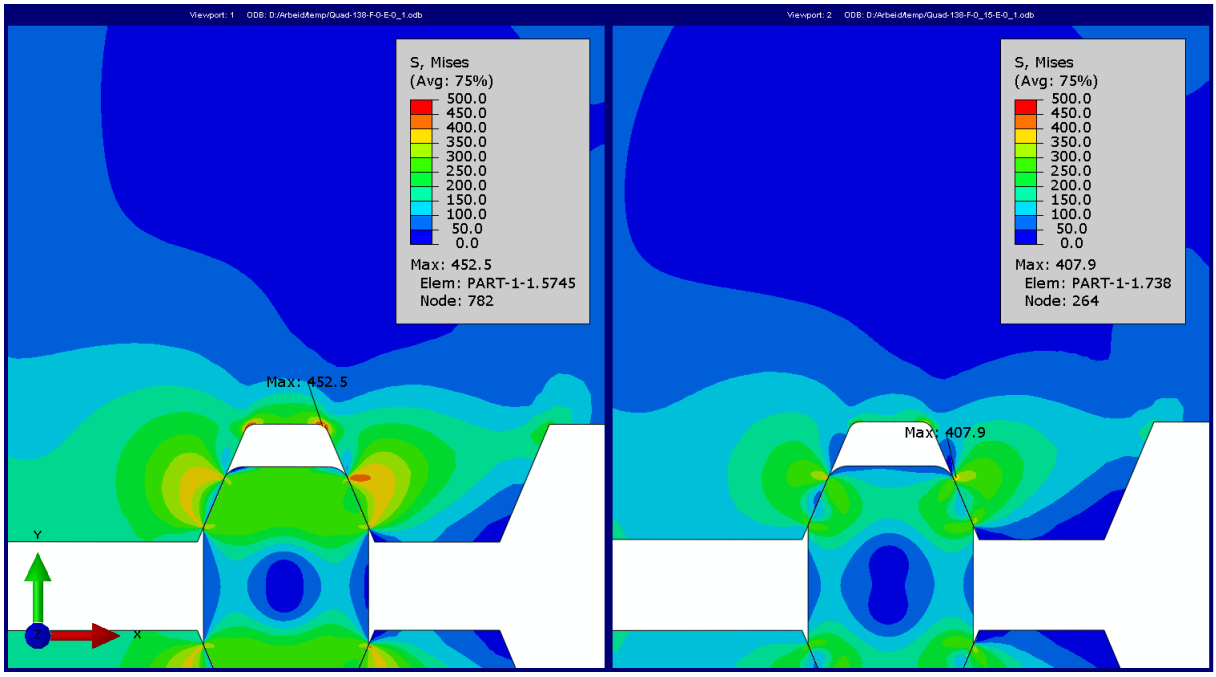


**Figure 86: Comparison between frictionless and frictional model, for equivalent bolt stress of 138 MPa, (left: frictionless, right: μ = 0.15).**

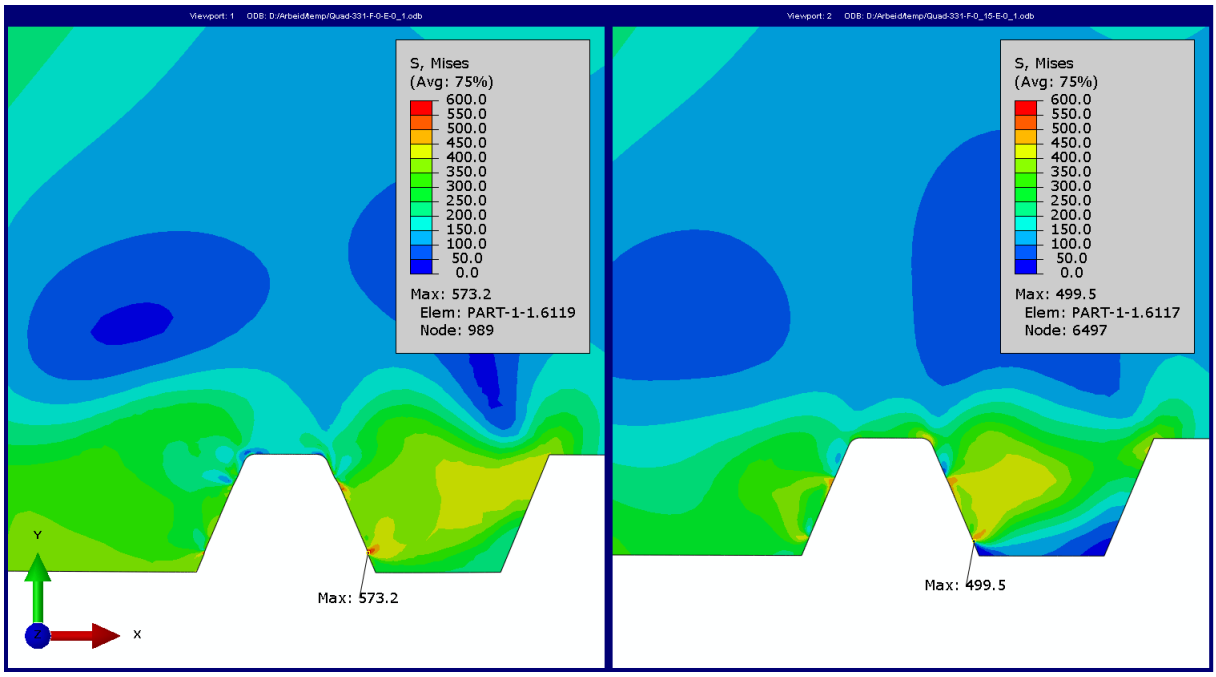


**Figure 87: Comparison between frictionless and frictional model, for equivalent bolt stress of 138 MPa, (left: frictionless, right: μ = 0.15).**

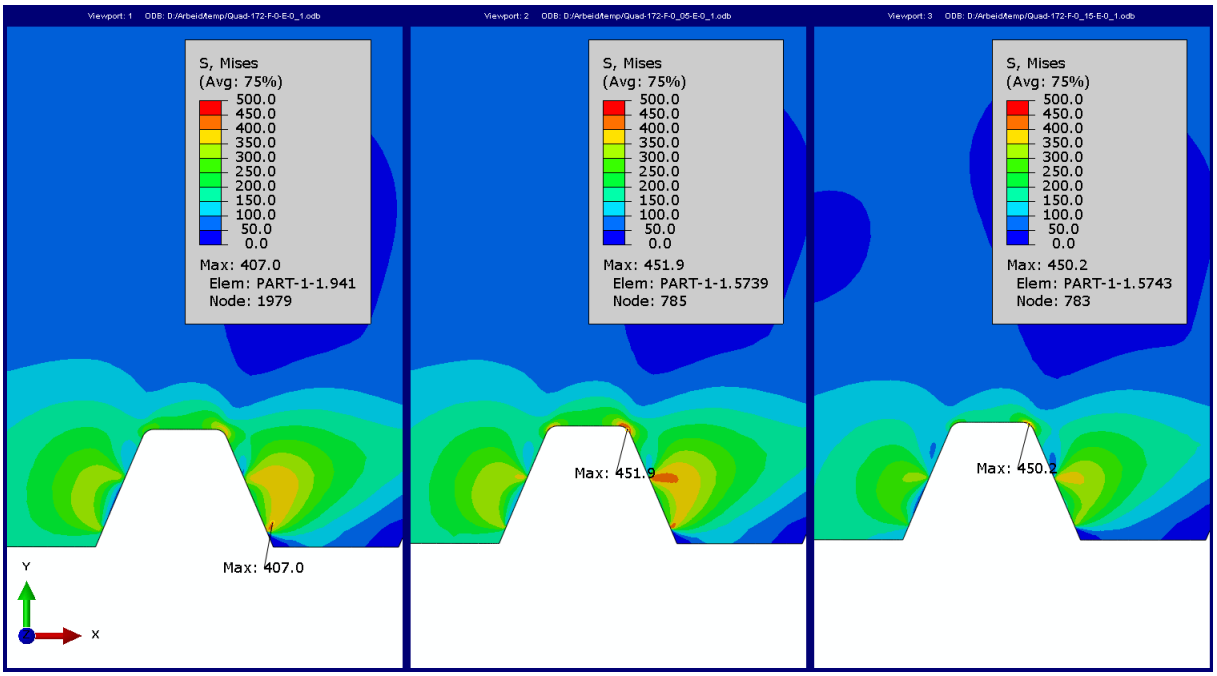


**Figure 88: Comparison of friction coefficients, for step Pressure 1, for equivalent bolt stress of 172 MPa, (left: μ = 0, middle: μ = 0.05, right: μ = 0.15)**

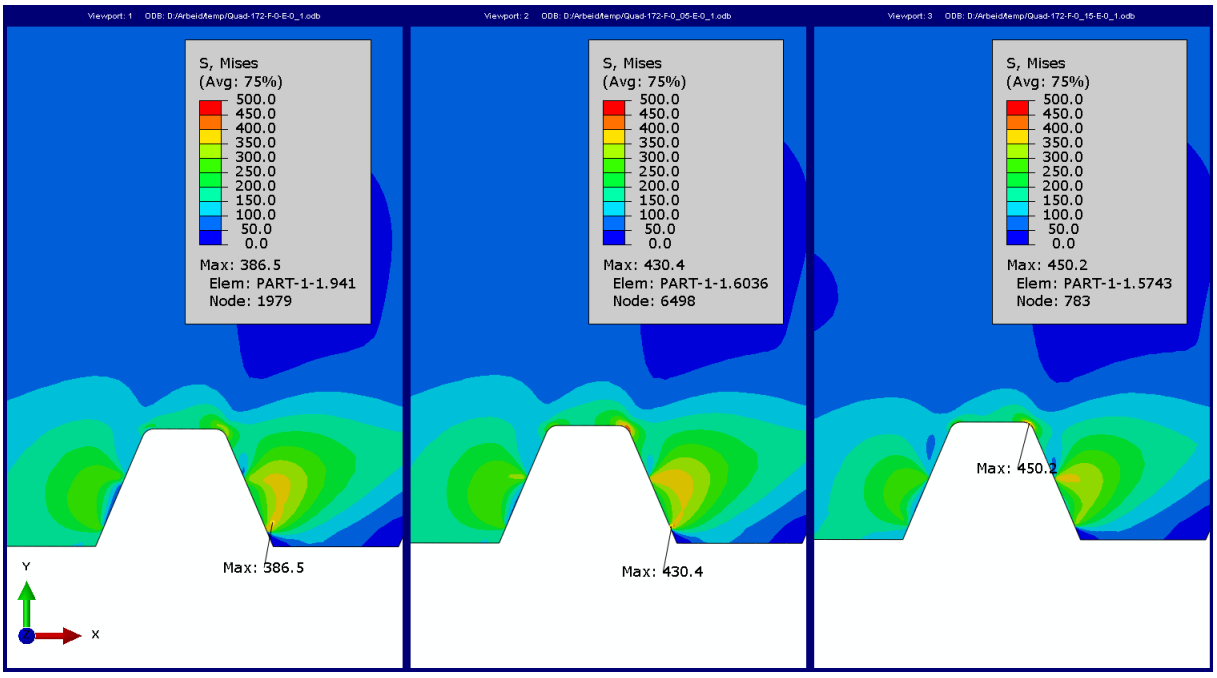


**Figure 89: Comparison of friction coefficients, for step Pressure 2, for equivalent bolt stress of 172 MPa, (left: μ = 0, middle: μ = 0.05, right: μ = 0.15)**

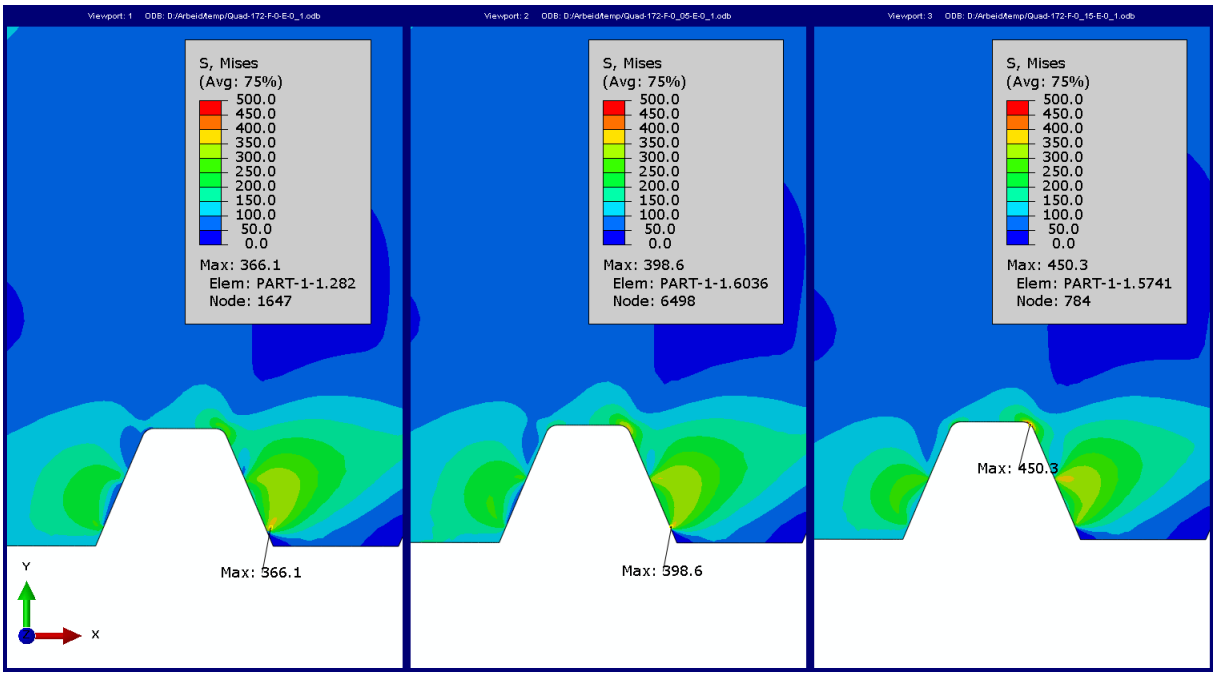


**Figure 90: Comparison of friction coefficients, for step Pressure 3, for equivalent bolt stress of 172 MPa, (left: μ = 0, middle: μ = 0.05, right: μ = 0.15)**

# Appendix G: Elastic Modulus Data for UNS S31803

**Table 60: Elastic modulus results for specimens originating from part A, for forged bar of 250 mm diameter.**

| Set | Test | Min Force | Max Force | Δ Force | Δ Extension | Δ Stress | Strain | E-module | Max Stress | Min Stress |
|---|---|---|---|---|---|---|---|---|---|---|
| - | # | N | N | N | mm | Mpa | mm/mm | Mpa | Mpa | Mpa |
| Set 1 | 1 | 1960,0 | 8070,0 | 6110,0 | 0,03750 | 153,0 | 0,000750 | 204038 | 202,1 | 49,1 |
| | 2 | 2004,0 | 8152,0 | 6148,0 | 0,03783 | 154,0 | 0,000757 | 203516 | 204,2 | 50,2 |
| | 3 | 1994,0 | 8474,0 | 6480,0 | 0,04008 | 162,3 | 0,000802 | 202464 | 212,2 | 49,9 |
| | 4 | 2112,0 | 8084,0 | 5972,0 | 0,03700 | 149,6 | 0,000740 | 202125 | 202,5 | 52,9 |
| | 5 | 2076,0 | 8148,0 | 6072,0 | 0,03733 | 152,1 | 0,000747 | 203692 | 204,1 | 52,0 |
| | | | | | | | | | | |
| Set 2 | 1 | 3960,0 | 10048,0 | 6088,0 | 0,04017 | 152,5 | 0,000803 | 189790 | 251,7 | 99,2 |
| | 2 | 4018,0 | 10060,0 | 6042,0 | 0,03992 | 151,3 | 0,000798 | 189536 | 252,0 | 100,6 |
| | 3 | 4000,0 | 10146,0 | 6146,0 | 0,04050 | 153,9 | 0,000810 | 190037 | 254,1 | 100,2 |
| | 4 | 3932,0 | 10100,0 | 6168,0 | 0,04058 | 154,5 | 0,000812 | 190341 | 253,0 | 98,5 |
| | 5 | 4014,0 | 10104,0 | 6090,0 | 0,04017 | 152,5 | 0,000803 | 189853 | 253,1 | 100,5 |
| | | | | | | | | | | |
| Set 3 | 1 | 6172,0 | 12140,0 | 5968,0 | 0,04075 | 149,5 | 0,000815 | 183401 | 304,1 | 154,6 |
| | 2 | 5956,0 | 12080,0 | 6124,0 | 0,04175 | 153,4 | 0,000835 | 183688 | 302,6 | 149,2 |
| | 3 | 6226,0 | 12190,0 | 5964,0 | 0,04050 | 149,4 | 0,000810 | 184410 | 305,3 | 155,9 |
| | 4 | 6144,0 | 12148,0 | 6004,0 | 0,04108 | 150,4 | 0,000822 | 183025 | 304,3 | 153,9 |
| | 5 | 5940,0 | 12080,0 | 6140,0 | 0,04183 | 153,8 | 0,000837 | 183815 | 302,6 | 148,8 |
| | | | | | | | | | | |
| Set 4 | 1 | 2026,0 | 4062,0 | 2036,0 | 0,01125 | 51,0 | 0,000225 | 226635 | 101,7 | 50,7 |
| | 2 | 1936,0 | 4132,0 | 2196,0 | 0,01208 | 55,0 | 0,000242 | 227649 | 103,5 | 48,5 |
| | 3 | 2032,0 | 4066,0 | 2034,0 | 0,01117 | 50,9 | 0,000223 | 228034 | 101,8 | 50,9 |
| | 4 | 2054,0 | 4066,0 | 2012,0 | 0,01117 | 50,4 | 0,000223 | 225567 | 101,8 | 51,4 |
| | 5 | 2176,0 | 3996,0 | 1820,0 | 0,01008 | 45,6 | 0,000202 | 226106 | 100,1 | 54,5 |
| | | | | | | | | | | |
| Set 5 | 1 | 3948,0 | 6142,0 | 2194,0 | 0,01417 | 54,9 | 0,000283 | 193896 | 153,8 | 98,9 |
| | 2 | 4044,0 | 6108,0 | 2064,0 | 0,01325 | 51,7 | 0,000265 | 195072 | 153,0 | 101,3 |
| | 3 | 4000,0 | 6148,0 | 2148,0 | 0,01383 | 53,8 | 0,000277 | 194497 | 154,0 | 100,2 |
| | 4 | 3980,0 | 6042,0 | 2062,0 | 0,01325 | 51,6 | 0,000265 | 194883 | 151,3 | 99,7 |
| | 5 | 3942,0 | 6154,0 | 2212,0 | 0,01425 | 55,4 | 0,000285 | 194389 | 154,1 | 98,7 |
| | | | | | | | | | | |
| Set 6 | 1 | 6020,0 | 8166,0 | 2146,0 | 0,01442 | 53,7 | 0,000288 | 186366 | 204,5 | 150,8 |
| | 2 | 5988,0 | 8202,0 | 2214,0 | 0,01492 | 55,5 | 0,000298 | 185827 | 205,4 | 150,0 |
| | 3 | 6106,0 | 8122,0 | 2016,0 | 0,01350 | 50,5 | 0,000270 | 187007 | 203,4 | 152,9 |
| | 4 | 6056,0 | 8232,0 | 2176,0 | 0,01458 | 54,5 | 0,000292 | 186897 | 206,2 | 151,7 |
| | 5 | 6014,0 | 8108,0 | 2094,0 | 0,01400 | 52,4 | 0,000280 | 187305 | 203,1 | 150,6 |
| | | | | | | | | | | |
| Set 7 | 1 | 7994,0 | 10056,0 | 2062,0 | 0,01408 | 51,6 | 0,000282 | 183395 | 251,9 | 200,2 |
| | 2 | 8064,0 | 10182,0 | 2118,0 | 0,01442 | 53,0 | 0,000288 | 183934 | 255,0 | 202,0 |
| | 3 | 7880,0 | 10110,0 | 2230,0 | 0,01525 | 55,9 | 0,000305 | 183120 | 253,2 | 197,4 |
| | 4 | 7934,0 | 10076,0 | 2142,0 | 0,01458 | 53,6 | 0,000292 | 183977 | 252,4 | 198,7 |
| | 5 | 7980,0 | 10132,0 | 2152,0 | 0,01467 | 53,9 | 0,000293 | 183702 | 253,8 | 199,9 |
| | | | | | | | | | | |
| Set 8 | 1 | 10250,0 | 12214,0 | 1964,0 | 0,01350 | 49,2 | 0,000270 | 182183 | 305,9 | 256,7 |
| | 2 | 10188,0 | 12218,0 | 2030,0 | 0,01392 | 50,8 | 0,000278 | 182624 | 306,0 | 255,2 |
| | 3 | 10231,3 | 12110,0 | 1878,7 | 0,01300 | 47,1 | 0,000260 | 180974 | 303,3 | 256,2 |
| | 4 | 10156,7 | 12164,0 | 2007,3 | 0,01375 | 50,3 | 0,000275 | 182815 | 304,7 | 254,4 |
| | 5 | 10062,0 | 12220,0 | 2158,0 | 0,01483 | 54,0 | 0,000297 | 182226 | 306,1 | 252,0 |

**Table 61: Elastic modulus results for specimens originating from part B, for radial position of 29 mm, for forged bar of 250 mm diameter.**

| Set | Test | Min Force | Max Force | Δ Force | Δ Extension | Δ Stress | Strain | E-module | Max Stress | Min Stress |
|---|---|---|---|---|---|---|---|---|---|---|
| - | # | N | N | N | mm | Mpa | mm/mm | Mpa | Mpa | Mpa |
| Set 1 | 1 | 2006,0 | 8140,0 | 6134,0 | 0,04017 | 156,2 | 0,000803 | 194484 | 207,3 | 51,1 |
| | 2 | 2012,0 | 8082,0 | 6070,0 | 0,03983 | 154,6 | 0,000797 | 194097 | 205,9 | 51,3 |
| | 3 | 2002,0 | 8174,0 | 6172,0 | 0,04042 | 157,2 | 0,000808 | 194478 | 208,2 | 51,0 |
| | 4 | 1980,0 | 8160,0 | 6180,0 | 0,04042 | 157,4 | 0,000808 | 194730 | 207,9 | 50,4 |
| | 5 | 2068,0 | 8084,0 | 6016,0 | 0,03933 | 153,2 | 0,000787 | 194816 | 205,9 | 52,7 |
| | | | | | | | | | | |
| Set 2 | 1 | 3984,0 | 10160,0 | 6176,0 | 0,04033 | 157,3 | 0,000807 | 195039 | 258,8 | 101,5 |
| | 2 | 4060,0 | 10368,0 | 6308,0 | 0,04117 | 160,7 | 0,000823 | 195143 | 264,1 | 103,4 |
| | 3 | 4048,0 | 10154,0 | 6106,0 | 0,03983 | 155,5 | 0,000797 | 195249 | 258,6 | 103,1 |
| | 4 | 4006,0 | 10156,0 | 6150,0 | 0,04008 | 156,7 | 0,000802 | 195429 | 258,7 | 102,0 |
| | 5 | 4034,0 | 10224,0 | 6190,0 | 0,04033 | 157,7 | 0,000807 | 195481 | 260,4 | 102,8 |
| | | | | | | | | | | |
| Set 3 | 1 | 5978,0 | 12050,0 | 6072,0 | 0,03967 | 154,7 | 0,000793 | 194944 | 306,9 | 152,3 |
| | 2 | 6034,0 | 12070,0 | 6036,0 | 0,03950 | 153,8 | 0,000790 | 194623 | 307,5 | 153,7 |
| | 3 | 6084,0 | 12104,0 | 6020,0 | 0,03933 | 153,3 | 0,000787 | 194946 | 308,3 | 155,0 |
| | 4 | 5962,0 | 12070,0 | 6108,0 | 0,03983 | 155,6 | 0,000797 | 195312 | 307,5 | 151,9 |
| | 5 | 6074,0 | 11966,0 | 5892,0 | 0,03842 | 150,1 | 0,000768 | 195320 | 304,8 | 154,7 |
| | | | | | | | | | | |
| Set 4 | 1 | 2168,0 | 4166,0 | 1998,0 | 0,01333 | 50,9 | 0,000267 | 190900 | 106,1 | 55,2 |
| | 2 | 2016,0 | 4330,0 | 2314,0 | 0,01533 | 58,9 | 0,000307 | 192248 | 110,3 | 51,4 |
| | 3 | 2111,3 | 4126,0 | 2014,7 | 0,01350 | 51,3 | 0,000270 | 190072 | 105,1 | 53,8 |
| | 4 | 2008,0 | 4122,0 | 2114,0 | 0,01417 | 53,8 | 0,000283 | 190010 | 105,0 | 51,1 |
| | 5 | 2082,0 | 4194,0 | 2112,0 | 0,01408 | 53,8 | 0,000282 | 191044 | 106,8 | 53,0 |
| | | | | | | | | | | |
| Set 5 | 1 | 4102,0 | 6134,0 | 2032,0 | 0,01333 | 51,8 | 0,000267 | 194149 | 156,2 | 104,5 |
| | 2 | 4058,0 | 6138,0 | 2080,0 | 0,01367 | 53,0 | 0,000273 | 193792 | 156,4 | 103,4 |
| | 3 | 3986,0 | 6238,0 | 2252,0 | 0,01475 | 57,4 | 0,000295 | 194454 | 158,9 | 101,5 |
| | 4 | 4098,0 | 6192,0 | 2094,0 | 0,01375 | 53,3 | 0,000275 | 193961 | 157,7 | 104,4 |
| | 5 | 4036,0 | 6216,0 | 2180,0 | 0,01433 | 55,5 | 0,000287 | 193754 | 158,3 | 102,8 |
| | | | | | | | | | | |
| Set 6 | 1 | 6188,0 | 8198,0 | 2010,0 | 0,01342 | 51,2 | 0,000268 | 190759 | 208,8 | 157,6 |
| | 2 | 6128,0 | 8324,0 | 2196,0 | 0,01450 | 55,9 | 0,000290 | 192888 | 212,0 | 156,1 |
| | 3 | 6020,0 | 8186,0 | 2166,0 | 0,01433 | 55,2 | 0,000287 | 192510 | 208,5 | 153,3 |
| | 4 | 5930,0 | 8178,0 | 2248,0 | 0,01483 | 57,3 | 0,000297 | 193062 | 208,3 | 151,1 |
| | 5 | 6012,0 | 8116,0 | 2104,0 | 0,01392 | 53,6 | 0,000278 | 192508 | 206,7 | 153,1 |
| | | | | | | | | | | |
| Set 7 | 1 | 8092,0 | 10240,0 | 2148,0 | 0,01417 | 54,7 | 0,000283 | 193066 | 260,8 | 206,1 |
| | 2 | 8122,0 | 10070,0 | 1948,0 | 0,01292 | 49,6 | 0,000258 | 192029 | 256,5 | 206,9 |
| | 3 | 8098,0 | 10214,0 | 2116,0 | 0,01400 | 53,9 | 0,000280 | 192499 | 260,2 | 206,3 |
| | 4 | 8063,3 | 10152,0 | 2088,7 | 0,01383 | 53,2 | 0,000277 | 192351 | 258,6 | 205,4 |
| | 5 | 8112,0 | 10188,0 | 2076,0 | 0,01375 | 52,9 | 0,000275 | 192294 | 259,5 | 206,6 |
| | | | | | | | | | | |
| Set 8 | 1 | 10160,0 | 12300,0 | 2140,0 | 0,01425 | 54,5 | 0,000285 | 191267 | 313,3 | 258,8 |
| | 2 | 9994,0 | 12186,0 | 2192,0 | 0,01475 | 55,8 | 0,000295 | 189274 | 310,4 | 254,6 |
| | 3 | 10030,0 | 12174,0 | 2144,0 | 0,01433 | 54,6 | 0,000287 | 190555 | 310,1 | 255,5 |
| | 4 | 10070,7 | 12234,0 | 2163,3 | 0,01450 | 55,1 | 0,000290 | 190016 | 311,6 | 256,5 |
| | 5 | 10176,0 | 12200,0 | 2024,0 | 0,01358 | 51,6 | 0,000272 | 189824 | 310,8 | 259,2 |

**Table 62: Elastic modulus results for specimens originating from part B, for radial position of 48 mm, for forged bar of 250 mm diameter.**

| Set | Test | Min Force | Max Force | Δ Force | Δ Extension | Δ Stress | Strain | E-module | Max Stress | Min Stress |
|---|---|---|---|---|---|---|---|---|---|---|
| - | # | N | N | N | mm | Mpa | mm/mm | Mpa | Mpa | Mpa |
| Set 1 | 1 | 2028,0 | 8130,0 | 6102,0 | 0,04150 | 155,4 | 0,000830 | 187269 | 207,1 | 51,7 |
| | 2 | 2116,0 | 7986,0 | 5870,0 | 0,04000 | 149,5 | 0,000800 | 186904 | 203,4 | 53,9 |
| | 3 | 2092,0 | 8134,0 | 6042,0 | 0,04108 | 153,9 | 0,000822 | 187323 | 207,2 | 53,3 |
| | 4 | 2000,0 | 8044,0 | 6044,0 | 0,04108 | 154,0 | 0,000822 | 187385 | 204,9 | 50,9 |
| | 5 | 2154,0 | 8100,0 | 5946,0 | 0,04050 | 151,5 | 0,000810 | 186987 | 206,3 | 54,9 |
| | | | | | | | | | | |
| Set 2 | 1 | 4014,0 | 10156,0 | 6142,0 | 0,04117 | 156,5 | 0,000823 | 190007 | 258,7 | 102,2 |
| | 2 | 4080,0 | 10196,0 | 6116,0 | 0,04100 | 155,8 | 0,000820 | 189987 | 259,7 | 103,9 |
| | 3 | 4130,0 | 10174,0 | 6044,0 | 0,04050 | 154,0 | 0,000810 | 190069 | 259,2 | 105,2 |
| | 4 | 3978,0 | 10252,0 | 6274,0 | 0,04208 | 159,8 | 0,000842 | 189893 | 261,1 | 101,3 |
| | 5 | 3974,0 | 10150,0 | 6176,0 | 0,04150 | 157,3 | 0,000830 | 189540 | 258,5 | 101,2 |
| | | | | | | | | | | |
| Set 3 | 1 | 6030,0 | 12164,0 | 6134,0 | 0,04067 | 156,2 | 0,000813 | 192093 | 309,8 | 153,6 |
| | 2 | 6156,0 | 12160,0 | 6004,0 | 0,03983 | 152,9 | 0,000797 | 191987 | 309,7 | 156,8 |
| | 3 | 5974,0 | 12130,0 | 6156,0 | 0,04057 | 156,8 | 0,000811 | 193257 | 309,0 | 152,2 |
| | 4 | 6182,0 | 12200,0 | 6018,0 | 0,03983 | 153,3 | 0,000797 | 192435 | 310,8 | 157,5 |
| | 5 | 6070,0 | 12064,0 | 5994,0 | 0,03967 | 152,7 | 0,000793 | 192440 | 307,3 | 154,6 |
| | | | | | | | | | | |
| Set 4 | 1 | 2162,0 | 4064,0 | 1902,0 | 0,01317 | 48,4 | 0,000263 | 183936 | 103,5 | 55,1 |
| | 2 | 2090,0 | 4128,0 | 2038,0 | 0,01417 | 51,9 | 0,000283 | 183179 | 105,2 | 53,2 |
| | 3 | 2124,0 | 4134,0 | 2010,0 | 0,01392 | 51,2 | 0,000278 | 183907 | 105,3 | 54,1 |
| | 4 | 2014,0 | 4130,0 | 2116,0 | 0,01475 | 53,9 | 0,000295 | 182711 | 105,2 | 51,3 |
| | 5 | 2046,0 | 4314,0 | 2268,0 | 0,01583 | 57,8 | 0,000317 | 182475 | 109,9 | 52,1 |
| | | | | | | | | | | |
| Set 5 | 1 | 4204,0 | 6144,0 | 1940,0 | 0,01317 | 49,4 | 0,000263 | 187611 | 156,5 | 107,1 |
| | 2 | 4004,0 | 6186,0 | 2182,0 | 0,01467 | 55,6 | 0,000293 | 189437 | 157,6 | 102,0 |
| | 3 | 4104,0 | 6254,0 | 2150,0 | 0,01458 | 54,8 | 0,000292 | 187812 | 159,3 | 104,5 |
| | 4 | 4014,0 | 6294,0 | 2280,0 | 0,01542 | 58,1 | 0,000308 | 188318 | 160,3 | 102,2 |
| | 5 | 4118,0 | 6154,0 | 2036,0 | 0,01375 | 51,9 | 0,000275 | 188589 | 156,8 | 104,9 |
| | | | | | | | | | | |
| Set 6 | 1 | 6037,3 | 8156,0 | 2118,7 | 0,01433 | 54,0 | 0,000287 | 188306 | 207,8 | 153,8 |
| | 2 | 6036,0 | 8158,0 | 2122,0 | 0,01433 | 54,1 | 0,000287 | 188599 | 207,8 | 153,8 |
| | 3 | 6080,0 | 8190,0 | 2110,0 | 0,01417 | 53,7 | 0,000283 | 189650 | 208,6 | 154,9 |
| | 4 | 6124,0 | 8162,0 | 2038,0 | 0,01367 | 51,9 | 0,000273 | 189879 | 207,9 | 156,0 |
| | 5 | 6064,0 | 8188,0 | 2124,0 | 0,01433 | 54,1 | 0,000287 | 188777 | 208,6 | 154,5 |
| | | | | | | | | | | |
| Set 7 | 1 | 8008,0 | 10032,0 | 2024,0 | 0,01358 | 51,6 | 0,000272 | 189824 | 255,5 | 204,0 |
| | 2 | 8098,7 | 10158,0 | 2059,3 | 0,01375 | 52,5 | 0,000275 | 190747 | 258,7 | 206,3 |
| | 3 | 8120,0 | 10164,0 | 2044,0 | 0,01375 | 52,1 | 0,000275 | 189330 | 258,9 | 206,8 |
| | 4 | 8102,0 | 10066,0 | 1964,0 | 0,01317 | 50,0 | 0,000263 | 189932 | 256,4 | 206,4 |
| | 5 | 8072,0 | 10162,0 | 2090,0 | 0,01400 | 53,2 | 0,000280 | 190134 | 258,9 | 205,6 |
| | | | | | | | | | | |
| Set 8 | 1 | 10132,0 | 12068,0 | 1936,0 | 0,01308 | 49,3 | 0,000262 | 188512 | 307,4 | 258,1 |
| | 2 | 10142,0 | 12154,0 | 2012,0 | 0,01358 | 51,3 | 0,000272 | 188699 | 309,6 | 258,3 |
| | 3 | 10058,0 | 12080,0 | 2022,0 | 0,01367 | 51,5 | 0,000273 | 188388 | 307,7 | 256,2 |
| | 4 | 10062,7 | 12228,0 | 2165,3 | 0,01458 | 55,2 | 0,000292 | 189148 | 311,5 | 256,3 |
| | 5 | 10044,0 | 12232,0 | 2188,0 | 0,01475 | 55,7 | 0,000295 | 188928 | 311,6 | 255,8 |

**Table 63: Elastic modulus results for specimens originating from part B, for radial position of 82 mm, for forged bar of 250 mm diameter.**

| Set | Test | Min Force | Max Force | Δ Force | Δ Extension | Δ Stress | Strain | E-module | Max Stress | Min Stress |
|---|---|---|---|---|---|---|---|---|---|---|
| - | # | N | N | N | mm | Mpa | mm/mm | Mpa | Mpa | Mpa |
| Set 1 | 1 | 2112,0 | 8134,0 | 6022,0 | 0,03900 | 150,0 | 0,000780 | 192284 | 202,6 | 52,6 |
| | 2 | 2136,0 | 8154,0 | 6018,0 | 0,03900 | 149,9 | 0,000780 | 192157 | 203,1 | 53,2 |
| | 3 | 2092,0 | 8082,0 | 5990,0 | 0,03867 | 149,2 | 0,000773 | 192895 | 201,3 | 52,1 |
| | 4 | 2074,0 | 8066,0 | 5992,0 | 0,03875 | 149,2 | 0,000775 | 192561 | 200,9 | 51,7 |
| | 5 | 2102,0 | 8146,0 | 6044,0 | 0,03908 | 150,5 | 0,000782 | 192592 | 202,9 | 52,4 |
| | | | | | | | | | | |
| Set 2 | 1 | 4054,0 | 10084,0 | 6030,0 | 0,03825 | 150,2 | 0,000765 | 196315 | 251,1 | 101,0 |
| | 2 | 4082,0 | 10116,0 | 6034,0 | 0,03825 | 150,3 | 0,000765 | 196445 | 251,9 | 101,7 |
| | 3 | 4036,0 | 10134,0 | 6098,0 | 0,03867 | 151,9 | 0,000773 | 196373 | 252,4 | 100,5 |
| | 4 | 4100,0 | 10134,0 | 6034,0 | 0,03825 | 150,3 | 0,000765 | 196445 | 252,4 | 102,1 |
| | 5 | 4080,0 | 10164,0 | 6084,0 | 0,03850 | 151,5 | 0,000770 | 196787 | 253,1 | 101,6 |
| | | | | | | | | | | |
| Set 3 | 1 | 6156,0 | 12174,0 | 6018,0 | 0,03767 | 149,9 | 0,000753 | 198941 | 303,2 | 153,3 |
| | 2 | 6134,0 | 12128,0 | 5994,0 | 0,03758 | 149,3 | 0,000752 | 198622 | 302,1 | 152,8 |
| | 3 | 6012,0 | 12162,0 | 6150,0 | 0,03875 | 153,2 | 0,000775 | 197638 | 302,9 | 149,7 |
| | 4 | 6208,0 | 12150,0 | 5942,0 | 0,03692 | 148,0 | 0,000738 | 200419 | 302,6 | 154,6 |
| | 5 | 6054,0 | 12082,0 | 6028,0 | 0,03767 | 150,1 | 0,000753 | 199272 | 300,9 | 150,8 |
| | | | | | | | | | | |
| Set 4 | 1 | 2044,0 | 4216,0 | 2172,0 | 0,01433 | 54,1 | 0,000287 | 188748 | 105,0 | 50,9 |
| | 2 | 2080,0 | 4138,0 | 2058,0 | 0,01358 | 51,3 | 0,000272 | 188718 | 103,1 | 51,8 |
| | 3 | 2026,0 | 4166,0 | 2140,0 | 0,01417 | 53,3 | 0,000283 | 188067 | 103,8 | 50,5 |
| | 4 | 2092,0 | 4156,0 | 2064,0 | 0,01367 | 51,4 | 0,000273 | 188022 | 103,5 | 52,1 |
| | 5 | 2010,0 | 4148,0 | 2138,0 | 0,01417 | 53,2 | 0,000283 | 187891 | 103,3 | 50,1 |
| | | | | | | | | | | |
| Set 5 | 1 | 4196,0 | 6194,0 | 1998,0 | 0,01292 | 49,8 | 0,000258 | 192575 | 154,3 | 104,5 |
| | 2 | 4090,0 | 6152,0 | 2062,0 | 0,01317 | 51,4 | 0,000263 | 194971 | 153,2 | 101,9 |
| | 3 | 4026,0 | 6168,0 | 2142,0 | 0,01375 | 53,3 | 0,000275 | 193992 | 153,6 | 100,3 |
| | 4 | 4102,0 | 6180,0 | 2078,0 | 0,01333 | 51,8 | 0,000267 | 194126 | 153,9 | 102,2 |
| | 5 | 4128,0 | 6174,0 | 2046,0 | 0,01308 | 51,0 | 0,000262 | 194790 | 153,8 | 102,8 |
| | | | | | | | | | | |
| Set 6 | 1 | 6104,0 | 8142,0 | 2038,0 | 0,01292 | 50,8 | 0,000258 | 196431 | 202,8 | 152,0 |
| | 2 | 6124,0 | 8130,0 | 2006,0 | 0,01258 | 50,0 | 0,000252 | 198572 | 202,5 | 152,5 |
| | 3 | 6046,0 | 8142,0 | 2096,0 | 0,01317 | 52,2 | 0,000263 | 198186 | 202,8 | 150,6 |
| | 4 | 6040,0 | 8106,0 | 2066,0 | 0,01308 | 51,5 | 0,000262 | 196694 | 201,9 | 150,4 |
| | 5 | 6120,0 | 8160,0 | 2040,0 | 0,01292 | 50,8 | 0,000258 | 196624 | 203,2 | 152,4 |
| | | | | | | | | | | |
| Set 7 | 1 | 8048,0 | 10186,0 | 2138,0 | 0,01358 | 53,2 | 0,000272 | 196054 | 253,7 | 200,4 |
| | 2 | 8116,7 | 10186,0 | 2069,3 | 0,01308 | 51,5 | 0,000262 | 197008 | 253,7 | 202,2 |
| | 3 | 8102,7 | 10162,0 | 2059,3 | 0,01300 | 51,3 | 0,000260 | 197262 | 253,1 | 201,8 |
| | 4 | 8042,0 | 10122,0 | 2080,0 | 0,01317 | 51,8 | 0,000263 | 196673 | 252,1 | 200,3 |
| | 5 | 8098,0 | 10204,0 | 2106,0 | 0,01333 | 52,5 | 0,000267 | 196742 | 254,1 | 201,7 |
| | | | | | | | | | | |
| Set 8 | 1 | 10156,0 | 12154,0 | 1998,0 | 0,01275 | 49,8 | 0,000255 | 195143 | 302,7 | 252,9 |
| | 2 | 10038,7 | 12102,0 | 2063,3 | 0,01308 | 51,4 | 0,000262 | 196437 | 301,4 | 250,0 |
| | 3 | 10111,3 | 12164,0 | 2052,7 | 0,01308 | 51,1 | 0,000262 | 195428 | 303,0 | 251,8 |
| | 4 | 10018,0 | 12146,0 | 2128,0 | 0,01350 | 53,0 | 0,000270 | 196293 | 302,5 | 249,5 |
| | 5 | 10094,7 | 12172,0 | 2077,3 | 0,01317 | 51,7 | 0,000263 | 196418 | 303,2 | 251,4 |

**Table 64: Elastic modulus results for specimens originating from part E, for radial position of approximately 82 mm, for forged bar of 250 mm diameter.**

| Set | Test | Min Force | Max Force | Δ Force | Δ Extension | Δ Stress | Strain | E-module | Max Stress | Min Stress |
|---|---|---|---|---|---|---|---|---|---|---|
| - | # | N | N | N | mm | Mpa | mm/mm | Mpa | Mpa | Mpa |
| Set 1 | 1 | 2066,0 | 8122,0 | 6056,0 | 0,03875 | 153,8 | 0,000775 | 198485 | 206,3 | 52,5 |
| | 2 | 2150,0 | 8114,0 | 5964,0 | 0,03842 | 151,5 | 0,000768 | 197149 | 206,1 | 54,6 |
| | 3 | 2098,0 | 8136,0 | 6038,0 | 0,03892 | 153,4 | 0,000778 | 197031 | 206,7 | 53,3 |
| | 4 | 2144,0 | 8000,0 | 5856,0 | 0,03767 | 148,7 | 0,000753 | 197433 | 203,2 | 54,5 |
| | 5 | 2030,0 | 8158,0 | 6128,0 | 0,03942 | 155,7 | 0,000788 | 197431 | 207,2 | 51,6 |
| | | | | | | | | | | |
| Set 2 | 1 | 4098,0 | 10022,0 | 5924,0 | 0,03775 | 150,5 | 0,000755 | 199302 | 254,6 | 104,1 |
| | 2 | 4092,0 | 10128,0 | 6036,0 | 0,03817 | 153,3 | 0,000763 | 200836 | 257,3 | 103,9 |
| | 3 | 4088,0 | 10170,0 | 6082,0 | 0,03900 | 154,5 | 0,000780 | 198059 | 258,3 | 103,8 |
| | 4 | 4102,0 | 10124,0 | 6022,0 | 0,03817 | 153,0 | 0,000763 | 200370 | 257,2 | 104,2 |
| | 5 | 4066,0 | 10174,0 | 6108,0 | 0,03867 | 155,1 | 0,000773 | 200603 | 258,4 | 103,3 |
| | | | | | | | | | | |
| Set 3 | 1 | 6192,0 | 12144,0 | 5952,0 | 0,03750 | 151,2 | 0,000750 | 201579 | 308,5 | 157,3 |
| | 2 | 6200,0 | 12022,0 | 5822,0 | 0,03658 | 147,9 | 0,000732 | 202135 | 305,4 | 157,5 |
| | 3 | 6090,0 | 12030,0 | 5940,0 | 0,03800 | 150,9 | 0,000760 | 198526 | 305,6 | 154,7 |
| | 4 | 5992,0 | 12130,0 | 6138,0 | 0,03933 | 155,9 | 0,000787 | 198206 | 308,1 | 152,2 |
| | 5 | 6132,0 | 12152,0 | 6020,0 | 0,03867 | 152,9 | 0,000773 | 197713 | 308,7 | 155,8 |
| | | | | | | | | | | |
| Set 4 | 1 | 2086,0 | 4100,0 | 2014,0 | 0,01300 | 51,2 | 0,000260 | 196757 | 104,1 | 53,0 |
| | 2 | 2104,0 | 4050,0 | 1946,0 | 0,01250 | 49,4 | 0,000250 | 197718 | 102,9 | 53,4 |
| | 3 | 2030,0 | 4070,0 | 2040,0 | 0,01308 | 51,8 | 0,000262 | 198078 | 103,4 | 51,6 |
| | 4 | 2040,0 | 4134,0 | 2094,0 | 0,01342 | 53,2 | 0,000268 | 198170 | 105,0 | 51,8 |
| | 5 | 2034,0 | 4154,0 | 2120,0 | 0,01367 | 53,8 | 0,000273 | 196961 | 105,5 | 51,7 |
| | | | | | | | | | | |
| Set 5 | 1 | 4094,0 | 6074,0 | 1980,0 | 0,01258 | 50,3 | 0,000252 | 199893 | 154,3 | 104,0 |
| | 2 | 4026,0 | 6106,0 | 2080,0 | 0,01317 | 52,8 | 0,000263 | 200582 | 155,1 | 102,3 |
| | 3 | 4046,0 | 6042,0 | 1996,0 | 0,01258 | 50,7 | 0,000252 | 201509 | 153,5 | 102,8 |
| | 4 | 4034,0 | 6076,0 | 2042,0 | 0,01300 | 51,9 | 0,000260 | 199492 | 154,3 | 102,5 |
| | 5 | 4030,0 | 6068,0 | 2038,0 | 0,01292 | 51,8 | 0,000258 | 200334 | 154,1 | 102,4 |
| | | | | | | | | | | |
| Set 6 | 1 | 6060,0 | 8036,0 | 1976,0 | 0,01250 | 50,2 | 0,000250 | 200766 | 204,1 | 153,9 |
| | 2 | 6084,0 | 8164,0 | 2080,0 | 0,01317 | 52,8 | 0,000263 | 200582 | 207,4 | 154,5 |
| | 3 | 6112,0 | 8118,0 | 2006,0 | 0,01267 | 51,0 | 0,000253 | 201080 | 206,2 | 155,2 |
| | 4 | 6074,0 | 8162,0 | 2088,0 | 0,01325 | 53,0 | 0,000265 | 200137 | 207,3 | 154,3 |
| | 5 | 6162,0 | 8118,0 | 1956,0 | 0,01242 | 49,7 | 0,000248 | 200014 | 206,2 | 156,5 |
| | | | | | | | | | | |
| Set 7 | 1 | 8090,0 | 10154,0 | 2064,0 | 0,01308 | 52,4 | 0,000262 | 200408 | 257,9 | 205,5 |
| | 2 | 8116,0 | 10104,0 | 1988,0 | 0,01258 | 50,5 | 0,000252 | 200701 | 256,6 | 206,2 |
| | 3 | 8124,0 | 10034,0 | 1910,0 | 0,01208 | 48,5 | 0,000242 | 200808 | 254,9 | 206,4 |
| | 4 | 8090,0 | 10064,0 | 1974,0 | 0,01250 | 50,1 | 0,000250 | 200563 | 255,6 | 205,5 |
| | 5 | 8064,0 | 10168,0 | 2104,0 | 0,01333 | 53,4 | 0,000267 | 200461 | 258,3 | 204,8 |
| | | | | | | | | | | |
| Set 8 | 1 | 10136,0 | 12040,0 | 1904,0 | 0,01200 | 48,4 | 0,000240 | 201511 | 305,8 | 257,5 |
| | 2 | 9904,0 | 12016,0 | 2112,0 | 0,01333 | 53,6 | 0,000267 | 201223 | 305,2 | 251,6 |
| | 3 | 10063,3 | 12186,0 | 2122,7 | 0,01350 | 53,9 | 0,000270 | 199696 | 309,5 | 255,6 |
| | 4 | 10172,7 | 12082,0 | 1909,3 | 0,01208 | 48,5 | 0,000242 | 200734 | 306,9 | 258,4 |
| | 5 | 10029,3 | 12054,0 | 2024,7 | 0,01267 | 51,4 | 0,000253 | 202954 | 306,2 | 254,8 |

**Table 65: Elastic modulus results for specimens originating from part F, for radial position of approximately 48 mm, for forged bar of 250 mm diameter.**

| Set | Test | Min Force | Max Force | Δ Force | Δ Extension | Δ Stress | Strain | E-module | Max Stress | Min Stress |
|---|---|---|---|---|---|---|---|---|---|---|
| - | # | N | N | N | mm | Mpa | mm/mm | Mpa | Mpa | Mpa |
| Set 3 | 1 | 2156,0 | 8160,0 | 6004,0 | 0,04142 | 156,0 | 0,000828 | 188328 | 212,0 | 56,0 |
| | 2 | 2066,0 | 8026,0 | 5960,0 | 0,04117 | 154,9 | 0,000823 | 188083 | 208,6 | 53,7 |
| | 3 | 2136,0 | 8212,0 | 6076,0 | 0,04192 | 157,9 | 0,000838 | 188313 | 213,4 | 55,5 |
| | 4 | 2070,0 | 8082,0 | 6012,0 | 0,04142 | 156,2 | 0,000828 | 188579 | 210,0 | 53,8 |
| | 5 | 2102,0 | 8136,0 | 6034,0 | 0,04167 | 156,8 | 0,000833 | 188133 | 211,4 | 54,6 |
| | | | | | | | | | | |
| Set 2 | 1 | 4110,0 | 10338,0 | 6228,0 | 0,04317 | 161,8 | 0,000863 | 187435 | 268,6 | 106,8 |
| | 2 | 4036,0 | 10100,0 | 6064,0 | 0,04208 | 157,6 | 0,000842 | 187227 | 262,4 | 104,9 |
| | 3 | 4028,0 | 10178,0 | 6150,0 | 0,04267 | 159,8 | 0,000853 | 187256 | 264,5 | 104,7 |
| | 4 | 4106,0 | 10174,0 | 6068,0 | 0,04225 | 157,7 | 0,000845 | 186596 | 264,4 | 106,7 |
| | 5 | 4014,0 | 10176,0 | 6162,0 | 0,04282 | 160,1 | 0,000856 | 186964 | 264,4 | 104,3 |
| | | | | | | | | | | |
| Set 1 | 1 | 6022,0 | 12110,0 | 6088,0 | 0,04200 | 158,2 | 0,000840 | 188326 | 314,7 | 156,5 |
| | 2 | 5980,0 | 12172,0 | 6192,0 | 0,04250 | 160,9 | 0,000850 | 189289 | 316,3 | 155,4 |
| | 3 | 6078,0 | 12192,0 | 6114,0 | 0,04217 | 158,9 | 0,000843 | 188367 | 316,8 | 157,9 |
| | 4 | 6048,0 | 12062,0 | 6014,0 | 0,04117 | 156,3 | 0,000823 | 189787 | 313,4 | 157,2 |
| | 5 | 6028,0 | 12300,0 | 6272,0 | 0,04308 | 163,0 | 0,000862 | 189154 | 319,6 | 156,6 |
| | | | | | | | | | | |
| Set 4 | 1 | 2048,0 | 4128,0 | 2080,0 | 0,01467 | 54,0 | 0,000293 | 184212 | 107,3 | 53,2 |
| | 2 | 2044,0 | 4072,0 | 2028,0 | 0,01425 | 52,7 | 0,000285 | 184900 | 105,8 | 53,1 |
| | 3 | 2032,0 | 4098,0 | 2066,0 | 0,01450 | 53,7 | 0,000290 | 185117 | 106,5 | 52,8 |
| | 4 | 2058,0 | 4170,0 | 2112,0 | 0,01483 | 54,9 | 0,000297 | 185028 | 108,4 | 53,5 |
| | 5 | 2012,0 | 4140,0 | 2128,0 | 0,01500 | 55,3 | 0,000300 | 184317 | 107,6 | 52,3 |
| | | | | | | | | | | |
| Set 5 | 1 | 4066,0 | 6096,0 | 2030,0 | 0,01392 | 52,7 | 0,000278 | 189470 | 158,4 | 105,7 |
| | 2 | 4078,0 | 6072,0 | 1994,0 | 0,01367 | 51,8 | 0,000273 | 189514 | 157,8 | 106,0 |
| | 3 | 4072,7 | 6116,0 | 2043,3 | 0,01408 | 53,1 | 0,000282 | 188544 | 158,9 | 105,8 |
| | 4 | 4088,0 | 6110,0 | 2022,0 | 0,01383 | 52,5 | 0,000277 | 189952 | 158,8 | 106,2 |
| | 5 | 4112,0 | 6092,0 | 1980,0 | 0,01350 | 51,4 | 0,000270 | 190553 | 158,3 | 106,8 |
| | | | | | | | | | | |
| Set 6 | 1 | 6148,0 | 8154,0 | 2006,0 | 0,01400 | 52,1 | 0,000280 | 186160 | 211,9 | 159,8 |
| | 2 | 6066,0 | 8162,0 | 2096,0 | 0,01467 | 54,5 | 0,000293 | 185629 | 212,1 | 157,6 |
| | 3 | 6114,0 | 8180,0 | 2066,0 | 0,01442 | 53,7 | 0,000288 | 186144 | 212,6 | 158,9 |
| | 4 | 6022,0 | 8060,0 | 2038,0 | 0,01442 | 53,0 | 0,000288 | 183621 | 209,4 | 156,5 |
| | 5 | 6116,0 | 8128,0 | 2012,0 | 0,01408 | 52,3 | 0,000282 | 185656 | 211,2 | 158,9 |
| | | | | | | | | | | |
| Set 7 | 1 | 8094,7 | 10176,0 | 2081,3 | 0,01475 | 54,1 | 0,000295 | 183327 | 264,4 | 210,3 |
| | 2 | 8072,0 | 10244,0 | 2172,0 | 0,01542 | 56,4 | 0,000308 | 183004 | 266,2 | 209,7 |
| | 3 | 8058,0 | 10190,0 | 2132,0 | 0,01517 | 55,4 | 0,000303 | 182594 | 264,8 | 209,4 |
| | 4 | 8086,7 | 10180,0 | 2093,3 | 0,01483 | 54,4 | 0,000297 | 183389 | 264,5 | 210,1 |
| | 5 | 8139,3 | 10116,0 | 1976,7 | 0,01408 | 51,4 | 0,000282 | 182399 | 262,9 | 211,5 |
| | | | | | | | | | | |
| Set 8 | 1 | 10018,0 | 12076,0 | 2058,0 | 0,01475 | 53,5 | 0,000295 | 181275 | 313,8 | 260,3 |
| | 2 | 10134,7 | 12174,0 | 2039,3 | 0,01467 | 53,0 | 0,000293 | 180607 | 316,3 | 263,3 |
| | 3 | 10051,3 | 12184,0 | 2132,7 | 0,01533 | 55,4 | 0,000307 | 180747 | 316,6 | 261,2 |
| | 4 | 10068,0 | 12204,0 | 2136,0 | 0,01533 | 55,5 | 0,000307 | 181027 | 317,1 | 261,6 |
| | 5 | 10079,3 | 12202,0 | 2122,7 | 0,01525 | 55,2 | 0,000305 | 180843 | 317,1 | 261,9 |

# Appendix H: Elastic Modulus Graphs for UNS S31803

**Table 66: Averaged elastic modulus for specimen obtained from part A, for forged bar of 250 mm diameter.**

| Symbol | Set 1 | Set 2 | Set 3 | Set 4 | Set 5 | Set 6 | Set 7 | Set 8 | Unit |
|---|---|---|---|---|---|---|---|---|---|
| E | 203167 | 189911 | 183668 | 226798 | 194547 | 186680 | 183625 | 182164 | MPa |
| St. Dev. | 827 | 300 | 514 | 458 | 458 | 585 | 365 | 717 | MPa |
| Avg(E) | 202675 | 188284 | 184157 | - | | | | | MPa |

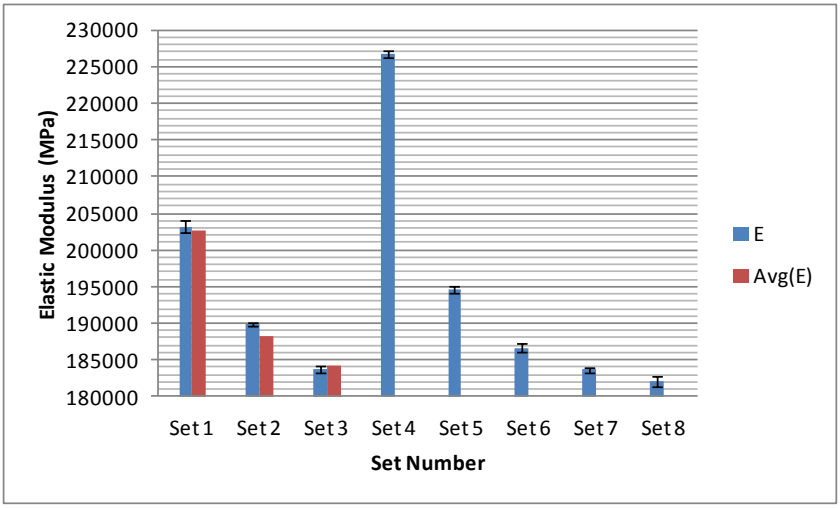


**Figure 91: Averaged elastic modulus for specimen obtained from part A, for forged bar of 250 mm diameter.**

**Table 67: Averaged elastic modulus for specimen obtained from part B, for radial position of 29 mm, for forged bar of 250 mm diameter.**

| Symbol | Set 1 | Set 2 | Set 3 | Set 4 | Set 5 | Set 6 | Set 7 | Set 8 | Unit |
|---|---|---|---|---|---|---|---|---|---|
| E | 194521 | 195268 | 195029 | 190855 | 194022 | 192345 | 192448 | 190187 | MPa |
| St. Dev. | 280 | 187 | 293 | 288 | 288 | 919 | 385 | 758 | MPa |
| Avg(E) | 192407 | 192939 | 191660 | - | | | | | MPa |

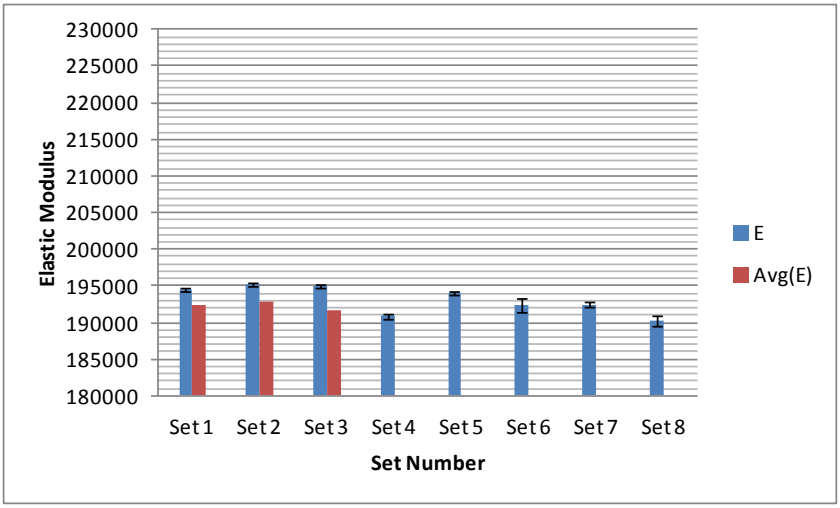


**Figure 92: Averaged elastic modulus for specimen obtained from part B, for radial position of 29 mm, for forged bar of 250 mm diameter.**

**Table 68: Averaged elastic modulus for specimen obtained from part B, for radial position of 48 mm, for forged bar of 250 mm diameter.**

| Symbol | Set 1 | Set 2 | Set 3 | Set 4 | Set 5 | Set 6 | Set 7 | Set 8 | Unit |
|---|---|---|---|---|---|---|---|---|---|
| E | 187174 | 189899 | 192442 | 183242 | 188353 | 189042 | 189993 | 188735 | MPa |
| St. Dev. | 214 | 211 | 498 | 721 | 721 | 685 | 515 | 308 | MPa |
| Avg(E) | 186879 | 189130 | 189257 | - | | | | | MPa |

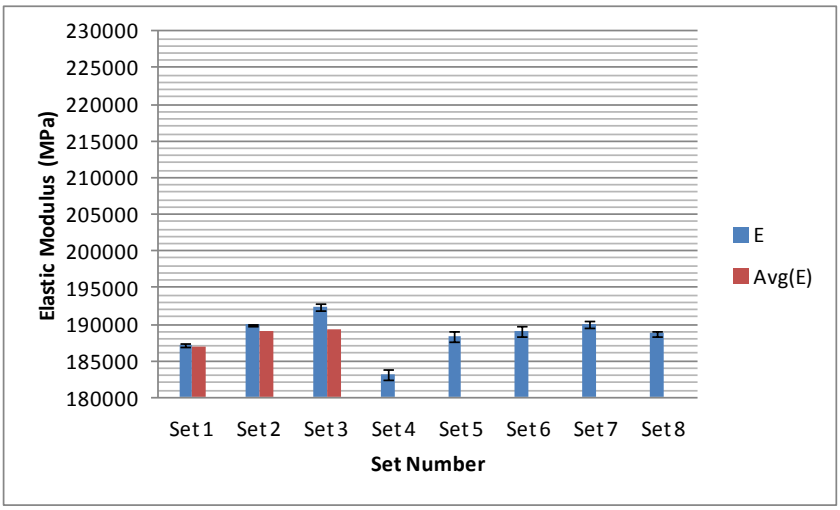


**Figure 93: Averaged elastic modulus for specimen obtained from part B, for radial position of 48 mm, for forged bar of 250 mm diameter.**

**Table 69: Averaged elastic modulus for specimen obtained from part B, for radial position of 82 mm, for forged bar of 250 mm diameter.**

| Symbol | Set 1 | Set 2 | Set 3 | Set 4 | Set 5 | Set 6 | Set 7 | Set 8 | Unit |
|---|---|---|---|---|---|---|---|---|---|
| E | 192498 | 196473 | 198979 | 188289 | 194091 | 197301 | 196748 | 195944 | MPa |
| St. Dev. | 288 | 184 | 1011 | 945 | 945 | 998 | 453 | 612 | MPa |
| Avg(E) | 193227 | 196047 | 196664 | - | | | | | MPa |

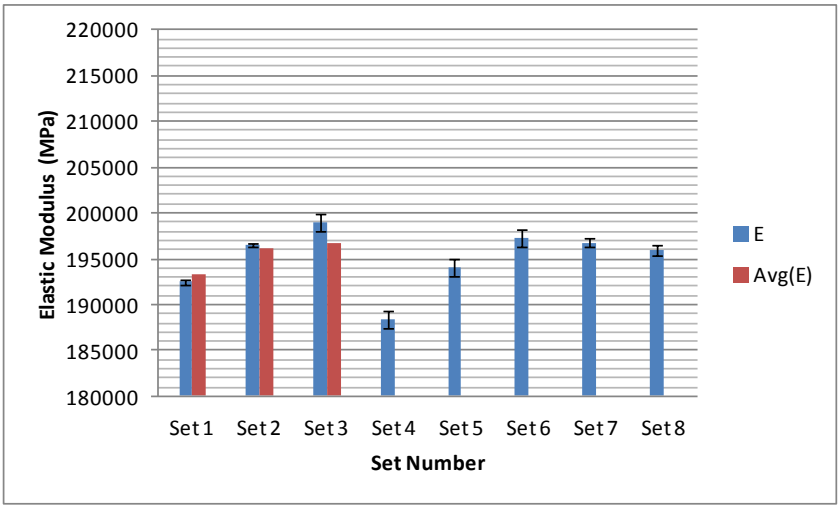


**Figure 94: Averaged elastic modulus for specimen obtained from part B, for radial position of 82 mm, for forged bar of 250 mm diameter.**

**Table 70: Averaged elastic modulus for specimen obtained from part B, for radial position of approximately 82 mm, for forged bar of 250 mm diameter.**

| Symbol | Set 1 | Set 2 | Set 3 | Set 4 | Set 5 | Set 6 | Set 7 | Set 8 | Unit |
|---|---|---|---|---|---|---|---|---|---|
| E | 197506 | 199834 | 199632 | 197537 | 200362 | 200516 | 200588 | 201224 | MPa |
| St. Dev. | 575 | 1153 | 2061 | 765 | 765 | 441 | 166 | 1189 | MPa |
| Avg(E) | 199472 | 200489 | 200776 | - | | | | | MPa |

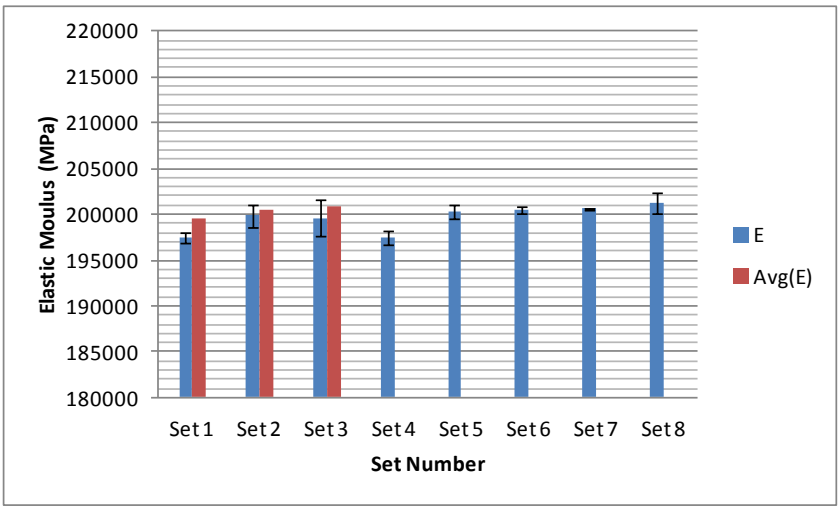


**Figure 95: Averaged elastic modulus for specimen obtained from part B, for radial position of approximately 82 mm, for forged bar of 250 mm diameter.**

**Table 71: Averaged elastic modulus for specimen obtained from part B, for radial position of approximately 48 mm, for forged bar of 250 mm diameter.**

| Symbol | Set 1 | Set 2 | Set 3 | Set 4 | Set 5 | Set 6 | Set 7 | Set 8 | Unit |
|---|---|---|---|---|---|---|---|---|---|
| E | 188287 | 187096 | 188985 | 184715 | 189607 | 185442 | 182943 | 180900 | MPa |
| St. Dev. | 195 | 326 | 629 | 737 | 737 | 1049 | 438 | 259 | MPa |
| Avg(E) | 186588 | 185997 | 183095 | - | | | | | MPa |

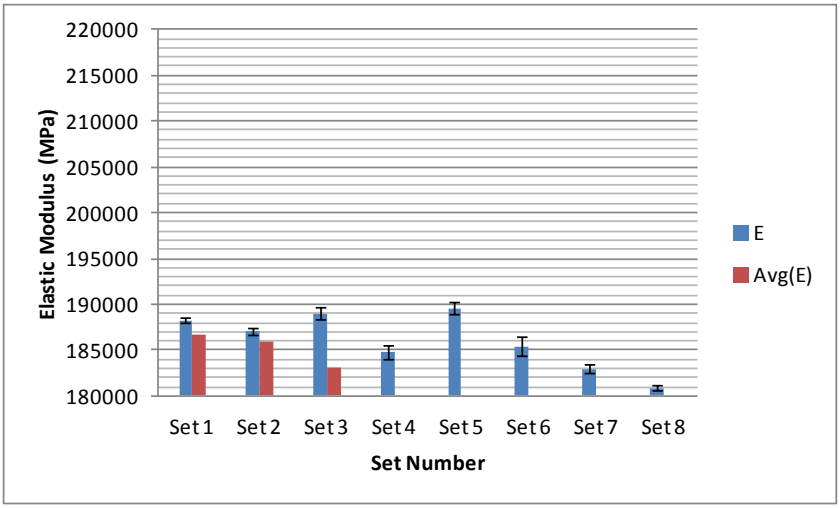


**Figure 96: Averaged elastic modulus for specimen obtained from part B, for radial position of approximately 48 mm, for forged bar of 250 mm diameter.**

# Appendix I: Stress-Strain Data for UNS S31803

**Table 72: Stress-strain data for UNS S31803, for 220 mm diameter forged bar.**

| | | Eng. Yield Strength | | | Eng. Tensile Strength | | |
|---|---|---|---|---|---|---|---|
| Radial Pos. | ID | Yield | Average | St. Dev | Tensile | Average | St. Dev. |
| mm | - | MPa | MPa | MPa | MPa | MPa | MPa |
| 29 | 220-LS-C-01 | 595,0 | 588,5 | 12,5 | 748,4 | 745,0 | 2,5 |
| 29 | 220-LS-C-02 | 592,0 | | | 744,0 | | |
| 29 | 220-LS-D-01 | 597,0 | | | 745,1 | | |
| 29 | 220-LS-D-02 | 570,0 | | | 742,6 | | |
| 48 | 220-LS-C-03 | 597,0 | 584,0 | 12,9 | 742,9 | 739,8 | 6,0 |
| 48 | 220-LS-C-04 | 571,0 | | | 732,9 | | |
| 48 | 220-LS-D-03 | 575,0 | | | 746,4 | | |
| 48 | 220-LS-D-04 | 593,0 | | | 737,0 | | |
| 82 | 220-LS-C-05 | 615,0 | 607,5 | 7,2 | 747,5 | 744,8 | 4,3 |
| 82 | 220-LS-C-06 | 604,5 | | | 749,5 | | |
| 82 | 220-LS-D-05 | 611,5 | | | 740,6 | | |
| 82 | 220-LS-D-06 | 599,0 | | | 741,7 | | |
| 47 | 220-TS-F-01 | 593,0 | 594,6 | 2,9 | 755,7 | 760,7 | 5,0 |
| 47 | 220-TS-F-02 | 598,0 | | | 762,7 | | |
| 47 | 220-TS-F-03 | 596,0 | | | 760,5 | | |
| 47 | 220-TS-F-04 | 590,5 | | | 756,5 | | |
| 47 | 220-TS-F-05 | 595,5 | | | 767,9 | | |
| 78,5 | 220-TS-E-01 | 598,0 | 595,1 | 8,9 | 758,0 | 758,5 | 4,3 |
| 78,5 | 220-TS-E-02 | 579,0 | | | 767,7 | | |
| 78,5 | 220-TS-E-03 | 593,0 | | | 756,4 | | |
| 78,5 | 220-TS-E-04 | 606,0 | | | 756,8 | | |
| 78,5 | 220-TS-E-05 | 591,0 | | | 759,1 | | |
| 78,5 | 220-TS-E-06 | 603,0 | | | 757,1 | | |
| 78,5 | 220-TS-E-07 | 596,0 | | | 754,4 | | |
| 23,5 | 220-RS-A-01 | 598,0 | 593,0 | 7,1 | 760,5 | 755,7 | 4,9 |
| 23,5 | 220-RS-A-02 | 586,0 | | | 753,8 | | |
| 23,5 | 220-RS-A-03 | 598,0 | | | 761,9 | | |
| 23,5 | 220-RS-A-04 | 590,0 | | | 751,8 | | |
| 23,5 | 220-RS-A-05 | 604,0 | | | 758,3 | | |
| 23,5 | 220-RS-A-06 | 585,0 | | | 748,3 | | |
| 23,5 | 220-RS-A-07 | 590,0 | | | 755,1 | | |
| 48 | 220-RS-A-08 | 607,0 | 605,0 | 4,0 | 752,4 | 752,9 | 3,9 |
| 48 | 220-RS-A-09 | 607,0 | | | 748,6 | | |
| 48 | 220-RS-A-10 | 611,0 | | | 759,8 | | |
| 48 | 220-RS-A-11 | 603,0 | | | 754,4 | | |
| 48 | 220-RS-A-12 | 601,0 | | | 750,8 | | |
| 48 | 220-RS-A-13 | 601,0 | | | 751,4 | | |
| 85,5 | 220-RS-A-15 | 590,0 | 596,1 | 7,8 | 746,5 | 754,0 | 6,0 |
| 85,5 | 220-RS-A-16 | 600,0 | | | 757,1 | | |
| 85,5 | 220-RS-A-17 | 583,0 | | | 746,3 | | |
| 85,5 | 220-RS-A-18 | 600,0 | | | 759,6 | | |
| 85,5 | 220-RS-A-19 | 601,5 | | | 756,9 | | |
| 85,5 | 220-RS-A-20 | 602,0 | | | 757,7 | | |

**Table 73: Stress-strain data for UNS S31803, for 250 mm diameter forged bar.**

| | | Eng. Yield Strength | | | Eng. Tensile Strength | | |
|---|---|---|---|---|---|---|---|
| Radial Pos. | ID | Value | Average | St. Dev | Tensile | Average | St. Dev. |
| mm | - | MPa | MPa | MPa | MPa | MPa | MPa |
| 29 | 250-LS-C-01 | 574,0 | 575,5 | 9,9 | 735,7 | 741,0 | 5,6 |
| 29 | 250-LS-C-02 | 589,0 | | | 747,0 | | |
| 29 | 250-LS-D-01 | 574,0 | | | 744,3 | | |
| 29 | 250-LS-D-02 | 565,0 | | | 736,8 | | |
| 48 | 250-LS-C-03 | 566,0 | 563,9 | 4,6 | 731,4 | 731,4 | 1,5 |
| 48 | 250-LS-C-04 | 566,0 | | | 733,1 | | |
| 48 | 250-LS-D-03 | 557,0 | | | 731,5 | | |
| 48 | 250-LS-D-04 | 566,5 | | | 729,4 | | |
| 82 | 250-LS-C-05 | 584,0 | 577,0 | 6,0 | 728,0 | 726,9 | 1,1 |
| 82 | 250-LS-C-06 | 580,0 | | | 727,2 | | |
| 82 | 250-LS-D-05 | 572,0 | | | 725,3 | | |
| 82 | 250-LS-D-06 | 572,0 | | | 727,2 | | |
| 47 | 250-TS-F-03 | 578,0 | 576,7 | 2,8 | 739,0 | 737,2 | 6,1 |
| 47 | 250-TS-F-04 | 572,0 | | | 737,0 | | |
| 47 | 250-TS-F-05 | 577,0 | | | 743,0 | | |
| 47 | 250-TS-F-06 | 579,5 | | | 727,0 | | |
| 47 | 250-TS-F-07 | 577,0 | | | 740,0 | | |
| 78,5 | 250-TS-E-01 | 581,5 | 582,3 | 3,8 | 724,9 | 740,7 | 9,6 |
| 78,5 | 250-TS-E-02 | 581,0 | | | 746,5 | | |
| 78,5 | 250-TS-E-03 | 577,0 | | | 743,6 | | |
| 78,5 | 250-TS-E-05 | 587,5 | | | 733,8 | | |
| 78,5 | 250-TS-E-06 | 586,0 | | | 751,0 | | |
| 78,5 | 250-TS-E-07 | 581,0 | | | 744,5 | | |
| 23,5 | 250-RS-A-01 | 577,0 | 574,9 | 5,2 | 743,8 | 740,6 | 3,3 |
| 23,5 | 250-RS-A-03 | 581,0 | | | 741,4 | | |
| 23,5 | 250-RS-A-04 | 572,5 | | | 741,3 | | |
| 23,5 | 250-RS-A-06 | 569,0 | | | 736,0 | | |
| 48 | 250-RS-A-08 | 581,0 | 579,0 | 4,8 | 746,4 | 742,1 | 4,9 |
| 48 | 250-RS-A-09 | 580,0 | | | 747,2 | | |
| 48 | 250-RS-A-10 | 587,0 | | | 747,8 | | |
| 48 | 250-RS-A-11 | 581,0 | | | 739,7 | | |
| 48 | 250-RS-A-12 | 572,0 | | | 736,8 | | |
| 48 | 250-RS-A-13 | 576,0 | | | 740,0 | | |
| 48 | 250-RS-A-14 | 576,0 | | | 736,6 | | |
| 85,5 | 250-RS-A-15 | 576,0 | 631,4 | 46,5 | 738,1 | 770,9 | 24,4 |
| 85,5 | 250-RS-A-16 | 590,0 | | | 750,3 | | |
| 85,5 | 250-RS-A-17 | 666,0 | | | 787,7 | | |
| 85,5 | 250-RS-A-18 | 582,0 | | | 747,1 | | |
| 85,5 | 250-RS-A-19 | 654,0 | | | 787,6 | | |
| 85,5 | 250-RS-A-20 | 670,0 | | | 792,1 | | |
| 85,5 | 250-RS-A-21 | 682,0 | | | 793,2 | | |

# Appendix J: Stress-Strain Curves for UNS S31803

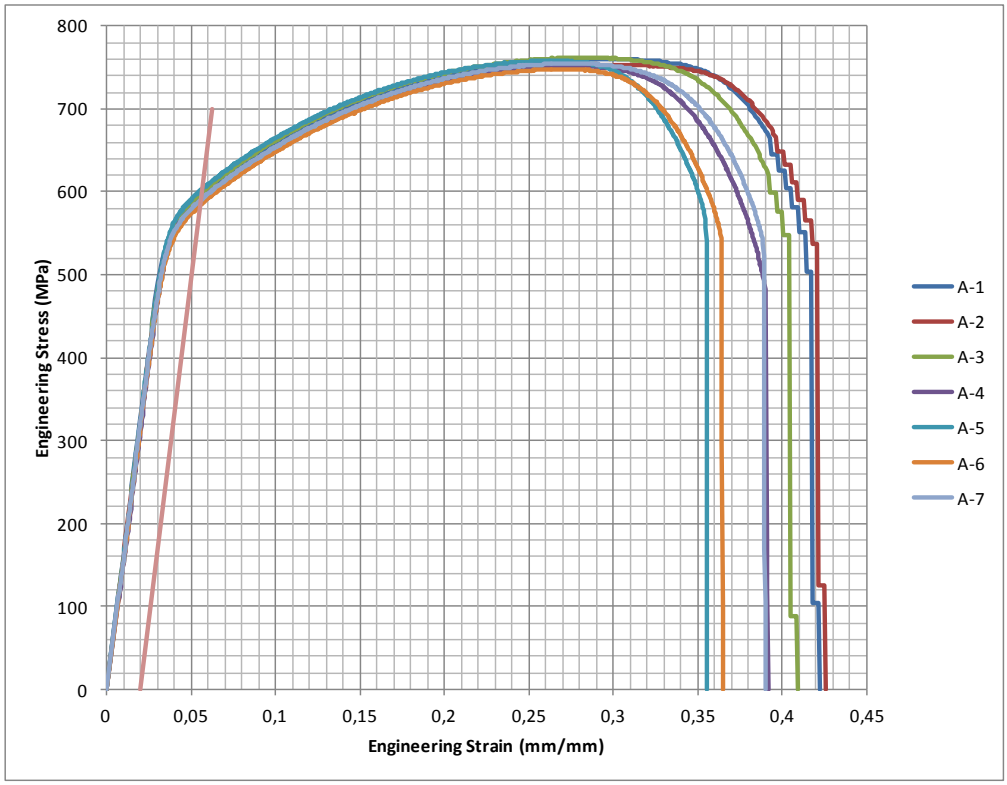


**Figure 97: Stress-strain curves for 220-A-23.5.**

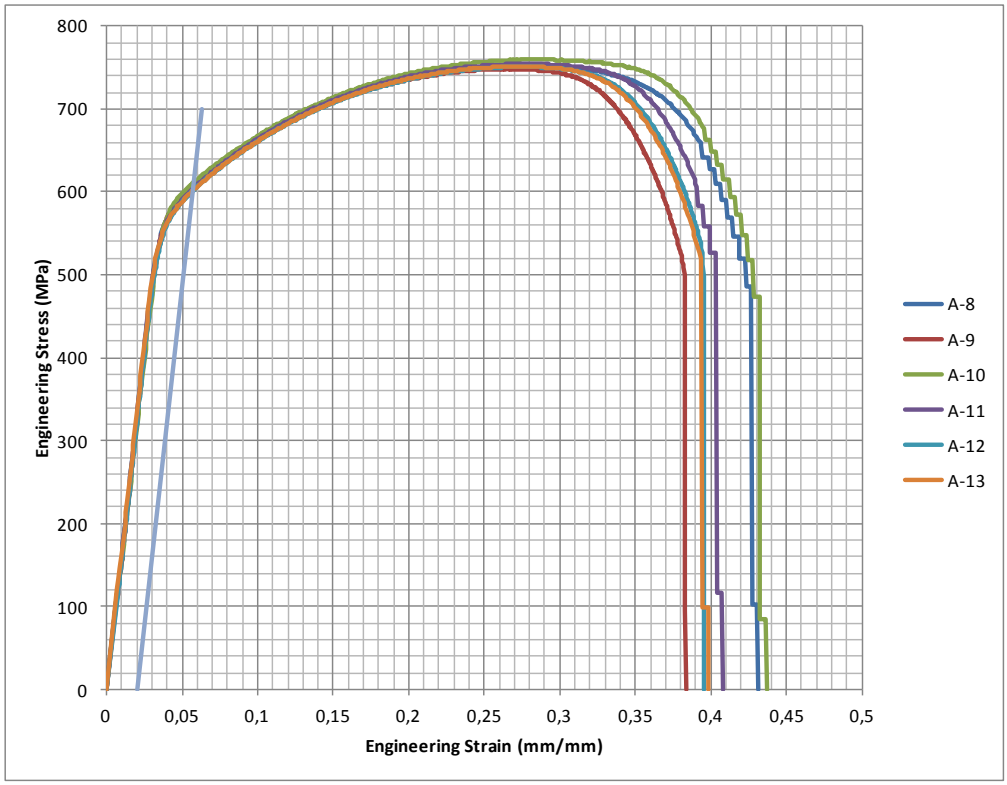


**Figure 98: Stress-strain curves for 220-A-48.**

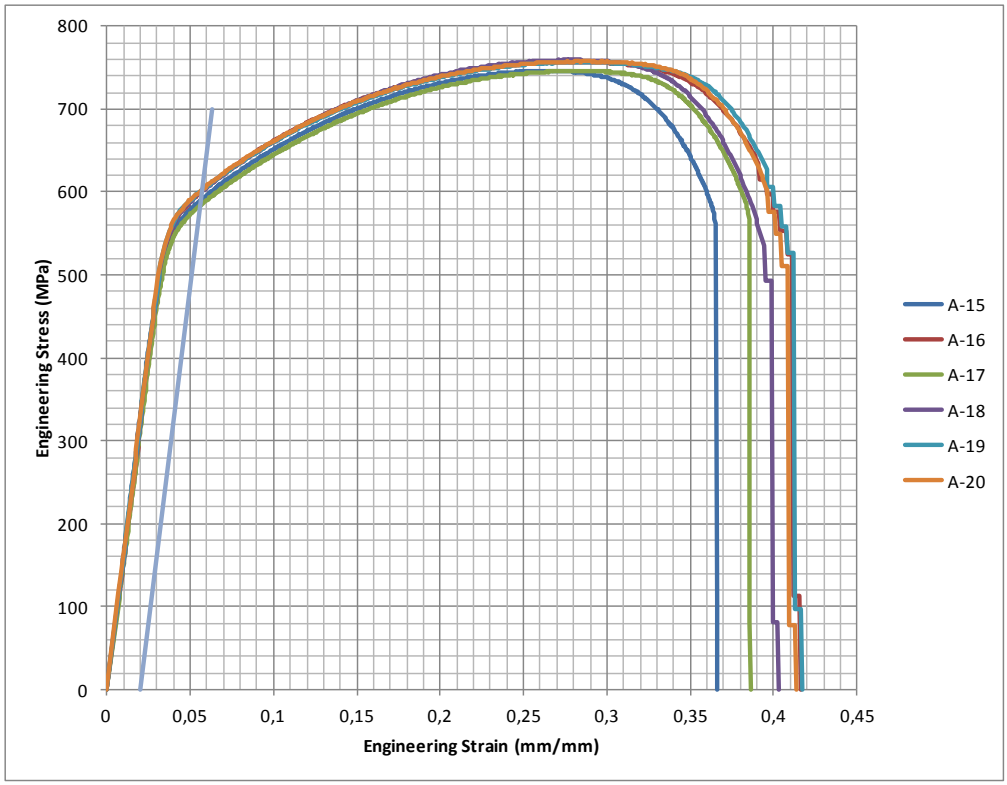


**Figure 99: Stress-strain curves for 220-A-85.5.**

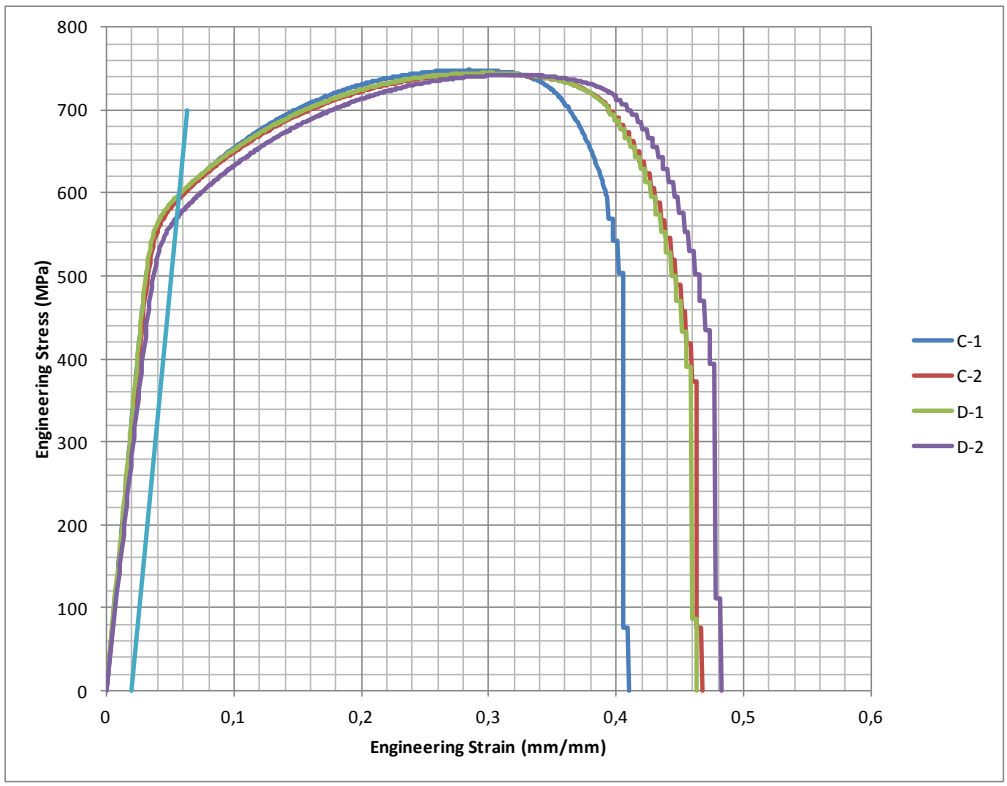


**Figure 100: Stress-strain curves for 220-C-29 and 220-D-29.**

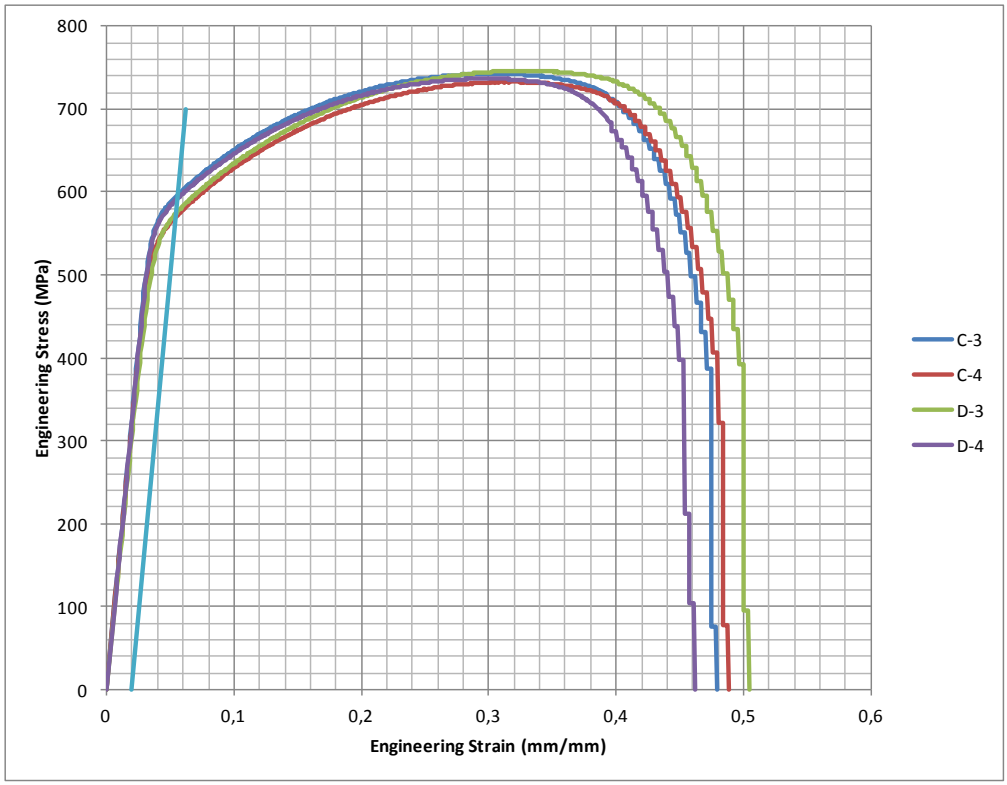


**Figure 101: Stress-strain curves for 220-C-48 and 220-D-48.**

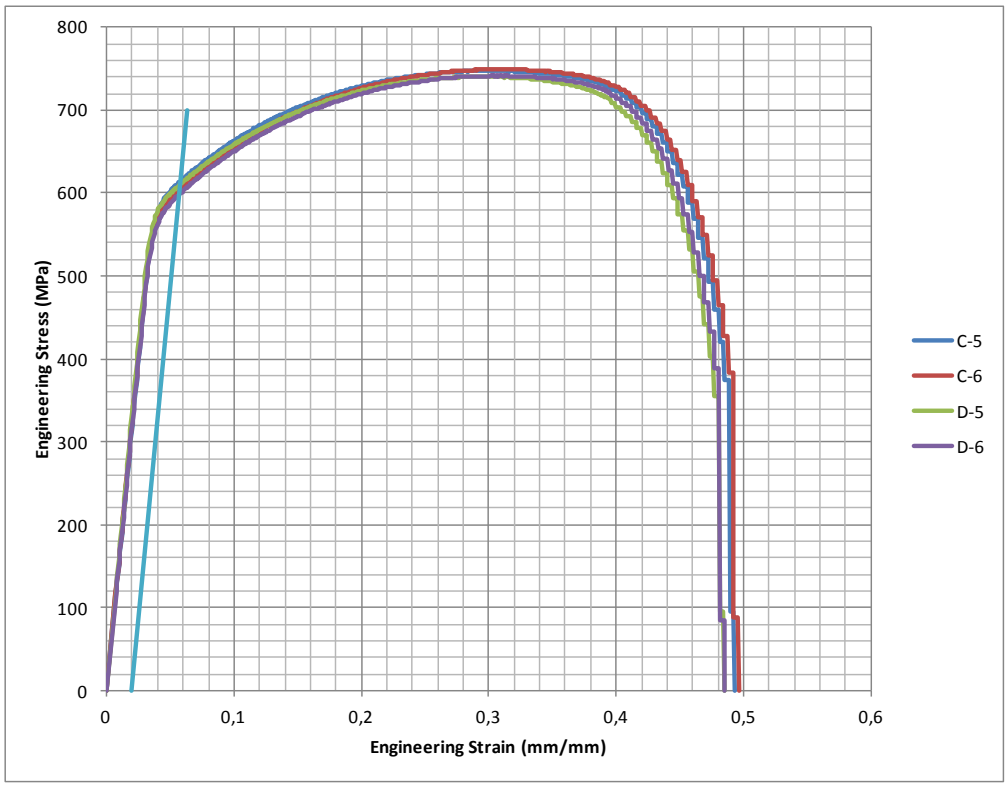


**Figure 102: Stress-strain curves for 220-C-82 and 220-D-82.**

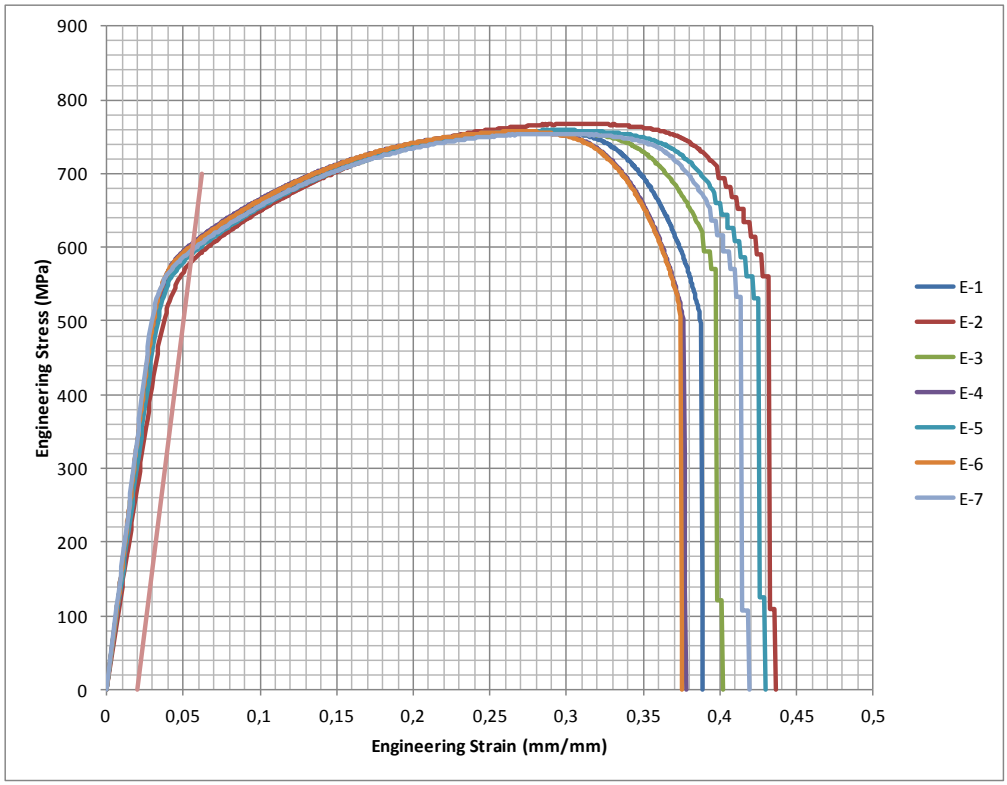


**Figure 103: Stress-strain curves for 220-E-78.5.**

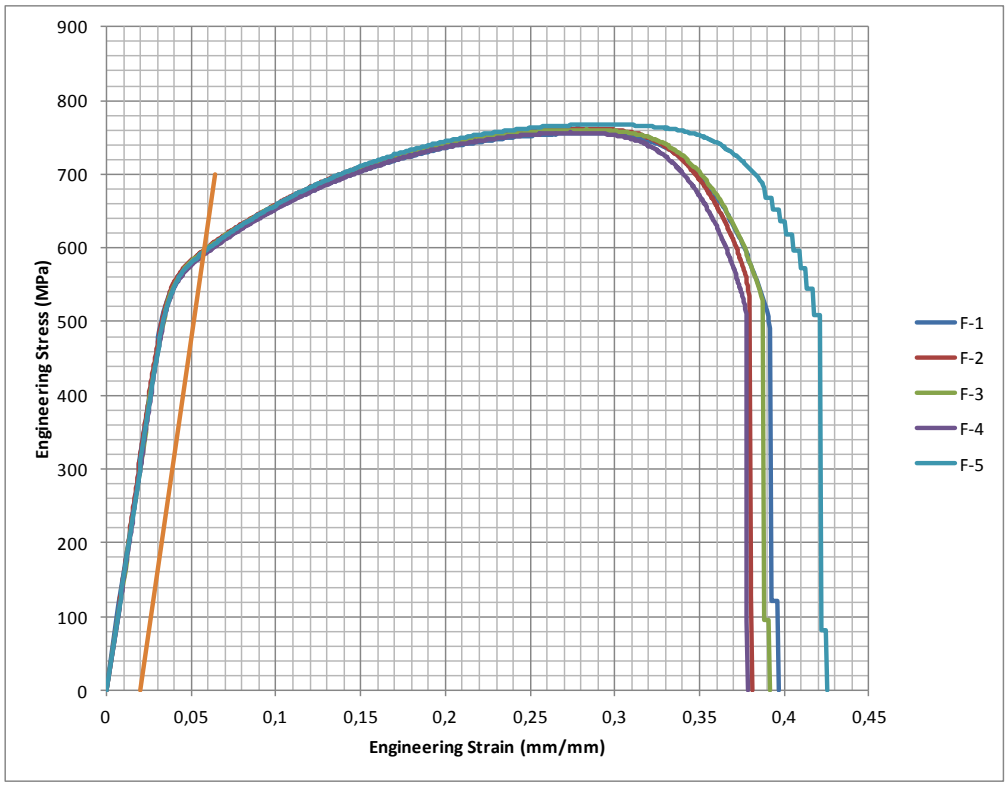


**Figure 104: Stress-strain curves for 220-F-47.**

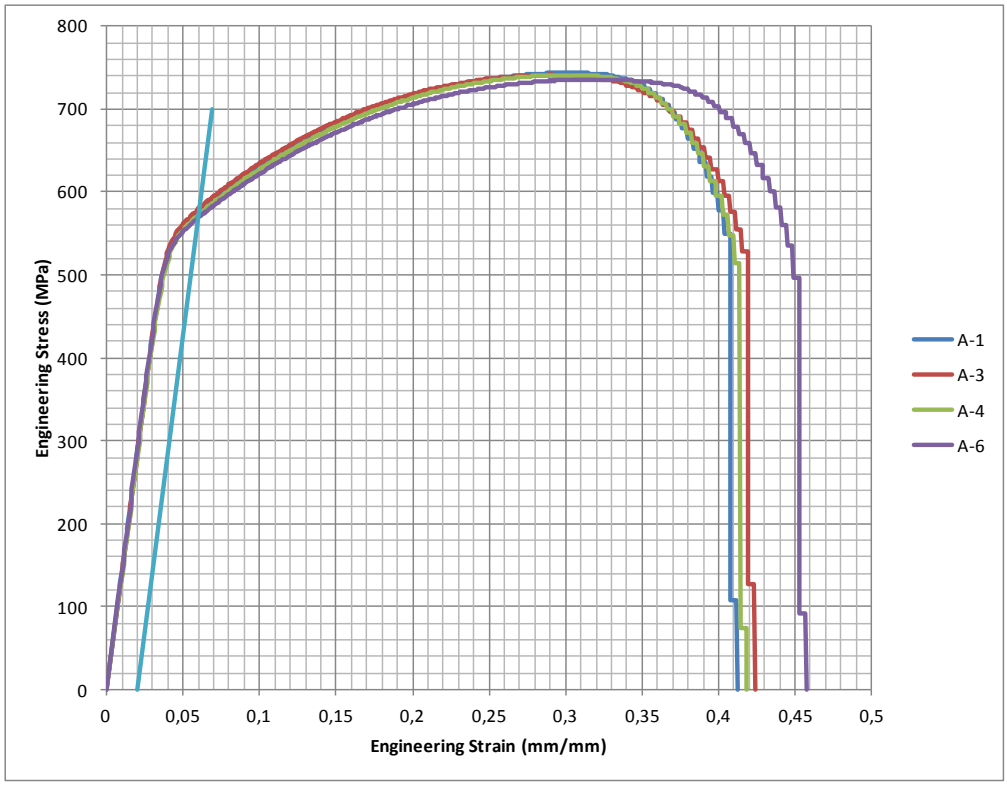


**Figure 105: Stress-strain curves for 250-A-23.5.**

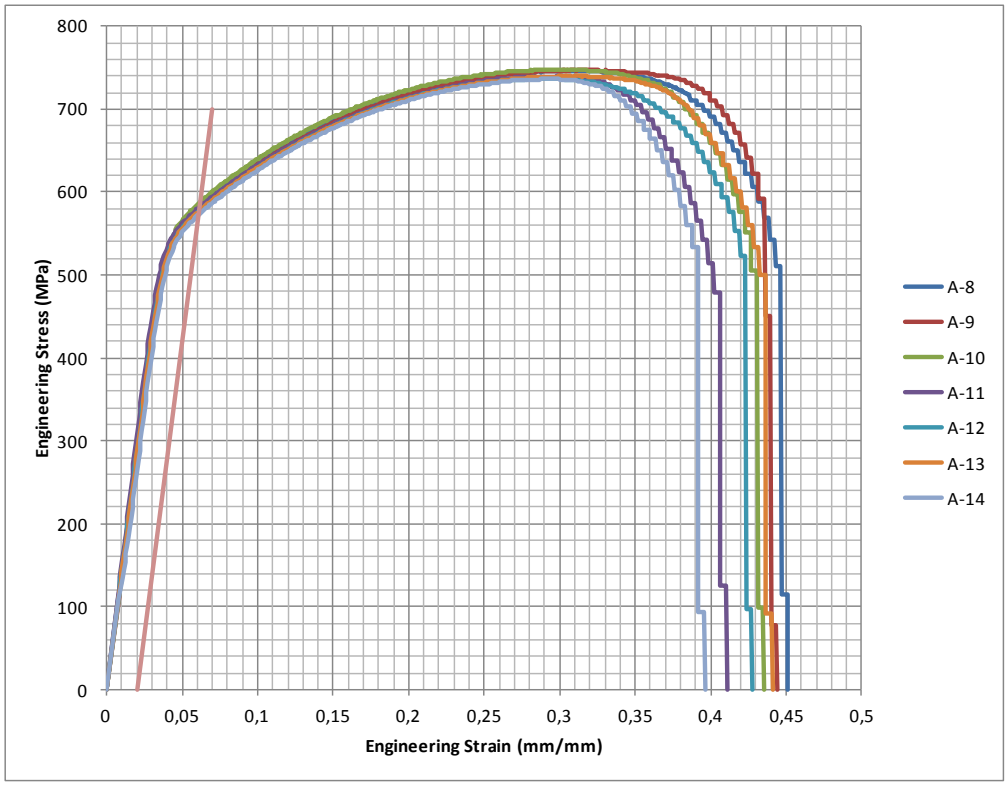


**Figure 106: Stress-strain curves for 250-A-48.**

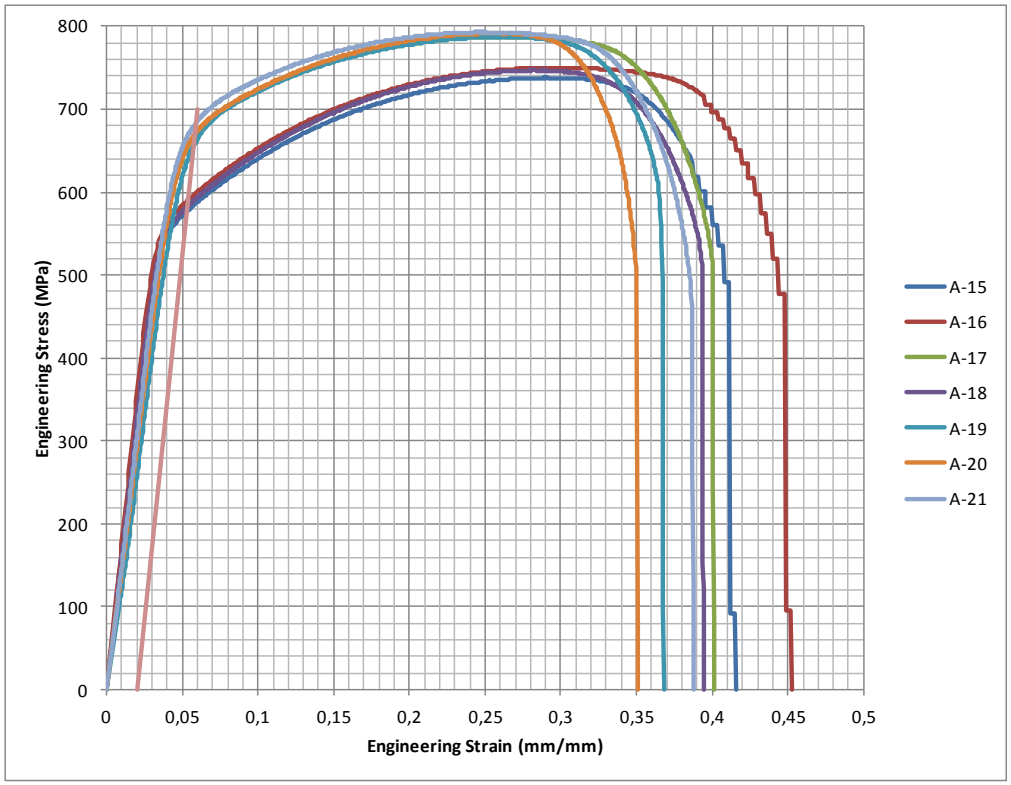


**Figure 107: Stress-strain curves for 250-A-85.5.**

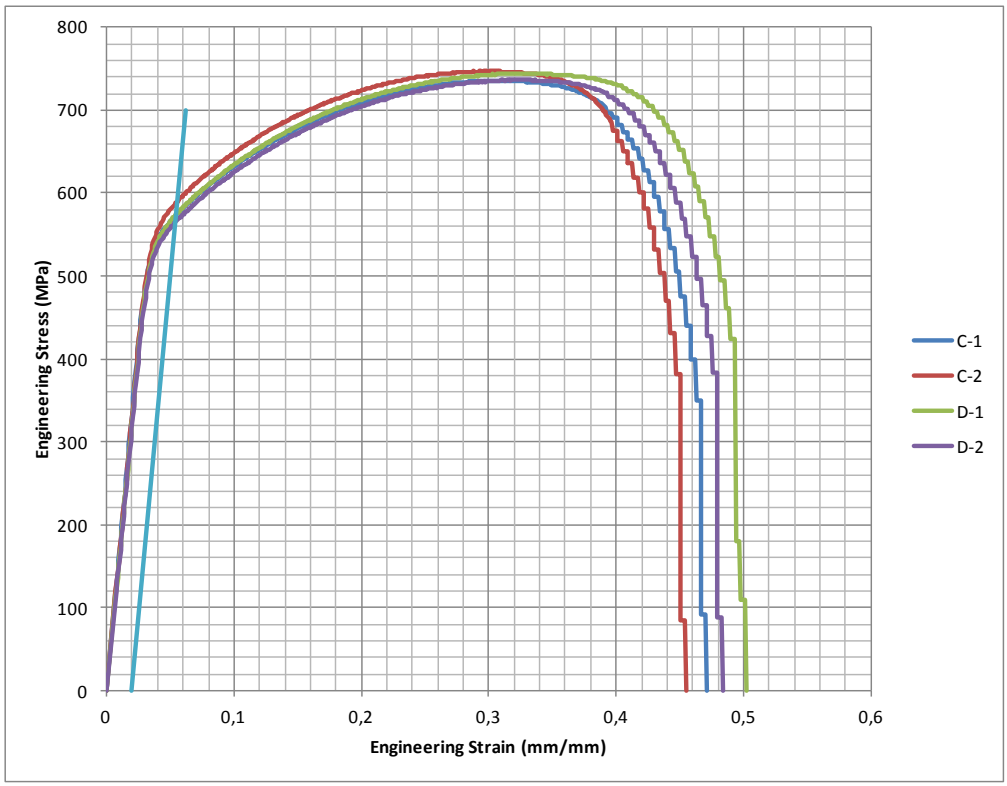


**Figure 108: Stress-strain curves for 250-C-29 and 250-D-29.**

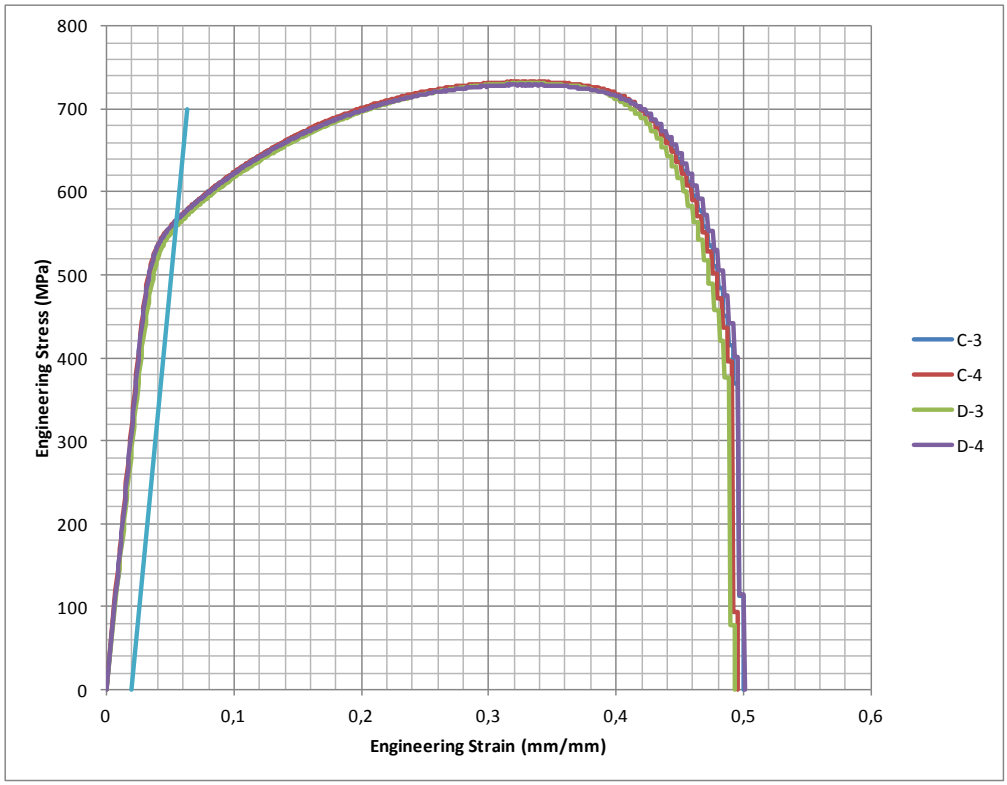


**Figure 109: Stress-strain curves for 250-C-48 and 250-D-48.**

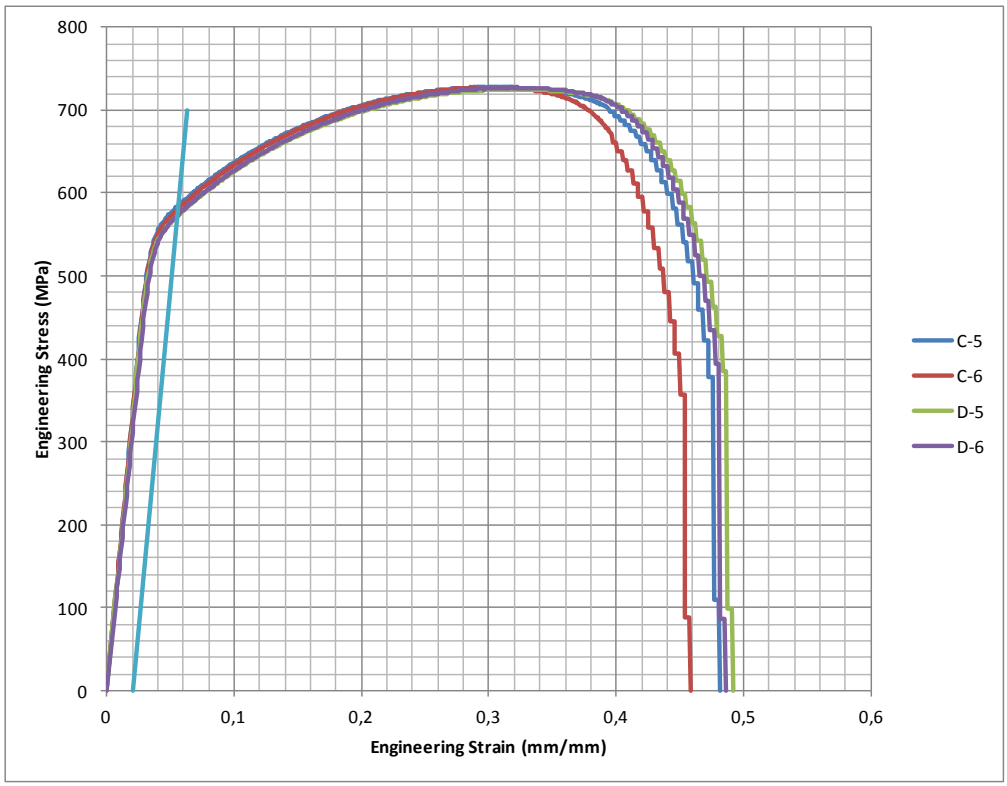


**Figure 110: Stress-strain curves for 250-C-82 and 250-D-82.**

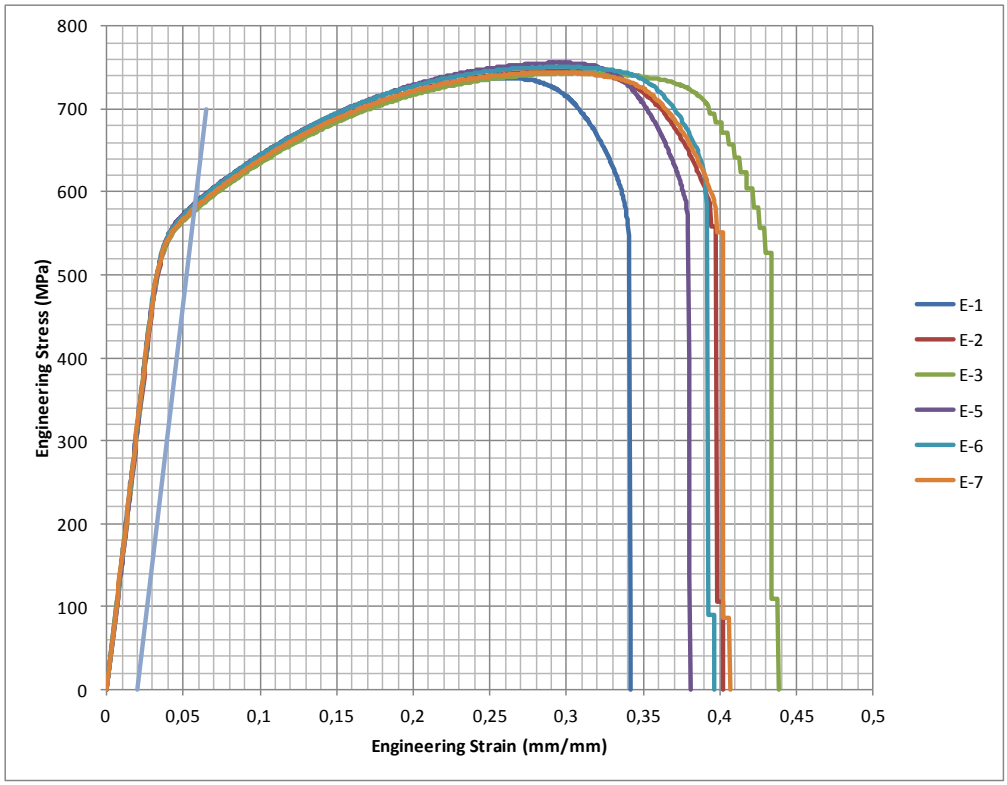


**Figure 111: Stress-strain curves for 250-E-78.5.**

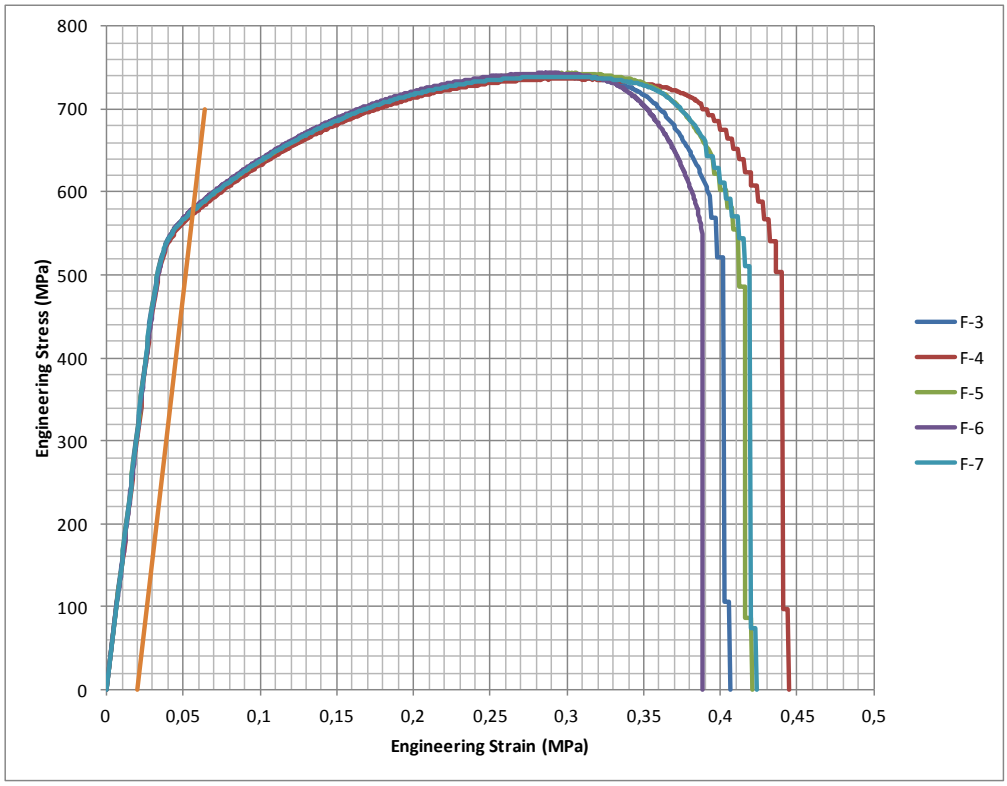


**Figure 112: Stress-strain curves for 250-F-47.**

## Appendix K: Manufacturer Data Sheets for Forged Bar



BGH

BGH Edelstahl Siegen GmbH

BGH Edelstahl Siegen GmbH Industriestr. 9 57076 Siegen

Sverdrup Hanssen Specialstaal A/S
Strandsvingen 2
4032 Stavanger
NORGE

Zeugnis-Nr. / Certificate no. / No. de certificat: 274448

Bescheinigung über Werkstoffprüfung nach DIN EN 10204
Certificate of material tests according to DIN EN 10204 3.1
Certificat des essais des matériaux selon DIN EN 10204

Die Lieferung entspricht den vereinbarten Lieferbedingungen.
Delivery in accordance with the agreed terms of delivery.
La livraison correspond aux conditions de livraison convenues.

Zeichen des Lieferwerkes / Trade mark / Signe du fournisseur
Stempel des Werkssachverständigen / Inspector's stamp / Poincon de l'inspecteur: BGH Q 33

Kunden-Bestell-Nr. / Customer order no. / Cde. no. du client: 476421

BGH-Auftrags-Nr. / BGH works no. / BGH référence: 860516-002-01

| | |
|---|---|
| Erzeugnisform / Product | Stab, rund, geschmiedet, geschält<br>Round bars,forged,peeled |
| Werkstoff / Quality | UNS S31803/S32205 |
| Anforderungen / Requirements | UNS S31803/S32205<br>UNS S31803 ,NACE MR 0175/ ISO15156-1 2004<br>UNS S31803 ,NORSOK M 650 Revision 3 04/04<br>UNS S31803 ,NORSOK MDS - D 47 Rev. 3<br>UNS S31803 ,NACE MR 0103 2005<br>UNS S31803, Sec. 5 Abs. 500-504 ,DNV-RP-F112 10/08<br>UNS S31803 ,ASTM A 479 /A479M - 10a<br>UNS S32205 ,ASTM A 479 /A479M - 10a<br>UNS S31803 ,ASTM A 276 - 10<br>UNS S32205 ,ASTM A 276 - 10<br>UNS S31803 - F51 ,ASTM A 182 /A 182M - 10a<br>F51 UNS S31803 ,Doc.-No. 6010-0329- D Rev. B 08/08<br>UNS S31803 ,Doc.-No. 43.200.024 Rev.C 11/05<br>UNS 31803 u. Kundeverb. vom 10.07.09 ,TR 2000 Sec. 6 MDS: DB101 18.06.09<br>KDV (DNV) Gefüge 11/10<br>Die MDS D44 kann von uns nicht bescheinigt werden, da wir über keine Zulassung verfügen.<br>BGH is not approved towards MDS D44, hence it can not be confirmed.<br>Zertifiziert nach DGRL 97/23/EG Anhang 1 Kap. 4.3; Zertifikat-Nr. 07-202-1405 WZ-1161/10,<br>Kenn-Nr. 0045; und AD 2000-Regelwerk W0/TRD100; Zertifikat-Nr. 07-202-1405 WP-1161/10<br>Certificated PED 97/23/EC Annex 1 Chap. 4.3; Certificate No. 07-202-1405 WZ-1161/10,<br>Registration No. 0045; and AD 2000 W0/TRD100; Certificate No. 07-202-1405 WP-1161/10 |

SVERDRUP HANSSEN SPESIALSTÅL 1407-11 APPROVED Q.C. DEPT.

| Besichtigung und Maßnachprüfung / Inspection and dimensional control / Inspection et contrôle de dimension | Erschmelzung/Nachbehandlung / Melting process/secondary refining / Mode d'élaboration/traitement ultérieur | Verwechslungsprüfung (spectroanalytisch) / Identification test (special-analysis) / examination d' identification(analyse spectrale) |
|---|---|---|
| ohne Beanstandung<br>without objection | E AOD | ohne Beanstandung<br>without objection |

| Pos. / Item | Anzahl / Quantity | Abmessung / Dimension | Gewicht / Weight kg | Schmelz-Nr. / Heat-No. |
|---|---|---|---|---|
| 2 | 1 | 220 mm dia. x 7444 mm | 2232 | 779980 |

| Schmelze / Heat % | C | Si | Mn | P | S | Cr | Mo | Ni | N | PRE |
|---|---|---|---|---|---|---|---|---|---|---|
| 779980 | 0,025 | 0,35 | 1,58 | 0,022 | 0,0006 | 22,10 | 3,21 | 5,80 | 0,1850 | 35,653 |

Wärmebehandlungszustand / Condition of heat treatment / Traitment thermique: lösungsgeglüht / solution annealed
1050°C 4h water - heat treat lot no. 8914
water temperature at start: 17°C, water temperature at end: 26°C

| Probe-Nr. / Test-No. | Lage / Loc. | Temp. °C | Rp0,2 N/mm² | | Rm N/mm² | A4 % | Z % | Kerbschlagarbeit / Impact value J | | Probenform / Shape of test piece Charpy-V | | Härte / Hardness HB | HRC |
|---|---|---|---|---|---|---|---|---|---|---|---|---|---|
| Soll/Req. | L | RT | >=485 | | >=655 | >=25 | >=45 | >=45 | | | -46°C | <=264 | <=28 |
| Soll/Req. | Q | RT | >=450 | | >=620 | >=20 | >=45 | >=27 | | | -46°C | | |
| 408K1 | L | RT | 490 | | 717 | 44 | 80 | 310 | 307 | 312 | -46°C | 220 | < 22 |

Anlagen / Encl. / Annexe: Gefügeaufnahme / Micrograph; Ofendiagramm / Furnace chart; US- + FE-Zeugnis / UT + PT cert.

Siegen,den / Place and date / Lieu et date: 14.06.2011

Abnahmebeauftragter / Inspector representative / Inspecteur de réception: M.Mertens

Das Zeugnis wurde maschinell erstellt und ist auch ohne Unterschrift gültig.

This certificate was generated by data system it must not be signed for validity as well.
Ce certificat a été établi sur système informatique et est valable sans signature aussi.

BGH

**BGH Edelstahl Siegen GmbH**

BGH Edelstahl Siegen GmbH Industriestr. 9 57076 Siegen

**Sverdrup Hanssen Specialstaal A/S**
**Strandsvingen 2**
**4032 Stavanger**
**NORGE**

**Zeugnis-Nr.** **274448**
**Certificate no.**
**No. de certificat**

Bescheinigung über Werkstoffprüfung nach DIN EN 10204
Certificate of material tests according to DIN EN 10204 **3.1**
Certificat des essais des matériaux selon DIN EN 10204

Die Lieferung entspricht den vereinbarten Lieferbedingungen.
Delivery in accordance with the agreed terms of delivery.
La livraison correspond aux conditions de livraison convenues.

Zeichen des Lieferwerkes
Trade mark
Signe du fournisseur

Stempel des Werkssachverständigen
Inspector's stamp
Poincon de l'inspecteur

BGH
Q 33

Kunden-Bestell-Nr. **476421**
Customer order no.
Cde. no. du client

BGH-Auftrags-Nr. **860516-002-01**
BGH works no.
BGH référence

| | | | | | | | | | | | |
|---|---|---|---|---|---|---|---|---|---|---|---|
| 408K1 | Q | RT | 481 | | 720 | 40 | 69 | 93 | 102 | 88 | -46°C |

| Probe-Nr. | Temp. | Lage | Laterale Breitung (mm) | | |
|---|---|---|---|---|---|
| Test-No. | °C | Loc. | Lateral extension (mm) | | |
| 408K1 | -46 | L | 2,5 | 2,5 | 2,6 |

Testing on prolongation of bar, in a quarter of thickness in accordance with ASTM A 370.

Corrosions test acc. ASTM G 48, method A - 24h at 25°C
No pitting at 20x magnification / Weight loss: 0.075 g/m²

Reduction ratio: 5.2 : 1

Ferrite content acc. ASTM E 562: 47 %

Microstructure: Ferrite / Austenite
The examined samples were extensively free from intermetallic phases and precipitates

No welding or weld repair

Radioactivity inspection without objection, the measured value is below the detection limit of 0.1 Bq/g.

UT examination:
ASTM A 388 / ASME SA-388
Acceptance criteria to ASME VIII, Div.2, AM 203.2 c)
without objection

Anlagen / Encl. / Annexe
Gefügeaufnahme / Micrograph
Ofendiagramm / Furnace chart
US- + FE-Zeugnis / UT + PT cert.

Siegen,den
Place and date
Lieu et date
14.06.2011

Abnahmebeauftragter
Inspector representative
Inspecteur de réception
**M.Mertens**

Das Zeugnis wurde maschinell erstellt und ist auch ohne Unterschrift gültig.

This certificate was generated by data system it must not be signed for validity as well.
Ce certificat a été établi sur système informatique et est valable sans signature aussi.

BGH

BGH Edelstahl Siegen GmbH

**Gefügeaufnahme**
**Micrograph**
**Microstructure**

-

| | |
|---|---|
| BGH-Auftragsnr.:<br>BGH works no.:<br>BGH référence: | 86051600201 |
| Charge:<br>Heat:<br>Coulée: | 779980 |
| Werkstoff:<br>Quality:<br>Matériel | 4462 |
| Probe-Nr.:<br>Test-No.:<br>Échant.: | 408 K |
| Ätzmittel:<br>Etchant:<br>Agent caustique: | NAOH 10% / elektrolytisch |
| Vergrößerung:<br>Magnification:<br>Agrandissement: | 500fach |

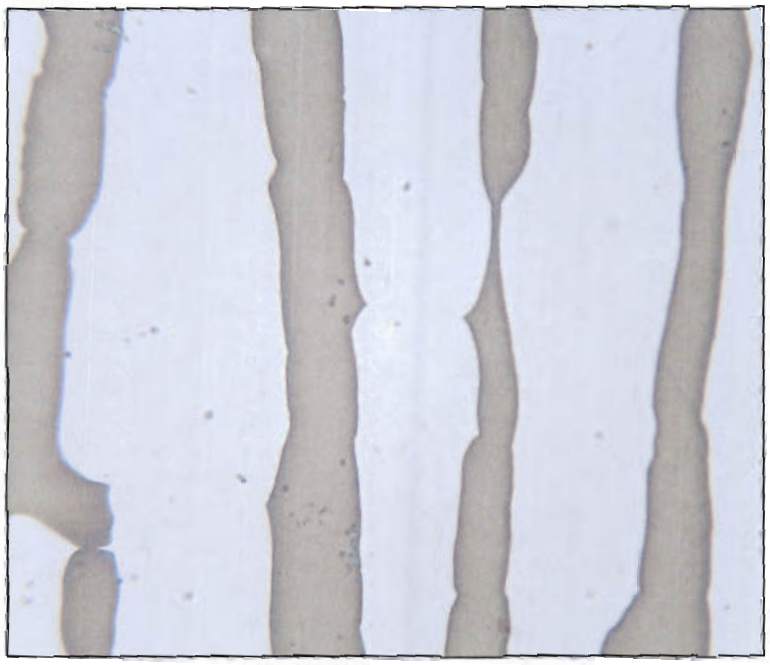

## Diagramm Ofen 426

BGH-Auftragsnr. 860516-002-01
Start: 16.05.2011 15:06 Uhr
Ende: 17.05.2011 00:39 Uhr
Gesamtzeit: 0 Tage 09:32 Stunden
Los-Nr.: 426/8914/1

**BGH Edelstahl Siegen GmbH**

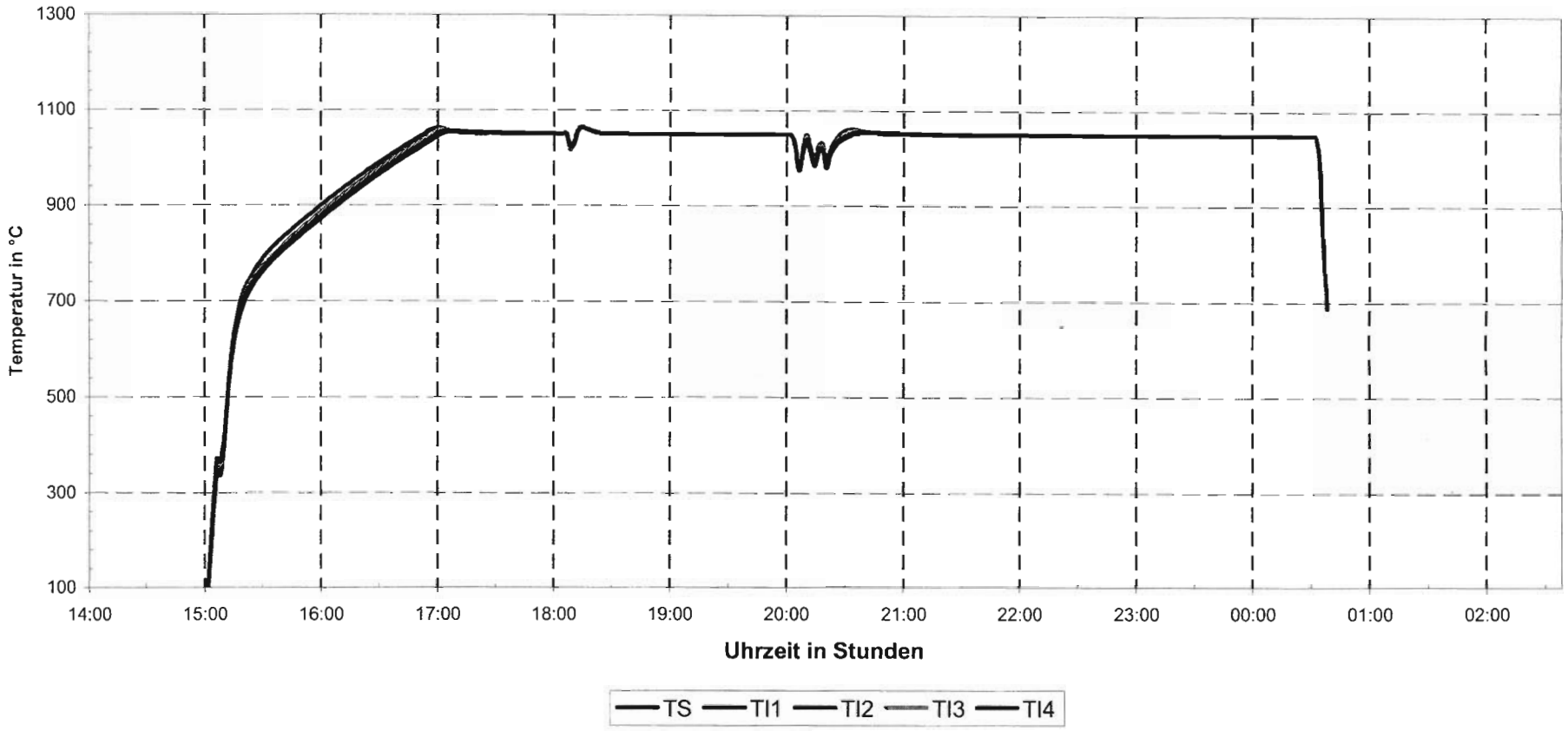

# US-Protokoll
Ultrasonic certificate

DIN EN 10204 3.1

BGH

**BGH Edelstahl Siegen GmbH**

Kunden-Bestell-Nr. **476421**
Customer order no.
Cde. no. du client

BGH-Auftrags-Nr. **860516-002-01**
BGH works no.
BGH référence

Zeugnis-Nr. **274448**
Certificate no.
No. de certificat

| | |
|---|---|
| Erzeugnisform<br>Product | : Stab, rund, geschmiedet, geschält<br>: Round bars, forged, peeled |
| Werkstoff/Quality | : UNS S31803/S32205 |
| Abmessung/Dimension | : 220 mm dia. x 7444 mm |
| Anzahl/Quantity | : 1 Gewicht /Weight : 2232 kg |
| Wärmebehandlungszustand<br>Condition of heat treat | : lösungsgeglüht<br>: solution annealed |

**Prüfrichtlinie**
Specification

Anforderungen nach API 6A, 20.Ausgabe Okt.2010/ISO 10423 Ausg.2009, PSL 3, Punkt 7.4.2.3.15(b)
Requirements per API 6A, 20.Edition Oct.2010/ISO 10423 Ed.2009, PSL 3, Point 7.4.2.3.15 (b)

| | |
|---|---|
| Prüfrichtlinie<br>Specification | : ASTM A 388 |
| Prüfgerät<br>Testing device | : Krautkrämer USM 35 |
| Prüfkopf<br>Search unit | : B2S |
| Prüffrequenz<br>Testing frequence | : 2 MHz |
| Kopplungsmittel<br>Couplant | : Wasser / Kleister<br>water / glue |
| Prüfumfang<br>Amount of inspection | : vollständig<br>completely |
| Prüfrichtung<br>Scanning direction | : radial<br>radial |
| Registriergrenze<br>Recording threshold | : 50 % Bezugslinie von 6,0 mm FBB<br>50 % reference line of 6.0 mm FBH |
| Befund<br>Result | : Keine registrierpflichtigen Anzeigen.<br>No reportable indications. |

| Siegen,den<br>Place and date<br>Lieu et date | Prüfer<br>Testing operator<br>Opérateur | Abnahmebeauftragter<br>Inspector representative<br>Inspecteur de réception | Überwacher<br>Supervisor<br>Surveilleur |
|---|---|---|---|
| 14.06.11 | Petri<br>Level II (SNT-TC-1A) | Jung<br>Level III (SNT-TC-1A)<br>BGH Q 30 | |

Das Zeugnis wurde maschinell erstellt und ist auch ohne Unterschrift gültig.

This certificate was generated by data system it must not be signed for validity as well.
Ce certificat a été établi sur système informatique et est valable sans signature aussi.

# Farbeindringprüfung
Dye penetrant inspection

DIN EN 10204 3.1

BGH

**BGH Edelstahl Siegen GmbH**

Kunden-Bestell-Nr. **476421**
Customer order no.
Cde. no. du client

BGH-Auftrags-Nr. **860516-002-01**
BGH works no.
BGH référence

Zeugnis-Nr. **274448**
Certificate no.
No. de certificat

Erzeugnisform : Stab, rund, geschmiedet, geschält
Product : Round bars, forged, peeled

Werkstoff/Quality : UNS S31803/S32205

Abmessung/Dimension : 220 mm dia. x 7444 mm

Anzahl/Quantity : 1 Gewicht /Weight : 2232 kg

Wärmebehandlungszustand : lösungsgeglüht
Condition of heat treat : solution annealed

**Prüfrichtlinie**
Specification

ASME V, Article 6
Acceptance criteria to ASME VIII, Div.1, Appendix 8

Prüfumfang : gesamte Prüfstückoberfläche
Amount of inspection : total test piece surface

Prüfsystem DIN EN 571-1 : II E d (EN 571-1)
Test system DIN EN 571-1

Prüfmittel : Karl Deutsch
Check medium

Penetrant : KD-Check, RDP-1, Charge: 4037
Penetrant

Eindringzeit : 30 Minuten
Dwell time : 30 minutes

Reinigungsmittel : Wasser und mit Reiniger getränkter Lappen
Detergent : wasser and with cleaner soaked cloth

Entwickler : KD-Check, SD-1, Charge: 4044
Developer

Ausblutzeit : 30 Minuten
Bleed out time : 30 minutes

Beurteilungszeitpunkt : Nach dem Antrocknen des Entwicklers und nach 30 Minuten.
Moment of evaluation : after drying of developer and after 30 minutes.

Befund : Keine registrierpflichtigen Anzeigen.
Result : No reportable indications.

| Siegen,den<br>Place and date<br>Lieu et date<br>14.06.11 | Prüfer<br>Testing operator<br>Opérateur<br>Petri<br>Level II (SNT-TC-1A) | Abnahmebeauftragter<br>Inspector representative<br>Inspecteur de réception<br>Jung<br>Level III (SNT-TC-1A)<br>BGH Q 30 | Überwacher<br>Supervisor<br>Surveilleur |
|---|---|---|---|

Das Zeugnis wurde maschinell erstellt und ist auch ohne Unterschrift gültig.

This certificate was generated by data system it must not be signed for validity as well.
Ce certificat a été établi sur système informatique et est valable sans signature aussi.

BGH

**BGH Edelstahl Siegen GmbH**

BGH Edelstahl Siegen GmbH Industriestr. 9 57076 Siegen

**Sverdrup Hanssen Specialstaal A/S**

**Strandsvingen 2**

**4032 Stavanger**

Bescheinigung zur Materialidentität
Certificate of material identity
Certificat d'identité du matériel
**159710**

Kunden-Bestell-Nr.
Customer order no.
Cde. no. du client
**801239**

BGH-Auftrags-Nr.
BGH works no.
BGH référence
**209617 7/610158_007**

| | |
|---|---|
| Erzeugnisform<br>Product | Stab, rund, geschmiedet, geschält<br>Round bars,forged,peeled |
| Werkstoff / Quality | 1.4462 UNS S31803 |
| Anforderungen<br>Requirements | M - 650 Rev. 3 04/04<br>ASTMA479/A479M - 11<br>NACE MR0175/15156-1<br>DIN EN 10088-3 9/05<br>MDS - D 47 Rev.3 |
| Wärmebehandlungszustand<br>Condition of heat treat | lösungsgeglüht<br>solution annealed |

| Pos.<br>Item | Anzahl<br>Quantity | Abmessung<br>Dimension | Gewicht kg<br>Weight kg | Schmelz-Nr.<br>Heat-No. |
|---|---|---|---|---|
| 1 | 1 | 250,0 RD | 2185 | 780834 |

Wir bestätigen, dass die gelieferten Teile aus unten genannter Zeugnis-Nr. entnommen wurden.We confirm that the delivered parts were taken from the certificate-no. mentioned below.

Ausgewiesen durch : Abnahmeprüfzeugnis nach / inspection certificate
Certified by as per EN 10204 / 3.2 / 3.1C / 3.1A
: x Werksabnahmeprüfzeugnis nach / works certificate
as per EN 10204 / 3.1

Die Stempelung / the stamping

Firmenzeichen/company´s sign.: ⌘
Schmelzen-Nr. / heat no. : 780834
Werkstoff / material : 4462
Probe-Nr. / speciemen-no. : 603M1

SVERDRUP HANSSEN SPESIALSTÅL
06091
APPROVED
Q.C. DEPT.

Bemerkung/remark:

Anlagen Kopie Zeugnis Nr.
Encl 276212
Annexe

Siegen,den
Place and date
Lieu et date
11.08.2011

Abnahmebeauftragter
Third Party Inspector
Inspecteur de réception
**HOMM**

BGH Q 18

Das Zeugnis wurde maschinell erstellt und ist auch ohne Unterschrift gültig.

This certificate was generated by data system it must not be signed for validity as well.
Ce certificat a été établi sur système informatique et est valable sans signature aussi.

**BGH Edelstahl Siegen GmbH**

BGH Edelstahl Siegen GmbH Industriestr. 9 57076 Siegen

**Zeugnis-Nr.** **276212**
**Certificate no.**
**No. de certificat**

Bescheinigung über Werkstoffprüfung nach DIN EN 10204
Certificate of material tests according to DIN EN 10204 **3.1**
Certificat des essais des matériaux selon DIN EN 10204

Die Lieferung entspricht den vereinbarten Lieferbedingungen.
Delivery in accordance with the agreed terms of delivery.
La livraison correspond aux conditions de livraison convenues.

Zeichen des Lieferwerkes
Trade mark
Signe du fournisseur

Stempel des Werkssachverständigen
Inspector's stamp
Poincon de l'inspecteur

BGH Q 33

Kunden-Bestell-Nr. **08539401400**
Customer order no.
Cde no. du client

BGH-Auftrags-Nr. **085394-014-01**
BGH works no.
BGH référence

| | |
|---|---|
| Erzeugnisform<br>Product | Stab, rund, geschält<br>Round bars, peeled |
| Werkstoff / Quality | 1.4462 X2CrNiMoN22-5-3 |
| Anforderungen<br>Requirements | BGH 1.4462 Rev. 3<br>1.4462 X2CrNiMoN22-5-3 ,DIN EN 10222- 5 02/00<br>1.4462 X 2 CrNiMoN 22 5 3 ,SEW 400 02/91<br>1.4462 X2CrNiMoN22-5-3 ,DIN EN 10250 04 02/00+Br.1 12/08<br>UNS S31803 ,NORSOK MDS - D 47 Rev. 3<br>UNS S31803 ,ASTM A 479 /A479M - 10a<br>UNS S31803 ,NACE MR 0175 ISO15156-1 2009 |

| Besichtigung und Maßnachprüfung<br>Inspection and dimensional control<br>Inspection et contrôle de dimension | Erschmelzung/Nachbehandlung<br>Meltingprocess/secondary refining<br>Mode d'élaboration/traitement ultérieur | Verwechslungsprüfung (spectroanalytisch)<br>Identification test (spectral-analysis)<br>examination d' identification(analyse spectrale) |
|---|---|---|
| ohne Beanstandung<br>without objection | E AOD | ohne Beanstandung<br>without objection |

| Pos.<br>Item | Anzahl<br>Quantity | Abmessung<br>Dimension | Gewicht<br>Weight kg | Schmelz-Nr.<br>Heat-No. |
|---|---|---|---|---|
| 14 | 1 | 250 mm rd. x 5663 mm | 2188 | 780834 |

| Schmelze<br>Heat | C | Si | Mn | P | S | Cr | Mo | Ni | N |
|---|---|---|---|---|---|---|---|---|---|
| | % | | | | | | | | |
| 780834 | 0,022 | 0,31 | 1,49 | 0,021 | 0,0007 | 22,20 | 3,15 | 5,70 | 0,1900 |

| | |
|---|---|
| Wärmebehandlungszustand<br>Condition of heat treat<br>Traitment thermique | lösungsgeglüht<br>solution annealed<br>1050°C Wasser/water |

| Probe-Nr.<br>Test-No. | Lage<br>Loc. | Temp.<br>°C | Rp0,2<br>N/mm² | | Rm<br>N/mm² | A4,A5<br>% | Z<br>% | Kerbschlagarbeit<br>Impact value<br>J | | Probenform<br>Shape of test piece<br>Charpy-V | | Härte<br>Hardness<br>HRC |
|---|---|---|---|---|---|---|---|---|---|---|---|---|
| Soll/Req. | L | RT | >=450 | | >=620 | >=25 | >=45 | >=50 | | | -46°C | <=28 |
| Soll/Req. | Q | RT | >=450 | | >=620 | >=25 | >=45 | >=27 | | | -46°C | |
| Soll/Req. | Q | RT | >=450 | | >=680<br><=880 | >=25 | | >=100 | | | RT | |
| 603M1 | L | RT | 474 | | 701 | 46 | 86 | 262 | 224 | 223 | -46°C | 19-20 |
| 603M1 | Q | RT | 486 | | 715 | 41 | 61 | 238 | 252 | 273 | -46°C | |
| 603M1 /K | Q | RT | 492 | | 719 | 39 | 58 | 400 | 394 | 399 | RT | |
| 603M1 /F | Q | RT | 501 | | 731 | 40 | 71 | 397 | 387 | 381 | RT | |

Reinheitsgrad nach DIN 50602 : K4 = 4
Degree of purity acc. DIN 50602:

Ferritgehalt nach ASTM E 562 : 46 %
Ferrite content acc. ASTM E 562:

Anlagen
Encl.
Annexe Gefügeaufnahme / Micrograph

Siegen,den
Place and date
Lieu et date
21.07.2011

Abnahmebeauftragter
Inspector representative
Inspecteur de réception
**M.Mertens**

Das Zeugnis wurde maschinell erstellt und ist auch ohne Unterschrift gültig.

This certificate was generated by data system it must not be signed for validity as well.
Ce certificat a été établi sur système informatique et est valable sans signature aussi.

BGH

**BGH Edelstahl Siegen GmbH**

BGH Edelstahl Siegen GmbH Industriestr. 9 57076 Siegen

**Zeugnis-Nr. 276212**
**Certificate no.**
**No. de certificat**

Bescheinigung über Werkstoffprüfung nach DIN EN 10204
Certificate of material tests according to DIN EN 10204 **3.1**
Certificat des essais des matériaux selon DIN EN 10204

Die Lieferung entspricht den vereinbarten Lieferbedingungen.
Delivery in accordance with the agreed terms of delivery.
La livraison correspond aux conditions de livraison convenues.

Zeichen des Lieferwerkes
Trade mark
Signe du fournisseur

Stempel des Werkssachverständigen
Inspector's stamp
Poincon de l'inspecteur

BGH Q 33

Kunden-Bestell-Nr. **08539401400**
Customer order no.
Cde. no. du client

BGH-Auftrags-Nr. **085394-014-01**
BGH works no.
BGH référence

IK-Test nach DIN EN ISO 3651-2, Verf. B und ASTM A 262, Verf. E wurde durchgeführt:
IC Test acc. DIN EN ISO 3651-2, pract. B and ASTM A 262, pract. E was done :
ohne Beanstandung / without objection

Kontrolle auf Radioaktivität ohne Befund, der Messwert liegt unter der Nachweisgrenze von 0,1 Bq/g.
Radioactivity inspection without objection, the measured value is below the detection limit of 0.1 Bq/g.

US-Prüfung / UT examination:
DIN EN 10228-4 - 10/99, Tab. 2 Type 1a (100%) + Tab. 4 QK/quality class 3
ASTM A 745 / ASME SA-745, QL 3
ohne Beanstandung / without objection

| Anlagen Encl. Annexe | Siegen,den Place and date Lieu et date | Abnahmebeauftragter Inspector representative Inspecteur de réception |
|---|---|---|
| Gefügeaufnahme / Micrograph | 21.07.2011 | **M.Mertens** |

Das Zeugnis wurde maschinell erstellt und ist auch ohne Unterschrift gültig.

This certificate was generated by data system it must not be signed for validity as well.
Ce certificat a été établi sur système informatique et est valable sans signature aussi.

BGH

BGH Edelstahl Siegen GmbH

**Gefügeaufnahme**
**Micrograph**
**Microstructure**

| | |
|---|---|
| BGH-Auftragsnr.:<br>BGH works no.:<br>BGH référence: | 08539401401 |
| Charge:<br>Heat:<br>Coulée: | 780834 |
| Werkstoff:<br>Quality:<br>Matériel | 4462 |
| Probe-Nr.:<br>Test-No.:<br>Échant.: | 603 M |
| Ätzmittel:<br>Etchant:<br>Agent caustique: | NAOH 10% / elektrolytisch |
| Vergrößerung:<br>Magnification:<br>Agrandissement: | 500fach |

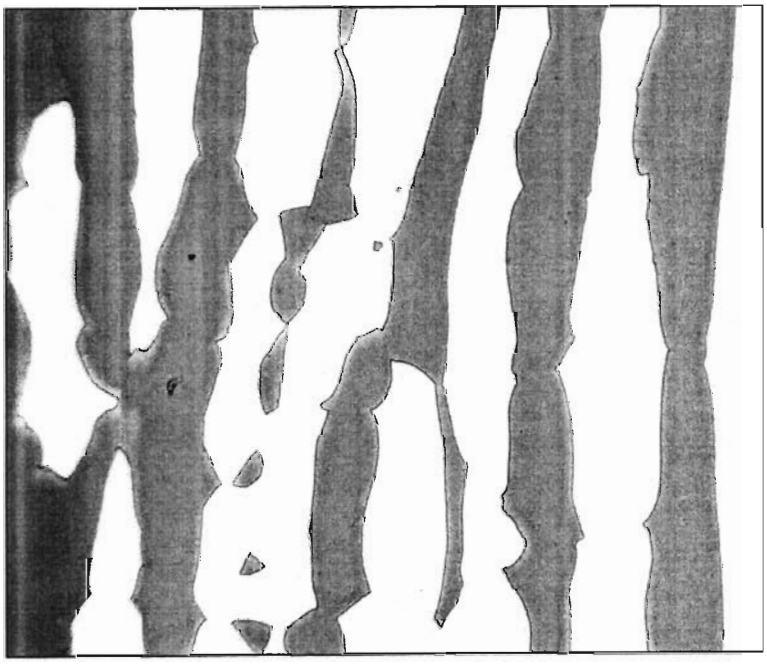

# Appendix L: ASME Design Rules for Flanged Joints



### 4.16 Design Rules for Flanged Joints

#### 4.16.1 Scope

**4.16.1.1** The rules in paragraph 4.16 shall be used to design circular flanges subject to internal and/or external pressure. These rules provide for hydrostatic end loads, gasket seating, and externally applied axial force and net-section bending moment.

**4.16.1.2** The rules in paragraph 4.16 apply to the design of bolted flange connections with gaskets that are entirely located within the circle enclosed by the bolt holes. The rules do not cover the case where the gasket extends beyond the bolt hole circle or where metal-metal contact is made outside of the bolt circle.

**4.16.1.3** It is recommended that bolted flange connections conforming to the standards listed in paragraph 4.1.11 be used for connections to external piping. These standards may be used for other bolted flange connections and dished covers within the limits of size in the standard and pressure-temperature ratings permitted in paragraph 4.1.11. The ratings in these standards are based on the hub dimensions given or on the minimum specified thickness of flanged fittings of integral construction. Flanges fabricated from rings may be used in place of the hub flanges in these standards provided that their strength and rigidity, calculated by the rules in this paragraph, are not less than that calculated for the corresponding size of hub flange.

**4.16.1.4** The rules of this paragraph should not be construed to prohibit the use of other types of flanged connections provided they are designed in accordance with Part 5.

#### 4.16.2 Design Considerations

**4.16.2.1** The design of a flange involves the selection of the flange type, gasket material, flange facing, bolting, hub proportions, flange width, and flange thickness. The flange dimensions shall be selected such that the stresses in the flange and the flange rigidity satisfy the acceptability criteria of this paragraph.

**4.16.2.2** In the design of a bolted flange connection, calculations shall be made for the following two design conditions, and the most severe condition shall govern the design of the flanged joint.

a) *Operating Conditions* – The conditions required to resist the hydrostatic end force of the design pressure and any applied external forces and moments tending to part the joint at the design temperature.

b) *Gasket Seating Condition* – The conditions existing when the gasket or joint-contact surface is seated by applying an initial load with the bolts during assembly of the joint, at atmospheric temperature and pressure.

**4.16.2.3** Calculations shall be performed using dimensions of the flange in the corroded and uncorroded conditions.

**4.16.2.4** In the design of flange pairs, each flange is designed for its particular design loads of pressure and gasket reactions. The bolt load used to design each flange, however, is that load common to the flange pair and equal to the larger of the bolt loads calculated for each flange individually. No additional rules are required for design of flange pairs. After the loads for the most severe condition are determined, calculations shall be made for each flange following the rules of this paragraph.

**4.16.2.5** In the design of flange pairs where pass partitions with gaskets are used, the gasket loads from the partition(s) shall be included in the calculation of bolt loads. Partition gaskets may have different gasket constants than the ring gasket inside the bolt circle. In the design of flanges with noncircular gaskets or with partitions of any shape, gasket reactions from all surfaces with gaskets shall be included in calculating bolt loads.

### 4.16.3 Flange Types

**4.16.3.1** For the purpose of computation, there are two major categories of flanges:

a) Integral Type Flanges – This type covers designs where the flange is cast or forged integrally with the nozzle neck, vessel or pipe wall, butt welded thereto, or attached by other forms of welding such that the flange and nozzle neck, vessel or pipe wall are structurally equivalent to integral construction. Integral flanges shall be designed considering structural interaction between the flange and the nozzle neck, vessel, or pipe wall, which the rules account for by considering the neck or wall to act as a hub. Integral type flanges are referenced below. The design flange and bolt loads are shown in Figures 4.16.1 and 4.16.2.

1) Integral type flanges – Figure 4.16.1 Sketch (a) and Table 4.2.9, Details 9 and 10

2) Integral type flanges where $g_1 = g_o$ – Figure 4.16.1 Sketch (b)

3) Integral type flanges with a hub – Figure 4.16.2 and Table 4.2.9, Details 6, 7, and 8

4) Integral type flanges with nut stops – Figure 4.16.3 and Figure 4.16.4

b) Loose Type Flanges – This type covers those designs in which the flange has no substantial integral connection to the nozzle neck, vessel, or pipe wall, and includes welded flange connections where the welds are not considered to give the mechanical strength equivalent of an integral attachment. Loose type flanges are referenced below. The design flange and bolt loads are shown in Figures 4.16.5 and 4.16.6.

1) Loose type flanges – Figure 4.16.5 and Table 4.2.9, Details 1,2,3 and 4

2) Loose type lap joint flanges – Figure 4.16.6 and Table 4.2.9, Detail 5

**4.16.3.2** The integral and loose type flanges described above can also be applied to reverse flange configurations. Integral and loose type reverse flanges are shown in Figure 4.16.7.

### 4.16.4 Flange Materials

**4.16.4.1** Materials used in the construction of bolted flange connections, excluding gasket materials, shall comply with the requirements given in Part 3.

**4.16.4.2** Flanges made from ferritic steel shall be given a normalizing or full-annealing heat treatment when the thickness of the flange section exceeds 75 mm (3 in.).

**4.16.4.3** Fabricated flanges with hub shall be in accordance with the following:

a) Flanges with hubs may be machined from a hot rolled or forged billet or forged bar. The axis of the finished flange shall be parallel to the long axis of the original billet or bar, but these axes need not be concentric.

b) Flanges with hubs, except as permitted in paragraph 4.16.4.3.a, shall not be machined from plate or bar stock material unless the material has been formed into a ring, and further provided that:

1) In a ring formed from plate, the original plate surfaces are parallel to the axis of the finished flange;

2) The joints in the ring are welded butt joints that conform to the requirements of Part 6. The thickness to be used to determine postweld heat treatment and radiographic requirements shall be $\min\left[t, (A-B)/2\right]$.

c) The back of the flange and the outer surface of the hub shall be examined by either the magnetic particle method or the liquid penetrant method in accordance with Part 7.

**4.16.4.4** Bolts, studs, nuts, and washers shall comply with the requirements of Part 3 and referenced standards. It is recommended that bolts and studs have a nominal diameter of not less than 12 mm (0.5 in.). If bolts or studs smaller than 12 mm (0.5 in.) are used, then ferrous bolting material shall be of alloy steel. Precautions shall be taken to avoid overstressing small-diameter bolts. When washers are used, they shall be through hardened to minimize the potential for galling.

### 4.16.5 Gasket Materials

**4.16.5.1** The gasket constants for the design of the bolt load ($m$ and $y$), are provided in Table 4.16.1. Other values for the gasket constants may be used if based on actual testing or data in the literature, as agreed upon between designer and the user.

**4.16.5.2** The minimum width of sheet and composite gaskets, $N$, is recommended to be no less than that given in Table 4.16.2.

NOTE: Gasket materials should be selected that are suitable for the design conditions. Corrosion, chemical attack, creep and thermal degradation of gasket materials over time should be considered.

### 4.16.6 Design Bolt Loads

**4.16.6.1** The procedure to determine the bolt loads for the operating and gasket seating conditions is shown below.

a) STEP 1 – Determine the design pressure and temperature of the flange joint.

b) STEP 2 – Select a gasket and determine the gasket factors $m$ and $y$ from Table 4.16.1, or other sources. The selected gasket width should comply with the guidelines detailed in Table 4.16.2.

c) STEP 3 – Determine the width of the gasket, $N$, basic gasket seating width, $b_0$, the effective gasket seating width, $b$, and the location of the gasket reaction, $G$, based on the flange and gasket geometry, the information in Table 4.16.3 and Figure 4.16.8, and the equations shown below. Note that for lap joint flanges, $G$ is equal to the midpoint of contact between the flange and the lap, see Figure 4.16.6 and Figure 4.16.8.

1) For $b_0 \le 6mm\ (0.25\ in.)$, $G$ is the mean diameter of the gasket contact face and

$$b = b_0 \tag{4.16.1}$$

2) For $b_0 > 6mm\ (0.25\ in.)$

$$b = 0.5C_{ul}\sqrt{\frac{b_0}{C_{ul}}} \tag{4.16.2}$$

$$G = G_C - 2b \tag{4.16.3}$$

d) STEP 4 – Determine the design bolt load for the operating condition.

$$W_o = 0.785G^2P + 2b\pi GmP \qquad for\ non-self-energized\ gaskets \tag{4.16.4}$$

$$W_o = 0.785G^2P \qquad for\ self-energized\ gaskets \tag{4.16.5}$$

e) STEP 5 – Determine the design bolt load for the gasket seating condition.

$$W_g = \left( \frac{A_m + A_b}{2} \right) S_{bg} \qquad (4.16.6)$$

The parameter $A_b$ is the actual total cross sectional area of the bolts that is selected such that $A_b \geq A_m$, where:

$$A_m = \max \left[ \left( \frac{W_o + F_A + \frac{4M_E}{G}}{S_{bo}} \right), \left( \frac{W_{gs}}{S_{bg}} \right) \right] \qquad (4.16.7)$$

$$W_{gs} = \pi b G (C_{us} y) \qquad \textit{for non-self-energized gaskets} \qquad (4.16.8)$$

$$W_{gs} = 0.0 \qquad \textit{for self-energized gaskets} \qquad (4.16.9)$$

Note: Where significant axial force is required to compress the gasket during assembly of a joint containing a self-energizing gasket, the value of $W_{gs}$ shall be taken as equal to that axial force. In addition, some self-energizing gaskets generate axial load due to their wedging action and this load shall be considered in setting the value of $W_{gs}$.

### 4.16.7 Flange Design Procedure

**4.16.7.1** The procedure in this paragraph can be used to design circular integral, loose or reverse flanges, subject to internal or external pressure, and external loadings. The procedure incorporates both a strength check and a rigidity check for flange rotation.

**4.16.7.2** The procedure to design a flange is shown below.

a) This STEP 1 – Determine the design pressure and temperature of the flange joint, and the external net-section axial force, $F_A$, and bending moment, $M_E$. If the pressure is negative, the absolute value of the pressure should be used in this procedure.

b) STEP 2 – Determine the design bolt loads for operating condition, $W_o$, and the gasket seating condition, $W_g$, and corresponding actual bolt area, $A_b$, from paragraph 4.16.6.

c) STEP 3 – Determine an initial flange geometry, in addition to the information required to determine the bolt load, the following geometric parameters are required:

1) The flange bore, $B$
2) The bolt circle diameter, $C$
3) The outside diameter of the flange, $A$
4) The flange thickness, $t$
5) The thickness of the hub at the large end, $g_1$
6) The thickness of the hub at the small end, $g_0$

7) The hub length, $h$

d) STEP 4 – Determine the flange stress factors using the equations in Tables 4.16.4 and 4.16.5.

e) STEP 5 – Determine the flange forces.

$$H_D = 0.785B^2P \tag{4.16.10}$$

$$H = 0.785G^2P \tag{4.16.11}$$

$$H_T = H - H_D \tag{4.16.12}$$

$$H_G = W_o - H \tag{4.16.13}$$

f) STEP 6 – Determine the flange moment for the operating condition using Equation (4.16.14) or Equation (4.16.15), as applicable. When specified by the user or his designated agent, the maximum bolt spacing ($B_{s\max}$) and the bolt spacing correction factor ($B_{sc}$) shall be applied in calculating the flange moment for internal pressure using the equations in Table 4.16.11. The flange moment $M_o$ for the operating condition and flange moment $M_g$ for the gasket seating condition without correction for bolt spacing $B_{sc} = 1$ is used for the calculation of the rigidity index in STEP 10. In these equations, $h_D$, $h_T$, and $h_G$ are determined from Table 4.16.6. For integral and loose type flanges, the moment $M_{oe}$ is calculated using Equation (4.16.16) where $I$ and $I_p$ in this equation are determined from Table 4.16.7. For reverse type flanges, the procedure to determine $M_{oe}$ shall be agreed upon between the Designer and the Owner.

$$M_o = \text{abs}\left[\left((H_Dh_D + H_Th_T + H_Gh_G)B_{sc} + M_{oe}\right)F_s\right] \quad \textit{for internal pressure} \tag{4.16.14}$$

$$M_o = \text{abs}\left[\left(H_D\left(h_D - h_G\right) + H_T\left(h_T - h_G\right) + M_{oe}\right)F_s\right] \quad \textit{for external pressure} \tag{4.16.15}$$

$$M_{oe} = 4M_E\left[\frac{I}{0.3846I_p + I}\right]\left[\frac{h_D}{\left(C - 2h_D\right)}\right] + F_Ah_D \tag{4.16.16}$$

g) STEP 7 – Determine the flange moment for the gasket seating condition using Equation (4.16.17) or Equation (4.16.18), as applicable.

$$M_g = \frac{W_g\left(C - G\right)B_{sc}F_s}{2} \qquad \textit{for internal pressure} \tag{4.16.17}$$

$$M_g = W_gh_GF_s \qquad \textit{for external pressure} \tag{4.16.18}$$

h) STEP 8 – Determine the flange stresses for the operating and gasket seating conditions using the equations in Table 4.16.8.

i) STEP 9 – Check the flange stress acceptance criteria. The two criteria shown below shall be evaluated. If the stress criteria are satisfied, go to STEP 10. If the stress criteria are not satisfied, re-proportion the flange dimensions and go to STEP 4.

1) Allowable Normal Stress – The criteria to evaluate the normal stresses for the operating and gasket seating conditions are shown in Table 4.16.9.

2) Allowable Shear Stresses – In the case of loose type flanges with lap, as shown in Fig. 4.16.6 where the gasket is so located that the lap is subjected to shear, the shearing stress shall not exceed $0.8S_{no}$ or $0.8S_{ng}$, as applicable, for the material of the lap. In the case of welded flanges where the nozzle neck, vessel, or pipe wall extends near to the flange face and may form the gasket contact face, the shearing stress carried by the welds shall not exceed $0.8S_{no}$ or $0.8S_{ng}$, as applicable. The shearing stress shall be calculated for both the operating and gasket seating load cases. Similar situations where flange parts are subjected to shearing stresses shall be checked using the same requirement.

j) STEP 10 – Check the flange rigidity criterion in Table 4.16.10. If the flange rigidity criterion is satisfied, then the design is complete. If the flange rigidity criterion is not satisfied, then re-proportion the flange dimensions and go to STEP 3. The flange moment $M_o$ for the operating condition (STEP 6) and flange moment $M_g$ for the gasket seating condition (STEP 7) without correction for bolt spacing $B_{sc}=1$ is used for the calculation of the rigidity index.

### 4.16.8 Split Loose Type Flanges

Loose flanges split across a diameter and designed under the rules given in this paragraph may be used under the following provisions.

a) When the flange consists of a single split flange or flange ring, it shall be designed as if it were a solid flange (without splits), using 200% of the total moment, $F_s=2.0$.

b) When the flange consists of two split rings, each ring shall be designed as if it were a solid flange (without splits), using 75% of the total moment, $F_s=0.75$. The pair of rings shall be assembled so that the splits in one ring are 90 degrees from the splits in the other ring.

c) The flange split locations should preferably be midway between bolt holes.

### 4.16.9 Noncircular Shaped Flanges with a Circular Bore

The outside diameter, $A$, for a noncircular flange with a circular bore shall be taken as the diameter of the largest circle, concentric with the bore, inscribed entirely within the outside edges of the flange. The bolt loads, flange moments, and stresses shall be calculated in the same manner as for a circular flange using a bolt circle whose size is established by drawing a circle through the centers of the outermost bolts.

### 4.16.10 Flanges with Nut Stops

When flanges are designed per paragraph 4.16, or are fabricated to the dimensions of ASME B16.5 or other acceptable standards, except that the dimension $0.5(C-B)-g_1$ is decreased to provide a nut-stop, the fillet radius shall be as shown in Figures 4.16.3 and 4.16.4 except that:

a) For flanges designed to this paragraph, the thickness of the hub at the large end, $g_1$, shall be the smaller of $2t_n$ or $4r_u$, but not less than 12 mm (0.5 in.).

b) For ASME B16.5 or other standard flanges, the thickness of the hub at the small end, $g_0$, shall be increased as necessary to provide a nut-stop.

### 4.16.11 Joint Assembly Procedures

Bolted joints should be assembled and bolted-up in accordance with a written procedure that has been demonstrated to be acceptable for similar joint configurations in similar services. Further guidance can be found in ASME PCC-1 "Guidelines for Pressure Boundary Bolted Flange Joint Assembly".

### 4.16.12 Nomenclature

| | |
|---|---|
| $A$ | outside diameter of the flange or, where slotted holes extend to the outside of the flange, the diameter to the bottom of the slots. |
| $A_b$ | cross-sectional area of the bolts based on the smaller of the root diameter or the least diameter of the unthreaded portion. |
| $A_m$ | total minimum required cross-sectional area of the bolts. |
| $a$ | nominal bolt diameter |
| $B$ | inside diameter of the flange. When $B < 20g_1$, $B_1$ may be used for $B$ in the equation for the longitudinal stress. |
| $B_1$ | $B + g_1$ for loose type flanges and for integral type flanges that have a value of $f$ less than 1.0, (although a minimum value of $f = 1.0$ is permitted). $B_1$ is equal to $B + g_0$ for integral type flanges when $f \geq 1.0$. |
| $B^*$ | inside diameter of the reverse flange. |
| $B_s$ | bolt spacing, The bolt spacing may be taken as the bolt circle circumference divided by the number of bolts or as the chord length between adjacent bolt locations. |
| $B_{s\max}$ | maximum bolt spacing |
| $B_{sc}$ | bolt spacing correction factor |
| $b$ | effective gasket contact width. |
| $b_0$ | basic gasket seating width. |
| $C$ | bolt circle diameter. |
| $C_{ul}$ | conversion factor for length, $C_{ul} = 1.0$ for US Customary Units and $C_{ul} = 25.4$ for Metric Units. |
| $C_{us}$ | conversion factor for stress, $C_{us} = 1.0$ for US Customary Units and $C_{us} = 6.894757E-03$ for Metric Units. |
| $d$ | flange stress factor. |
| $d_r$ | flange stress factor $d$ for a reverse type flange. |
| $E_{yg}$ | Modulus of Elasticity at the gasket seating load case temperature. |
| $E_{yo}$ | Modulus of Elasticity at the operating load case temperature. |
| $e$ | flange stress factor. |
| $e_r$ | flange stress factor $e$ for a reverse type flange. |
| $F$ | flange stress factor for integral type flanges. |
| $F_A$ | value of the external tensile net-section axial force. Compressive net-section forces are to be neglected and for that case, $F_A$ should be taken as equal to zero. |
| $F_L$ | flange stress factor for loose type flanges. |
| $F_s$ | moment factor used to design split rings (see paragraph 4.16.8), $F_s = 1.0$ for non-split rings. |
| $f$ | hub stress correction factor for integral flanges. |
| $G$ | diameter at the location of the gasket load reaction (see Figure 4.16.8). |
| $G_{avg}$ | average of the hub thicknesses $g_1$ and $g_0$. |
| $G_c$ | outside diameter of the gasket contact area (see Figure 4.16.8). |
| $g_0$ | thickness of the hub at the small end. |

$g_1$ thickness of the hub at the large end.

$H$ total hydrostatic end force.

$H_D$ total hydrostatic end force on the area inside of the flange.

$H_G$ gasket load for the operating condition.

$H_T$ difference between the total hydrostatic end force and hydrostatic end force on the area inside the flange.

$h$ hub length.

$h_o$ hub length parameter.

$h_{or}$ hub length parameter for a reverse flange.

$h_D$ moment arm for load $H_D$.

$h_G$ moment arm for load $H_G$.

$h_T$ moment arm for load $H_T$.

$I$ bending moment of inertia of the flange cross-section.

$I_p$ polar moment of inertia of the flange cross-section.

$J$ flange rigidity index.

$K$ ratio of the flange outside diameter to the flange inside diameter.

$K_R$ rigidity index factor.

$L$ flange stress factor.

$L_r$ flange stress factor $L$ for a reverse type flange.

$M_E$ absolute value of the external net-section bending moment.

$M_g$ flange design moment for the gasket seating condition.

$M_o$ flange design moment for the operating condition.

$M_{oe}$ component of the flange design moment resulting from a net section bending moment and/or axial force.

$m$ factor for the gasket operating condition.

$N$ gasket contact width, N = 0.0 for self-energizing gaskets.

$P$ design pressure.

$r_1$ radius to be at least $0.25g_1$ but not less than 5 mm (0.1875 in.).

$r$ radius of the undercut on a flange with nut stops.

$S_{bg}$ allowable stress from Annex 3.A for the bolt evaluated at the gasket seating temperature.

$S_{bo}$ allowable stress from Annex 3.A for the bolt evaluated at the design temperature.

$S_{fg}$ allowable stress from Annex 3.A for the flange evaluated at the gasket seating temperature.

$S_{fo}$ allowable stress from Annex 3.A for the flange evaluated at the design temperature.

$S_{ng}$ allowable stress from Annex 3.A for the nozzle neck, vessel, or pipe evaluated at the gasket seating temperature.

$S_{no}$ allowable stress from Annex 3.A for the nozzle neck, vessel, or pipe evaluated at the design temperature.

$S_H$ flange hub stress.

$S_R$ flange radial stress.

| | |
|---|---|
| $S_T$ | flange tangential stress. |
| $S_{T1}$ | flange tangential stress at the outside diameter of a reverse flange. |
| $S_{T2}$ | flange tangential stress at the inside diameter of a reverse flange. |
| $T$ | flange stress factor. |
| $T_r$ | flange stress factor $T$ for a reverse flange. |
| $t$ | flange thickness, including the facing thickness or the groove depth if either do not exceed 2 mm (0.0625 in.); otherwise, the facing thickness or groove depth is not included in the overall flange thickness. |
| $t_n$ | nominal thickness of the shell, pipe, or nozzle to which the flange is attached. |
| $t_x$ | is $2g_0$ when the design is calculated as an integral flange, or two times the minimum required thickness of the shell or nozzle wall when the design is based on a loose flange, but not less than 6 mm ( 0.25 in.). |
| $U$ | flange stress factor. |
| $U_r$ | flange stress factor $U$ for a reverse type flange. |
| $V$ | flange stress factor for integral type flanges. |
| $V_L$ | flange stress factor for loose type flanges. |
| $W_g$ | design bolt load for the gasket seating condition. |
| $W_o$ | design bolt load for the operating condition. |
| $w$ | width of the nubbin. |
| y | factor for the gasket seating condition |
| $Y$ | flange stress factor. |
| $Y_r$ | flange stress factor $Y$ for a reverse type flange. |
| $Z$ | flange stress factor. |

### 4.16.13 Tables

**Table 4.16.1 – Gasket Factors For Determining The Bolt Loads**

| Gasket Material | Gasket Factor m | Min. Design Seating Stress y, MPa (psi) | Column in Table 4.16.3 | Facing Sketch In Table 4.16.3 |
|---|---|---|---|---|
| Self-energizing types (O rings, metallic, elastomer, other gasket types considered as self-sealing) | 0 | 0 | --- | --- |
| Elastomers without fabric or high percent of mineral fiber:<br>• below 75 A Shore Durometer<br>• 75 A or higher Shore Durometer | <br>0.50<br>1.00 | <br>0<br>1.4 (200) | II | (1a), (1b), (1c), (1d), (4), (5) |
| Mineral fiber with suitable binder for operating conditions:<br>• 3.2 mm (1/8 inch) thick<br>• 1.6 mm (1/16 inch) thick<br>• 0.8 mm (1/32 inch) thick | <br>2.00<br>2.75<br>3.50 | <br>11 (1,600)<br>26 (3,700)<br>45 (6,500) | II | (1), (1b), (1c), (1d), (4), (5) |
| Elastomers with cotton fabric insertion | 1.25 | 2.8 (400) | II | (1a), (1b), (1c), (1d), (4), (5) |
| Elastomers with mineral fiber insertion (with or without wire reinforcement):<br>• 3-ply<br>• 2-ply<br>• 1-ply | <br>2.25<br>2.50<br>2.75 | <br>15 (2200)<br>20 (2,900)<br>26 (3,700) | II | (1), (1b), (1c), (1d), (5) |
| Vegetable fiber | 1.75 | 7.6 (1,100) | II | (1a), (1b), (1c), (1d), (4), (5) |
| Spiral-wound metal, mineral fiber filler<br>• Carbon steel<br>• Stainless steel, Monel, and nickel-base alloy | <br>2.50<br>3.00 | <br>69 (10,000)<br>69 (10,000) | II | (1a), (1b) |
| Corrugated metal, mineral fiber inserted, or corrugated metal, jacketed mineral fiber filled:<br>• Soft aluminum<br>• Soft copper or brass<br>• Iron or soft steel<br>• Monel or 4% - 6% chrome<br>• Stainless steels and nickel-base alloys | <br>2.50<br>2.75<br>3.00<br>3.25<br>3.50 | <br>20 (2,900)<br>26 (3,700)<br>31 (4,500)<br>38 (5,500)<br>45 (6,500) | II | (1a), (1b) |
| Corrugated metal:<br>• Soft aluminum<br>• Soft copper or brass<br>• Iron or soft steel<br>• Monel or 4% - 6% chrome<br>• Stainless steels and nickel-base alloys | <br>2.75<br>3.00<br>3.25<br>3.50<br>3.75 | <br>26 (3,700)<br>31 (4,500)<br>38 (5,500)<br>45 (6,500)<br>52 (7,600) | II | (1a), (1b), (1c), (1d) |

**Table 4.16.1 – Gasket Factors For Determining The Bolt Loads**

| Gasket Material | Gasket Factor m | Min. Design Seating Stress y, MPa (psi) | Column in Table 4.16.3 | Facing Sketch In Table 4.16.3 |
|---|---|---|---|---|
| Flat metal, jacketed mineral fiber filled: | | | | |
| • Soft aluminum | 3.25 | 38 (5,500) | II | (1a), (1b), (1c), (1d), (2) |
| • Soft copper or brass | 3.50 | 45 (6,500) | | |
| • Iron or soft steel | 3.75 | 52 (7,600) | | |
| • Monel | 3.50 | 55 (8,000) | | |
| • 4% - 6% chrome | 3.75 | 62 (9,000) | | |
| • Stainless steels and nickel-base alloys | 3.75 | 62 (9,000) | | |
| Grooved Metal: | | | | |
| • Soft aluminum | 3.25 | 38 (5,500) | II | (1a), (1b), (1c), (1d), (2), (3) |
| • Soft copper or brass | 3.50 | 45 (6,500) | | |
| • Iron or soft steel | 3.75 | 52 (7,600) | | |
| • Monel or 4% - 6% chrome | 3.75 | 62 (9,000) | | |
| • Stainless steels and nickel-base alloys | 4.25 | 70 (10,100) | | |
| Sold flat metal: | | | | |
| • Soft aluminum | 4.00 | 61 (8,800) | I | (1a), (1b), (1c), (1d), (2), (3), (4), (5) |
| • Soft copper or brass | 4.75 | 90 (13,000) | | |
| • Iron or soft steel | 5.50 | 124 (18,000) | | |
| • Monel or 4% - 6% chrome | 6.00 | 150 (21,800) | | |
| • Stainless steels and nickel-base alloys | 6.50 | 180 (26,000) | | |
| Ring joint: | | | | |
| • Iron or soft steel | 5.50 | 124 (18,000) | I | (6) |
| • Monel or 4% - 6% chrome | 6.00 | 150 (21,800) | | |
| • Stainless steel and nickel-base alloys | 6.50 | 180 (26,000) | | |

Note: This table gives a list of commonly used gasket materials and contact facings with suggested values of m and y that have generally proved satisfactory in actual service when using effective gasket seating width b. The design values and other details given in this table are suggested only and are not mandatory.

**Table 4.16.2 – Recommended Minimum Gasket Contact Width**

| Gasket Contact Width, $N$ | | | | | |
|---|---|---|---|---|---|
| **Gasket Type** | **Gasket Outside Diameter** | | | | |
| | **< 150 mm (6 inch)** | **< 300 mm (12 inch)** | **< 600 mm (24 inch)** | **< 900 mm (36 inch)** | **900 mm (36 inch) and Over** |
| Sheet Gaskets Including Laminated Sheets Gaskets With Or Without A Metal Core | 9 mm (0.375in) | 12 mm (0.5in) | 16 mm (0.625in) | 16 mm (0.625in) | 19 mm (0.75in) |
| Preformed Composite Gaskets Including Spiral Wound, Jacketed, And Solid Flat Metal Gaskets | 6 mm (0.25in) | 9 mm (0.375in) | 12 mm (0.5in) | 16 mm (0.625in) | 16 mm (0.625in) |

**Table 4.16.3 – Effective Gasket Width For Determining The Bolt Loads**

| Facing Sketch | Facing Sketch Detail (Exaggerated) | Basic Gasket Seating Width $b_o$ | |
|---|---|---|---|
| | | Column I | Column II |
| 1a | 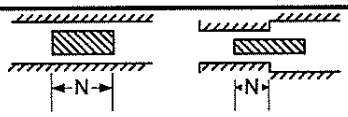  | $\frac{N}{2}$ | $\frac{N}{2}$ |
| 1b | 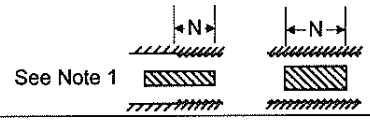  | | |
| 1c | 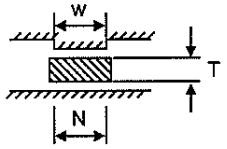  w ≤N | $\min\left[\frac{w+T}{2}, \frac{w+N}{4}\right]$ | $\min\left[\frac{w+T}{2}, \frac{w+N}{4}\right]$ |
| 1d | 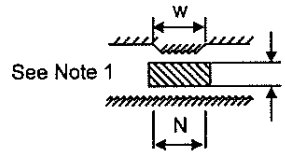  w ≤ N | | |
| 2 | 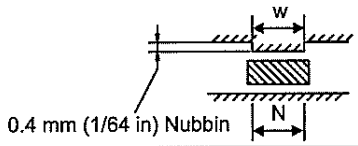  w ≤ N/2 | $\frac{w+N}{4}$ | $\frac{w+3N}{8}$ |
| 3 | 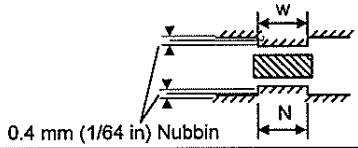  w ≤ N/2 | $\frac{N}{4}$ | $\frac{3N}{8}$ |
| 4 | 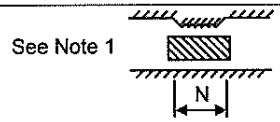  | $\frac{3N}{8}$ | $\frac{7N}{16}$ |
| 5 | 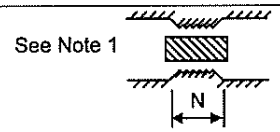  | $\frac{N}{4}$ | $\frac{3N}{8}$ |
| 6 | 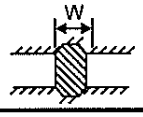  | $\frac{w}{8}$ | --- |

Notes:
1. Where serrations do not exceed 0.4 mm, (0.0156in) depth and 0.8mm (0.0313in) width spacing, Sketches (1b) and (1d) shall be used.
2. The gasket factors listed in this table only apply to flanged joints in which the gasket is contained entirely within the inner edges of the bolt holes.

**Table 4.16.4 – Flange Stress Factors Equations Involving Diameter**

| Flange Type | Stress Factors Involving Diameter |
|---|---|
| Integral Type Flange and Loose Type Flange with a Hub | $K = \frac{A}{B}$<br>$Y = \frac{1}{K-1}\left[0.66845 + 5.71690\left(\frac{K^2 \log_{10} K}{K^2-1}\right)\right]$<br>$T = \frac{K^2\left(1+8.55246\log_{10} K\right)-1}{\left(1.04720+1.9448K^2\right)\left(K-1\right)}$<br>$U = \frac{K^2\left(1+8.55246\log_{10} K\right)-1}{1.36136\left(K^2-1\right)\left(K-1\right)}$<br>$Z = \frac{\left(K^2+1\right)}{\left(K^2-1\right)}$<br>$L = \frac{te+1}{T} + \frac{t^3}{d}$<br>$e = \frac{F}{h_o}$ *for Integral Type Flanges*<br>$e = \frac{F_L}{h_o}$ *for Loose Type Flanges with a Hub*<br>$d = \frac{Ug_o^2 h_o}{V}$ *for Integral Type Flanges*<br>$d = \frac{Ug_o^2 h_o}{V_L}$ *for Loose Type Flanges with a Hub*<br>$h_o = \sqrt{Bg_0}$<br>$X_g = \frac{g_1}{g_0}$<br>$X_h = \frac{h}{h_o}$ |

**Table 4.16.4 – Flange Stress Factors Equations Involving Diameter**

| Flange Type | Stress Factors Involving Diameter |
|---|---|
| Reverse Integral Type Flange and Reverse Loose Type Flanges with a Hub | The parameters $K$, $T$, $U$, $Y$, and $Z$ are determined using the equations for Integral and Loose Type Flanges with:<br>$K = \frac{A}{B^*}$<br>Then, the reverse flange parameters are computed as follows:<br>$Y_r = \alpha_r Y$<br>$T_r = \frac{(Z+0.3)}{(Z-0.3)}\alpha_r T$<br>$U_r = \alpha_r U$<br>$L_r = \frac{te_r+1}{T_r} + \frac{t^3}{d_r}$<br>$\alpha_r = \frac{1}{K^2}\left[1+\frac{0.668(K+1)}{Y}\right]$<br>$e_r = \frac{F}{h_{or}}$ *for Integral Type Flanges*<br>$e_r = \frac{F_L}{h_{or}}$ *for Loose Type Flanges with a Hub*<br>$d_r = \frac{U_r g_o^2 h_{or}}{V}$ *for Integral Type Flanges*<br>$d_r = \frac{U_r g_o^2 h_{or}}{V_L}$ *for Loose Type Flanges with a Hub*<br>$h_{or} = \sqrt{Ag_0}$<br>$X_g = \frac{g_1}{g_0}$<br>$X_h = \frac{h}{h_{or}}$ |

**Table 4.16.5 – Flange Stress Factor Equations**

| Flange Type | Stress Factors |
|---|---|
| Integral Type Flange, Reverse Integral Type Flange | $F = \left( \begin{array}{l} 0.897697 - 0.297012 \ln X_g + 9.5257\left(10^{-3}\right) \ln X_h + \\ 0.123586\left(\ln X_g\right)^2 + 0.0358580\left(\ln X_h\right)^2 - 0.194422\left(\ln X_g\right)\left(\ln X_h\right) - \\ 0.0181259\left(\ln X_g\right)^3 + 0.0129360\left(\ln X_h\right)^3 - \\ 0.0377693\left(\ln X_g\right)\left(\ln X_h\right)^2 + 0.0273791\left(\ln X_g\right)^2\left(\ln X_h\right) \end{array} \right)$<br><br>*For* $0.1 \le X_h \le 0.5$<br>$V = \left( \begin{array}{l} 0.500244 + \dfrac{0.227914}{X_g} - 1.87071 X_h - \dfrac{0.344410}{X_g^2} + 2.49189 X_h^2 + \\ 0.873446\left(\dfrac{X_h}{X_g}\right) + \dfrac{0.189953}{X_g^3} - 1.06082 X_h^3 - 1.49970\left(\dfrac{X_h^2}{X_g}\right) + \\ 0.719413\left(\dfrac{X_h}{X_g^2}\right) \end{array} \right)$<br>*For* $0.5 < X_h \le 2.0$<br>$V = \left( \begin{array}{l} 0.0144868 - \dfrac{0.135977}{X_g} - \dfrac{0.0461919}{X_h} + \dfrac{0.560718}{X_g^2} + \dfrac{0.0529829}{X_h^2} + \\ \dfrac{0.244313}{X_g X_h} + \dfrac{0.113929}{X_g^3} - \dfrac{0.00928265}{X_h^3} - \dfrac{0.0266293}{X_g X_h^2} - \dfrac{0.217008}{X_g^2 X_h} \end{array} \right)$<br><br>$f = \max\left[ 1.0, \left( \begin{array}{l} \dfrac{0.0927779 - 0.0336633 X_g + 0.964176 X_g^2 + }{1 - 5.96093(10^{-3}) X_g + 1.62904 X_h + } \\ \dfrac{0.0566286 X_h + 0.347074 X_h^2 - 4.18699 X_h^3}{3.49329 X_h^2 + 1.39052 X_h^3} \end{array} \right) \right]$ |

**Table 4.16.5 – Flange Stress Factor Equations**

| Flange Type | Stress Factors |
|---|---|
| Loose Type Flange with a Hub, Reverse Loose Type Flange with a Hub | $F_L = \left( \begin{array}{l} 0.941074 + 0.176139\left(\ln X_g\right) - 0.188556\left(\ln X_h\right) + 0.0689847\left(\ln X_g\right)^2 + \\ 0.523798\left(\ln X_h\right)^2 - 0.513894\left(\ln X_g\right)\left(\ln X_h\right) \\ \hline 1 + 0.379392\left(\ln X_g\right) + 0.184520\left(\ln X_h\right) - 0.00605208\left(\ln X_g\right)^2 - \\ 0.00358934\left(\ln X_h\right)^2 + 0.110179\left(\ln X_g\right)\left(\ln X_h\right) \end{array} \right)$ <br> *For* $0.1 \le X_h \le 0.25$ <br> $\ln\left[V_L\right] = \left( \begin{array}{l} 6.57683 - 0.115516X_g + 1.39499\sqrt{X_g}\left(\ln X_g\right) + \\ 0.307340\left(\ln X_g\right)^2 - 8.30849\sqrt{X_g} + 2.62307\left(\ln X_g\right) + \\ 0.239498X_h\left(\ln X_h\right) - 2.96125\left(\ln X_h\right) + \dfrac{7.035052(10^{-4})}{X_h} \end{array} \right)$ <br> *For* $0.25 < X_h \le 0.50$ <br> $V_L = \left( \begin{array}{l} 1.56323 - 1.80696\left(\ln X_g\right) - \dfrac{1.33458}{X_h} + 0.276415\left(\ln X_g\right)^2 + \\ \dfrac{0.417135}{X_h^2} + \dfrac{1.39511\left(\ln X_g\right)}{X_h} + 0.0137129\left(\ln X_g\right)^3 + \\ \dfrac{0.0943597}{X_h^3} - \dfrac{0.402096\left(\ln X_g\right)}{X_h^2} - \dfrac{0.101619\left(\ln X_g\right)^2}{X_h} \end{array} \right)$ <br> *For* $0.50 < X_h \le 1.0$ <br> $V_L = \left( \begin{array}{l} -0.0213643 - \dfrac{0.0763597}{X_g} + \dfrac{0.102990}{X_h} + \dfrac{0.725776}{X_g^2} - \dfrac{0.160603}{X_h^2} - \\ \dfrac{0.0918061}{X_g \cdot X_h} + \dfrac{0.472277}{X_g^3} + \dfrac{0.0873530}{X_h^3} + \dfrac{0.527487}{X_g \cdot X_h^2} - \dfrac{0.980209}{X_g^2 \cdot X_h} \end{array} \right)$ <br> *For* $1.0 < X_h \le 2.0$ <br> $V_L = \left( \begin{array}{l} 7.96687(10^{-3}) - \dfrac{0.220518}{X_g} + \dfrac{0.0602652}{X_h} + \dfrac{0.619818}{X_g^2} - \dfrac{0.223212}{X_h^2} + \\ \dfrac{0.421920}{X_g \cdot X_h} + \dfrac{0.0950195}{X_g^3} + \dfrac{0.209813}{X_h^3} - \dfrac{0.158821}{X_g \cdot X_h^2} - \dfrac{0.242056}{X_g^2 \cdot X_h} \end{array} \right)$ <br> $f = 1.0$ |

**Table 4.16.6 – Moment Arms For Flange Loads For The Operating Condition**

| Flange Type | $h_D$ | $h_T$ | $h_G$ |
|---|---|---|---|
| Integral Type Flanges | $\frac{C-B-g_1}{2}$ | $\frac{1}{2}\left[\frac{C-B}{2}+h_G\right]$ | $\frac{C-G}{2}$ |
| Loose Type Flanges, except Lap Joint Flanges | $\frac{C-B}{2}$ | $\frac{h_D+h_G}{2}$ | $\frac{C-G}{2}$ |
| Loose Type Lap Joint Flanges | $\frac{C-B}{2}$ | $\frac{C-G}{2}$ | $\frac{C-G}{2}$ |
| Reverse Integral Type Flanges | $\frac{C+g_1-2g_o-B}{2}$ | $\frac{1}{2}\left(C-\frac{B+G}{2}\right)$ | $\frac{C-G}{2}$ |
| Reverse Loose Type Flanges | $\frac{C-B}{2}$ | $\frac{1}{2}\left(C-\frac{B+G}{2}\right)$ | $\frac{C-G}{2}$ |

**Table 4.16.7 – Flange Moments Of Inertia**

| Flange Type | $I$ | $I_p$ |
|---|---|---|
| Integral Type Flange with a Hub | $I = \dfrac{0.0874 L g_o^2 h_o B}{V}$ | $I_p = K_{AB} + K_{CD}$<br>$K_{AB} = \left(A_A B_B^3\right)\left[\dfrac{1}{3} - 0.21\left(\dfrac{B_B}{A_A}\right)\left(1 - \dfrac{1}{12}\left\{\dfrac{B_B}{A_A}\right\}^4\right)\right]$<br>$K_{CD} = \left(C_C D_{DG}^3\right)\left[\dfrac{1}{3} - 0.105\left(\dfrac{D_{DG}}{C_C}\right)\left(1 - \dfrac{1}{192}\left\{\dfrac{D_{DG}}{C_C}\right\}^4\right)\right]$ |
| Loose Type Flange with a Hub | $I = \dfrac{0.0874 L g_o^2 h_o B}{V_L}$ | $A_R = 0.5\left(A - B\right)$<br>$G_{avg} = 0.5\left(g_0 + g_1\right)$<br>*If* $t \geq G_{avg}$ :<br>$A_A = A_R,\ \ B_B = t,\ \ C_C = h,\ \ D_{DG} = G_{avg}$<br>*If* $t < G_{avg}$ :<br>$A_A = h + t,\ \ B_B = G_{avg},\ \ C_C = A_R - G_{avg},\ \ D_{DG} = t$ |
| Loose Type Flange without a Hub | $I = \dfrac{B t^3 \ln K}{6}$ | $I_p = A_R t^3\left[\dfrac{1}{3} - 0.21\left(\dfrac{t}{A_R}\right)\left(1 - \dfrac{1}{12}\left\{\dfrac{t}{A_R}\right\}^4\right)\right]$<br>$A_R = 0.5\left(A - B\right)$ |

**Table 4.16.8 – Flange Stress Equations**

| Flange Type | Stress Equations | |
|---|---|---|
| | Operating Condition | Gasket Seating Conditions |
| Integral Type Flange or Loose Type Flange with a Hub | $S_H = \frac{fM_o}{Lg_1^2B}$<br>$S_R = \frac{(1.33te+1)M_o}{Lt^2B}$<br>$S_T = \frac{YM_o}{t^2B} - ZS_R$ | $S_H = \frac{fM_g}{Lg_1^2B}$<br>$S_R = \frac{(1.33te+1)M_g}{Lt^2B}$<br>$S_T = \frac{YM_g}{t^2B} - ZS_R$ |
| Loose Type Flange without a Hub | $S_T = \frac{YM_o}{t^2B}$ | $S_T = \frac{YM_g}{t^2B}$ |
| Reverse Integral Type Flange or Reverse Loose Type Flange with a Hub | $S_H = \frac{fM_o}{L_r g_1^2 B^*}$<br>$S_R = \frac{(1.33te_r+1)M_o}{L_r t^2 B^*}$<br>$S_{T1} = \frac{Y_r M_o}{t^2 B^*} - \frac{ZS_R(0.67te_r+1)}{(1.33te_r+1)}$<br>$S_{T2} = \left[Y - \frac{2K^2(0.67te_r+1)}{(K^2-1)L_r}\right]\frac{M_o}{t^2B^*}$ | $S_H = \frac{fM_g}{L_r g_1^2 B^*}$<br>$S_R = \frac{(1.33te_r+1)M_g}{L_r t^2 B^*}$<br>$S_{T1} = \frac{Y_r M_g}{t^2 B^*} - \frac{ZS_R(0.67te_r+1)}{(1.33te_r+1)}$<br>$S_{T2} = \left[Y - \frac{2K^2(0.67te_r+1)}{(K^2-1)L_r}\right]\frac{M_g}{t^2B^*}$ |
| Reverse Loose Type Flange without a hub | $S_T = \frac{YM_o}{t^2B^*}$ | $S_T = \frac{YM_g}{t^2B^*}$ |

**Table 4.16.9 – Flange Stress Acceptance Criteria**

| Flange Type | Stress Acceptance Criteria | |
|---|---|---|
| | Operating Condition | Gasket Seating Conditions |
| Integral Type Flange or Loose Type Flange with a Hub | $S_H \le \min\left[1.5S_{fo}, 2.5S_{no}\right]$ (1)<br>$S_H \le 1.5S_{fo}$ (2)<br>$S_R \le S_{fo}$<br>$S_T \le S_{fo}$<br>$\frac{(S_H + S_R)}{2} \le S_{fo}$<br>$\frac{(S_H + S_T)}{2} \le S_{fo}$ | $S_H \le \min\left[1.5S_{fg}, 2.5S_{ng}\right]$ (1)<br>$S_H \le 1.5S_{fg}$ (2)<br>$S_R \le S_{fg}$<br>$S_T \le S_{fg}$<br>$\frac{(S_H + S_R)}{2} \le S_{fg}$<br>$\frac{(S_H + S_T)}{2} \le S_{fg}$ |
| Loose Type Flange without a Hub | $S_T \le S_{fo}$ | $S_T \le S_{fg}$ |
| Reverse Integral Type Flange or Reverse Loose Type Flange with a Hub | $S_H \le 1.5S_{fo}$<br>$S_R \le S_{fo}$<br>$S_{T1} \le S_{fo}$<br>$\frac{(S_H + S_R)}{2} \le S_{fo}$<br>$\frac{(S_H + S_{T1})}{2} \le S_{fo}$<br>$S_{T2} \le S_{fo}$ | $S_H \le 1.5S_{fg}$<br>$S_R \le S_{fg}$<br>$S_{T1} \le S_{fg}$<br>$\frac{(S_H + S_R)}{2} \le S_{fg}$<br>$\frac{(S_H + S_{T1})}{2} \le S_{fg}$<br>$S_{T2} \le S_{fg}$ |
| Reverse Loose Type Flanges | $S_T \le S_{fo}$ | $S_T \le S_{fg}$ |

Notes:
1. For integral flanges with hubs welded to a nozzle neck, pipe, or vessel shell
2. For loose type flanges with a hub.
3. Flanges made of non-ductile material, such as cast iron, are not addressed by this section.

**Table 4.16.10 – Flange Rigidity Criterion**

| Flange Type | Rigidity Criterion | |
|---|---|---|
| | Operating Condition | Gasket Seating Conditions |
| Integral Type Flange | $J=\frac{52.14VM_o}{LE_{yo}g_0^2K_Rh_o}\le 1.0$ | $J=\frac{52.14VM_g}{LE_{yg}g_0^2K_Rh_o}\le 1.0$ |
| Loose Type Flange with a Hub | $J=\frac{52.14V_LM_o}{LE_{yo}g_0^2K_Rh_o}\le 1.0$ | $J=\frac{52.14V_LM_g}{LE_{yg}g_0^2K_Rh_o}\le 1.0$ |
| Reverse Integral Type Flange | $J=\frac{52.14VM_o}{L_rE_{yo}g_0^2K_Rh_o}\le 1.0$ | $J=\frac{52.14VM_g}{L_rE_{yg}g_0^2K_Rh_o}\le 1.0$ |
| Reverse Loose Type Flange with a Hub | $J=\frac{52.14V_LM_o}{L_rE_{yo}g_0^2K_Rh_o}\le 1.0$ | $J=\frac{52.14V_LM_g}{L_rE_{yg}g_0^2K_Rh_o}\le 1.0$ |
| Loose Type and Reverse Loose Type Flange without a Hub | $J=\frac{109.4M_o}{E_{yo}t^3K_R(\ln K)}\le 1.0$ | $J=\frac{109.4M_g}{E_{yg}t^3K_R(\ln K)}\le 1.0$ |

Notes:

1. For an integral type flange, $K_R=0.3$ unless other values are specified by the user.
2. For a loose type flange with or without a hub, $K_R=0.2$ unless other values are specified by the user.

**Table 4.16.11 - Bolt Spacing Equations**

| Flange Type | Bolt Spacing Factors |
|---|---|
| All | $B_{s\max}=2a+\frac{6t}{m+0.5}$ |
| | $B_{sc}=\sqrt{\frac{B_s}{2a+t}}$ |

### 4.16.14 Figures

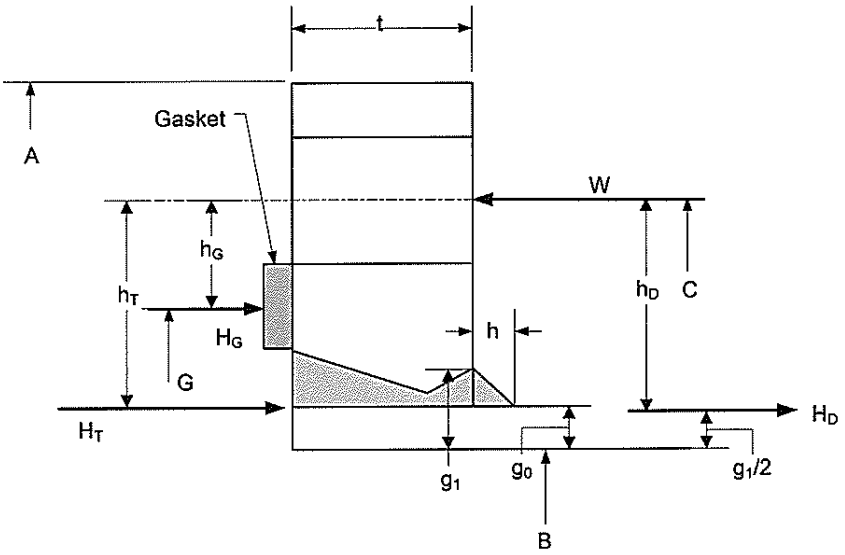


(a) Integral Flange Without A Hub

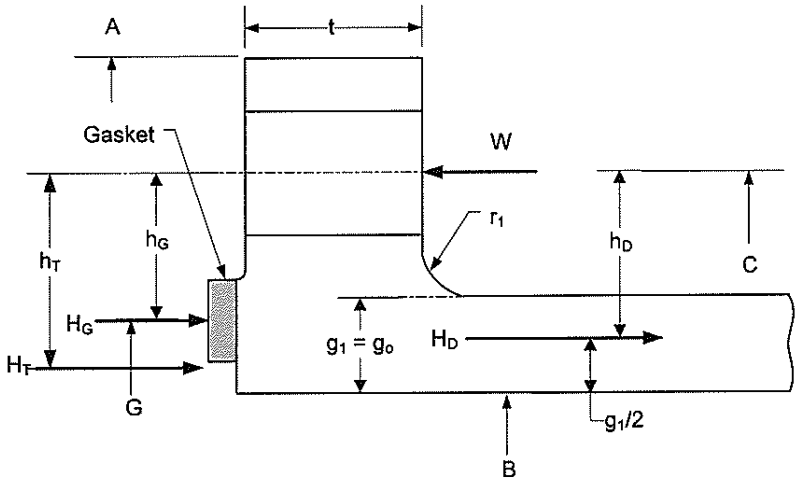


(b) Integral Flange with $g_o$=$g_1$

**Figure 4.16.1 – Integral Type Flanges**

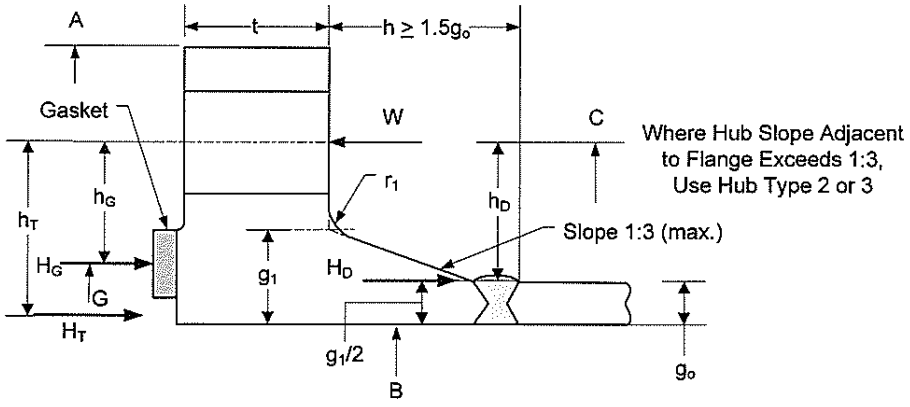


(a) Hub Type 1

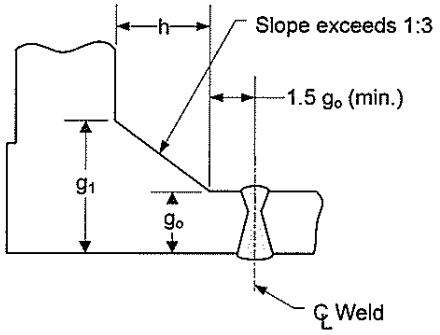


(b) Hub Type 2

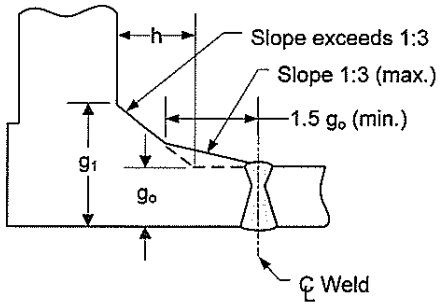


(c) Hub Type 3

**Figure 4.16.2 – Integral Type Flanges with a Hub**

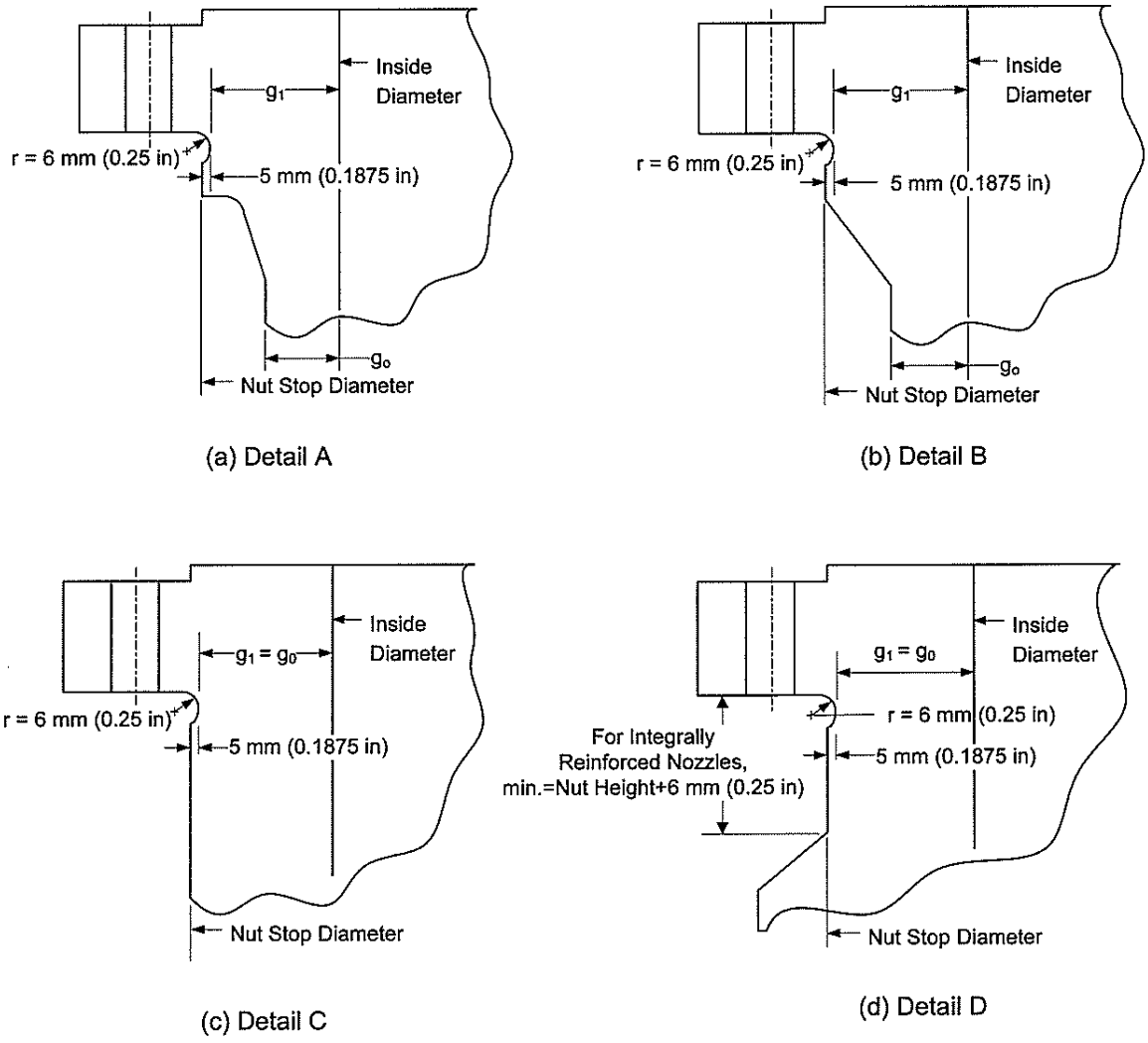


**Figure 4.16.3 – Integral Type Flanges With Nut Stops – Diameter Less Than or Equal To 450mm (18 Inches)**

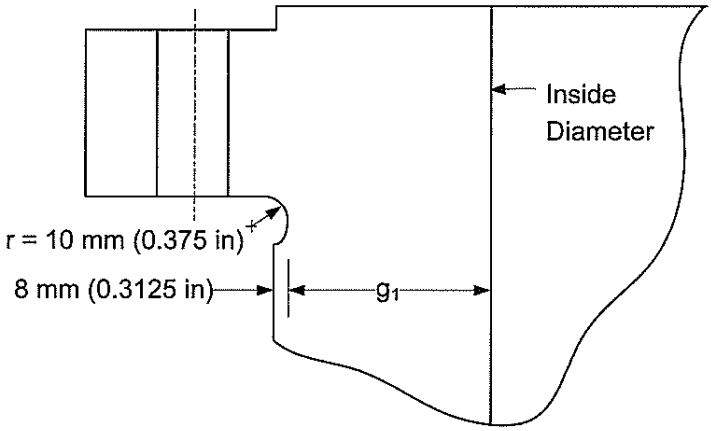


Note: All other details per Figure 4.16.3

**Figure 4.16.4 – Integral Type Flanges With Nut Stops – Diameter Greater Than 450mm (18 Inches)**

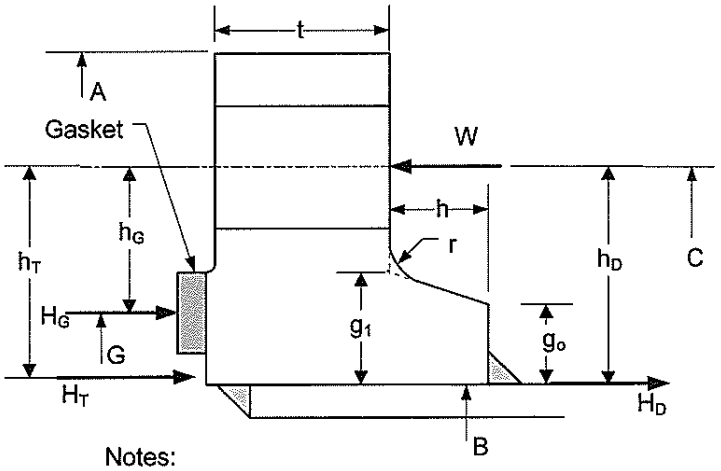


Notes:
1) For Hub Tapers 6° or Less, Use $g_0 = g_1$

(a) Loose Flange With A Hub

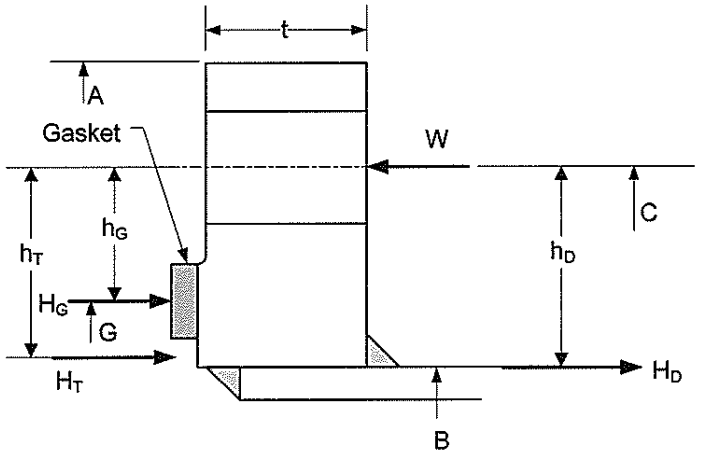


(b) Loose Flange Without A Hub

**Figure 4.16.5 – Loose Type Flanges**

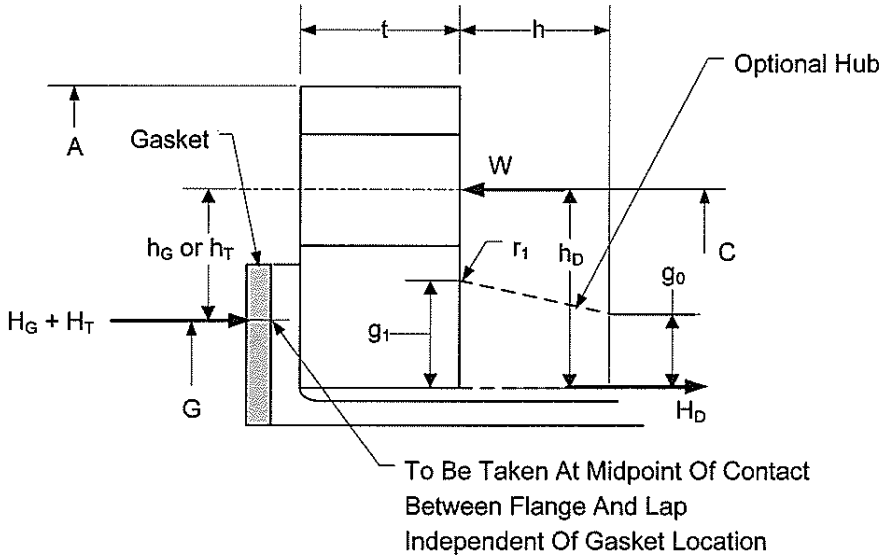


Notes (Loose Type Flanges):
(1) For Hub Tapers 6° or Less, Use $g_0 = g_1$

**Figure 4.16.6 – Loose Type Lap Joint Type Flanges**

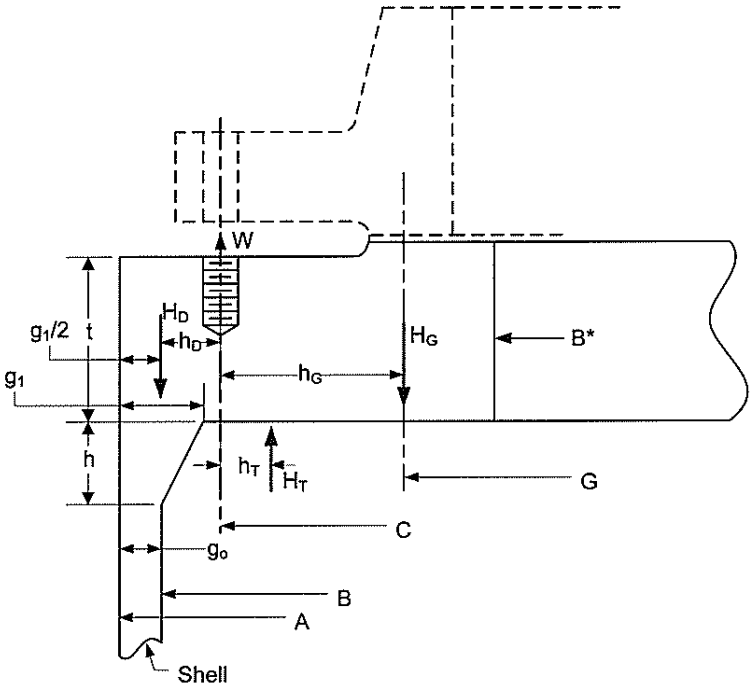


(a) Integral Type Reverse Flange

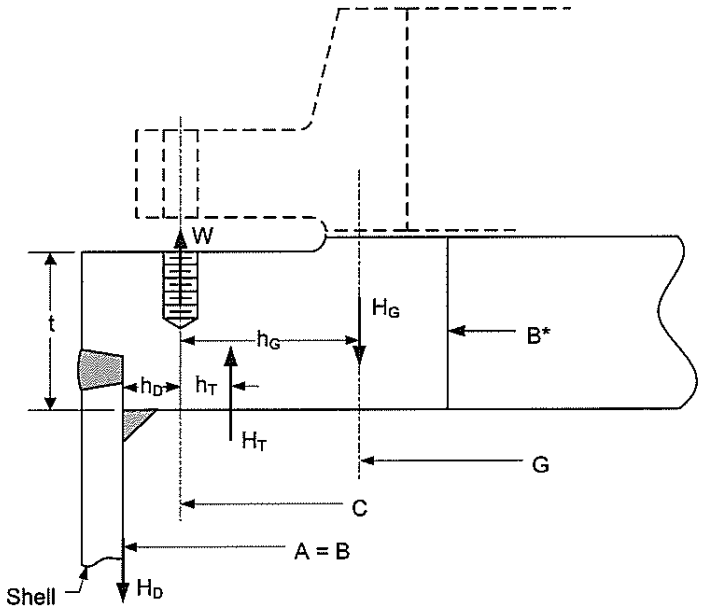


(b) Loose Type Reverse Flange

**Figure 4.16.7 – Reverse Flanges**

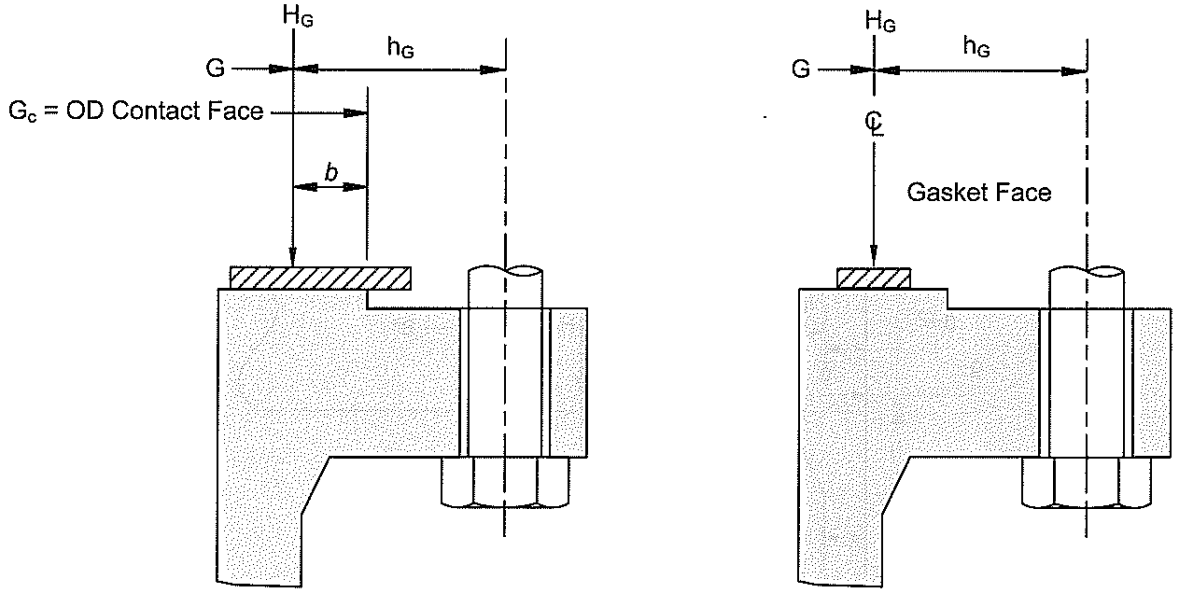


For $b_o$ > 6 mm (0.25in.)

For $b_o \leq$ 6 mm (0.25in.)

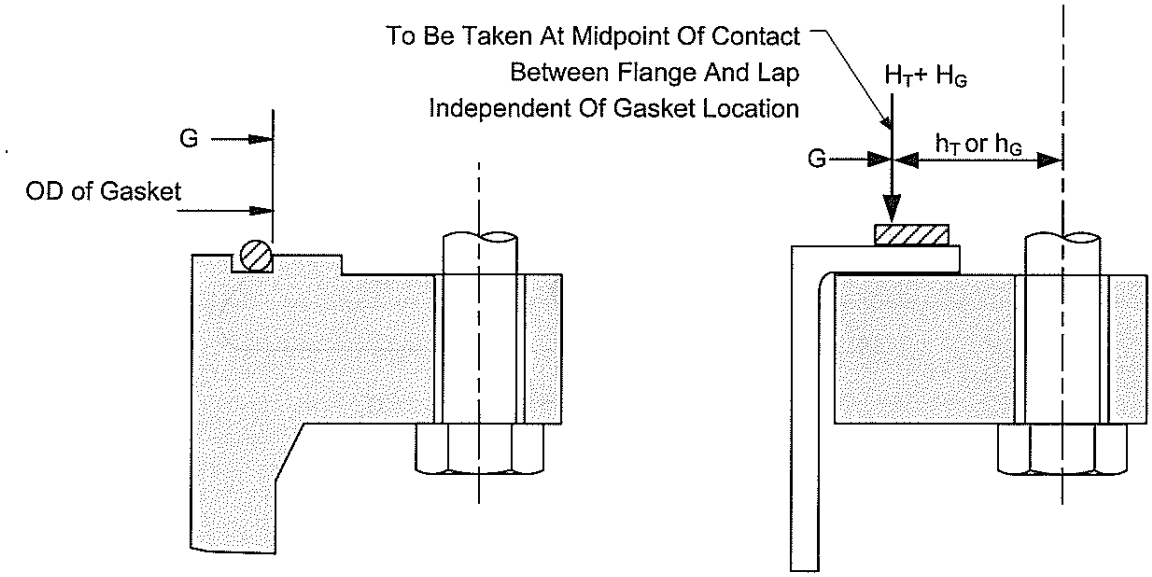


Self-Energizing Gaskets

Lap Type Joints

**Figure 4.16.8 – Location of Gasket Reaction Load Diameter**